Differential Response to Photon versus Proton Radiotherapy

Biological implications for new indications and combined treatment concepts

---

Dissertation

zur

Erlangung der naturwissenschaftlichen Doktorwürde

(Dr. sc. nat.)

vorgelegt der

Mathematisch-Naturwissenschaftlichen Fakultät

der

Universität Zürich

von

Simon Deycmar

aus

Wien / Österreich

Promotionskomitee

Prof. Dr. Martin Pruschy (Leitung der Dissertation und Vorsitz)

Prof. Dr. Alessandro Sartori

Prof. Dr. Antony Lomax

Prof. Dr. med. Oliver Riesterer

Zürich, 2020

Declaration

I confirm that this thesis is entirely my own work. All sources and quotations have been fully acknowledged in the appropriate places with adequate footnotes and citations. Quotations have been properly acknowledged and marked with appropriate punctuation. The works consulted are listed in the bibliography. This thesis has not been submitted to another examination panel in the same or a similar form.

…….. ……..

Place, Date Signature

Abstract

Nearly half of cancer patients are eligible for radiotherapy at least once during the course of disease. The current main pillar is photon radiotherapy but particle-based approaches such as proton and carbon beams are stepping out of their niche. In contrast to photon irradiation, proton irradiation allows to reduce the dose deposited to healthy tissue as well as the specific sparing of critical structures. Furthermore, proton irradiation not just exhibits superior beam characteristics but also induces a different cellular response. The higher linear-energy transfer (LET) of proton beams is predicted to induce more complex DNA double-strand breaks which explains the subsequently different recruitment and utilization of DNA repair machineries. In detail, an increased necessity and utilization of homologous-recombination repair (HRR) was observed in response to proton irradiation. As a result, the extrinsic abrogation of HRR provides a promising rational to specifically sensitize cancer cells for proton radiotherapy.

In this PhD project, we investigate the combination of HSP90 inhibitor Ganetespib with protons administered at a proximal and a distal position in a Spread-Out Bragg peak (SOBP) in reference to conventional photon irradiation. HSP90 is a chaperon and upregulated in cancer cells due to the elevated intrinsic proteotoxic stress. HSP90 inhibition in turn demonstrated to downregulate numerous HRR-relevant proteins such as BRCA1, BRCA2, and Rad51 and conclusively impairs HRR. We investigated clonogenic cell survival in A549 non-small cell lung cancer (NSCLC) and FaDu head and neck squamous cell carcinoma (HNSCC) cell lines treated with or without low-dosed Ganetespib and either irradiated with 200kV photons or protons at a proximal (LET 2.1keV/µm) or at a distal (LET 4.5keV/µm) position in a SOBP. Ganetespib treatment significantly radiosensitized both investigated cancer cell lines for SOBP proton irradiation but only negligible when combined with photon irradiation. Higher and more persistent protein levels of Rad51 were determined in proton-treated A549 cells and the downregulation of Rad51 upon Ganetespib treatment confirmed. In comparison to photon-irradiation cells, proton-irradiated cells exhibited a more pronounced accumulation in S/G2/M phase at 8h and 24h after irradiation. Ganetespib abrogated this accumulation and decreased the fraction of cells in S/G2/M phase at each investigated time point and conclusively limits the availability of HRR in these cells. Irrespective of the type of administered irradiation, a similar number of γH2AX foci was induced and also foci removal

was indifferent. Furthermore, foci removal was also not altered by Ganetespib treatment despite the observed reduction in Rad51 protein levels and the restricted access to HRR. These findings suggest that HRR capacity either remained sufficient or missing HRR capacity was replaced by Rad51-independent but more error-prone repair pathways.

In conclusion, we are the first ones to demonstrate a specific radiosensitization for SOBP proton irradiation by HSP90 inhibitor Ganetespib. In both cell lines investigated, RBE increases of up to 30% were observed in Ganetespib-treated cells. Additionally, we highlighted the role of Rad51 in response to proton radiotherapy. Overall, our generated data supports the promising rational of combining SOBP proton radiotherapy with HSP90 inhibitors and fosters continuing preclinical and clinical investigation.

Keywords: proton radiotherapy, SOBP, LET, Ganetespib, Rad51, HSP90 inhibition

Acknowledgements

Per aspera ad astra

The relief in handing in this thesis and manuscript is immeasurable. This thesis was not just a challenge in regards of cancer biological questions but also a logistical and a personal one. Nevertheless, a huge number of people supported me during this long and cumbersome path.

The first ones to mention are the other early-stage researchers involved in the ITN Radiate program. Regular meetings throughout Europe allowed us to grow on each other's experience and this accumulation of open minds fostered friendship that goes far beyond business networking. I also want to thank Dr. Nagma Khan who managed this sack full of fleas while always providing each of us with an open ear and useful advice.

In addition, I want to thank the members of the group headed by Prof. Dr. Pruschy who allowed me to reflect on and proceed with my work, kept me mentally sane and my spirit alive. I especially want to acknowledge Dr. Ivo Grgic who provided me with asylum in F-Lab and supported me during unpleasant times. I also want to thank Dr. Philip Knobel and Verena Waller who assisted me with flow cytometry and provided me with critical thoughts regarding my data. Last but not least, I also want to thank Erica Faccin who pushed urgent orders and investigated on delayed ones while always having a smile on her face and a positive attitude in her mind.

Needless to say, I also want to thank the people involved in my work at MedAustron. Dr. Sylvia Gruber, Elisabeth Mara and Karin Posch not just hosted but included me and supported me with cell culture but also with planning the experiments and analysing the obtained data. This little bubble in Austria allowed me to implement my own ideas and conduct research in proton irradiation in an incredibly inspiring environment. Conclusively, I also want to mention Anton Kerschbaum who assisted me in understanding the basics of proton delivery and interactions and represents the scientifically open and curious environment at the MedAustron.

Most importantly, I want to acknowledge my parents. They not just supported me during my childhood and education but were truly involved in this project. I was able to stay at my parents` house and use my dad`s car for free. Without this support (and the wake-up calls at 3 in the morning on a Sunday) I would not have been able to be at the proton shifts in Wiener Neustadt and conduct my project in this exciting and outstanding field of research. They never scrutinized their efforts but provided me with all I could have ever asked for.

List of Abbreviations

CTV	clinical target volume
dCDP	deoxycytidine diphosphate
dCTP	Deoxycytidine triphosphate
DNA	deoxyribonucleic acid
dNTP	deoxynucleoside triphosphate
DSB	double-strand break
dsDNA	double-stranded DNA
G1/S/G2/M phase	phases of cell cycle
HDACi	histone deacetylase inhibitor
HNSCC	head and neck squamous cell carcinoma
HPV	human papillomavirus
HRR	homologous recombination repair
HSP90	heat shock protein 90
HSP90i0	HSP90 inhibitor
LET	linear energy transfer [keV/µm]
LINAC	linear accelerator
MDSC	myeloid-derived suppressor cells
MMEJ	microhomology-mediated end joining
MMR	mismatch repair
NER	nucleotide excision repair
NGS	Next-Generation Sequencing
NHEJ	non-homologous end joining
NSCLC	non-squamous cell lung carcinoma
OAR	organ-at-risk
PD-L1	programmed death-ligand 1
PMMA	poly(methyl methacrylate)
PTV	planning target volume
RBE	relative biological effectiveness
SOBP	Spread-Out Bragg peak
ssDNA	single-stranded DNA
TAM	tumor-associated macrophages
Treg	T regulatory cells
WHO	World Health Organisation
wt /mutTP53	wild type / mutated TP53
γH2AX	p.S139 histone 2AX

Table of Contents

1. Introduction

1.1 Cancer

1.1.1 Carcinogenesis and the Global Incidence of Cancer

Cancer, malignancies, tumor stage, or metastasis are words describing a disease and its features and impose an imminent negative connotation. Cancer is a group of disease affecting all groups of people worldwide independent of age, wealth or country and is becoming more and more relevant in an aging population. While tremendous advantages in versatile clinical fields such as antibiotics, surgery or vaccines have extended the overall life expectance, cancer remains a threat. The mortality rates of appendicitis, infected teeth, pox or tetanus is marginal in developed countries. Unfortunately, these rates remain high for lung, pancreas or oesophagus cancer and thus illustrate the urgent demand for a deeper understanding and novel treatment approaches. To further elaborate on this demand, open access global statistics collected and provided by the IARC (see Error! Reference source not f ound.) illustrate the vast numbers of patients worldwide as well as cancer sides with a worse outcome than others.

Table 1 Global cancer incidence and mortality rates 2018 (modified from [1])
More than half of cancer patients will succumb to their disease with lung tumors at a high incidence as well as mortality rate (84.1%). Breast cancer on the other hand also occurs at high rates but the mortality rate (30.0%) is fortunately lower as for liver (92.9%) or stomach cancer (75.7%).

	Incidence rate		Mortality rate		Estim. risk of death
Total	**18.078.957**	**100.0%**	**9.555.027**	**100.0%**	**52.9%**
Lung	2.093.876	11.6%	1.761.007	18.4%	**84.1%**
Breast	2.088.849	11.6%	626.679	6.6%	**30.0%**
Colon/Rectum	1.849.518	10.2%	880.792	9.2%	**47.6%**
Prostate	1.276.106	7.1%	358.989	3.8%	**28.1%**
Stomach	1.033.701	5.7%	782.685	8.2%	**75.7%**
Liver	841.080	4.7%	781.631	8.2%	**92.9%**
Oesophagus	572.034	3.2%	508.585	5.3%	**88.9%**
Cervix uteri	569.847	3.2%	311.365	3.3%	**54.6%**
Thyroid	567.233	3.1%	41.071	0.4%	**7.2%**
Bladder	549.393	3.0%	199.922	2.1%	**36.4%**
Non-Hodgkin Lymphoma	509.590	2.8%	248.724	2.6%	**48.8%**
Pancreas	458.918	2.5%	432.242	4.5%	**94.2%**
Other	5.668.812	31.4%	3.302.301	34.6%	**58.3%**

These cancer cases provide an overview about global case numbers but there are differences between sexes, age groups, race and global region. The difference between sexes in cancer incidence and mortality is also illustrated in a graph provided by the open access World Cancer Report 2014.

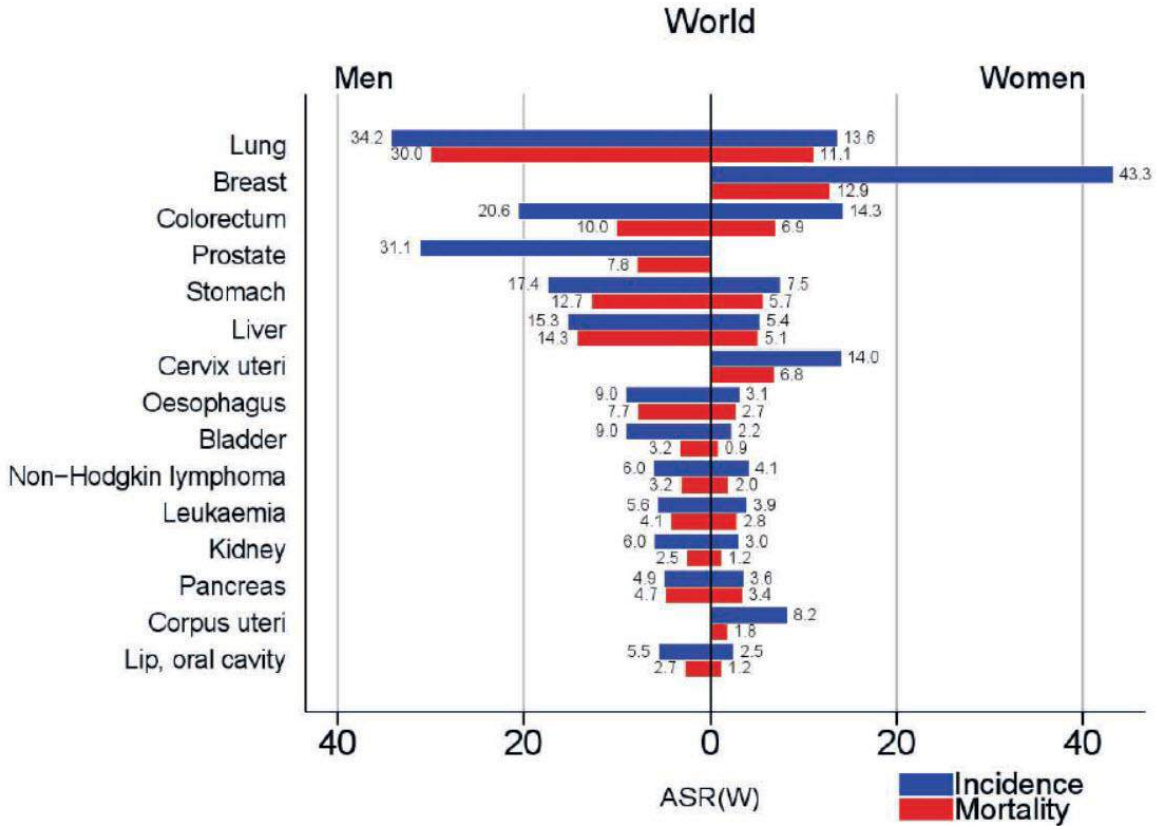

Figure 1 Illustration of the global incidence and mortality rate (per 100.000) in the respective sexes in 2012 [2]

A strong deviation of cancer incidence can be found between the sexes with usually higher incidence rates in man than woman. These deviations are also apparent in different ethnic groups, regions and age groups but not illustrated here due to simplicity.

Aggravatingly, these incidence numbers are expected to rise to 25 million annual cases in the next two decades which is based on a growing as well as aging population. Despite all efforts, risk factors such as infectious disease or low food quality persist in low developed regions and/or got replaced by the contradictory risk factors of an industrial lifestyle such as high caloric diet, obesity, and reduced exercise.[3-5] In addition, tobacco consumption is persisting or increasing in low and middle income countries while fortunately having peaked in high income countries.[6]

Improvements such as HPV vaccination [7, 8], stricter ruling to reduce tobacco as well as alcohol consumption and a reversal of the industrial lifestyle with a more balanced diet and exercise [9] could be a huge game changer and reduce cancer risk, morbidity and mortality as well as the risk for versatile other accompanying disease. Nevertheless, improvements in anti-tumor therapy will be essential to reduce the public and personal burden of cancer which occurred despite preventive efforts or just by “bad luck”.

1.1.2 Hallmarks of Cancer

The conversion from a normal cell towards a pathologically relevant neoplastic phenotype which ultimately becomes malignant and metastasises is a multistep process of highly diverse developmental patterns. In 2000, Hanahan and Weinberg published a system which attempted to organize this multifarious processes by defining hallmark capabilities.[10] These initially 6 hallmarks were expanded to 10 in 2011 by the same authors due to increasing knowledge in cancer biology.[11]

The purpose of the following paragraphs is to bring all readers on the same page and either introduce or refresh certain topics and features of cancer. I therefore intend to provide an overview of these hallmarks, their role in tumorigenesis as well as their significance for choice of therapy.

1.1.2.1 Sustaining Proliferative Signaling

One of the most obvious features of cancer cells is their capability to maintain a continuously proliferative phenotype. Normal cells receive versatile cues from their environment such as growth factors in a paracrine context. Versatile known and unknown factors are part of this signalling and control growth factor release, sequestration, degradation or the final response by the influenced cell. This complex regulatory network may be corrupted by cancer cells by simply producing growth factor ligands themselves or stimulating normal cells to do so. This provides cancer cells with a proliferative signalling in an autocrine or paracrine manner, respectively. Cancer cells can also receive increased proliferative signalling by upregulation of receptors, rendering these cells hypersensitive for defined ligands, or alterations within the receptor structure resulting in the continuous signalling of such. These proliferative signalling may also be induced by alterations in downstream signalling proteins such as KRAS, BRAF or PI3K.[12, 13] In addition, not just activating events but also abolishing the action of negative regulators can result in cell proliferation. An example of such abrogated negative regulator may be PTEN which is involved in downregulating PI3K and AKT signalling and thus limiting tumorigenic signalling.[14, 15] Nevertheless, cells with excessively high proliferative capacity may still sense their corrupted state by feedback loops and undergo oncogene-induced apoptosis or senescence.[16, 17] This demonstrates the nature of excessively high proliferative signalling as two-edged sword with aggressive cellular expansion and detrimental cellular stress as the extremes of the scale.

A typical example for a constitutively activated pathway is the mutation of BRAF in melanoma. The substitution of glutamic acid for valine at the 600th codon (V600E) results in a constitutive activation of BRAF and is present in 40 to 60% of melanomas.[18] Due to the exclusivity of V600E-mutated BRAF in tumor cells, this kinase is an outstanding target for

inhibitors which interfere with tumor signaling but theoretically not interfere with normal cells.

Vemurafenib, an inhibitor of aforementioned V600E-mutated BRAF, can be orally administered and demonstrated its efficacy in multiple clinical trials. Vemurafenib induced partial or complete response in V600E-mutated melanoma patients with response rates of 48 to 69% and improved overall and progression-free survival.[18, 19] Due to these tremendous results, Zelboraf (Vemurafenib) received marketing authorization in 2011 by the FDA and 2012 in the EU.[20, 21]

Another example of cancer cell growth signal inhibition is Imatinib. Imatinib is a kinase inhibitor targeting the cancer-associated fusion protein BCR-ABL [22] but also platelet-derived growth factor receptor (PDGFR).[23] The aforementioned fusion protein BCR-ABL is the result of a chromosome translocation between chromosomes 9 and 22 and results in the so called Philadelphia chromosome (a shortened chromosome 22). This translocation results in an elevated tyrosine kinase activity and is present in more than 90% of chronic myelogenous leukemia and some patients with acute leukemia. These clonally expanded cancer cells are more dependent on specific driver proteins and thus strongly respond to inhibition of such while normal cells receive signaling cues from versatile pathways and are thus less dependent. In conclusion, the improved patient outcome was demonstrated in clinical trials [24] and resulted in the approval of Gleevec (Imatinib) in 2001 by the FDA for multiple neoplastic entities such as leukemia or gastrointestinal stromal tumors.[25]

Versatile other drugs also interfere with more or less tumor-specific growth signaling pathways such as Erbitux (Cetuximab) preventing ligand binding to EGFR [26, 27], Xalkori (Crizotinib) administered against ALK positive NSCLC [28-30], or Tarceva (Erlotinib) interfering with the kinase activity of EGFR. [31, 32]

These drugs can prevent the transmission of growth signals by targeting the extracellular part of receptor kinases and preventing ligand binding in case of antibodies and their fragments. Small molecule drugs on the other hand mostly block intracellularly the receptor tyrosine kinase activity.

1.1.2.2 Evading Growth Repressors

Negative regulators of cellular proliferation are important throughout the whole existence of the organism and act as safety switches and way to clear unwanted cells may it be because of virus infection or tissue remodelling. Moreover, these negative signals also prevent unwanted proliferation of intrinsically deregulated cells and thus act as tumor suppressors. The most famous of these tumor suppressors are TP53 and RB.

RB (retinoblastoma protein) is a protein involved in steering the cell cycle.[33, 34] RB prevents cyclin E and A synthesis by repressing E2F-dependent transcription via recruitment of histone deacetylases (HDAC) and thus prevents entry into S phase.[35] Mitogenic signalling on the other hand induces the synthesis of cyclinD which forms a complex with CDK4/6 and finally deactivates RB by phosphorylation to pRB and thus triggers the cell to progress into S phase. In conclusion, abolishing RB function by inherited or acquired loss-of function mutations as well as hyperactivation of the cyclinD/CDK4/6 complex obviously abrogates this regulatory function. While RB may be described as the gate keeper of the cell cycle, TP53 is often described as the guardian of the genome.

For TP53 action, it must be stabilized, bind to DNA in a sequence-specific manner, and transcriptionally activate target genes.[36] In a healthy cell, TP53 is continuously produced but also continuously ubiquitinylated by MDM2 and thus marked for proteasomal degradation. Cellular stress such as DNA damage results in the activation of kinases such as ATM, ATR, CHK1, and CHK2 which in turn phosphorylate TP53 and this way stabilize TP53. As an example, TP53 then can induce transcription of p21 which is an inhibitor of CDKs or it represses CDC25 and thus arrests cell cycle.

Needless to say, these processes are highly complex and interconnected but already single missense point mutations for example in the DNA binding region of TP53 can cause an imbalance in this system and are a frequent event in tumors. This illustrates the necessity to overcome this growth repression during tumorigenesis to become pathologic while transformed cells that retain this control mechanism are unlikely to be ever recognized.

Another pathologic condition which abrogates these growth suppressors is HPV infection.[37] HPV virus can introduce the protein E6 which interacts with TP53 and initiates its degradation. Another protein introduced by the virus is E7 which competes with E2F for RB protein and thus releases E2F from repression and abrogates RB function. This inactivation of checkpoints and regulatory pathways clearly states the tumorigenic nature of HPV infection which is coherently considered to be involved in nearly all cervical cancer, 90% of anal cancer, 40% of penile, vaginal and vulvar cancers as well as 25% of oral cavity and 35% of oropharyngeal cancers.[38]

Fortunately, prophylactic vaccines against HPV such as Gardasil are spreading globally and could reduce cancer incidence in the upcoming generation independent of sex or socioeconomic status. [39, 40]

1.1.2.3 Resisting Cell Death

Similarly to overcoming growth repressors, cancer cells also need to overcome cell-death-inducing signalling.

Cell death is regulated by versatile proteins sensing and translating external and internal signal cues. This balance between pro- and anti-apoptotic signals shifts and triggers apoptosis by elevated oncogenic signals, DNA damage due to hyperproliferation or FasL in the cellular environment as well as versatile other factors.[11, 41] To specify, anti-apoptotic Bcl-2 and further proteins can sequester pro-apoptotic Bax and Bak which are located in the outer mitochondrial membrane. A relieve from inhibition therefore results in the disruption of the mitochondrial membrane and the release of cytochrome c which in turn activates a cascade of caspases. These caspases ultimately trigger apoptosis via their proteolytic activity.

Crosstalk between cell death and growth repression are evident with TP53 as illustrative example. In addition to arresting the cell cycle, stabilized TP53 can also trigger apoptosis.[36] TP53 can activate genes and proteins such as Bax, CD95 (Fas), PUMA, and a vast number of other pro-apoptotic factors as well as inducing mitochondrial outer membrane permeabilization and thus initiating the release of pro-apoptotic factors from the intermembrane space. Conclusively, TP53 dysfunction by mutation or degradation also abolishes this cell-death-inducing pathway. A similar non-responsive phenotype can be achieved by overexpression of anti-apoptotic (Bcl-2) or downregulation of pro-apoptotic factors (Bax, PUMA).

1.1.2.4 Enabling Replicative Immortality

Normal cells can only replicate for a predefined number of cycles until they will run into senescence.[11, 42] This cellular replication limit was established against the dogma at the time in 1961 by Leonard Hayflick und is thus called Hayflick limit. Cells in senescence are non-replicative but viable while cells ignoring this limit are expected to run into cellular crisis.

These effects can be explained by telomeres and their length at the end of chromosomes.[43] Repetitive terminal DNA sequences enable the DNA to form loops and thus hide and protect the DNA ends from unwanted “repair” and ligation with other DNA fragments. The reason of telomere shortening is based on the process of DNA replication during S phase and termed end-replication problem.[42] The DNA polymerizing protein complex cannot assemble right at the end of the DNA strand but requires a certain length of DNA to assemble to. Therefore, the 3’ end of the lagging DNA is used for assembly, lies upstream the polymerization site and is conclusively not replicated but lost. This loss in telomeric DNA shortens the telomeres with each DNA replication cycle and functions as intracellular counting mechanism.

Cells incapable of restricting cell replication will run into cellular crisis and shorten their telomeres until DNA looping and thus protection is abolished. These unprotected DNA ends are mistaken by DNA repair proteins and can be ligated by processes such as Non-Homologous End Joining (as described in **1.3.5 Repair**). Needless to say, unintended ligation of chromosome ends can result in dicentric chromosomes which in turn can induce mitotic arrest, aneuploidy, and genomic instability and apparently threaten the cell viability.

A protein to counteract this counting mechanism and cellular crisis is telomerase which can add telomeric repeats to the DNA ends. Throughout the organism, telomerase activity is highly regulated and almost absent in normal differentiated cells but high in cells which are determined for infinite replication such as stem cells and germ cells.[44, 45] On the other hand, the vast majority of 85-90% of cancer cells gained a high telomerase activity to overcome prementioned obstacles.[43] This mechanism of replicative immortalization and the high frequency it occurs in cancer cells demonstrates its hallmark role and how detrimental these obstacles and how essential bypassing is.

1.1.2.5 Inducing Angiogenesis

While neovascularization, the assembly and formation of new vessels, is limited to embryogenesis, angiogenesis, the sprouting of vessels from existing ones, persists throughout lifetime. Angiogenesis is a regular process during wound healing and female reproductive cycling but otherwise quiescent.

Due to the increasing demand of nutrients and oxygen by hyperactive and proliferative tumor cells, the supply of such becomes a growth limiting factor. Attracting blood vessels to provide a sustainable supply is essential to become pathological while lesions incapable to do so will remain widely unrecognized.

Vascular endothelial growth factor (VEGF) family is a key player for blood vessel growth as well as homeostasis and gene expression can be upregulated by hypoxia and HIF-1 and HIF-2 [46, 47] as well as oncogenic signalling.[48-50] Due to this imbalanced chronically activated angiogenesis, these newly formed vessels are commonly distorted, enlarged and/or immature which results in erratic blood flow, leakiness and haemorrhage.

Therefore, angiogenesis and blood vessel formation is an obvious clinically relevant target for anti-cancer therapy. Bevacizumab, clinically known as Avastin, is an antibody sequestering VEGF and has proven its efficacy in versatile clinical trials.[51] It received marketing authorization by the FDA in 2004 [52] and the EMA in 2005 for the treatment of cancers originating at sites such as colon, rectal, breast, lung, kidney, ovarian, fallopian tube and cervix.

Also radiotherapy interacts with angiogenesis and oxygen supply (as discussed in **1.3.3 Reoxygenation**) by inducing vessel normalization and thus improved tumor perfusion. In addition, tumor vessel dysfunction can also limit delivery of small-molecule chemotherapeutics. On the other hand, vessel leakiness may be exploited by the enhanced permeability and retention (EPR) effect by utilizing nanoparticles for drug delivery approaches such as pegylated liposomes.[53-55] Nanoparticles are less probable to extravasate through a mature continuous endothelial layer while the wide fenestration in immature tumor-associated blood vessels enables the entry into the tissue and the targeted release of the cytotoxic cargo. This effect not just increases the uptake of drug into the tumor but also limits the uptake into healthy tissue.

1.1.2.6 Activating Invasion and Metastasis

Pathologically growing cancer cells ultimately require space for their proliferative phenotype. In differentiated epithelial cells, as progenitors of carcinoma and surrounding tissue, E-cadherin and EpCAM may restrict the available space by tight adhesion between cells or by the engulfing effect of dense extracellular matrix (ECM).[11, 56] The loss of cell adhesion molecules such as E-cadherin is a feature of epithelial-mesenchymal transition (EMT) in cancer cells which results in a more motile and invasive phenotype. EMT is considered a pro-metastatic event and describes versatile possible changes in cytoskeletal components, reassemble of cell-cell contacts and cell motility but also gene expression and exocytosis of altered ECM components. Factors involved in the onset of EMT are versatile and include Wnt, Notch, hedgehog, cytokines and as most prominent one TGF-β. To increase complexity, some metastatic cancer lesions revert to an epithelial phenotype via mesenchymal-epithelial transition (MET) while others retain a mesenchymal phenotype and thus question the role of MET in metastasis establishment and growth.[57]

In addition, clinical patterns of cancer spreading can also be correlated to patterns in non-coding RNA networks such as miRNA, lncRNA, and circRNA.[58] Peritoneal spreading is a common symptom in ovarian cancer patients and present with a miliary (vast numbers of small millet-like lesions) or non-miliary (few but bulky lesions) pattern. Data suggested EMT (-MET) being more relevant for bulky non-miliary lesions as well as a possible spreading via the blood/lymphatic system in manner of a regular distant metastasizing. On the other hand, miliary-spreading tumor cells retain their epithelial phenotype and globally decrease gene expression by enhanced miRNA regulation and as a result are more adapted for spreading via anaerobic ascites and implantation on the peritoneal surface.

As enabling factor of invasion and metastasis, the degradation of extracellular matrix and membranes should not remain undiscussed.[59-61] The process of ECM degradation is important for repair, development and growth of normal tissue but being hijacked by cancer cells. A famous family of proteases, matrix metalloprotease (MMP), is commonly overexpressed in various cancers and associated with tumor invasion, metastasis and a poor prognosis. These endopeptidases degrade essentially all ECM components such as collagen of various types, laminin, and fibronectin. Precursor MMPs are extracellularly activated by proteolysis but MMP activity can also be dampened by TIMPs (tissue inhibitors of metalloproteinases) expressed by tumor or host cells. While MMPs are proven to facilitate cell motility and metastasis, TIMPs demonstrated to reduce invasion and metastatic capacity. Moreover, MMPs may not only be expressed in tumor cells themselves but can be induced in fibroblasts by tumor-cell-derived factors.

As already prementioned, not only tumor cells themselves determine invasiveness but also accompanying cells such as fibroblasts and pericytes.[62] As an example, cancer-cell-secreted PDGF-BB was found to induce pericyte-fibroblast transition (PFT) in pericytes which in turn gain mesenchymal features and expressed stromal fibroblasts and myofibroblasts markers. Pericytes transformed in this manner were strikingly found to promote tumor dissemination and invasion. This clearly states the need to not just investigate tumor cells but also take accompanying cells and the tumor microenvironment into account.

1.1.2.7 Genome Instability and Mutation

In regular cells, mutation rate is kept at a low sustainable rate by versatile genome maintenance systems. These are commonly abrogated in cancer cells to foster the acquiring of essential mutant genes and in conclusion facilitate tumorigenesis. As a result, the mutational burden in a tissue correlates with the cancer incidence rate in it. [63]

High mutation rates are based on dysfunctions in DNA repair, DNA modifications or during DNA replication.[64] Additionally, mutation rates can also be increased by external factors such as tobacco smoke, exposure to ultraviolet light and ionizing radiation, or food borne mutagens such as polycyclic aromatic hydrocarbons.[65, 66]

The prevalence of mutations is highly variable between and within cancer subtypes and can range between 0.001 to 400 mutations per megabase of DNA.[67] Factors such as age relates into this with childhood cancers usually carrying fewer mutations while chronic mutagen exposure explains the high mutation prevalence in lung cancer and melanoma. An example for deviations in mutation rate within cancers can be found in prementioned lung cancers. NSCLCs of smokers exposed to mutagens demonstrate a 10-fold higher mutation rate than NSCLCs in never-smokers.[68]

In addition to higher mutation rates, the type of mutation induced also correlates with the carcinogen exposed to.[69] As an example, C→A mutations are frequent in lung cancer due to polycyclic aromatic hydrocarbon exposure from tobacco smoke while melanoma show a high frequency of C→T mutations induced by misrepair of UV-induced DNA damage. These findings can be summed up to a subset of approximately 140 genes being defined as promoting tumorigenesis when mutated with tumors typically displaying 2 to 8 of these driver mutations.[70]

Increased mutation rates can also be inherited with BRCA1 and BRCA2 as most well-known gene defects. BRCA1 and 2 are key players in maintaining genetic integrity and DNA repair (in detail at **1.3.5 Repair**) and germline mutations go along with a drastically increased lifetime risk of developing breast or ovarian cancer.[71-73] Interestingly, upon treatment with DNA damaging drugs, which BRCA1/2 deficient cancer cells are sensitive to, a selection for cancer cells which regained BRCA1/2 can be observed.[74] This reversion mutation can be seen as resistance mechanism but also demonstrates that genome instability may promote tumorigenesis at an early stage but becomes obsolete in an established cancer lesion.

Another inherited repair deficiency as an example is Xeroderma pigmentosum.[75] This disease originates from a deficiency in Nucleotide Excision Repair (NER) by mutations in essential repair proteins. Symptoms include neurological impairments but also hypersensitivity to UV-light-induced DNA lesions and thus a 1000-fold increased risk for skin cancers. Preventing UV light exposure is a preventive measure but life expectancy is nevertheless drastically reduced.

In summary, genome instability as newly added hallmark is considered to play an enabling role in providing cancer cells with vast numbers of mutations and as a result the chance to gain new hallmark capabilities, adapt to an altered environment or resist a therapy.[76] Obviously, this hallmark is a double-edged sword and can also cause detrimental gene loss and cell death. As long as this balance remains more or less positive within the tumor and more than half of the daughter cells are viable, it may slow down cancer progression in short-term but in long-term it increases the clonal landscape and accelerates the selection for more aggressive/resistant/proliferative phenotypes.

1.1.2.8 Tumor-Promoting Inflammation

Inflammation can play a major role for tumorigenesis.[11] During normal immune response, alarm signals such as invading microbes or tissue damage will alert versatile immune cells which help to clear the area of pathogens and secrete factors to activate epithelial cells.[77] This secretion accelerates the repair of dysfunctional barriers before the immune response

converts back to homeostasis. In tumorigenesis, not a microbe but oncogenic events can lead to epithelial dysfunction. The triggered immune response thereafter may not remove the transformed cells but nevertheless provide cytokines and inflammatory factors which as a result drive tumor proliferation instead of tissue regeneration.

In detail, the inflammatory environment can be induced externally by local tissue damage such as chronic inhalation of small particles like asbestos which in turn triggers lung and airway inflammation. [78] Asbestos-exposed tissue is known to recruit macrophages which interact with the carcinogenic fibers, release IL-1β and as a result increase mesothelial proliferation. In addition to cytokines released, also reactive oxygen species (ROS) are set free which fosters mesothelial cell transformation (see also **1.1.2.7 Genome Instability and Mutation**). This unwanted ROS release is based on the length of the inorganic asbestos fibers which cannot be fully phagocytosed and engulfed by the macrophages and thus cause accidental leakage into the surrounding tissue.

The inflammatory environment can also be systemic when caused by internal cues such as obesity.[79] Adipocytes are becoming hypertrophic and die during weight gain which shifts the previously type 2 (anti-inflammatory) cytokine rich environment towards a type 1 (pro-inflammatory) state with increased TNF, IFN-γ, and IL-1β levels. Overnutrition is also found to suppress anti-inflammatory signaling in classic dendritic cells which results in dendritic cell activation and continuous antigen presentation, triggering a T-cell-mediated response and in turn T cell exhaustion due to continuous activation.

Strikingly, also metastasis is facilitated by obesity-induced inflammation.[80] Lung neutrophilia induced by obesity fosters breast cancer metastasis which could be reverted by weight loss. This effect was demonstrated to be linked to elevated GM-CSF and IL-5 levels in obese mice and clearly demonstrates a link between inflammatory phenotypes and cancer.

These inflammatory patterns in cancer induction are versatile and further prominent examples of inflammation-promoted tumors are inflammatory bowel disease, chronic hepatitis, Helicobacter-induced gastritis, and schistostoma-induced inflammation of the bladder.[77]

1.1.2.9 Reprogramming Energy Metabolism

Deregulated and high proliferation within cancer obviously also requires an altered metabolism to fuel tumor growth.[11] Already in 1920, an altered metabolism in cancer cells was described by Otto Warburg.[81] This anomalous upregulation of glycolysis despite aerobic conditions was thus termed Warburg effect. To counterbalance the lower ATP production efficiency of glycolysis, an increased glucose consumption is found in cancer cells

which is sustained by a higher expression of glucose transporters such as GLUT1 and thus an increased glucose uptake.

Factors influencing the metabolism include HIF-1, Ras, Myc, or Akt which foster glycolysis with mTORC1 being a key player in induction of anabolic growth. Interestingly, also TP53 plays a role in energy metabolism and lowers glycolysis rates while enhancing mitochondrial respiration. This is accomplished by running a counteractive program and lowering expression of glucose transporter GLUT1 and GLUT4. On the other hand, pyruvate conversion to Acetyl-CoA is increased and made available for mitochondrial respiration while being excluded as substrate for lactate production by lactate dehydrogenase. Obviously, a loss in TP53 reverts this glycolysis limiting steps and increases lactate production.

1.1.2.10 Evading Immune Destruction

Immune surveillance not just targets exogenic pathogens but also incipient cancer cells.[11] Deficiency in immune surveillance, such as in immunocompromised patients due to HIV infection or after organ transplantation, increases the cancer incidence rates strikingly.[82] Moreover, tumor infiltration by cytotoxic T cells is a positive prognostic factor for overall survival in versatile solid tumors.[83-88] Thus, they may not only be enriched in this tissue by chemical cues but actually play an active role in confining and eradicating tumor cells.

This illustrates the necessity for an emerging cancer to evade recognition respectively destruction by immune cells. To further specify, both the innate immune system such as NK cells but also the adaptive immune cells such as T cells play a role in tumor eradication. This was supported by genetically engineered mice where a deficiency in one or the other facilitated the growth of tumors.[89-91] Moreover, tumor incidence could be further increased by a deficiency in both, T cells and NK cells demonstrating at least partial non-redundancy and different targets for the respective immune cell arms.

Condensing this data results in the paradigm of elimination-equilibrium-escape as three E's of tumor development.[92] During elimination phase, effector immune cells such as effector T cells are capable of recognizing tumor antigens and eradicating the transformed cells. During equilibrium phase, the effector immune cells are counterbalanced by suppressive mechanisms such as regulatory T cells allowing the tumor lesion to persist in a confined environment. The escape phase is the most pathological phase where immunosuppressive cues outcompete the activation cues and thus abrogate the eradication of tumor cells.

Advances in research broadened our knowledge and clearly point out the role of the immune system in counteracting tumor development as well as providing an outstanding and novel approach to treat cancer (see at **1.2.4 Immunotherapy**).

1.2 Cancer Treatment

1.2.1 Cancer Screening and Diagnostic

The more specific and earlier cancer is diagnosed, the better is the outcome for a patient.[93] Often, early-detected, local and not-metastasized cancers can easily be resected with a favourable prognosis while advanced disease still imposes a poor outlook. In addition, regular screened patients were less likely to develop cancer and diagnosed at an earlier stage than unscreened patients. [94] This demonstrates the importance of screening for diagnosis but also the preventive effect of screenings by promoting interactions with medical personnel.

Screening tests for cancer are [95]:

1. Physical Examination and History

- Anamnesis for drinking or smoking habits, familial medical history, etc.
- Are lumps palpable? cachexia? visual abnormalities? (melanoma [96] or during colonoscopy [97])

2. Laboratory Tests

- Differences in cell morphology (Pap Smear [98], skin biopsy [99])
- Changes in marker levels in blood or urine (PSA [100], CA125[101])

3. Imaging procedures

Lesions can be found by versatile methods [102, 103] such as

- Mammography
- X-rays
- computer tomography (CT) scan
- magnetic resonance imaging (MRI) scan
- positron emission tomography (PET) scan
- ultrasound

Abnormal lesions usually need to be confirmed by biopsies to ensure the diagnosis. Imaging also helps in staging and conclusively in treatment planning.

4. Genetic tests

- Screening for BRCA1 and BRCA2 mutations [104]
- Stool DNA test to screen for DNA alterations associated with colon cancer [105]
- TP53 mutations in tubal lavage for ovarian cancer screening [106-108]

Similar tests are also conducted throughout the course of disease to follow-up progression, therapy response or relapse.

While the set of screening and diagnostic tests is continuously expanding and improving, a lot of problems remain unresolved.[95] Screening results can be misleading, have side effects, be false-positive or false-negative and may not improve the person`s life expectance. In detail, defining the tumor marker`s cutoff level for a positive result is crucial. Unfortunately, deviations in protein levels may not be induced by a tumor but idiopathically and thus are the rule not the exception. As an example, versatile markers for ovarian cancer such as CA125, CA15.3, HE4 and CA72.4 were found to differ in respect of reproductive and lifestyle factors such as smoking.[101, 109] Non-pathological but common marker deviations thus impede a straightforward binary test result.

Another example for overdiagnosis and overtreatment can be illustrate by prostate cancer and PSA screening. [110, 111] While PSA screening may be beneficial to preserve the patient's life in cases of aggressive tumors, it may be detrimental in low-risk tumors which are unlikely to become life-threatening. Prostate cancer therapy such as radical prostatectomy or radiotherapy is associated with a variety of severe side effects such as urinary, sexual and bowel dysfunction.[112] In conclusion, overdiagnosis can initiate unnecessary treatments which drastically reduce the quality-of-live (QOL) without a significant clinical benefit.

In summary, the risk for false test results can either delay therapy initiation or impose a huge cut in life accompanied by anxiety and emotional reactions. Thus, a close follow-up and interaction with experienced medical personnel is essential for cancer diagnosis and patient outcome to carefully evaluate the test results and decide on the most beneficial clinical intervention.

Once the tumor is diagnosed, it will be staged in reference to its aggressiveness respectively local or distant spread. The most widely-spread staging system is the tumor, node, metastasis (TNM) staging system.[113] Each parameter is given a scaled number respectively code with higher numbers usually being less favourable. While T describes the local extend of the primary tumor such as size and adjacent tissue infiltration, the N describes the involvement and distance of the involved lymph nodes and M describes the presence and spreading of metastasis.

Consecutively to cancer diagnosis and staging, the patient and involved physicians can decide on curative or palliative actions and treatments to undergo.

1.2.2 Surgery

Resecting the neoplastic tissue with a defined safety margin seems as straightforward method of choice in locally confined lesions.[114, 115] On the other hand, extensive operations of deep-situated tumors such as Whipple operations for pancreas tumors can go along with extensive side effects and limit life expectance themselves.[116] Additionally, sometimes tumors and the healthy margin cannot be fully resected due to involvement of vital structures and thus impose a risk for remaining or relapsing disease.

While at an early stage surgery is often the only therapy, advanced disease commonly requires the combination with chemo- and radiotherapy. This is either done in an adjuvant setting by surgical tumor debulking prior to secondary therapy or a neoadjuvant setting where chemo- or radiotherapy is applied to reduce tumor mass prior to surgical resection.

An example where preventive surgeries can also help to reduce cancer risk is mastectomy and salpingo-oophorectomy in BRCA1/2 mutation carrier or abnormal skin lesions and colon polyps. Moreover, surgery can also be conducted in palliative cases where it is performed to relieve side effects by the tumor such as bleeding or restore skeletal functions.

Clinical outcome highly varies in dependence of tumor localization and patient characteristics while technological improvements such as endoscopy and the spreading of robot-assisted surgery helps to reduce side effects and improve the outcome

1.2.3 Chemotherapy

Chemotherapy describes a vast range of drugs which can be administered systemically via oral, intravenous or intraperitoneal administration but also topical by skin creams.[117, 118]

In contrast to surgery, systemic chemotherapy can also target cancer cells which may not be reached by surgery or radiotherapy due to tumor localization. Moreover, it can also target small cancer lesions which may not be detected by imaging such as tissue-infiltrating cells or distant metastasis.

This systemic off-site effects also describes the major disadvantage of chemotherapy and conclusively can cause severe side effects throughout the whole body. Due to the high metabolic and proliferative rate, cancer cells are most susceptible for substances interfering with mitosis, crosslinking DNA and preventing DNA untangling by topoisomerases. Unfortunately, healthy proliferative cells are also affected and displaying detrimental responses. This cellular response translates into versatile clinical side effects such as fatigue, hair loss, nausea and vomiting, mucosal inflammation, and changes in the blood count. Depending on severity, treatment discontinuation must be considered to limit side effects but also lowers tumor control.[119] Thus, the treatment response and side effects must be closely surveilled to allow treatment adaptation.

The most common types of chemotherapy used in clinics [120, 121] are:

1. DNA-interfering agents

- Platinum-based agents: Cisplatin/Carboplatin (crosslinking DNA)
- Anthracyclines: Doxorubicin/Daunorubicin (DNA intercalation)
- Mustard gas derivatives: Cyclophosphamide (DNA alkylation)

2. Microtubule-interfering agents

- Taxanes: Paclitaxel, Docetaxel (microtubule stabilisation)
- Vinca alkaloids: Vincristin/Vinorelbin (microtubule destabilisation)

3. Antimetabolites

- Folic acid antagonist: Methotrexate
- Pyrimidine antagonist: 5-Flourouracil, Capecitabine, Gemcitabine

4. Topoisomerase inhibitors

- Topoisomerase I inhibitor: Irinotecan, Topotecan
- Topoisomerase II inhibitor: Etoposide

5. Kinase inhibitors

- EGFR inhibitors: Cetuximab, Erlotinib
- VEGFR inhibitor: Bevacizumab

(see also **1.1.2.1 Sustaining Proliferative Signaling**)

Mustard gas derivatives are a man-made drug, while versatile other classes of chemotherapeutics such as vinca alkaloids, taxanes and anthracyclines derivate from plants or microorganisms. Adaptations in the chemical structure helped to generate prodrugs or improve the pharmacological profile with higher target specificity and less off-target effects.

Nevertheless, targeting a pristine cancer-specific proteins such as fusion protein BCR-ABL by Imatinib is often not possibly.[22] Therefore, advances in chemotherapeutics mainly focused on further improving the administration and targeting of cancer cells to reduce effects in healthy tissue. An example is the exploitation of leaky tumor vasculature by the enhanced permeability and retention (EPR) effect (as discussed in **1.1.2.5 Inducing Angiogenesis**). Nanoparticles such as liposomes are more likely to be trapped in this vasculature and thus impose a promising approach to increase drug concentration in the tumor and limit it systemically.[53-55, 122]

1.2.4 Immunotherapy

Due to importance and the ongoing development in clinical application, cancer-immune system interactions shall be further elaborated on, despite being broached above (**1.1.2.10 Evading Immune Destruction**).

More and more research data facilitates the development of novel therapies to exploit immune cells for therapy or prohibiting tumor cells from evading immune recognition and destruction.[92] To counteract and harness the immune system, understanding of the escape mechanisms is essential.

The most obvious mechanism to avoid immune recognition is by downregulation of antigen processing respectively presentation by downregulation of MHC-I, LMP2, LMP7, or tapasin to avoid T cell recognition. IFN signalling on the other hand may increase the antigen presentation and therefore may also be negatively regulated in tumor cells. Moreover, cancer cells can exhaust T cells by increasing their PD-L1 and B7-1/2 presentation to PD-1 and CTLA-4, respectively. As an example, overactivation of the proliferation-driving AKT pathway by PTEN deficiency could contribute to the immunosuppressive increase in PD-L1 expression.

Not just surface bound down or upregulations of tumor proteins but also secreted factors such as TGF-β, IL-8, IL-10, or VEGF dampen T cell function. Aggravatingly, these secreted factors also attract additional immunosuppressive cell populations such as T regulatory cells (Treg), myeloid-derived suppressor cells (MDSC) and tumor-associated macrophages (TAM). Another immunosuppressive trait can be derived from the high metabolic turnover rate of tumor cells which depletes the tumor environment from oxygen, glucose, amino acids and lowers the pH (see also **1.1.2.9 Reprogramming Energy Metabolism**) which as a result interferes with T cell function.

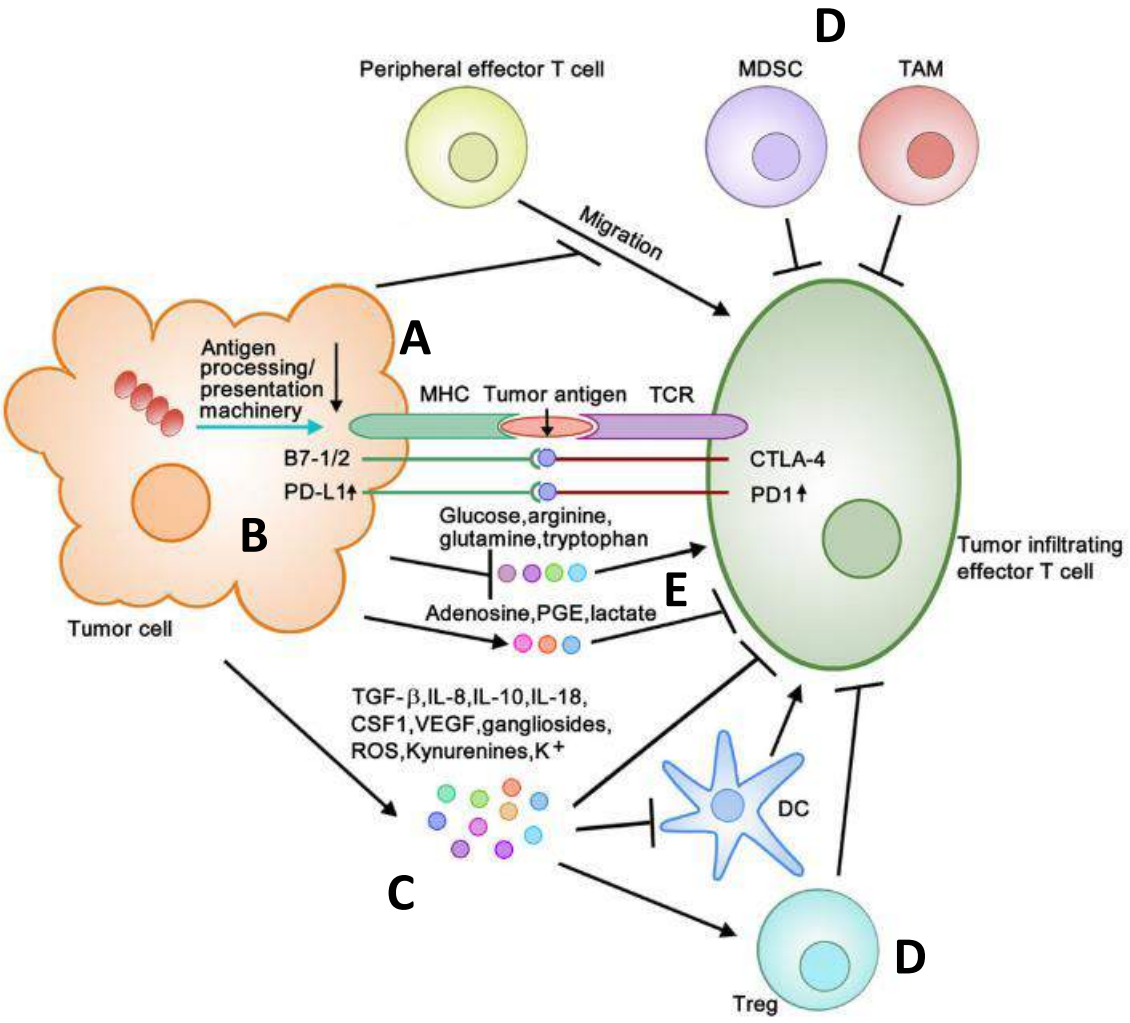

Figure 2 Overview of the tumor-immune cell Interface (modified from [92])
Tumor cells can counteract effector T cell activity by: A) reduced antigen processing/presentation, B) T cell exhaustion by B7-1/2 & PD-L1 upregulation, C) secretion of immunosuppressive factors such as TGF-β or IL-8, D) attraction of immunosuppressive cell populations such as Treg, MDSC, and TAM, and E) by generating an unfavourable metabolic environment

Immunotherapies are changing the paradigm in cancer therapy and brought hope for previously only palliatively treated cancer cases. Versatile approaches such as cancer vaccination, modified immune cells such as chimeric antigen receptor (CAR) T cells, and bispecific antibodies activating T cells are currently under investigation.[123] At the present time, the most widely applied immunotherapy in clinics is immune checkpoint blockade targeting CTLA-4 and PD-1 signalling to release the brakes of effector T cells and to facilitate a persisting activation. While low PD-L1 expression in antigen-presenting cells (APC) is linked to autoimmune disease systemic lupus erythematosus[124], it is commonly overexpressed in tumor cells suppressing T-cell activating pathways.[125] This illustrates that this mechanism is clearly essential in modulating self-tolerance but can obviously be hijacked by cancer cells and high PD-L1 levels conclusively linked to a bad prognosis.[88] The research and the

elucidation of these pathways was game changing and consequently awarded with the Nobel Prize in 2018. It moreover resulted in multiple clinically applied antibodies such as nivolumab (PD-1), pembrolizumab (PD-1), atezolizumab (PD-L1), avelumab (PD-L1), durvalumab (PD-L1) [126], and ipilimumab (CTLA-4)[127] which proved efficacy and are shifting to first-line in treatment schedule.[128-131]

In summary, immunotherapy is a hot topic in oncology since it opened up a fully unexplored field in cancer therapy with versatile treatment approaches and room for advancements. Nonetheless, some patients are experiencing cancer cure while others are non-responding. Elucidating the factors involved and predicting which patients are eligible for immune therapy is therefore considered to be as relevant as increasing, initiating or modulating the immune response. Broadening our knowledge will enable to choose the right off-shelf therapy respectively ease the generation of personalized medicine such as (due to brevity unexpounded) CAR T cells or cancer vaccines.

1.2.5 Radiotherapy

1.2.5.1 History of Radiotherapy

Radiotherapy emerged at the turn of the 20th century [132] and remains an essential therapy with approximately 50% of cancer patients requiring radiotherapy and increasing patient numbers worldwide.[133] While additional isotopes, types of radiation and treatment options were found and utilized without deep understanding, it was not until 1932 that measuring the radiation dose become possible by the first ionization chambers. The first cancer therapeutic approaches mainly consisted of local brachytherapy with radium and external X-ray beams from 50 to 200kV X-ray tubes for deep situated tumors. The tremendous developments in electric, electronics and computing drastically improved present day irradiation machines to become safer, more sophisticated in size and precision and more optimized in treatment planning. In addition to radioactive seeds and X-rays, also particle beams such as especially proton and carbon beams are currently becoming more powerful and convenient with center numbers increasing steadily.

The main principle of radiotherapy is killing tumor cells and halting their reproduction which is consistent throughout all application methods and radiation types.[132] The most investigated and detrimental effect of radiation is the damaging of DNA which is expected to result in mutations and chromosomal aberrations which lead to arrested cell cycles, apoptosis, necrosis, mitotic catastrophe and ideally cancer control.[134] What makes DNA especially vulnerable for radiation is the huge size of the molecule offering a vast number of potentially broken covalent bonds. Additionally, proteins and lipids also get damaged but in contrast to DNA can easily by compensated for by the vast number of copies and spare molecules. In DNA on the other hand, there is no spare “reserve” and even a single unrepaired or wrongly repaired lesion could result in point mutations, deletions, insertions and lost or rearranged chromosomal sections and turn out as lethal for the cell.

The following sections are intended to provide an overview of the physical principles, the present most common clinically applied forms of cancer radiotherapy and their respective basics, instrumentation and pros and cons.

1.2.5.2 Physical basics of radiotherapy

Depending on the transmitted energy, radiation can be ionizing or non-ionizing.[135] The ionizing potential for elements ranges from 3.9eV to 24.6eV for cesium and helium respectively and is 12.6eV for the ionization of water.[136] In dependence of type of radiation, ionizing radiation can be further divided in directly or indirectly ionizing radiation. While charged particles such as electrons, protons, alpha particles or heavy ions can directly interact with orbital electrons via Coulomb interactions, photons and neutrons are considered to ionize by a two-step process. Photons release electrons and neutrons release protons or heavier ions which then in turn can interact with orbital electrons in a similar manner as described.

1.2.5.3 Brachytherapy

Brachytherapy is one of the oldest applied radiotherapies [132] and describes the treatment of cancer by short distance application with radionuclide sources such as ^{60}Co, ^{137}Cs, ^{192}Ir, ^{125}I, and ^{103}Pd.[135] These sources are mostly applied to the tumor mass intracavitarily by taking advantage of adjacent body cavities for short term exposure or implanted interstitially into the tumor for long term exposure. Typical examples are cervix cancer therapy respectively permanent prostate implants. The benefit of brachytherapy is the localized delivery of photon, beta, or neutron emitting sources to the tumor mass while limiting healthy tissue exposure. This advantage also describes the major drawback since only small, localized and well defined tumors are eligible for brachytherapy.

1.2.5.4 External Beam - Photon therapy

Physics and Interactions of Photons

Photons are interacting with matter in versatile processes with some of them being eventually ionizing. These interactions include [135]:

1) Photoelectric effect

The photon interacts with a tightly bound orbital electron and disappears. The electron on the other hand is ejected from the atom as a photoelectron with the kinetic energy E_{kin} given as:

$$E_{kin} = h\nu - E_{binding}$$

E_{kin}	…	kinetic energy of the photo electron
h	…	Planck's constant
v	…	photon frequency
$E_{binding}$	…	binding energy of the ejected electron

2) Coherent (Rayleigh) scattering

The photon interacts with a bound orbital electron and gets scattered by a small angle but does not transfer respectively lose energy.

3) Compton effect (incoherent scattering)

The photon interacts with an orbital electron, ejects it but does not disappear. The photon energy must be much larger than the binding energy, hence this effect is most prominent with loosely bound electrons and high-energy photons. As a result, the incident photon energy is shared between the kinetic energy of the ejected electron and the scattered photon with an accordingly lower wavelength/energy. The distribution of energy between photon and electron depends on the scattering angle of the photon and is highest for backscattered photons.

4) Pair production

The photon disappears within the nuclear Coulomb field with an electron-positron pair being produced. The combined kinetic energy is the incident photon energy minus the energy required to produce the mass of an electron and a positron.

$$E_{kin,comb} = h\nu - 2 * m_e c^2$$

$E_{kin,comb}$	…	combined kinetic energy of positron and electron
h	…	Planck's constant
v	…	photon frequency
m_e	…	mass of an electron
c	…	speed of light

Pair production is limited to photon energies above 1.02MeV which is consumed for producing the electron and positron ($2 * m_e c^2$). If pair production occurs in the field of an orbital electron, these 3 particles share the kinetic energy.

5) Photonuclear reactions

High energy photons can be absorbed by the nucleus and result in the emission of a proton or neutron and the transmutation of the atom. This reaction requires MeV photon energies and is less relevant for treatment but for safety and shielding considerations. Produced neutrons and radioactivity impose a health risk and must be dealt with by improved shielding and improved room ventilation

These discussed photon-matter interactions and their probability strongly depend on the photon energy and the atomic number of the irradiated matter and the respective probability can be seen in the following graph (see **Figure 3**)

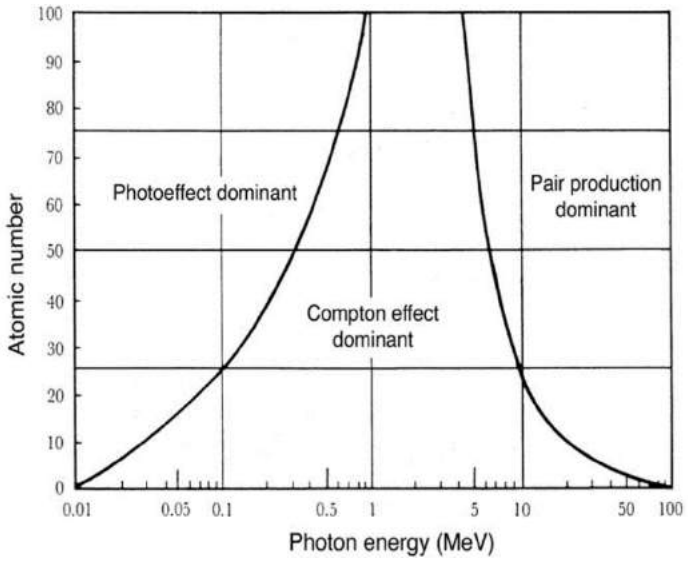

Figure 3 Probability of photon interactions in dependence of the atomic number of the target atom and the energy of the incident photon [135]

Direct ionizing effects in biomolecules only account for a small fraction of induced damage which is superimposed by the indirect effect via the generation of versatile reactive species from water molecules due to the vast excess of water molecules.[137] The radiolysis and ionization of water generates free electrons, reactive species with unpaired electrons and free radicals as well as recombination products such as hydrogen peroxide. This conversion of photon energy to chemical carriers then allows reactive species to diffuse and react with biomolecules in close proximity. A special focus must be drawn to the generation of hydrogen peroxide and hydroxyl radicals which is enhanced in dependence of elevated oxygen concentration within the solution. This demonstrates the importance of oxygenation for photon radiotherapy to increase the yield of reactive species and thus biological effect and is a key consideration for fractionation schemes (see also **1.3.3 Reoxygenation**)

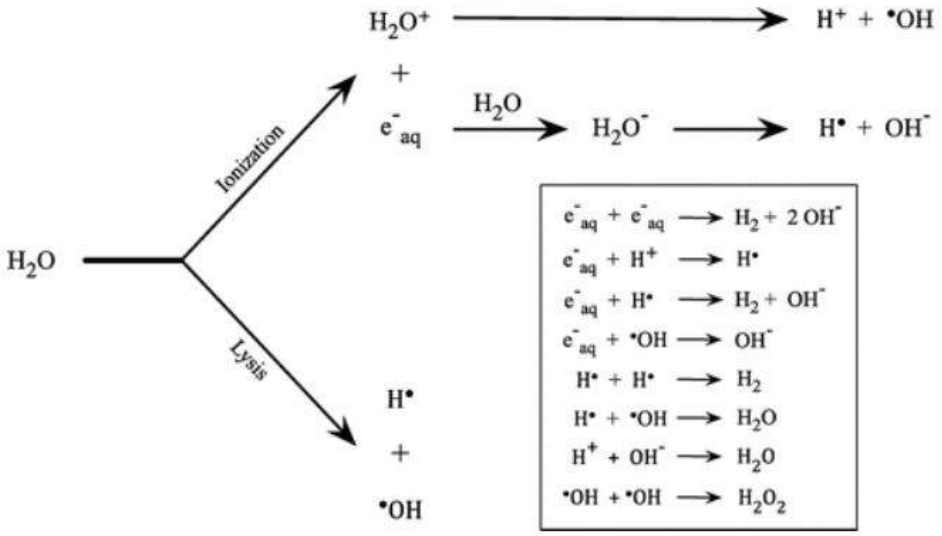

Figure 4 Radiolysis and ionization of water and accompanying reactions [137]

Clinical application, generation and instrumentation

External beam therapy utilizes high-energy photons from nuclear reactions (gamma rays) or electrons interacting with a target (X-rays). Radioactive ^{60}Co emits clearly defined photons with 1.17MeV and 1.33MeV but source intensity declines by time due to the radioactive decay.

The energy of X-rays on the other hand can be more easily adjusted. Electrons are ejected from a heated filament in an evacuated tube and accelerated towards an anodic target. The voltage difference between filament cathode and anode describes the acceleration of the electrons and can easily be adjusted. These accelerated electrons are aimed at a metallic target where they decelerate and interact with matter. Unfortunately, most of the electrons`

kinetic energy is transformed to heat requiring target cooling and only a small fraction converted to X-ray photons.

These incident electrons can interact with orbital electrons and eject them from their shell position. The filling of the vacancy by a higher level shell electron requires the filling electron to lose energy. This energy difference is emitted as photon and a characteristic for the target material.

Bremsstrahlung on the other hand, results from interactions of the incident electrons with nuclei. Kinetic energy of the electron is emitted as photons during deceleration in the target material. Bremsstrahlung is thus material independent and provides photons in a range of zero up to the kinetic energy of the incident electron.

Conclusively, the line spectrum of X-rays consists of target material specific peaks and a continuous broad bremsstrahlung spectra. The low energy photons in the splash of Bremsstrahlung are less penetrant and would cause undesirable dose deposit at the surface. Therefore, these low-energy photons are filtered out by thin layers of metal (such as 1mm Al or 0.3mm Cu) and excluded from the spectrum before the X-rays leave the beam generator.

In addition to different filter set-ups, also the electron acceleration changes the spectrum. The faster the accelerated electrons are, the less pronounced are the characteristic photons in the total spectrum. Additionally, the average direction of photons emitted shifts from a 90° angle at low energies (10-150kV) to a forward direction at megavoltage energies (1-50MV) and thus also influence the construction of the X-ray source. Moreover, also the electron current and thus X-ray intensity can be increased by increasing the temperature of the filament.

In previous times, the shape profile of the photon beam could be customized and personalized by often handmade metallic collimators absorbing the unwanted beam fraction.[138] This modulation is obviously limited to only a single angle of beam delivery despite tumor size being expected to change throughout treatment. A more advanced method are so called multi-leaf collimators where absorbing wedges can be moved in and out of the beam path to shape the beam profile. This also enabled more complex multi-angle treatment plans by rotating gantries where the beam shape must be modulated during irradiation. In addition to collimator improvements, also the photon sources improved drastically. Modern linear accelerators (LINAC) enable much higher electron velocities and thus photon energies which broadened the spectrum of available X-rays. Condensing all capabilities of modulating photon beams, resulted in the so called Intensity Modulated radiotherapy (IMRT) as present state-of-the-art in photon radiotherapy. For IMRT, not just the beam shape but also the intensity is modulated throughout an irradiation session. [139] Obviously, this advance in dose delivery also benefits from advances in imaging and sophisticated computer simulations and planning programs to optimize dose distribution and demonstrates the multidisciplinarity of radiotherapy

In summary, X-ray radiation can be adjusted more easily and is more versatile than gamma ray sources but requires more complex instrumentation and control units. Conclusively, external gamma radiation lost market shares in developed countries by the emergence of safer and non-radioactive linear accelerator technology.

1.2.5.5 External Beam - Proton therapy

Proton beam therapy was first proposed in 1946 but remained a niche treatment until present time.[140] Despite the recent opening of multiple proton therapy centers, the number of patients being treated conventionally remains more than 100-fold higher.[139]

Proton therapy is generally more complex, more expensive and more difficult to establish compared to standard X-rays. Also the meter-thick concrete shielding, the beam dump and beam lines require space which is usually not available in historically-grown hospitals or adjacent city areas and conclusively prevents the integration of proton radiotherapy in existing facilities. As a result, most proton radiotherapy centers are located at separated locations with national but commonly also international patients being referred to. Nevertheless, current advancements in accelerator technology, a higher general interest in this technology and the growing market will reduce price, complexity, as well as required space with a so called “one-room solution” by a single provider as the final goal.[138]

Differences in Photon and Proton Physics

A spatially different dose distribution profile compared to photon beams make proton and other particles beams superior in reducing radiation damage to healthy tissue . [141-143]

Photon beams have a lower entrance dose deposition within the first millimeters until the splash of ejected electrons is established and sums up with the inciding photons to the highest dose deposition within 2-3cm. Afterwards, the dose deposition is steadily declining due to absorbed photons but extends throughout the beam path. This obviously represents the deposition of considerable amounts of dose to superficial tissues such as skin but also behind the treated tumor mass. Moreover, a deep-situated tumor is expected to receive less dose than the entry tissue and therefore multiple angle beams must be combined to build up the dose in the target and dilute the dose to healthy tissue by increasing the co-irradiated volume.

Protons on the other hand are following a nearly ballistic trajectory and pass through the tissue. The protons interact with matter, deposit their energy and decelerate. The slower the protons get, the more energy can be deposited per atom passed respectively distance travelled until they are ultimately stopped. The term describing this is the linear energy transfer (LET) which increases drastically towards the end of the trajectory and peaks in the

so called Bragg Peak where the highest dose deposition and LET is found, followed by a steep decline. The region of highest dose deposition can therefore be calculated and designed to be in the tumor by accelerating the protons to the required velocity. By overlaying multiple of these pristine Bragg peaks, a so called spread-out Bragg peak (SOBP) is generated which homogeneously covers the defined depth range with ionizing radiation. The deposited dose is highest in the tumor and lower in the entry tissue and conclusively reduces the need for multi-angle approaches. In addition, healthy tissue beyond the Bragg peak can be consequently spared since the protons are stopped in their trajectory.

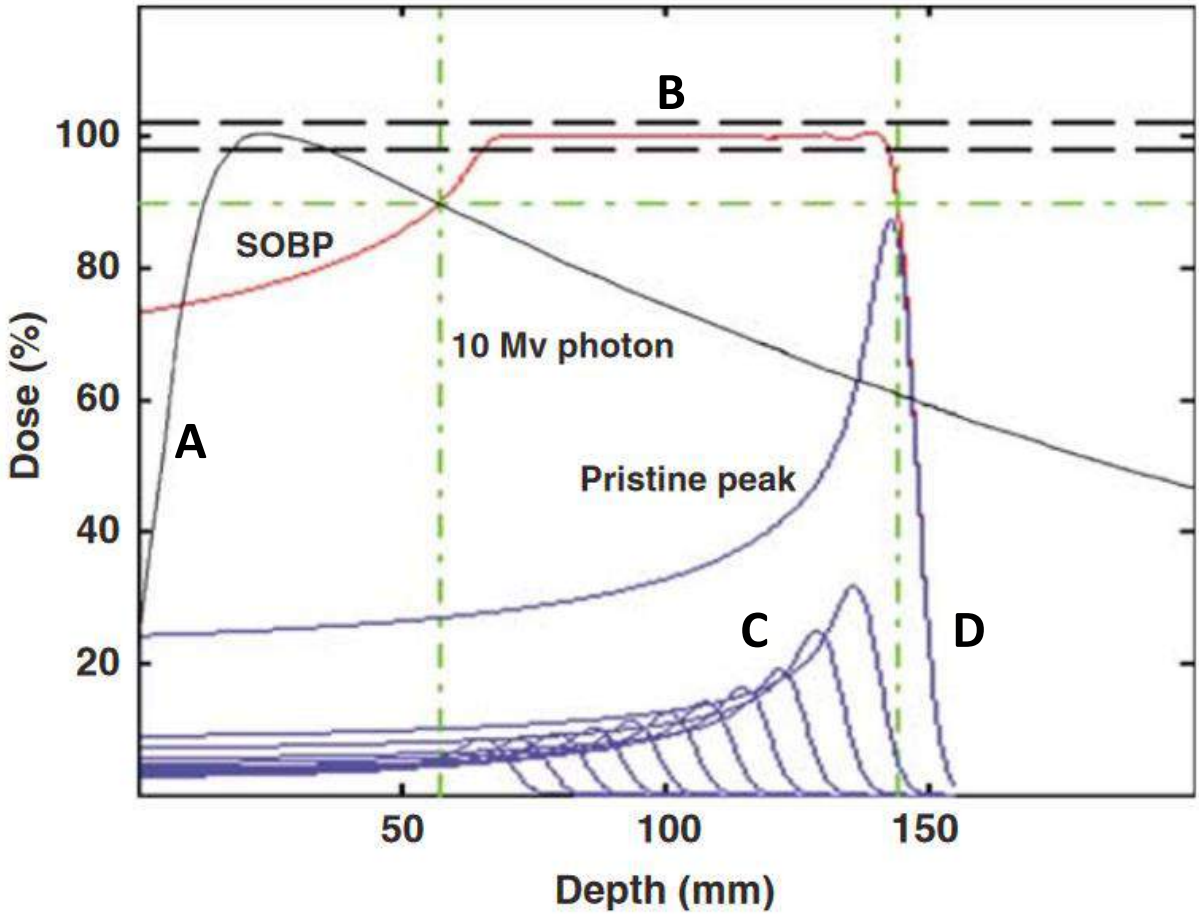

Figure 5 Dose-deposition profile of 10MV photons, pristine and SOBP protons (modified from [141])

A 10MV photon beam (A, black line) is described by a build-up in dose deposition at the entry side followed by a steady decline in dose deposition. A SOBP proton profile (B, red line) consists of multiple pristine proton beams (C, blue lines) which results in the consistent coverage of the tumor volume while depositing no dose beyond the SOBP (D)

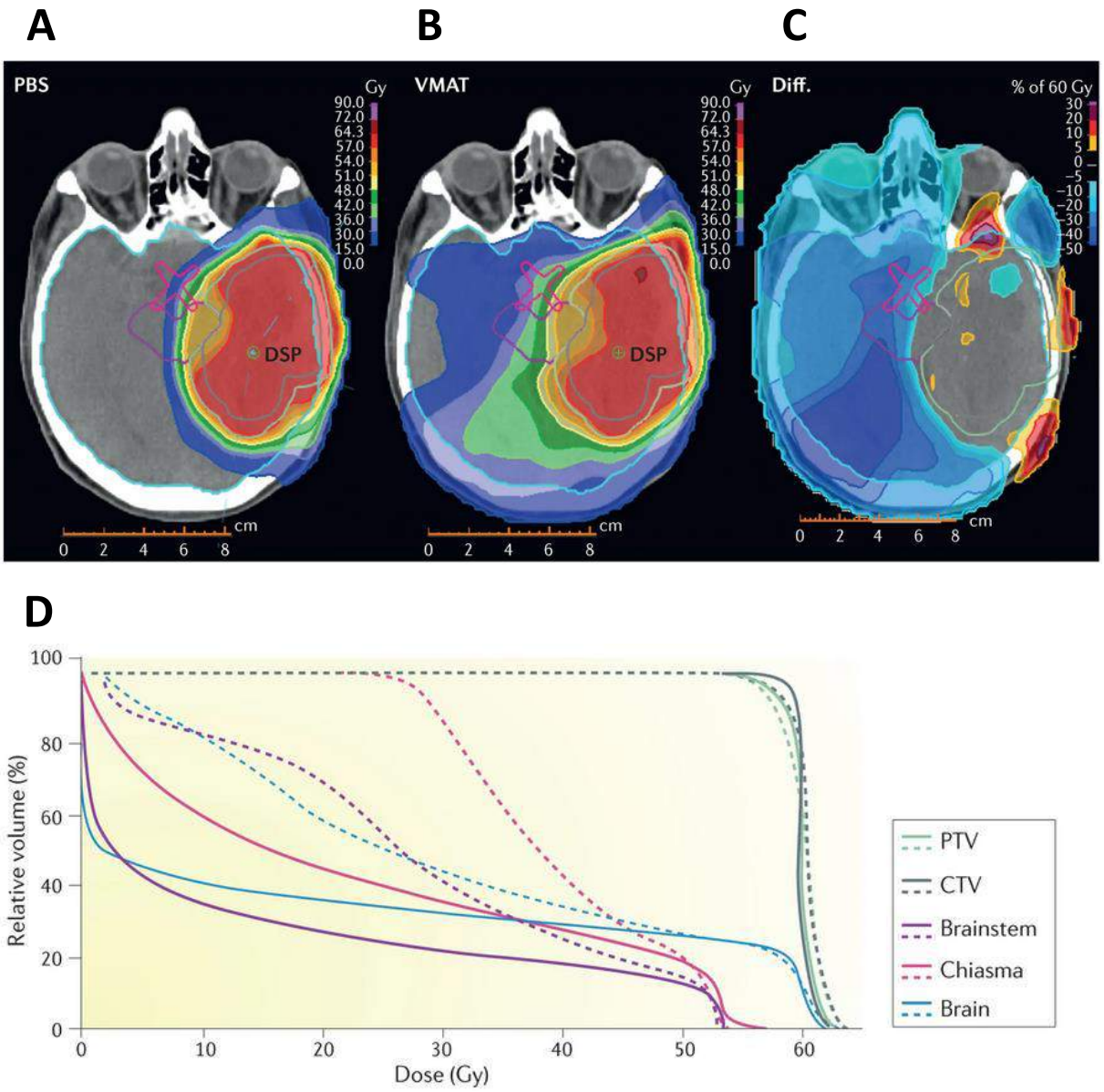

Figure 6 Comparing Photon versus. Proton treatment plans (modified from [144])
Pencil beam scanning (A) clearly demonstrates a lower coverage of healthy tissue in a high-grade glioma patient than the photon beam plan (B). The difference (C) is concisely illustrated by a decreased dose (in blue) in most of the healthy tissue and only marginally increased dose depositions (in red) adjacent to the tumor volume. The dose volume histogram (D) shows the proportional dose deposited by the photon (dashed line) or proton treatment plan (solid line). A similar coverage of planning and clinical target volume (PTV and CTV) is achieved but more healthy tissue is receiving higher doses in the photon treatment plan.

Clinical application, generation and instrumentation

To generate and deliver protons, a complex system consisting of linear accelerator tubes, cyclic accelerators such as synchrotrons and cyclotrons or mixed types as well as magnetic-focusing and beam lines is requires.

In general, hydrogen atoms will be stripped for their electrons by thin foils and first linearly accelerated before being sourced into a cyclic accelerator. Cyclotrons work in a continuous manner, accelerating protons to a fixed velocity which can be reduced subsequently by a range shifter slowing protons down to the desired velocity.[138] The proton velocity can be more easily modulated in synchrotrons which accelerate a batch of protons to the desired velocity at once but work discontinuously. The ejected proton beam is guided by magnetic lenses through a pipe system where further controlling of beam characteristics such as beam current or beam profile is conducted. While only one room can be served at a time, multiple treatment rooms are connected to one beam line to switch between rooms where patients are aligned and prepared for radiotherapy. This helps to avoid unused downtimes of the accelerator during patient set up and alignment. Investment in additional treatment rooms is therefore essential to utilize most of the available beam time and exploit this usually limiting factor of proton therapy.

Once the protons leave the pipe system, the beam must be shaped to cover the target volume. The earlier, less complex and still applied method for eye tumors is passive scattering. The two-dimensional beam shape is ensured by copper collimators and the beam axis depth profile by a compensator which protons permeate but are slowed down in a controlled manner. For in-treatment Bragg peak shifting, a prementioned range shifter/modulator is inserted into the beam. This allows to supply a Spread-out Bragg peak (SOBP) into the tumor without complex planning or magnetic beam modulation but handcrafted collimators and compensators.

The more advanced and also for this project utilized method is pencil beam scanning (PBS) respectively spot scanning. Based on imaging, the tumor is dissected in layers and a treatment software defines single spots for each layer. The protons are directed to a spot by magnetic steering in the nozzle and so a defined dose applied before targeting the next spot. This process is repeated throughout the respective layer until all spots are scanned. By adjusting the velocity of ejected protons from the accelerator, the depth and thus the target layer in the tissue is shifted and again all calculated spots scanned. This enables to variate the number of spots in each layer and the location as well as the dose of each individual spot and is thus more conformal than passive scattering and handmade collimators.

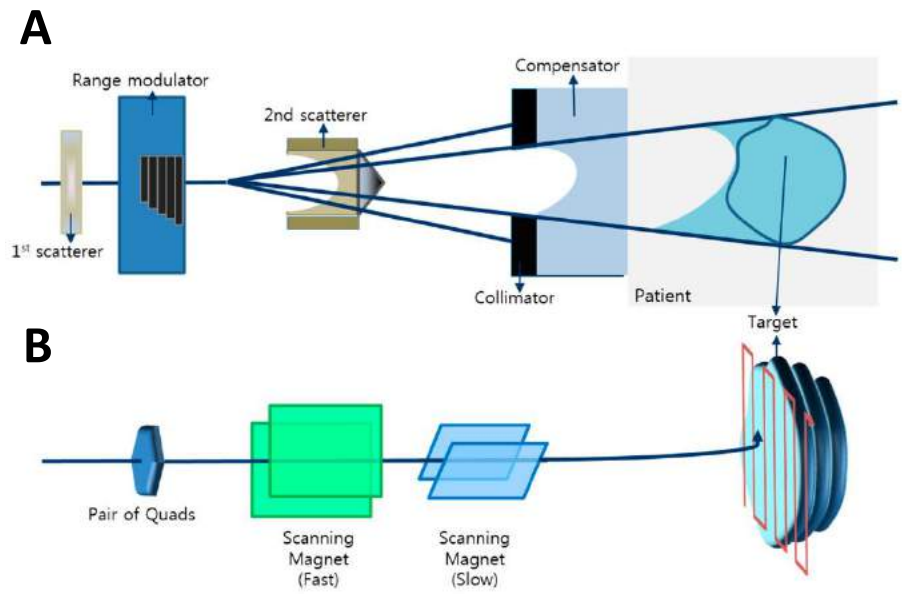

Figure 7 Proton beam delivery by passive scattering (A) and pencil beam scanning (B) (modified from [145])

For passive scattering (A), the focussed proton beam is scattered and shape and depth profile modulated by collimator and compensator, respectively. Pencil beam scanning (B) is achieved by steering the proton beam using magnets to pursue a programmed track. Numerous spots of proton splashes are administered along this track to homogeneously fill up the volume with dose. Both methods work by superimposing layers to generate a SOBP which is achieved by either inserting plates to reduce proton velocity or by a lower proton velocity supplied from the accelerator.

1.2.5.6 Differences Photon versus Proton radiotherapy

Despite the obvious physical differences between photon and proton radiotherapy, also the biological and cellular response differs.[146-149] Present treatment plans and estimations mostly utilize a generic relative biological effectiveness (RBE) of 1.1 as factor for dose calculations to account for a higher efficacy of protons compared to photons.

This value was determined by extensive testing but probably generalizes and covers up its variable nature. The RBE increases along the SOBP which clearly implies a different nature and response to low LET photons or fast entering protons in contrast to high LET, decelerating, and stopping protons. The LET of carbon ions is even higher than for protons and so is the RBE of carbon ions.[150] Conclusively, once establishing a different biological response in dependence of irradiation species or a LET dependence, there is room to exploit it due to the widely fluctuating patient backgrounds and tumor. Shifting the paradigm to a biologically variable RBE also opens the door towards combinatorial approaches to target cellular pathways and redundancies and modulate the treatment response actively.

Another relevant consideration in radiotherapy is the exact definition of the tumor volume and the exact patient positioning before treatment.[144] Photon treatment plans deposit

higher doses into adjacent healthy tissue which can be avoided by proton beams and is therefore commonly more confined. As a result, exfiltrated tumor cells and adjacent tumor colonies which are not visualized by imaging are not planned into the treatment volume and probably not irradiated by a confined treatment plan. On the other hand, less confined photon treatment plans probably still deposit substantial doses of “unintended” radiation into these regions.

Defining the precise tumor depth is also more relevant for finite proton beam paths than for less depth-restricted photon beams. Proton beams are prone to tissue movements in the beam axis and both overshooting into the healthy tissue as well as underdosing the distal tumor section a relevant issue. A way to increase robustness in pencil beam scanning is by reirradiation. The full tumor volume is scanned as stated in the steering file but the prescribed dose is split up and only a fraction applied. This allows to run multiple scanning rounds and reduces the risk that a piece of tissue is always out of the beam path and remains unirradiated. Versatile other ways of reducing tumor motion or increasing targeting robustness are breath holding and breath restriction by fixtures as well as live imaging of the patient and computer-processed counteractions by the patient bed to keep the tumor in the treatment field.

More extensive and detailed reviews dealing with the differences of photon and proton irradiation, how to probably exploit differences in DNA repair dependency and future concepts can be found in **3.2 Combined Treatment Modalities for High-Energy Proton Irradiation: Exploiting Specific DNA Repair Dependencies** [142] and **3.3 The Relative Biological Effectiveness of Proton Irradiation in Dependence of DNA Damage Repair**.[143]

1.3 The 5 R`s of Radiotherapy

1.3.1. Radiosensitivity

Cells and tissue are described by a cell intrinsic sensitivity to radiation.[134] The extremes range from radiation resistant tissues and tumors such as brain tissue and sarcomas to more radiation sensitive tissues such as the haematopoietic system or the oral mucosa. This can be seen by versatile factors such as cell cycle state when being irradiated but also on a cellular signalling level. In general, normal cells with intermediate DNA damage can activate cell cycle arrest, slow down proliferation by proteins such as TP53 and conclusively buy sufficient time for correctly repairing the lesions. On the other hand, tumor cells are in general more dysfunctional and checkpoints and growth repressors incapacitated which results in shorter repair periods and a higher probability of prematurely proceeding in cell cycle and running into mitotic catastrophe. Healthy cells on the other hand are in general more presumable to undergo apoptosis or senescence which is less probable in tumor cells where these pro- and anti-apoptotic pathways are commonly dysregulated.

This said, it becomes obvious that tissues and tumors provide different radiation sensitivities already upfront treatment start.

1.3.2 Redistribution

Radiosensitivity is a function of cell cycle state. The sensitivity to DNA damage increases from late S phase > early S phase > G1 and early G2 > late G2/M phase. Cells during S phase have the option to undergo error-free homologous recombination repair with DNA repair proteins available and DNA accessible. Late G2/M phase cells on the other hand, have double the DNA and thus error-sides while already having passed cell cycle checkpoints. Cells in early G2 may have double DNA and thus double damage sides than G1 cells, but can still utilize HRR.

The significance of this differential sensitivity is that mitotic cells are more likely to be cleared off by radiotherapy while latent G1 or S phase cells may persist. By repetitive irradiations, these cells are probable to undergo redistribution and thus may become more radioresistant at the next treatment session. This effect of redistribution is probably more extensive in tumor cells with deregulated cell cycle checkpoints while healthy cells are more capable of arresting and persisting in less sensitive cell cycle states. Therefore, time between fractions becomes relevant but efforts to time it in respect of the tumor treated is made obsolete by the tumor heterogeneity and different growth kinetics.

1.3.3 Reoxygenation

The efficacy of radiotherapy in dependence of oxygen can be clearly seen when comparing X-ray-irradiated oxic and hypoxic cells.[134] The sensitization by oxygen follows a sigmoidal response curve with the largest increase between 0.5 to 20mmHg and typical oxygen concentrations in venous and arterial blood ranging from 40 to 100mmHg. In conclusion, most normal tissue is considered well oxygenated while primitive vasculature in the high metabolic tumor mass results in oxygen-deprived regions.

While the oxygenated tumor cells are expected to be killed by a considerable single dose, tumor cells from the hypoxic region may persist and survive. What follows is a process termed reoxygenation which describes the oxygenation of previously hypoxic regions due to less or no oxygen consumption in damaged cells respectively dead cells and increased oxygen diffusion distances. As a result, repetitive irradiation enables the killing of previously hypoxic but now reoxygenized cells in each treatment session. However, hypoxia is not a homogenous and predictable trait and differs between tumor entities, between patients and even within regions of a single tumor mass. Therefore imaging hypoxia and predicting treatment response is a huge challenge in todays practice

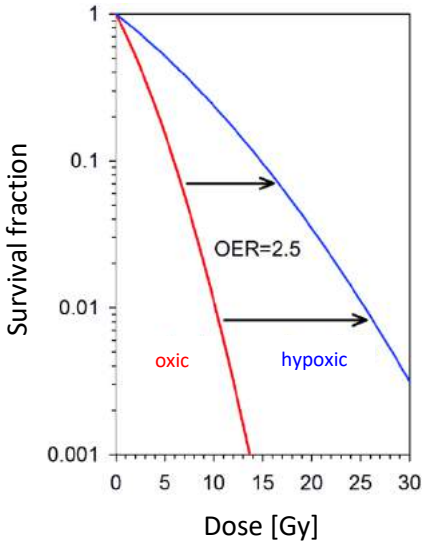

Figure 8 Radiosensitizing effect of oxygen (modified from [151])
The radiosensitizing effect of oxygen is described by the oxygen enhancement ratio (OER) which is about 2.5. This implies that hypoxic cells can be considered as more radioresistant than oxygenated cells.

Interestingly, the dependence on oxygenation status is decreasing for higher LET radiation such as provided by proton and carbon beams.[152-154] Nevertheless, adjusting the LET by LET painting and accounting for hypoxic regions is unfeasible by prementioned flaws in hypoxia imaging and tumor heterogeneity.

1.3.4 Repopulation

Radiation does not differ between transformed and normal cells and thus also harm the healthy tissue.[134] To counteract the loss in cell number, inhabiting stem cells can initiate a number of processes. Tissue-homed stem cells can adapt within a week of lag time until increasing their proliferation to allow replacement of destroyed and damaged cells. Stem cells can also switch from asymmetric to symmetric divisions to regain the required stem cell pool. Moreover, even doomed stem cells that lost their infinite replication potential may be able to give rise to a finite number of offspring in so called abortive divisions as a short-term relieve for tissue homeostasis. These processes are termed repopulation and describe the mechanism in which healthy tissue can resist and adapt to radiation and endure higher total doses in a fractionated scheme than a single treatment. Unfortunately, tumor cells can also adapt to radiation by accelerated repopulation so the decision of fractionation scheme to protect normal tissue while maximizing damage to tumor cells must be considered thoroughly.

1.3.5 Repair

Versatile cellular processes can mediate the outcome of radiotherapy. An essential task is the repair of induced DNA lesions by DNA repair processes.[134] As mentioned above (see at **1.1.2.7 Genome Instability and Mutation**), DNA repair is commonly abrogated in tumors. DNA repair deficiency can even be the tumorigenic factor for example in BRCA1/2 mutation carriers where homologous recombination repair (HRR) is abrogated. Obviously, these repair-deficient tumors will be more challenged by DNA lesions and misrepaired or missed out lesions become more probable than fully functional healthy cells. These tumor specific repair deficiencies are utilized in oncology by inhibiting repair redundancies for example by PARP inhibitors such as Olaparib in prementioned HRR-deficient BRCA1/2 carriers.[155]

Due to the importance and rational of DNA repair for this project, I would like to further elaborate on this topic and provide more details. The most commonly induced lesions by radiotherapy are DNA base damage, abasic sites, and DNA single strand breaks while DNA double-strand breaks and complex DNA damage consisting of multiple lesions within close proximity only accounts for a minor fraction. The following table provides an overview of DNA lesions induced by radiation and the associated repair pathways.

Table 2 Overview of DNA lesions induced by ionizing irradiation (modified from [156])

Lesion	No./Gy/cell	Repair machinery	Sensing/signalling proteins
Base damage	**1000**	Base-excision repair (BER)	DNA glycosylases [157]
Single-strand break (SSB)	**500-1000**	Single-strand break repair (SSBR)	PARP1 [158]
Double-strand breaks (DSB)	**~40**	A) Non-homologous end joining (NHEJ, all cell cycle phases) B) Homologous recombination repair (HRR, S & G2 phase)	1) MRN→ATM→γH2AX 2) Ku→DNA-PK_{cs}→γH2AX 3) ATR→γH2AX [134]

Despite their lower occurrence, DNA DSBs are considered as most lethal and most detrimental lesion. Therefore, BER and SSBR which are relevant for repair of ionizing-radiation-induced DNA lesions are not further elaborated on as well as mismatch repair (MMR) and nucleotide excision repair (NER). Conclusively, I want to draw your attention to non-homologous end-joining (NHEJ) and homologous recombination repair (HRR) which are the two main repair pathways of DSBs and are therefore more extensively discussed in the following paragraphs.

1.3.5.1 NHEJ

NHEJ is a relatively fast and straightforward process and accounts for the majority of repaired DNA DSBs.[159] NHEJ is not limited to a specific cell phase and is initiated by the binding of a Ku70/80 heterodimer to both free ends.[160] The high abundance of Ku with about 400.000 molecules per cell accounts for it as being considered the first protein binding and stabilizing the broken DNA ends. The Ku heterodimer can be further considered as tool belt for the recruitment of DNA-PK_{cs} and other processing enzymes. Trimming can be required and accomplished by nucleases such as Artemis or gaps filled by DNA polymerases (Polμ or Polλ). A complex of LIG4, XRCC4, and XLF then finalizes the repair by ligating the ends. Terminal microhomologies can simplify processing during NHEJ and already a 4-nucleotide overhang is sufficient for religation by only the XRCC4/LIG4 complex.

End processing by nucleases and polymerases imposes a risk for the introduction of errors respectively a recombination of different ends than intended. The risk of chromosomal rearrangements or mutations must therefore be considered but is overweight by the benefit of a fast repair.

1.3.5.2 HRR

HRR requires more processing in comparison to NHEJ and is limited to S and G2 phase where sister chromatids are present.[159] Whereas HRR can result in loss of heterozygosity, it is less prone to errors since a template is used for end processing and strand replication. HRR is irreversibly initiated by the exonucleolytic 5'-3' resection of the DNA ends and facilitated by the MRN complex and CtIP. The generated single-stranded overhang is initially coated with RPA which gets replaced by RAD51 by the action of BRCA2. The nucleoprotein filament is then capable of invading the sister chromatid and searching for sequence homologies. Once the strands are aligned, the undamaged strand is utilized as a template for strand extension beyond the previous DSB site. This restores any lost sequence before the complex DNA structure involving two Holliday junctions is resolved by different complexes involving proteins such as BLM, GEN1, MUS81, or SLX4.[161, 162]

Despite the benefit of theoretical error-free repair, a tight regulation of HRR is essential since end resection in not yet copied DNA regions during S phase and uncontrolled end resection itself could cause massive DNA fragmentation.[163]

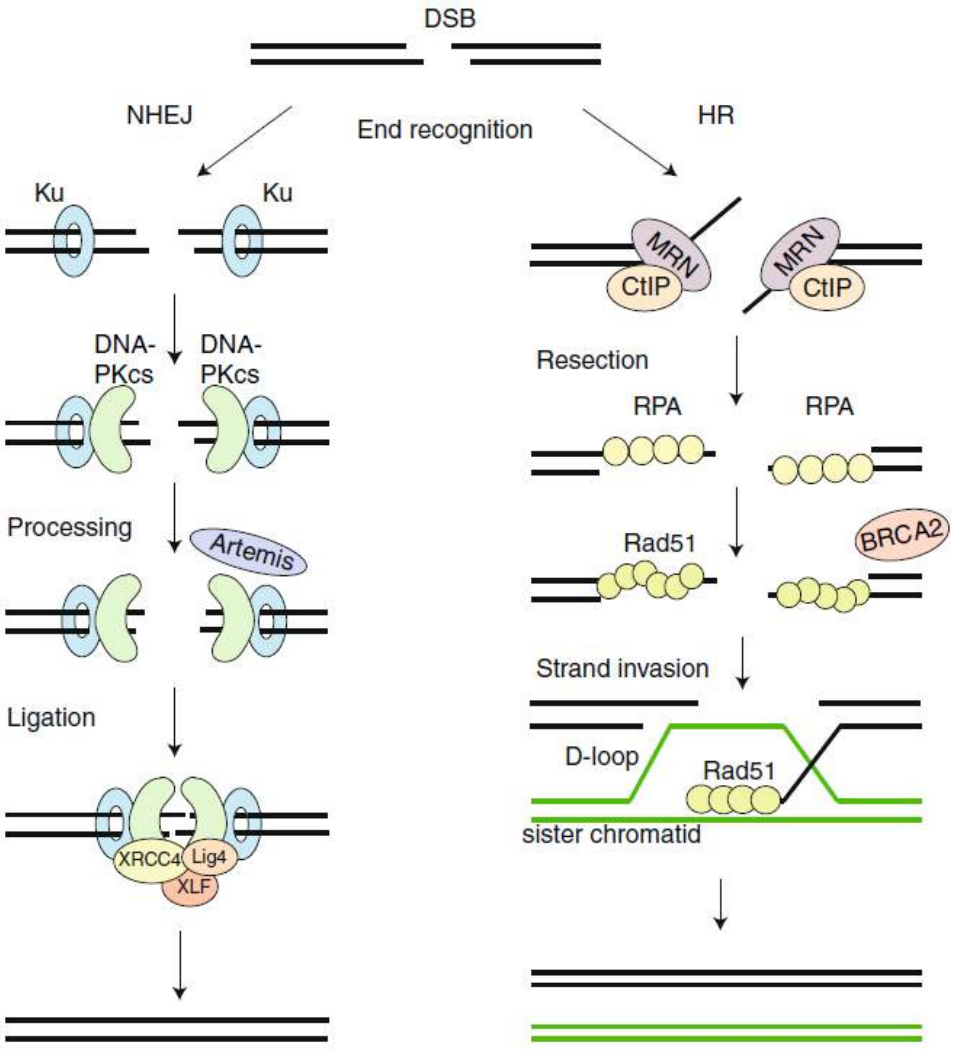

Figure 9 Schematic overview of NHEJ and HRR (modified from [159])

1.3.5.3 Pathway choices during DNA DSB repair

The main cues for pathway choice is by cell cycle and can be illustrated by CtIP. End resection requires CtIP phosphorylation which is achieved by S/G2-specific cyclin-dependent kinases (CDKs). Moreover, CtIP is proteasomally degraded during G1 phase and end resection therefore prevented. Also NBS1, part of the MRN complex, is phosphorylated by CDK1 during S, G2 and M phase adding another layer of regulation. Moreover, structural proteins such as cohesion, condensin and SMC5/6 are utilized to confine HRR to already replicated stretches of DNA.

The fluctuations of DSB repair choice become self-evident at the example of 53BP1 and BRCA1.[164, 165] 53BP1, a protein associated with foci of DNA repair, prevents DNA end resection, therefore promotes NHEJ and is counteracted by BRCA1. Mutations in BRCA1 occurring spontaneously or inherited, thus limit DSB repair to NHEJ. This can be exploited by inhibition of PARP1 which is essential in marking single-strand breaks which therefore remain unrecognized. When an unrepaired SSB is channeled into a replication fork during S phase, it generates the complex situation of a dsDNA with a SSB and another strand with a

free double-stranded end triggering DNA DSB repair. Realignment with the corresponding homologous site and restarting the fork requires a functional HRR machinery and cannot satisfyingly be replaced by NHEJ. This repair deficiency underlies the sensitivity of HRR-deficient cells for PARP1 inhibitors such as Olaparib.[155] To close the circle, a secondary mutation disabling 53BP1 in these cancer cells relieves the breaks on end resection and restores HRR capacity. 53BP1 mutation is therefore a considerable mechanism for chemoresistance in BRCA1-deficient cancer cells by shifting the DSB repair pathway choice.

Obviously, versatile other repair processes, examples and repair proteins would be worth nodding but would go beyond the scope of this thesis.

1.4 Difficulties of cancer therapy and overcoming approaches

1.4.1 What is the tumor?

Cancer describes not a single pathogen causing a specific symptom but describes the uncontrolled growth of patient-originating cells. As versatile as the patients are the tumors emerging and even within a single tumor mass, a huge variability of cancer cells is evident. The breathtaking advances in Next-Generation Sequencing (NGS) and computational power of systems biology provide the scientific community with new insights on tumor heterogeneity.[166, 167] Previously, oncologists were able to determine the originating tissue, the histologic morphology and maybe a handful of tumor mutations or driving events. Today, cancer biologists got the tools to define subsets of subsets of cancer cells, to simulate evolution within a tumor and sometimes even predict upcoming therapy resistances.

This already points out to the essential problem of cancer therapy. In most cases, not a single clone of similar cells is being treated but an army of cells harnessed with more or less resistance mechanisms, being nutrient-deprived or highly metabolic, undergoing fast cell cycle alternations or being dormant for month. The harsh and hostile environment for cancer cells results in selection pressure where evolution steps in and diverse clones then outcompete others for faster growth or less immunogenicity. Aggravatingly, it is commonly not the primary tumor being lethal but the aggressive offspring and metastasis interfering with the delicate balance of life. What must also be considered is that administering anti-tumor therapy may reduce tumor mass but could also raise the selection pressure and promote the emergency of more aggressive clones.

Exploiting the more adaptable immune cells by cancer immunotherapy added a novel tool but also proton radiotherapy may provide clinicians with a new flavor of therapy. The slightly different response to protons than compared with conventional photons could become important in certain tumor cases or when combined with certain therapies.

It is therefore evident that further research is required to elucidate the features and clonal origins of cells, to understand what therapy is most helpful for a specific tumor and what combinations should be administered to block resistances beforehand and stay ahead of tumor evolution.

1.4.2 Normal tissue toxicity

Next to understanding the tumor, it is also pivotal to reduce side effects in normal tissue. Severe side effects can drastically reduce quality of life (QOL) and turn cancer therapy into a disadvantageous and harming treatment. Moreover, side effects not just reduce QOL as one of the most important patient read outs but also compromise treatment efficacy by forcing treatment interruptions or terminations. Needless to say, this not just provides healthy cells with time for recovery but also tumor cells. Thus, all treatment options must be weigh before decisions are taken with a huge demand for improved and novel therapies to reduce normal tissue toxicity.

An obvious improvement in radiotherapy could be provided by particle beams limiting co-irradiation of healthy tissue. Proton radiotherapy reduces the whole-body dose [168-170] and current data suggests reduced side effects but clear clinical data is just being produced.[171-173] Thus, a more widespread application of particle beam therapy can be predicted but treatment slots and centers must be expected to remain the limiting factor.

1.4.3 Where is the tumor located?

The most evident factor and currently also main decision factor for proton radiotherapy is the location of the tumor. A variety of organs at risk (OAR) such as brainstem, oral mucosa, or the heart are known to be sensitive to radiotherapy and should be spared from irradiation. Tumors adjacent or in front of OAR thus impose an imminent threat and co-irradiation becomes an unavoidable trade off to tumor control. The more widespread application of particle beams on the other hand provides radiation oncologist with a versatile tool to deliver a homogeneous dose into the tumor volume despite sparing OARs.

The patient population most prone for late side effects after radiotherapy are paediatric patients.[174, 175] This is on the one hand reasoned by their long life expectance subsequent to therapy but on the other hand by their smaller body size narrowing down the safety margins and increasing the proportion of co-irradiated tissue compared to an adult. In conclusion, paediatric cancer patients clearly benefit from proton radiotherapy.

In summary, proton radiotherapy could ascend from a niche treatment to a key player in cancer therapy. Advances in accelerator technology lowering the price are expected to increase access to this therapy and remove economic barriers. In addition, obvious physical

benefits in superior dose distribution and healthy tissue sparing support the more extensive prescription of proton radiotherapy. In contrast to the confirmed physical benefits, there is an urgent demand for further research to elucidate the radiobiological aspects of proton radiotherapy and the widely unestablished factors triggering the prementioned differential cellular response and RBE deviations.

2. Aims of the study

Proton treatment provides a superior dose distribution profile but remains a niche treatment in comparison to photon radiotherapy with less than 1% of patients receiving protons. Despite the financial burden, huge efforts are taken worldwide to increase the numbers of treatment facilities and improve patient access. This increase is furthermore expected to be facilitated by advances in accelerator and beam line instrumentation which lower financial and spatial requirements of new facilities and conclusively promote availability to the public.

Nevertheless, the differential biological processes subsequent to irradiation with proton beams remain a black box for radiation oncologists. A different type of physical induction implies a strong rational for a different type of biological response which in turn implies a chance for clinical exploitation.

This PhD project therefore aims to shed light on proton radiobiology, cellular responses and in particular DNA DSB repair to ultimately provide a rational for novel radio-chemotherapeutic approaches. Thus, our specific aim was to further specify the role of HRR in response to proton radiotherapy and the rational-driven selection of a promising small-molecule inhibitor in consideration of a potential future clinical application. Versatile methods were utilized to broaden our current knowledge and reveal the underlying mechanism of differential response to photon respectively proton radiotherapy.

Our specific aims is the investigation of small-molecule inhibitors with a rational to suppress HRR and are thus hypothesized to more extensively sensitize for SOBP proton than for conventional photon irradiation. A549, H1299, FaDu, and HeLa cells are combined with either Ganetespib, Gemcitabine, or Triapine at varying doses and photon irradiation to define the respective sublethal dose range by proliferation assay and clonogenic cell survival assay. Due to beam time limitations, only A549 and FaDu cells and only Ganetespib are further investigated in combination with proton irradiation of a lower (2.1keV/µm) and a higher (4.5keV/µm) LET. This resembles a SOBP as clinically administered to the gross tumor volume. The influence of Ganetespib and irradiation on Rad51 protein levels, cell cycle distribution and DNA repair are investigated by Western Blotting, flow cytometry and immunofluorescence microscopy, respectively.

3. Results

3.1 HSP90i by Ganetespib selectively radiosensitizes cancer cells for proximal and distal Spread-Out Bragg peak (SOBP) proton irradiation

Simon Deycmar, MSc[1], Elisabeth Mara, MSc[2,3], Sylvia Gruber, PhD[2,4], Verena Waller, MSc[1], Antony John Lomax, PhD[5,6], and Martin Pruschy, PhD[1]

[1]Department of Radiation Oncology, Laboratory for Applied Radiobiology, University Hospital Zurich, Zurich, Switzerland

[2]Department of Radiation Oncology, Medical University of Vienna

[3]University of Applied Science, Wiener Neustadt, Austria

[4]EBG MedAustron GmbH, Wiener Neustadt, Austria

[5]Paul Scherrer Institute, Center for Proton Therapy, Switzerland

[6]Department of Physics, ETH Zurich, Switzerland

Corresponding Author:

Martin Pruschy, PhD

Email: martin.pruschy@uzh.ch

Department of Radiation Oncology, Laboratory for Applied Radiobiology, University Hospital Zurich, Zurich, Switzerland

Winterthurerstr. 190, Y23-K84

8057 Zürich, Switzerland

Status of the manuscript: To be submitted in IJROBP 2020

Author contribution Simon Deycmar:

- Literature Research
- Project design and evolvement
- Drafting and conduction of **all** experiments
- Drafting and proofreading of the manuscript
- Managing collaboration

HSP90i by Ganetespib selectively radiosensitizes cancer cells for proximal and distal Spread-Out Bragg peak (SOBP) proton irradiation

Running Title: Ganetespib radiosensitizes for SOBP protons

Simon Deycmar, MSc[1], Elisabeth Mara, MSc[2,3], Sylvia Gruber, PhD[2,4], Verena Waller, MSc[1], Antony John Lomax, PhD[5,6], and Martin Pruschy, PhD[1]

[1]Department of Radiation Oncology, Laboratory for Applied Radiobiology, University Hospital Zurich, Zurich, Switzerland

[2]Department of Radiation Oncology, Medical University of Vienna

[3]University of Applied Science, Wiener Neustadt, Austria

[4]EBG MedAustron GmbH, Wiener Neustadt, Austria

[5]Paul Scherrer Institute, Center for Proton Therapy, Switzerland

[6]Department of Physics, ETH Zurich, Switzerland

Corresponding Author:

Martin Pruschy, PhD

Email: martin.pruschy@uzh.ch

Department of Radiation Oncology, Laboratory for Applied Radiobiology, University Hospital Zurich, Zurich, Switzerland

Winterthurerstr. 190,

8057 Zürich, Switzerland

Conflicts of Interest

The authors have no conflicts of interest to disclose

Funding

Simon Deycmar is an early stage researcher and Martin Pruschy is a beneficiary in the RADIATE-ITN and as such have received funding from the European Union's Horizon 2020 research and innovation programme under the Marie Sklodowska-Curie grant agreement (No. 642623) and support by the Swiss State Secretariat for Education, Research and Innovation (SBFI, No. 15.0066).

Acknowledgements

We want to acknowledge Christina and Gerhard Deycmar, the parents of Simon Deycmar, who selflessly provided accommodation and a car during the irradiation shifts in Austria. We moreover want to thank the people at MedAustron for their assistance, treatment plans and beam operation. We also acknowledge the assistance and support by the team of the Flow Cytometry Core Facility and the Center for Microscopy and Image Analysis, both at the University of Zurich.

Ganetespib radiosensitizes for SOBP protons

Abstract

Background and purpose

This study investigates the radiosensitizing effect of Ganetespib for proton irradiation at a proximal and distal position in a SOBP in comparison to photon irradiation. Rad51, a key protein of homologous recombination repair (HRR), is downregulated by Ganetespib which provides a promising rational for a specifically proton-sensitizing combinatorial approach.

Methods and Materials

A549 and FaDu cells were treated with low-dose (2nM resp. 1nM) HSP90-inhibiting Ganetespib and irradiated with 200kV photons. Proton irradiation was administered at a proximal, low linear energy transfer (LET, 2.1keV/µm) and a distal, higher LET (4.5keV/µm) position within a SOBP. Cellular survival was determined by clonogenic assay and relative biological effectiveness (RBE) and dose-modifying factor (DMF) calculated. Cell cycle distribution was investigated by flow cytometry, Rad51 protein levels by western blotting and γH2AX foci by immunofluorescence microscopy.

Results

Our results indicate a significant sensitization by Ganetespib in both cancer cell lines exclusively for proton irradiation of both investigated LETs. Upon proton irradiation, a more pronounced accumulation of cells in S/G2/M phase became evident with Ganetespib reducing this population. Without irradiation, Ganetespib had no influence on the cell cycle distribution. Rad51 protein levels were more extensively and more persistently elevated in proton- than in photon-irradiated samples. Additionally, Rad51 protein levels were suppressed by Ganetespib administration at each investigated time point. Immunofluorescence staining demonstrated a similar induction and removal of γH2AX foci independent of Ganetespib administration which suggests compensation by more error-prone Rad51-independent repair pathways.

Conclusion

Low-dosed Ganetespib is sufficient to significantly sensitize cancer cells for proximal and distal SOBP proton irradiation. Ganetespib downregulates Rad51 protein and reduces the S/G2/M fraction of cells and is thus considered to suppress HRR. Hence, this study explicitly supports pursuing research on the novel combination of Ganetespib with proton radiotherapy for a prospective clinical exploitation.

Keywords:

Proton Radiotherapy, Linear Energy Transfer, Rad51, Ganetespib, HSP90

Introduction

The superior dose distribution profile of proton radiotherapy is widely accepted in the present discourse [1] but a differential proton radiobiology and the biological factors involved remain widely unestablished. Nevertheless, a generic 10% higher cell killing efficacy respectively RBE of 1.1 is applied in present-day clinical treatment planning of proton radiotherapy. This paradigm of a constant RBE is questioned by findings and simulations of multiple research groups with ongoing efforts to elaborate on variable RBEs, the role of LET and the biological background.[2-5] Defining the appropriate RBE is unfortunately becoming complicated due to a dependence of RBE on various factors such as end point, tissue, or model investigated.

Needless to say, a broadened knowledge on differently balanced cellular processes subsequent to proton in comparison to photon irradiation will shed light on these questions and supply radiation oncologists with a novel rational for combinatorial approaches with RBE-modulating agents.

The outstanding radiobiological characteristics of proton radiotherapy is the increase in LET towards the distal end of the SOBP which translates into more clustered DNA lesions than yielded by conventional photon irradiation.[6] These more complex lesions are defined as DNA double strand breaks (DSB) clustering with additional lesions such as single-strand breaks within a vicinity of 20 base pairs and are considered more challenging for DNA repair.

The two canonical pathways involved in DNA DSB repair are non-homologous end joining (NHEJ) and homologous recombination repair (HRR). In detail, NHEJ can be summarized as a fast process, responsible for the vast number of repaired DSBs and present throughout cell cycle.[7] NHEJ also involves minor DNA end processing and as a result comprises the risk of accidental mutations prior to relegation of the strands. HRR on the other hand is limited to the presence of copied DNA during S- and G2 phase, involves extensive single-strand resection, Rad51-mediated strand invasion for recombination, DNA polymerization and the resolution of the resulting complex DNA structure. As a result, HRR is slower and consumes more cellular resources but is ultimately less error-prone than

NHEJ. Recapitulating, the cellular response to radiation-induced DSBs is a fine-tuned balance of repair mechanisms which depend on cell cycle phase and are essential to maintain genome integrity.

The particular importance of HRR in response to proton irradiation was demonstrated by diverse approaches. HRR deficiency in Chinese hamster ovary cells resulted in a proton irradiation-sensitive phenotype as indicated by increased RBEs.[8] Similar conclusions could be drawn from human cancer cell lines and could be replicated by SAHA- [9] or siRNA-mediated downregulation of Rad51.[10] These findings were further supported by a screening of lung cancer cell lines.[11] Resulting data indicated a correlation of HRR deficiency with an increased RBE and in contrast a decreased RBE in cells with elevated levels of Rad51 mRNA and protein. Additional research on deficiencies in HRR key proteins such as Slx4 and Mus81[12] also suggest an increased importance of HRR in response to proton than in response to conventional photon irradiation. Consequently, interference with HRR constitutes a promising target to sensitize cancer cells for proton radiotherapy.

Unfortunately, modulation of HRR is a clinically difficult target and many inhibitors of HRR are limited to the use in *in vitro* experiments. This limitation is based on the necessity to provide pharmaceutically unachievably high concentrations or due to severe side effects provoked in the patient. A possible alternative is provided by HSP90-inhibiting Ganetespib which downregulates versatile DSB repair proteins including Rad51 and BRCA2 [13-16] and conclusively suppresses HRR. Furthermore, the elevated intrinsic proteotoxic stress in tumor cells upregulates the activated, high-affinity form of chaperone HSP90 and hence provides a certain tumor-specific vulnerability.[17] In addition, Ganetespib demonstrated a good tissue penetrance and pharmaceutical profile [18, 19] and was moreover administered in numerous clinical trials.[20-22] However, current research is limited to high-LET carbon ions in combinations with HSP90 inhibitors [23-26] and despite the promising findings and a potential translatability to proton irradiation, it remained unexplored.

This study investigates the radiosensitizing effect of HSP90 inhibitor Ganetespib in combination with reference photon and SOBP proton irradiation of two different LETs, respectively. Ganetespib

administration and proton radiotherapy are designed to replicate the clinical situation as close as feasible to reduce undesirable uncertainties and foster a prospective clinical application.

Materials and Methods

The human cancer cell lines A549 (NSCLC, wtTP53) and FaDu (HNSCC, mutTP53) were obtained from ATCC and used for all *in vitro* experiments (see supplementary materials (***Suppl. Methods E1***). The cells were treated with Ganetespib 1h prior to irradiation with proton and reference photon irradiation and maintained in drug-containing medium until harvest. A similar amount of DMSO was added as sham treatment (0nM) to exclude effects by the solvent. Horizontal beam setups were utilized for photon and proton irradiation and closable slide flasks conclusively filled air bubble-free with the respective cell culture medium antecedent to irradiation. 200kV photon irradiation was administered in an irradiation cabinet at 1.28Gy/min (see also ***Suppl. Methods E2***). For proton irradiation, a dosimetrically-defined PMMA/water phantom [27] was utilized with cell layers being positioned at the proximal (55mm depth) and distal end (105mm depth) of a SOBP (range 40-120mm) (see also ***Suppl. Methods E3, Suppl. Fig. E3***). These positions provide protons of a lower (2.1keV/µm) and a higher dose-averaged LET (4.5keV/µm).

Clonogenic cell survival assays were conducted for both cell lines and cells seeded after irradiation in technical sextuplicates in 6-well plates at adjusted cell concentrations to obtain 20-300 clones per well. Resulting clones were fixated after incubation for 7 (A549) or 14 (FaDu) days at regular cell culture conditions and three independent biological replicates generated for each data point (***Suppl. Methods E4***).

Clonogenic survival data was fitted using a linear-quadratic model to obtain RBE and DMF values at 50% (RBE_{50}, DMF_{50}), 25% (RBE_{25}, DMF_{25}), and 10% (RBE_{10}, DMF_{10}) survival fraction, respectively. Additionally, cells were harvested to investigate cell cycle distribution by flow cytometry and Rad51 protein levels by western blotting 8h, 24h, and 48h after irradiation (***Suppl. Methods E5-E6***). Nuclear

γH2AX foci were utilized as surrogate marker for DSBs and investigated 0.5h and 24h after irradiation to determine DSB induction and removal, respectively (*Suppl. Methods E7*).

Statistical analysis was performed using GraphPad Prism (Version 5.03) and parameters of cell survival compared by two-tailed T-test. All error bars and quoted uncertainties are represented as standard deviation of the mean.

Results

Ganetespib significantly sensitized A549 cells for proton irradiation administered as a SOBP in comparison to reference photon treatment (Fig. 1A-1B). This is illustrated by consistently increased RBEs in Ganetespib-treated cells. In detail, RBE_{50} increased from 0.93 ±0.05 to 1.34 ±0.10 for the proximal and from 0.92 ±0.11 to 1.33 ±0.10 for the distal position in the proton SOBP (Fig. 1C). Similar findings were determined for RBE_{25} which was increased in Ganetespib-treated cells from 0.99 ±0.03 to 1.27 ±0.07 and from 1.01 ±0.05 to 1.29 ±0.07 as well as for RBE_{10} which was increased from 1.07 ±0.05 to 1.22 ±0.05 and 1.11 ±0.04 to 1.25 ±0.04 for the proximal and distal position, respectively (see also ***Suppl. Table E1***). This sensitization was limited to proton treatment as particularly indicated by the DMFs of Ganetespib. The DMF_{50}, DMF_{25}, and DMF_{10} for the proximal position were 1.32 ±0.05, 1.23 ±0.03, and 1.16 ±0.01 and for the distal position 1.33 ±0.12, 1.23 ±0.06, and 1.15 ±0.02, respectively. These DMFs are significantly higher than the DMF_{50}, DMF_{25}, and DMF_{10} for photon-irradiated cells which were determined to be 0.92 ±0.05, 0.97 ±0.02, and 1.02 ±0.02, respectively (***Suppl. Table E1 & Fig. E1***). Conclusively, radiosensitization by Ganetespib in A549 cells demonstrated to be limited to proton irradiation and absent in photon-irradiated cells.

In accordance with our findings in A549 cells, also FaDu cells were specifically sensitized by Ganetespib for SOBP proton irradiation (Fig. 2A-2B). RBE_{50}, RBE_{25}, and RBE_{10} values were increased in Ganetespib-treated cells from 1.10 ±0.04 to 1.29 ±0.04, from 1.16 ±0.01 to 1.36 ±0.03, and from 1.22 ±0.02 to 1.38 ±0.02 for the proximal position in the SOBP and from 1.32 ±0.04 to 1.68 ±0.09, from 1.33 ±0.03 to 1.59 ±0.03, and from 1.34 ±0.07 to 1.52 ±0.03 for the distal position, respectively. (Fig. 2C-2E, ***Suppl. Table E2***). These increased RBEs in Ganetespib-treated cells translate into DMF_{50}, DMF_{25}, and DMF_{10} values of 1.25 ±0.04, 1.17 ±0.01, and 1.09 ±0.01 for the proximal and comparable values of 1.35 ±0.06 , 1.19 ±0.00, and 1.09 ±0.04 for the distal position, respectively. (see also ***Suppl. Table E2 & Fig. E2***) In contrast, no sensitization by Ganetespib was observed in photon-irradiated FaDu cells as indicated by DMF_{50}, DMF_{25}, and DMF_{10} values of 1.06 ±0.02, 1.00 ±0.01, and 0.96 ±0.01, respectively.

To elucidate the cellular response to irradiation and potential alterations induced by Ganetespib, we performed flow cytometry of A549 cells treated with 4Gy of irradiation. Single cells were gated for their cellular DNA content as indicated by propidium iodide and for BrdU uptake by staining with fluorophore-labelled antibody.

Pretreatment with Ganetespib as conducted in all experiments did not alter cell cycle distribution at the time point of irradiation (Fig. 3A). This excludes cell cycle synchronization as a factor for radiosensitization. After 4Gy irradiation, a strong accumulation in G2 phase was observed at the 8h time point (Fig. 3B). Interestingly, the fraction of cells in S/G2/M phase was more pronounced and approximately 6% larger in proton-irradiated cells. At the 24h time point (Fig. 3C), this accumulation in G2 was observed to shift towards an accumulation in G1 phase. However, proton irradiation similarly induced an approximately 5% larger fraction of cells persisting in S/G2/M phase. At the 48h time point, most of the irradiated cells accumulated in G1 phase and the more pronounced fraction of cells in S/G2/M phase as seen at the 24h time point in proton-treated cells, was mostly vanished. Interestingly, 10nM Ganetespib decreased the fraction of cells in S/G2/M phase throughout the investigated time points and especially suppressed DNA-replicating cells as seen at the 48h time point.

Importantly, Ganetespib treatment without irradiation only marginally affected cell cycle distribution and did not accumulate cells in a specific cell phase. The time-dependently increasing G1 fraction in unirradiated cells is expected to be induced by contact inhibition. An explanation was provided by microscopic visualization and despite sufficient space for proliferation at the outer clonal rim, more densely packed central regions in the growing clones observable.

Protein levels of Rad51 in A549 cells were investigated 8h (Fig. 4A), 24h (Fig. 4B), and 48h (Fig. 4C) subsequent to irradiation with 4Gy and concomitant treatment with Ganetespib. Within 8h, an upregulation of Rad51 protein levels became evident in cells irradiated with protons of both investigated LETs. This pronounced upregulation of Rad51 protein levels in proton-irradiated cells was not displayed by photon-irradiated cells and further increased in manifestation at the 24h time point.

48h after irradiation, Rad51 protein levels were only marginal in photon-irradiated cells while proton-irradiated cells retained relevant levels of Rad51. Importantly, Rad51 proteins levels were persistently downregulated by 10nM Ganetespib within 8h and within 24h upon treatment with 2nM Ganetespib. In summary, cells intend to more extensively upregulate Rad51 protein levels upon treatment with proton irradiation which is at least partially counteracted by Ganetespib administration.

To investigate DSB repair in response to photon (Fig. 3A), proximal SOBP (Fig. 3B), or distal SOBP (Fig. 3C) proton irradiation, the number of γH2AX foci per cell nucleus were evaluated in A549 cells 0.5h and 24h after irradiation with a dose of 2 Gy, respectively. As proposed by previous research [8], a similar number of foci were induced independent of the type of irradiation administered. Moreover, 24h after irradiation, foci were removed in a uniform efficiency independent of photon or proton irradiation. In addition, Ganetespib administration did neither alter the number of foci induced nor the number of foci remaining after 24h. This suggests Rad51 protein levels being either sufficient for effective HRR or a shift from Rad51-dependent HRR to more error-prone Rad51-independent NHEJ or alternative repair pathways.

Discussion

This study provides insights into the cellular response to radiotherapy of different nature and linear energy transfer. Experiments were designed to elaborate on RBE variations of proton radiotherapy and a future exploitability by a combined treatment modality with a chemotherapeutical agent. We accomplished this by replicating the clinical irradiation situation as close as feasible which involved a dosimetrically-defined treatment phantom to mimic relevant tissue depths, the accurate sample positioning at the proximal and distal end of a defined SOBP to obtain different LETs, as well as most advanced spot scanning for proton administration. We also established the cell-specific sublethal Ganetespib dose to draw the focus on the combinatorial approach and to limit cellular alterations by Ganetespib itself.

We demonstrate for the first time an exclusively proton-sensitizing effect of low-dosed HSP90 inhibitor Ganetespib. To do so, we investigated RBEs and DMFs at 50%, 25% and 10% cell survival to cover the survival fractions as achieved by a single dose of a hypo- or conventionally fractionated regimen. In compliance with previous research [11], we confirmed the RBE values of sham-treated A549 cells to be approximately 1.0, which represents similar sensitivity for photon and proton radiotherapy. Strikingly, the RBE values of both types of proton irradiation were significantly increased by 20% to 30% in cells treated with 2nM Ganetespib. These findings could be reproduced in a second cell line, namely in HNSCC FaDu cells. The RBE values in FaDu were also significantly increased by 15% to 30% in Ganetespib-treated cells which closely resembles previously determined RBE increases in HRR-deficient lung cancer cells compared to HRR-proficient cell lines [11] respectively as determined by siRNA-mediated knockdown of Rad51 in A549 and CHO cells.[8, 10] Interestingly, we could not observe a LET dependency for radiosensitization by Ganetespib and the relative RBE increases were similar in A549 and FaDu cells for the proximal and the distal position in the SOBP, respectively. Previous research on LET and DNA repair [28] suggested an increasing relative role of HRR upon increases in LET. In detail, the highest investigated LET was 7.3keV/µm which resembles a LET as

achieved in the more distal fall off region of a SOBP. The LETs investigated in this study are 2.1keV/µm and 4.5keV/µm and are potentially too low and too less apart to define a clear correlation of LET and radiosensitization by Ganetespib. Nevertheless, chosen LETs closely replicate the clinical situation in a SOBP covering the gross tumor volume and higher LETs are frequently limited to the healthy rim of the distal safety margin. Conclusively, our experimental design more closely resembles the LET situation in the tumor than in the distal normal tissue.

Investigating the cell cycle distribution in A549 cells subsequent to irradiation illustrated a strong accumulation of sham-treated cells in S/G2/M phase within 8h which was more pronounced in response to proton than in response to photon irradiation. In general, most cells shifted into G1 phase within 24h after irradiation. However, a larger fraction of proton-irradiated cells persisted in S/G2/M phase. This difference was mostly levelled out at the 48h time point when the majority of irradiated cells accumulated in G1 phase. Pretreatment with Ganetespib did not shift the cell cycle distribution which conclusively excluded radiosensitization by cell cycle synchronization. However, in combination with irradiation, 10nM Ganetespib decreased the fraction of cells in S/G2/M phase at each investigated time point. Limiting the S/G2/M phase bears the potential to also limit cellular access to HRR and thus shifting DNA repair pathway choice away from HRR. In addition, also the prementioned larger fraction of sham-treated cells in S/G2/M phase in response to proton irradiation could indicate a more available respectively more utilized HRR. Due to beam time limitations, the exact reason, cell cycle checkpoints triggered and resulting implications for pathway choices were not further investigated.

Our findings further demonstrated that protein levels of Rad51 are downregulated upon HSP90 inhibition. To investigate this, we determined Rad51 protein levels at the particular same time points as applied for cell cycle analysis. We found a nearly 2-fold upregulation of Rad51 protein levels within 8h after proton irradiation but only marginally after photon irradiation. Rad51 levels persisted at this high level for 24h in proton-irradiated cells but remained unaltered in photon-irradiated cells. Moreover, 48h after photon irradiation, Rad51 levels are mostly vanished which correlates with a high

fraction of G1 phase cells. In contrast, 48h after proton irradiation cells retained relevant levels of Rad51 despite a comparably extensive fraction of G1 cells. Most importantly, 10nM Ganetespib persistently downregulated Rad51 protein levels within 8h and 2nM Ganetespib within 24h. This indicates a HRR-suppressive role of Ganetespib and in particular counteracts the cellular upregulation of Rad51 upon proton irradiation. Nevertheless, the exact mechanism of Rad51 downregulation upon HSP90 inhibition remains elusive due to the vast number of HSP90 client proteins and HSP90 inhibition could thus directly affect Rad51 protein but could also affect the upstream signalling of Rad51 activity and expression. Nevertheless, the particle-specific sensitization as well as the reduction in Rad51 protein levels by HSP90 inhibition match previous findings generated with carbon irradiation.[23-26]

Conclusively, we also investigated the emergence and removal of γH2AX foci in A549 cells as surrogate for DSBs in response to 2Gy of ionizing irradiation. Similar numbers of foci were induced by photon and proton radiotherapy of both LETs as suggested by previous research.[8] Additionally, also 24h after irradiation the number of remaining foci was similar and independent of the nature of irradiation administered. Remarkably, despite the suppression of Rad51 protein, neither γH2AX foci induction nor removal was altered in Ganetespib-treated cells. Conclusively, Rad51 protein levels either remained sufficient to accomplish HRR or redundancies in DSB repair replaced the decreased capacity in Rad51-dependent HRR with more error-prone but Rad51-independent alternative pathways. A possible shift towards NHEJ or not further specified alternatives such as microhomology-mediated end joining (MMEJ)[29] contradicts the cellular upregulation of Rad51 protein upon proton irradiation and implies a potential mode of action of Ganetespib.

Conclusion

We demonstrated that low doses of HSP90 inhibitor Ganetespib are sufficient to sensitize A549 cancer cell lines exclusively for proton radiotherapy but not for conventional photon irradiation. This proton-sensitizing effect of Ganetespib was confirmed in FaDu cells and similar increases in RBE of up to 30% obtained in both cell lines and at both investigated LETs of 2.1keV/µm and 4.5keV/µm, respectively.

A LET dependency of this effect was not observed in this study but cannot be excluded at elevated LETs as predicted by Bright et al [28] or when combined with high-LET carbon irradiation.

This study is the first to demonstrate radiosensitization for clinically relevant SOBP proton radiotherapy by HSP90 inhibition. We thus strongly propose further research investigating the response of normal cells in combination with HSP90i and with protons of higher LETs as frequently administered to the healthy safety margin of treatment fields. Additionally, more extensive research on the DNA repair pathway choice and the balance between NHEJ, HRR, and alternative repair pathways is strongly suggested. Taken together, we generated reliable data that promotes the combination of proton radiotherapy with HSP90 inhibition as a novel rational-driven clinical approach against cancer.

References

1. Vitti, E.T. and J.L. Parsons, *The Radiobiological Effects of Proton Beam Therapy: Impact on DNA Damage and Repair.* Cancers (Basel), 2019. **11**(7).
2. Paganetti, H., *Nuclear interactions in proton therapy: dose and relative biological effect distributions originating from primary and secondary particles.* Phys Med Biol, 2002. **47**(5): p. 747-64.
3. Chen, Y., et al., *Impact of potentially variable RBE in liver proton therapy.* Phys Med Biol, 2018. **63**(19): p. 195001.
4. Giovannini, G., et al., *Variable RBE in proton therapy: comparison of different model predictions and their influence on clinical-like scenarios.* Radiat Oncol, 2016. **11**: p. 68.
5. Marshall, T.I., et al., *Investigating the Implications of a Variable RBE on Proton Dose Fractionation Across a Clinical Pencil Beam Scanned Spread-Out Bragg Peak.* Int J Radiat Oncol Biol Phys, 2016. **95**(1): p. 70-7.
6. Mavragani, I.V., et al., *Ionizing Radiation and Complex DNA Damage: From Prediction to Detection Challenges and Biological Significance.* Cancers (Basel), 2019. **11**(11).
7. Brandsma, I. and D.C. Gent, *Pathway choice in DNA double strand break repair: observations of a balancing act.* Genome Integr, 2012. **3**(1): p. 9.
8. Grosse, N., et al., *Deficiency in homologous recombination renders Mammalian cells more sensitive to proton versus photon irradiation.* Int J Radiat Oncol Biol Phys, 2014. **88**(1): p. 175-81.
9. Gerelchuluun, A., et al., *Histone Deacetylase Inhibitor Induced Radiation Sensitization Effects on Human Cancer Cells after Photon and Hadron Radiation Exposure.* Int J Mol Sci, 2018. **19**(2).
10. Fontana, A.O., et al., *Differential DNA repair pathway choice in cancer cells after proton- and photon-irradiation.* Radiother Oncol, 2015. **116**(3): p. 374-80.

11. Liu, Q., et al., *Lung cancer cell line screen links fanconi anemia/BRCA pathway defects to increased relative biological effectiveness of proton radiation.* Int J Radiat Oncol Biol Phys, 2015. **91**(5): p. 1081-9.
12. Liu, Q., et al., *Disruption of SLX4-MUS81 Function Increases the Relative Biological Effectiveness of Proton Radiation.* Int J Radiat Oncol Biol Phys, 2016. **95**(1): p. 78-85.
13. Kramer, D., et al., *Strong antitumor synergy between DNA crosslinking and HSP90 inhibition causes massive premitotic DNA fragmentation in ovarian cancer cells.* Cell Death Differ, 2017. **24**(2): p. 300-316.
14. He, S., et al., *The HSP90 inhibitor ganetespib has chemosensitizer and radiosensitizer activity in colorectal cancer.* Invest New Drugs, 2014. **32**(4): p. 577-86.
15. Jiang, J., et al., *Ganetespib overcomes resistance to PARP inhibitors in breast cancer by targeting core proteins in the DNA repair machinery.* Invest New Drugs, 2017. **35**(3): p. 251-259.
16. Vriend, L.E.M., et al., *Boosting the effects of hyperthermia-based anticancer treatments by HSP90 inhibition.* Oncotarget, 2017. **8**(57): p. 97490-97503.
17. Kamal, A., et al., *A high-affinity conformation of Hsp90 confers tumour selectivity on Hsp90 inhibitors.* Nature, 2003. **425**(6956): p. 407-10.
18. Ying, W., et al., *Ganetespib, a unique triazolone-containing Hsp90 inhibitor, exhibits potent antitumor activity and a superior safety profile for cancer therapy.* Mol Cancer Ther, 2012. **11**(2): p. 475-84.
19. Goldman, J.W., et al., *A first in human, safety, pharmacokinetics, and clinical activity phase I study of once weekly administration of the Hsp90 inhibitor ganetespib (STA-9090) in patients with solid malignancies.* BMC Cancer, 2013. **13**: p. 152.
20. Ramalingam, S., et al., *A randomized phase II study of ganetespib, a heat shock protein 90 inhibitor, in combination with docetaxel in second-line therapy of advanced non-small cell lung cancer (GALAXY-1).* Ann Oncol, 2015. **26**(8): p. 1741-8.
21. Pillai, R.N., et al., *Randomized Phase III Study of Ganetespib, a Heat Shock Protein 90 Inhibitor, With Docetaxel Versus Docetaxel in Advanced Non-Small-Cell Lung Cancer (GALAXY-2).* J Clin Oncol, 2019: p. JCO1900816.
22. Cardin, D.B., et al., *A Phase II Study of Ganetespib as Second-line or Third-line Therapy for Metastatic Pancreatic Cancer.* Am J Clin Oncol, 2018. **41**(8): p. 772-776.
23. Hirakawa, H., et al., *The combination of Hsp90 inhibitor 17AAG and heavy-ion irradiation provides effective tumor control in human lung cancer cells.* Cancer Med, 2015. **4**(3): p. 426-36.
24. Segawa, T., et al., *Radiosensitization of human lung cancer cells by the novel purine-scaffold Hsp90 inhibitor, PU-H71.* Int J Mol Med, 2014. **33**(3): p. 559-64.
25. Lee, Y., et al., *The purine scaffold Hsp90 inhibitor PU-H71 sensitizes cancer cells to heavy ion radiation by inhibiting DNA repair by homologous recombination and non-homologous end joining.* Radiother Oncol, 2016. **121**(1): p. 162-168.
26. Li, H.K., et al., *PU-H71, a novel Hsp90 inhibitor, as a potential cancer-specific sensitizer to carbon-ion beam therapy.* J Radiat Res, 2016. **57**(5): p. 572-575.
27. Clausen, M., et al., *Phantom design and dosimetric characterization for multiple simultaneous cell irradiations with active pencil beam scanning.* Radiat Environ Biophys, 2019. **58**(4): p. 563-573.
28. Bright, S.J., et al., *Nonhomologous End Joining Is More Important Than Proton Linear Energy Transfer in Dictating Cell Death.* Int J Radiat Oncol Biol Phys, 2019. **105**(5): p. 1119-1125.
29. Seol, J.H., E.Y. Shim, and S.E. Lee, *Microhomology-mediated end joining: Good, bad and ugly.* Mutat Res, 2018. **809**: p. 81-87.

Deycmar et al., 2020

HSP90i by Ganetespib selectively radiosensitizes cancer cells for proximal and distal Spread-Out Bragg peak (SOBP) proton irradiation

Summary

Low-dosed Ganetespib renders cancer cells exclusively sensitive for SOBP proton radiotherapy. Higher and more persistent Rad51 protein levels and a more pronounced fraction of cells in S/G2/M phase were detected in proton-irradiated than compared to photon-irradiated cells. Rad51 levels and S/G2/M phase fraction were reduced upon Ganetespib treatment. However, a similar DSB removal was observed which suggests that reduced HRR capacity is being replaced by Rad51-independent but more error-prone pathways.

Deycmar et al., 2020

HSP90i by Ganetespib selectively radiosensitizes cancer cells for proximal and distal Spread-Out Bragg peak (SOBP) proton irradiation

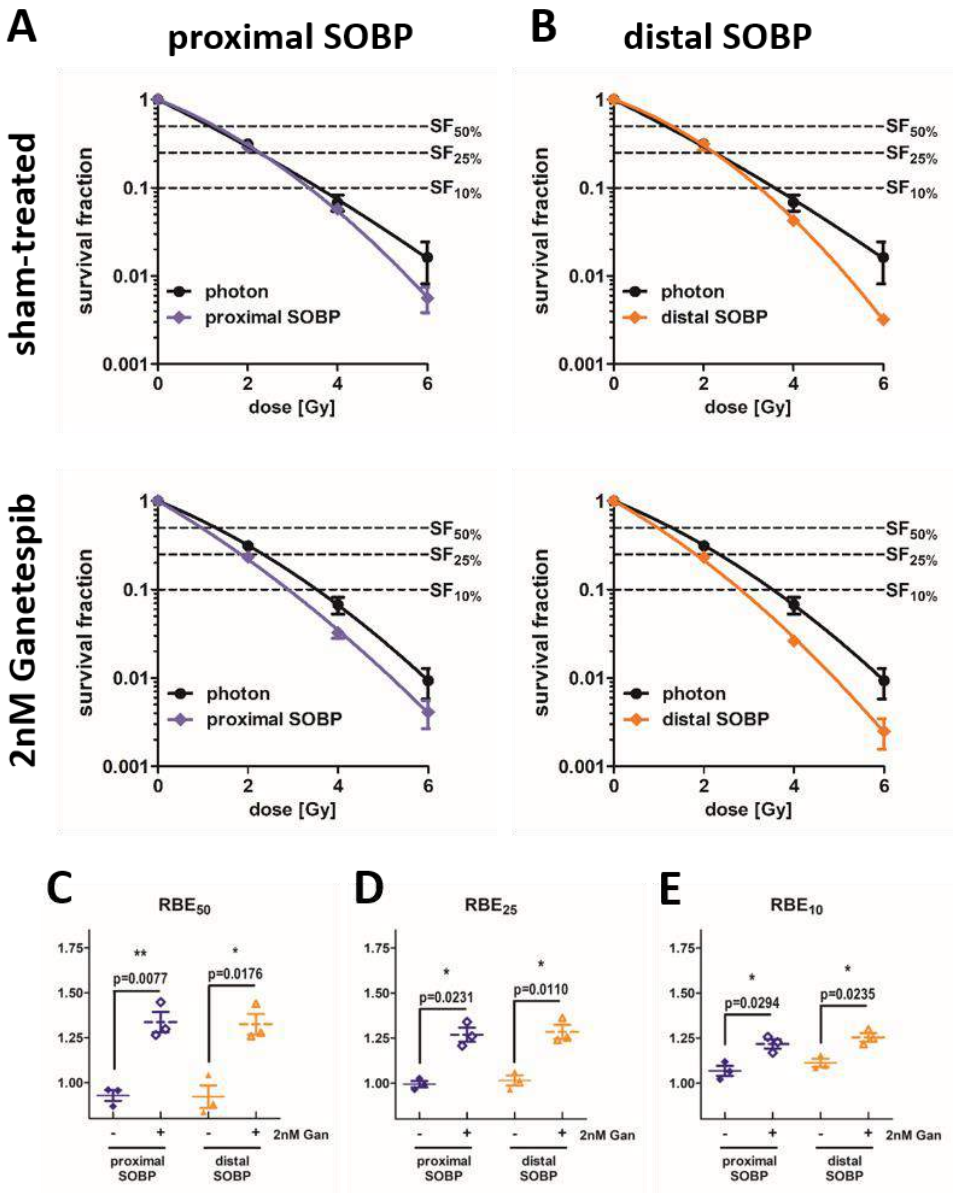

Figure 1 Clonogenic cell survival of A549

Clonogenic cell survival of A549 cells treated with and without Ganetespib (2nM) and 200kV reference photon or proton irradiation at the proximal (A) or distal (B) position of a SOBP with LETs of 2.1 and 4.5keV/µm, respectively. The relative biological effectiveness (RBE) at (C) 50%, (D) 25%, and (E) 10% cell survival was significantly increased in Ganetespib-treated cells.

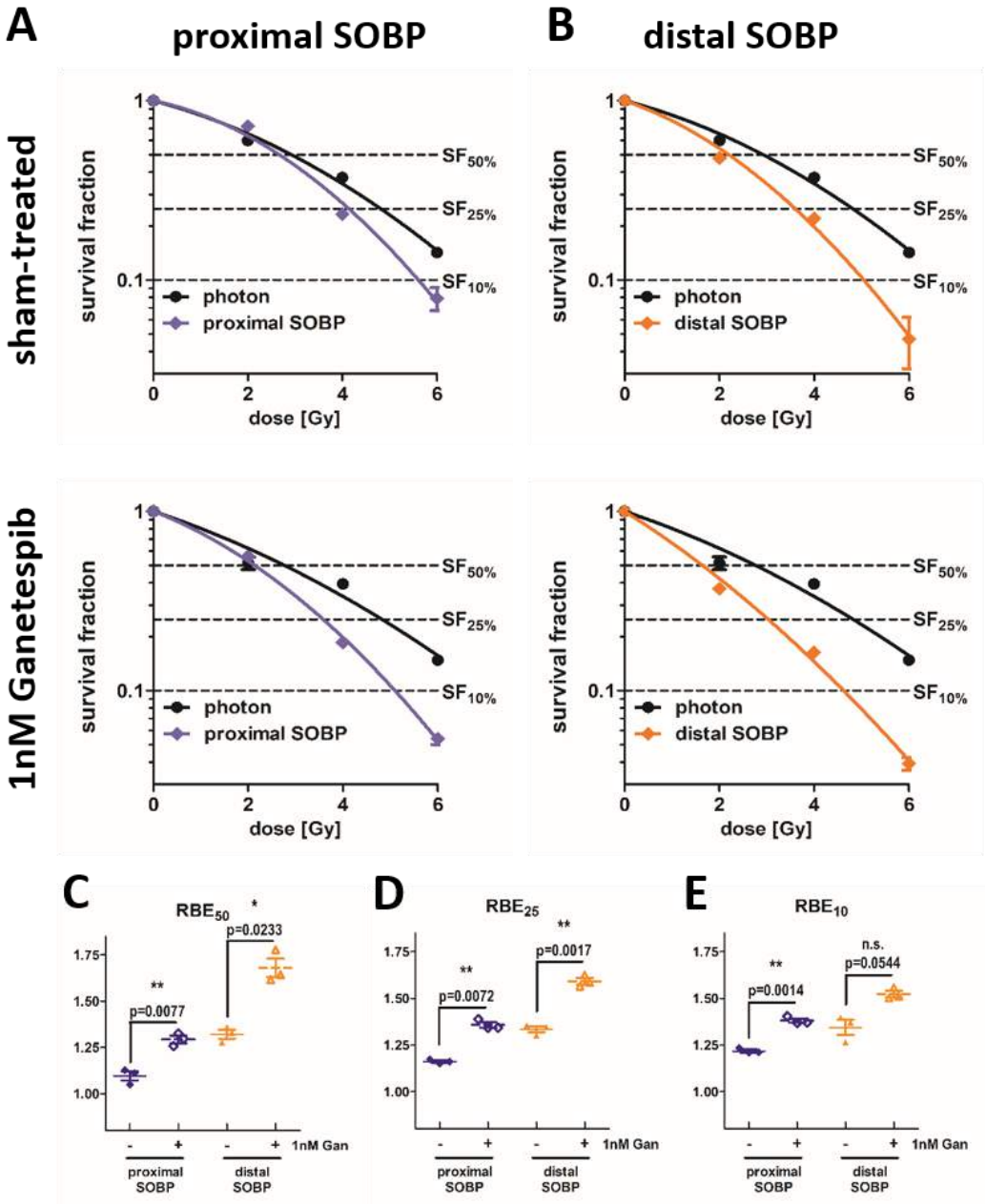

Figure 2 Clonogenic cell survival of FaDu

Clonogenic cell survival of FaDu cells treated with and without Ganetespib (1nM) and 200kV reference photon or proton irradiation at the proximal (A) or distal (B) position of a SOBP with LETs of 2.1 and 4.5keV/µm, respectively. The relative biological effectiveness (RBE) at (C) 50%, (D) 25%, and (E) 10% cell survival was significantly increased in Ganetespib-treated cells.

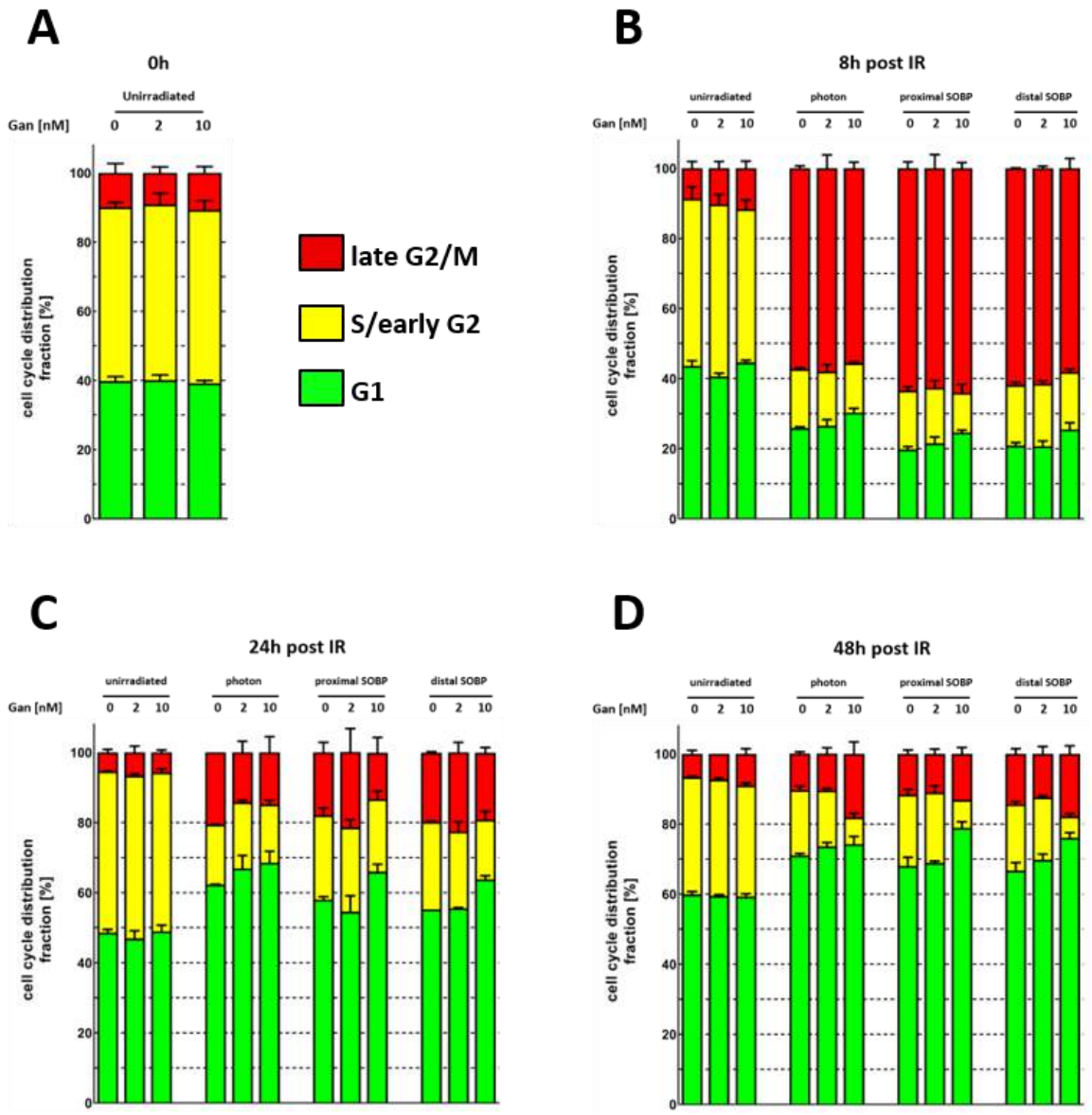

Figure 3 Cell cycle analysis of A549

A549 cells received 4 Gy of the respective irradiation and were analyzed at (A) 0h, (B) 8h, (C) 24h, and (D) 48h after irradiation. Cell cycle phases were gated in single cells by DNA content and BrdU uptake. A duplicate of data points could be obtained with error bars indicating the standard deviation.

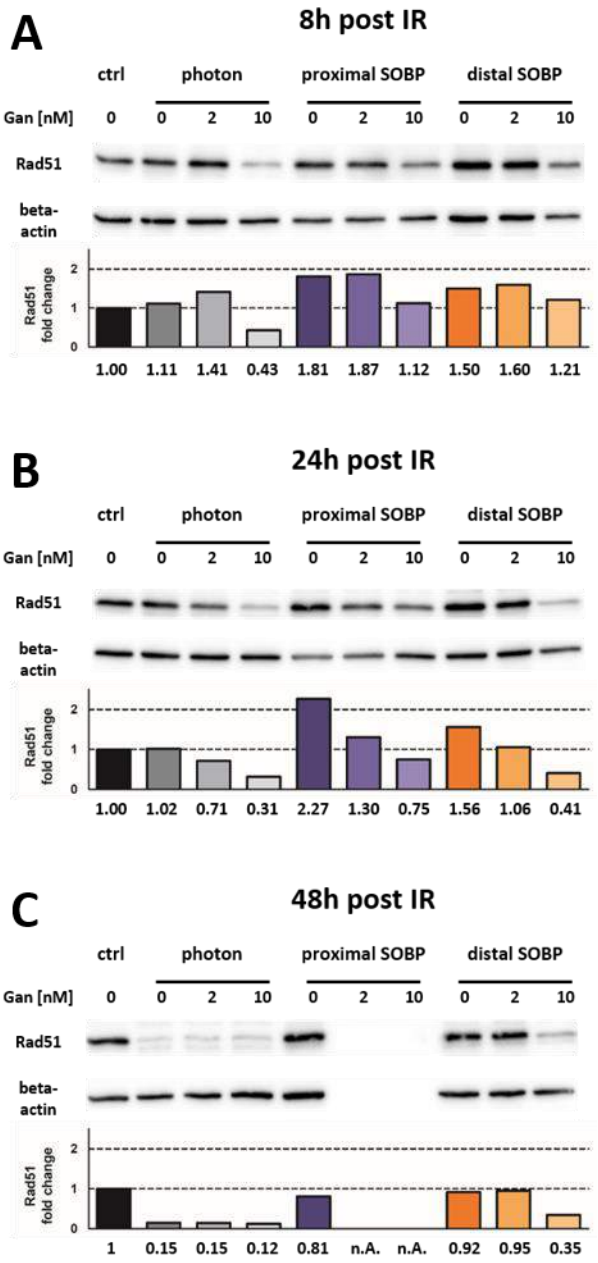

Figure 4 Western Blot analysis of A549

Analysis of Rad51 protein levels in response to photon, proximal SOBP proton or distal SOBP proton irradiation. A549 cells were harvested (A) 8h, (B) 24h, and (C) 48h subsequent to 4Gy of the indicated type of irradiation and analyzed by immunoblotting. The first lane (ctrl, 0), which represents an unirradiated, untreated control lysate, was utilized for normalizing protein levels in between the membranes. Two lysates of the 48h time point could not be obtained due to beam time limitations.

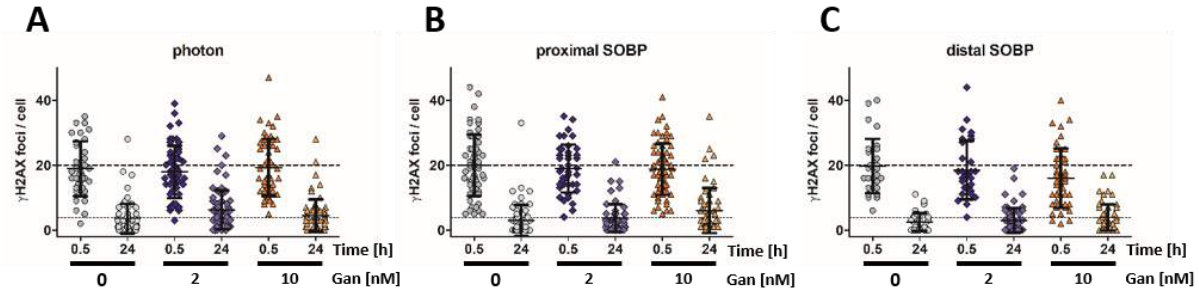

Figure 5 Nuclear γH2AX foci analysis of A549

A549 cells were fixated 0.5h and 24h subsequent to irradiation with 2Gy (A) photons, (B) proximal SOBP, or (C) distal SOBP protons. Nuclear γH2AX foci were stained with fluorophore-labelled antibody and DAPI as nuclear counterstain. Cells were investigated by immunofluorescence microscopy, at least 50 cells imaged per condition and the number of γH2AX foci per nucleus counted.

Deycmar et al., 2020

HSP90i by Ganetespib selectively radiosensitizes cancer cells for proximal and distal Spread-Out Bragg peak (SOBP) proton irradiation

Supplementary information

Tab. E1 Clonogenic cell survival RBEs and DMFs of A549

A549 cells were pretreated 1hr prior to irradiation with 2nM Ganetespib or sham treatment. Subsequent to irradiation, a defined numbers of cells were plated in Ganetespib or sham-treated medium as described in Methods E4. Three independent clonogenic assay sets were generated and utilized to calculate the DMFs and RBEs at 50%, 25% and 10% cell survival, respectively.

RBE_{50}	mean	stdev	p value
proximal SOBP, sham	0.928	0.052	0.0077
proximal SOBP, 2nM	1.337	0.098	
distal SOBP, sham	0.921	0.108	0.0176
distal SOBP, 2nM	1.325	0.099	

RBE_{25}	mean	stdev	p value
proximal SOBP, sham	0.994	0.031	0.0231
proximal SOBP, 2nM	1.269	0.067	
distal SOBP, sham	1.014	0.049	0.0110
distal SOBP, 2nM	1.285	0.067	

RBE_{10}	mean	stdev	p value
proximal SOBP, sham	1.068	0.049	0.0294
proximal SOBP, 2nM	1.218	0.045	
distal SOBP, sham	1.112	0.039	0.0235
distal SOBP, 2nM	1.254	0.042	

DMF_{50}	mean	stdev	p value*
photon	0.9183	0.050	
proximal SOBP	1.322	0.048	0.0021
distal SOBP	1.327	0.123	0.0031

DMF_{25}	mean	stdev	p value*
photon	0.9667	0.024	
proximal SOBP	1.234	0.027	0.0010
distal SOBP	1.226	0.061	0.0205

DMF_{10}	mean	stdev	p value*
photon	1.021	0.015	
proximal SOBP	1.164	0.014	0.0011
distal SOBP	1.151	0.020	0.0028

***Compared to photon irradiation, two-tailed T test**

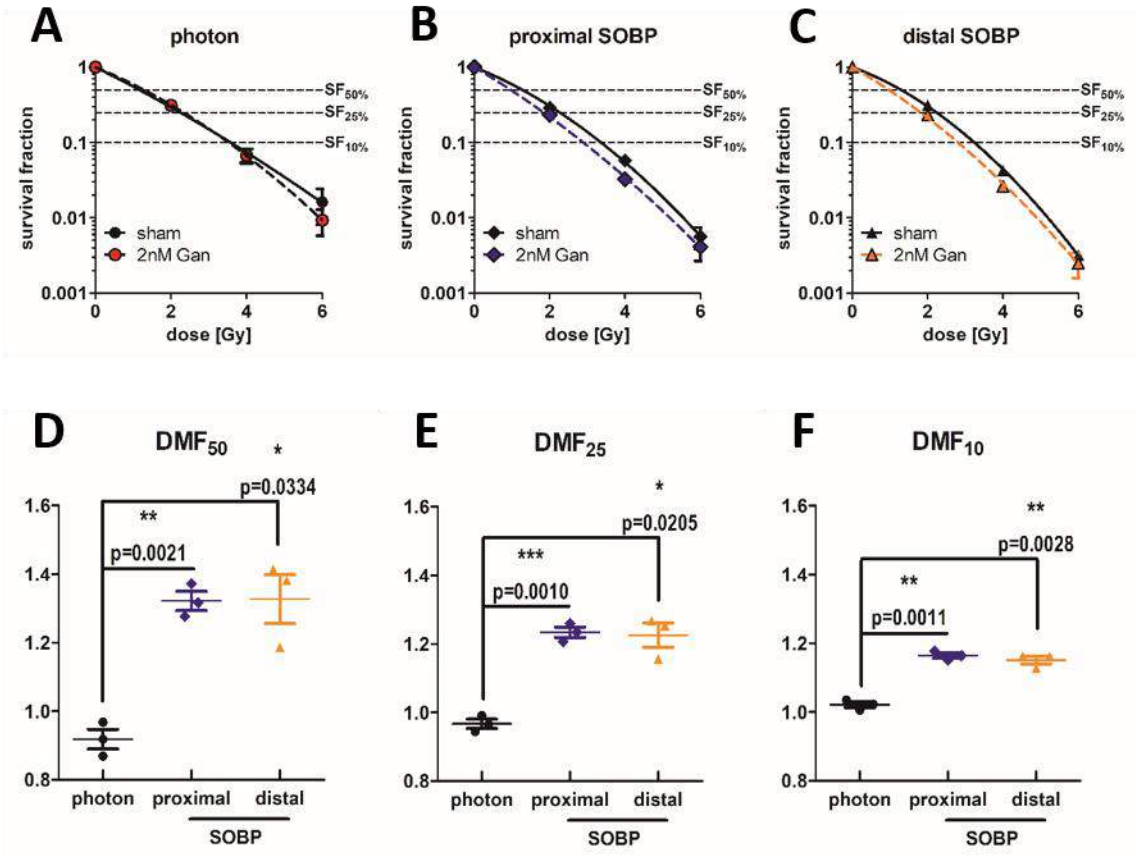

Fig. E1 Clonogenic cell survival - DMFs of A549

Fig. E1. Clonogenic cell survival of A549 cells treated with and without Ganetespib (2nM) and (A) 200kV reference photon or proton irradiation at the (B) proximal or (C) distal position of a SOBP with LETs of 2.1 and 4.5keV/µm, respectively. The sensitizing effect of Ganetespib was determined by the dose-modifying factor at (D) 50%, (E) 25%, and (F) 10% cell survival.

Tab. E2 Clonogenic cell survival RBEs and DMFs of FaDu

FaDu cells were pretreated 1hr prior to irradiation with 1nM Ganetespib or sham treatment. Subsequent to irradiation, a defined numbers of cells were plated in Ganetespib or sham-treated medium as described in Methods E4. Three independent clonogenic assay sets were generated and utilized to calculate the DMFs and RBEs at 50%, 25% and 10% cell survival, respectively.

DMF_{50}	mean	stdev	p value*
photon	1.058	0.021	
proximal SOBP	1.249	0.037	0.0044
distal SOBP	1.345	0.055	0.0139

DMF_{25}	mean	stdev	p value*
photon	0.997	0.010	
proximal SOBP	1.165	0.010	0.0003
distal SOBP	1.190	0.002	0.0010

DMF_{10}	mean	stdev	p value*
photon	0.960	0.008	
proximal SOBP	1.088	0.010	0.0004
distal SOBP	1.089	0.035	0.0248

***Compared to photon, two-tailed T test**

RBE_{50}	mean	stdev	p value
proximal SOBP, sham	1.095	0.041	0.0077
proximal SOBP, 1nM	1.293	0.035	
distal SOBP, sham	1.321	0.042	0.0233
distal SOBP, 1nM	1.679	0.087	

RBE_{25}	mean	stdev	p value
proximal SOBP, sham	1.161	0.011	0.0072
proximal SOBP, 1nM	1.358	0.027	
distal SOBP, sham	1.334	0.029	0.0017
distal SOBP, 1nM	1.592	0.030	

RBE_{10}	mean	stdev	p value
proximal SOBP, sham	1.218	0.015	0.0014
proximal SOBP, 1nM	1.381	0.020	
distal SOBP, sham	1.344	0.070	0.0544
distal SOBP, 1nM	1.523	0.030	

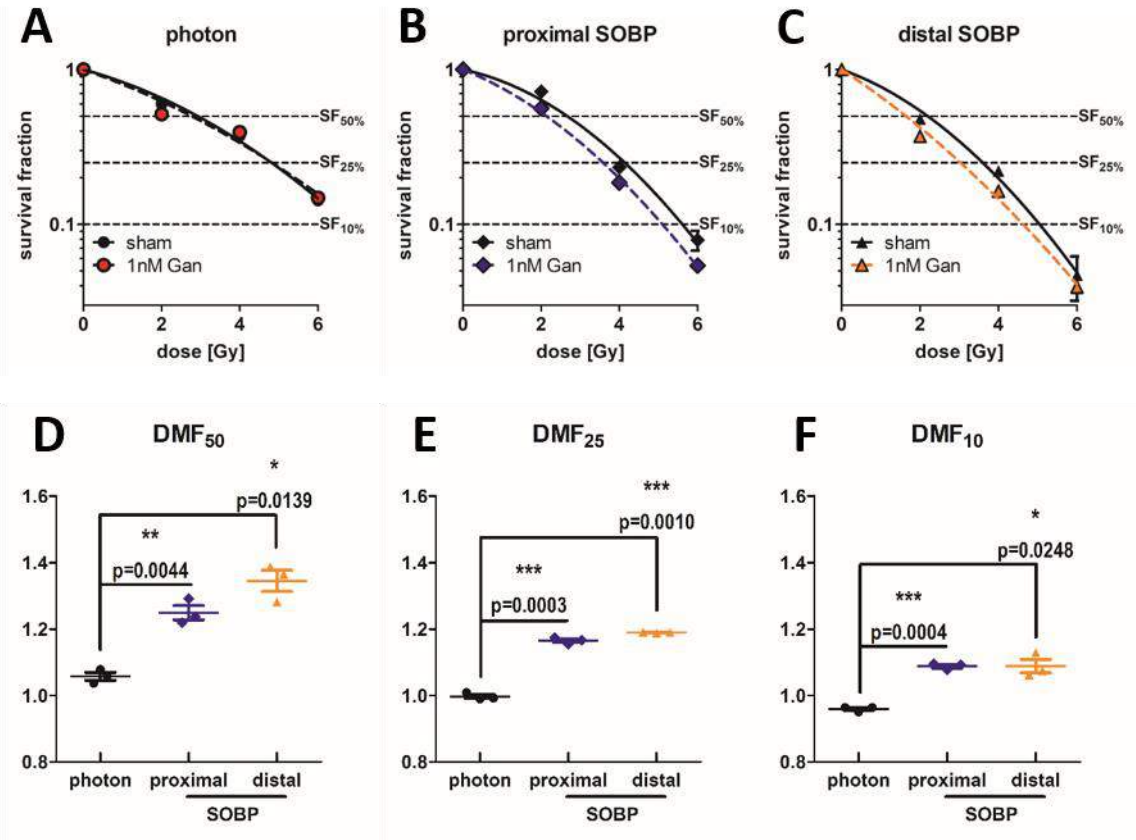

Fig. E2 Clonogenic cell survival - DMFs of FaDu

Fig. E2. Clonogenic cell survival of FaDu cells treated with and without Ganetespib (1nM) and (A) 200kV reference photon or proton irradiation at the (B) proximal or (C) distal position of a SOBP with LETs of 2.1 and 4.5keV/µm, respectively. The sensitizing effect of Ganetespib was determined by the dose-modifying factor at (D) 50%, (E) 25%, and (F) 10% cell survival.

Methods E1. Cell culture conditions and Ganetespib treatment

A549 and FaDu cells were cultured in RPMI 1640 containing 2mM L-glutamine, 10% FBS, 1mM sodium pyruvate, 25mM HEPES and 100U/ml penicillin, 100µg/ml streptomycin, and 0.25µg/ml amphotericin B. All cells were maintained at 37°C in a humidified atmosphere with 5% CO2. Prior to reaching confluency, cells were detached with trypsin-EDTA (0.05%) and subcultured in T25 and T75 cell culture flasks. Cells were regularly tested mycoplasma-free by a commercial kit (Lonza, MycoAlert) and during microscopy with DAPI (5µg/ml in PBS) as DNA-intercalating dye.

For drug treatment, Ganetespib was dissolved and diluted in DMSO to achieve a stock concentration of 10µM and stored at -20°C. For treatment, fresh supplemented medium was mixed with Ganetespib to achieve the defined concentration and used to replace the previous growth medium approximately 1 hour before irradiation. For sham treatment, the same amount of DMSO was added to the medium and exchanged similarly to exclude effects by DMSO itself. Cells were retained in drug/sham-containing medium until fixation/harvesting.

For experiments, exponentially growing cells were seeded in 9cm² slide flasks at a cell density of 5.000 to 15.000 cells/cm^2 and at least 36h prior to irradiation to allow cell cycle redistribution. For horizontal irradiation, the flasks had to be turned upwards and were consequently filled air-bubble free with the respective cell culture medium. This is essential to eliminate undesirable proton beam inaccuracies. After irradiation, the medium was completely removed and replaced with fresh drug/DMSO-containing medium to restore gas exchange.

Methods E2. Photon irradiation

For reference irradiation, 200kV photons were administered using a horizontal irradiation cabinet (YXLON, TU32-D03, 20mA, 5.5FOC, filtration: 3mm Be + 3mm Al + 0.5mm Cu). Slide flasks where positioned at 40cm distance from the beam exit window in a PMMA holder to provide a homogeneous distribution and a dose rate of 1.28Gy/min.

Methods E3. Proton irradiation

Slide flasks were submerged in a water/PMMA phantom at a proximal (55mm depth, LET 2.1keV/µm) and a distal position (105mm depth, LET 4.5keV/µm) of a SOBP. The SOBP ranged from 40 to 120mm depth which correlates to proton beam energies ranging from 66.5MeV to 136MeV. The submersion in water is essential to avoid uncertainties and mimic beam alterations by the aqueous environment in human tissue. Dose-averaged LETs are obtained from Monte Carlo simulations by the treatment planning software (RayStation). Protons were administered by spot scanning with dosimetric characterization and treatment plans as described in the following publication.

Reference

Clausen, M., et al. (2019). "Phantom design and dosimetric characterization for multiple simultaneous cell irradiations with active pencil beam scanning." Radiat Environ Biophys **58**(4): 563-573.

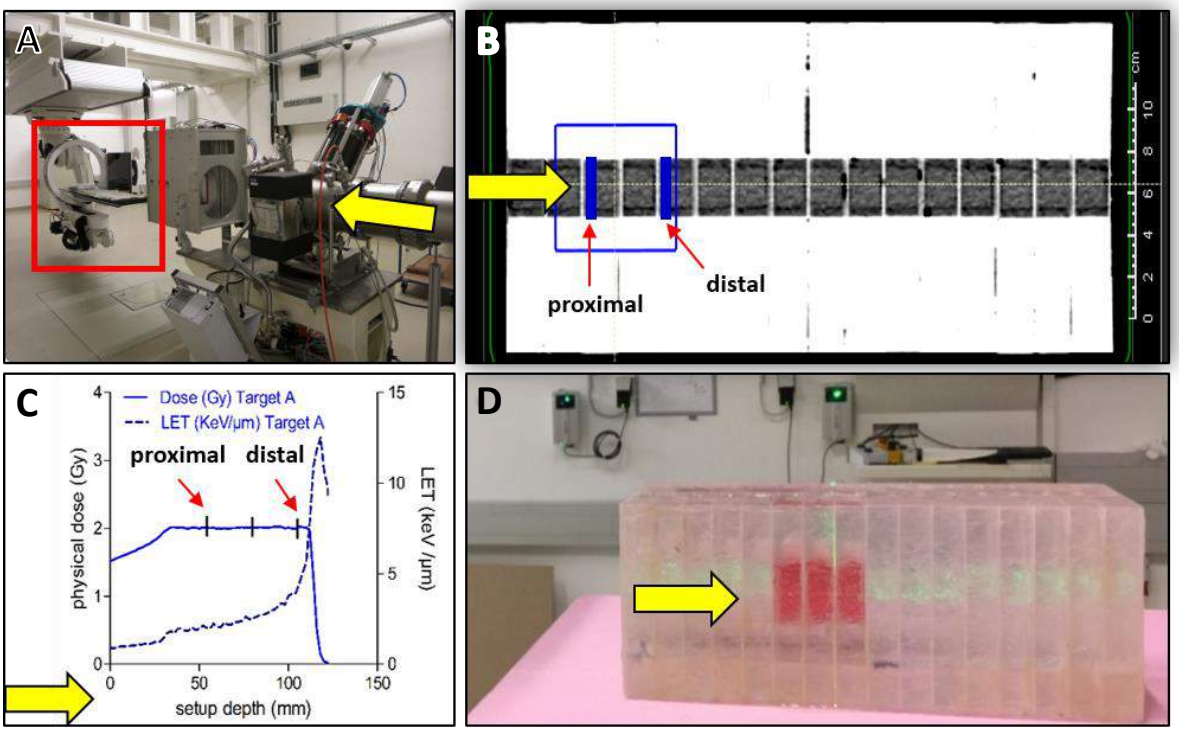

Fig. E3. Proton irradiation: instrumentation, phantom, and set-up

Fig. E3 (A) Fixed horizontal proton beam line. The phantom is placed on the robotic patent stage as marked with a red box. Beam direction is marked by a bright yellow arrow. (B) CT image (top view) of the PMMA/water phantom. The blue box illustrates the planned treatment field and the blue lines the position of the cell layers in the treatment field as indicated by red arrows. (C) Dose/LET simulation of the administered SOBP. The respective depths of the cell layers in the SOBP are indicated by red arrows and the corresponding dose-averaged LET illustrated by dashed line. (D) Accurate and reproducible alignment of the PMMA/water phantom was assured by positioning lasers in the treatment room.

Methods E4. Clonogenic cell survival assay

Exponentially growing cells were seeded and drug-treated as described above. Samples received an irradiation dose of 2Gy, 4Gy, and 6Gy, respectively. Reference non-irradiated samples (0Gy) were treated similarly and placed in the treatment room but not the beam line for a comparable time.

Subsequent to irradiation, the cells were detached from the slide flasks, counted, diluted accordingly and plated into 6-well plates in sextuplicate to achieve approximately 20 to 300 clones per well. After 7 (A549) respectively 14 days (FaDu), the cells were washed with PBS, fixed with MeOH:HAc (3:1), air-dried and subsequently stained with crystal violet (2%). Counting was performed manually in a blinded fashion and clones above 50 cells considered as a surviving cell.

The plating efficiency was derived from unirradiated samples and considered when calculating the fraction of surviving clones. The clonogenic assays were conducted in triplicate and a linear-quadratic model applied to allow calculation of DMF and RBE value according to following equations:

Linear-quadratic model:

$$y=\exp(-(\alpha * x + \beta * x^{\wedge}2)$$

y surviving fraction

x dose [Gray]

weighted by $1/y^2$ (minimizing relative squares)

Relative biological effectiveness:

$$RBE_y = dose_{y\ survival,\ photon,\ sham} / dose_{y\ survival,\ proton,\ sham}$$

respectively $dose_{y\ survival,\ photon,\ Ganetespib\text{-}treated} / dose_{y\ survival,\ proton,\ Ganetespib\text{-}treated}$

Dose-modifying factor:

$$DMF_y = dose_{y\ survival,\ sham} / dose_{y\ survival,\ Ganetespib\text{-}treated}$$

The dose to achieve 50%, 25%, and 10% survival rate corresponds to radiation doses administered by hypo- and regular fractionation schemes

For statistical analysis, DMF and RBE values were plotted in GraphPad Prism (Version 5.03) and two-tailed T-test applied.

Methods E5. Flow Cytometry – Cell cycle distribution

Cells were seeded, treated and irradiated with a dose of 4Gy as described above. Cells were harvested at 0h, 8h, 24h, and 48h to investigate the initial cell cycle distribution as well as irradiation-induced cell cycle alterations. Consequently, medium was replaced with BrdU-containing (10µM) medium 1hr before fixation to label DNA-polymerizing cells . At the respective time points, cells were trypsinised, washed with PBS, resuspended in 100µl PBS and fixated by addition of 1ml ice-cold EtOH (80%) while vortexing. Fixed cells were stored at -20°C until staining took place.

For staining, cells were washed with PBS, treated with 4M HCl (10min) to denature DNA, neutralized with PBS, incubated in blocking buffer (1hr, room temperature) and subsequently in staining solution (1.5hrs, dark, room temperature). Stained cells were washed with PBS, filtered through a cell strainer prior to flow cytometry (FACSCanto II, BD Biosciences) and the obtained data analyzed with FlowJo (Version 10.5.2).

For cell cycle analysis, a duplicate of A549 samples was seeded, irradiated, and stained independently. A third iteration could not be obtained due to strict limitations in proton beam time.

Hierarchy - Cell cycle distribution		**PI content**	**BrdU**
Single cells (FSC-H/FSC-A)			
→	G1 phase	2N	negative
→	S & early G2 phase	between 2N to 4N	positive
→	Late G2 & M phase	4N	negative

	Compound	**concentration**	**notes**
Blocking Buffer	BSA	0.5%	In 1xPBS
	Tween 20	0.1%	
	RNase A solution	0.5%	

	Compound	**concentration**	**notes**
Staining solution	antiBrdU-FITC	5µg/ml	in blocking buffer
	Propidium iodide	5µg/ml	
	RNase A solution	add. 1.5% (2% total)	

Methods E6. Western Blotting

A549 cells were handled similarly to the flow cytometry samples and seeded, treated, and irradiated with a dose of 4Gy as described above. Upon harvest at 8h, 24h, and 48h post-irradiation, cells were washed with PBS, lysis buffer added and distributed homogenously by a cell scraper. The obtained lysates were heated for 95°C (10min) and stored at -20°C. Due to similar cell numbers seeded and low protein concentrations as determined in pilot experiments, no dilution step was performed.

For SDS-PAGE, a separation gel (10% acrylamide, 1.5mm thick) with stacking gel on top was self-cast and a gel electrophoresis system utilized. Samples were mixed with 5x sample buffer (containing 10% freshly added 2-mercaptoethanol) and 30 µl of this mixture loaded per gel slot.

The proteins were electrophoretically separated (80V until front reaches separation gel, 100V until front reaches end of separation gel), blotted onto a PVDF membrane (70min, 80V), the membrane blocked for 1hr with blocking buffer and incubated overnight at 4°C with primary antibody diluted in blocking buffer. Membranes were washed three times for 10min each with TBS-T, incubated with secondary HRP-labelled antibody (1hr, room temperature) and subsequently washed again as described. Protein detection was accomplished by overlaying the membrane with HRP substrate and the resulting chemiluminescence imaged with a photo cabinet. Protein quantification of the respective bands was enabled by Fiji (Version 1.52g) and results normalized to the β-actin loading control as well as an untreated control sample which was included in each run in the first lane. This enables comparison of protein levels also in between membranes.

Reference
Schindelin, J., et al. (2012). "Fiji: an open-source platform for biological-image analysis." Nat Methods **9**(7): 676-682.

Buffer & PAGE gel compositions

	compound	concentration	notes
Lysis Buffer	Tris	50mM	Adjust pH to 6.8
	SDS	2%	
	Glycerin	10%	

	compound	concentration	notes
5x Loading Buffer	Tris	125mM	In deionized water pH 6.8
	SDS	5%	
	Glycerin	25%	
	Bromophenol blue	0.25%	
	2-Mercaptoethanol	10%	added right before mixing with samples

	compound	concentration	notes
APS (10%)	Ammonium persulfate	10%	in deionized water

	compound	concentration	notes
Running Gel Buffer	Tris	182g/l (1.5M)	Adjust pH to 8.8
	SDS	1g/l (0.1%)	

	compound	concentration	notes
Stacking Gel Buffer	Tris	60g/l (0.5M)	Adjust pH to 6.8
	SDS	1g/l (0.1%)	

	compound	concentration	notes
Running Buffer (10x)	Tris	30g/l	dissolved in 1l deionized water and diluted accordingly
	Glycine	144g/l	
	SDS	10g/l	

	compound	concentration	notes
Blotting Buffer (10x)	Tris	60g	dissolved in 1l deionized water and diluted accordingly
	Glycine	144g	
	SDS	2g	
	Methanol	20%	Added upon dilution

		volumes exemplified for 2 gels (1.5mm thick)	Final Concentration
Running Gel	deionized water	6.25ml	
	Running Gel Buffer (pH 8.8)	3.75ml	
	Acrylamide (30%)	5ml	10%
	TEMED	8.5µl	
	APS (10%)	85µl	
	overlay with 2-propanol and allow time for polymerization		
Stacking gel	deionized water	4.27ml	
	Stacking Gel Buffer (pH 6.8)	1.75ml	
	Acrylamide (30%)	0.91ml	3.9%
	TEMED	7µl	
	APS (10%)	35µl	
	insert sample comb (10wells) and allow time for polymerization		

	compound	concentration	notes
TBS-T (10x)	NaCl	80g/l	dissolved in 1l deionized water and adjust pH to 7.4
	KCl	2g/l	
	Tris	30g/L	
	Tween 20	0.1%	Added upon dilution

	compound	concentration	notes
Blocking Buffer	Non-fat dry milk	5%	Dissolved in TBS-T

Methods E7. Immunofluorescent nuclear γH2AX foci staining

A549 cells were seeded, treated and irradiated with a dose of 2Gy as described above. Cells were fixed 0.5h and 24h subsequent to irradiation with formaldehyde-based fixative (4%. 15min, 4°C) and slide flasks filled up with PBS for transport and storage at 4°C.

For staining, the upper chamber part was carefully removed and the fixed cells on the plastic microscopy slide made accessible for following staining steps. Homogenous antibody and dye distribution was assured by careful overlay with parafilm. Cells were incubated with blocking buffer (1hr, room temperature) followed by staining solution (overnight, 4°C, dark) and washed three times with blocking buffer. Slides were subsequently stained with DAPI (30min, room temperature, dark) before washing three times in PBS. Anti-fade mounting medium and a cover slip were subsequently overlayed and the edges sealed with nail polish for storage at 4°C in the dark.

Microscopy was accomplished by utilizing an immunofluorescence microscope (Leica Thunder). Foci numbers were assessed by applying the “find maxima”-function of open source Fiji (Version 1.52g) and the data plotted in GraphPad Prism (Version 5.03).

	Compound	concentration	notes
Blocking Buffer	FCS	10%	in 1x PBS
	Triton X-100	0.2%	

	Compound	concentration	notes
Staining solution	anti – γH2AX-AF647	1:50 (no absolute conc. retrievable)	in blocking buffer

	Compound	concentration	notes
DAPI solution	DAPI	5µg/ml	In 1x PBS

Reference
Schindelin, J., et al. (2012). "Fiji: an open-source platform for biological-image analysis." Nat Methods **9**(7): 676-682.

Methods E8 Lists of Reagents, Antibodies & Dyes, and Instruments

Reagents and consumables

Reagent	Manufacturer/supplier	Order code	Described in
Nunc™ Lab-Tek™ Flask on Slide	ThermoFisher Scientific	170920	E1
Ganetespib	Selleckchem	S1159	E1
Dimethyl Sulfoxide (DMSO)	Sigma-Aldrich	D8418-500ML	E1
RPMI-1640 (+ 2mM L-Glutamine)	Gibco	11875-085	E1
HEPES (1M, 40x)	Gibco	15630-080	E1
Sodium pyruvate (100mM, 100x)	Gibco	11360-039	E1
FBS, heat inactivated	Gibco	10500-064	E1
0.05% Trypsin-EDTA (1x)	Gibco	25300-054	E1
Anti-Anti (100x) Antibiotic-Antimycotic	Gibco	15240-062	E1
PBS (1x, Dulbecco`s Phosphate Buffered Saline)	Gibco	14190-094	E1
MycoAlert™ mycoplasma detection kit	Lonza	LT03-318	E1
Methanol 99%	Thommen-Furler AG	203-Cl03K	E4, E6
Acetic acid (glacial)	Merch KGaA	1.00063.1000	E4
Crystal violet	Sigma-Aldrich	C6158-100G	E4
Ethanol (absolute)	Honeywell	10311036	E5
Hydrochloric acid (32%)	Merck KGaA	1.00319.1000	E5
Bovine Serum Albumin	Sigma-Aldrich	A9647-500G	E5
5ml polystyrene round-bottom tube with cell-strainer cap	Falcon	352235	E5
RNase A Solution	Sigma-Aldrich	R6148-25ML	E5
10% SDS solution	Applichem	146132.1315	E6
Trizma base (Tris)	Sigma-Aldrich	93352-1KG	E6
Acrylamide BioAcryl-P (30%, 37.5:1)	AlfaAesar	J61505	E6
TEMED	Bio Rad	1610800	E6
Ammonium Persulfate (APS)	Bio Rad	1610700	E6
2-Mercaptoethanol	Sigma-Aldrich	M3148-250ML	E6
Glycerin	Fluka	49767	E6
Glycine	Sigma-Aldrich	G7126-1KG	E6
Cell scraper	TPP	99002	E6
Sodium chloride (NaCl(	Sigma-Aldrich	71380-1KG	E6
Potassium chloride (KCl)	Sigma-Aldrich	P9541-500G	E6
TWEEN 20	Sigma-Aldrich	P2287-100ML	E6
Western blotting membrane, PVDF, Hybond P, pore size 0.45µm	GE Healthcare	10600023	E6
Blotting-Grade Blocker – non-fat dry milk	Bio Rad	1706404	E6
ECL™ Prime Western Blotting Detection Reagents	GE Healthcare	RPN2232	E6
2-Propanol	Sigma-Aldrich	I9516-500ML	E6
Full Range Rainbow™ Recombinant Protein Molecular Weight Marker	GE Healthcare	RPN800E	E6

ROTI HistoFix 4%	Roth AG	P087.5	E7
Laboratory Film, Parafilm	Sigma-Aldrich	P6543-1EA	E7
Triton X-100	Sigma-Aldrich	T8787-100ML	E7
ProLong Gold Antifade reagent	Invitrogen	P36930	E7

Antibodies and dyes

Reagent	Species	stains…	Concentration applied	Supplier	Order code	Method
5-Bromo-2'-deoxyuridine (BrdU)		incorporated into polymerizing DNA	10µM	Sigma-Aldrich	B5002-5G	E5
anti-BrdU-FITC	mouse	BrdU	5µg/ml	Roche	11202693001	E5
Propidium iodide		DNA	5µg/ ml	Fluka	81845-100MG	E5
anti-Rabbit-IgG-HRP	mouse	rabbit IgG	1:3000	Santa Cruz Biotechnology	sc-2357	E6
anti-mouse-IgG-HRP	sheep	mouse IgG	1:3000	GE Healthcare	NA931V	E6
anti-Rad51	rabbit	Rad51	1:1000	BioAcademia	70-002	E6
anti-β-actin	mouse	β-actin (loading control)	1:4000	Sigma-Aldrich	A5441-.2ML	E6
4',6-Diamidino-2-phenylindole dihydrochloride (DAPI)		DNA	5µg/ml	Sigma-Aldrich	D9542-10MG	E7
anti H2AX(pS139)-AF647	mouse	H2AX(pS139)	1:50	BD Pharmingen	560447	E7

Instruments

Name	Supplier	Method
Vi-Cell XR (cell counter)	***Beckman Coulter Life Sciences***	E4
FACSCanto II (flow cytometer)	***BD Biosciences***	E5
FUSION FX7 edge (Photo cabinet)	***Vilber***	E6
Mini-PROTEAN TetraCell	***BioRad***	E6
Mini-PROTEAN TetraCell Casting Module	***BioRad***	E6
PowerPac HC (power Supply)	***BioRad***	E6
THUNDER (immunofluorescence microscope)	***Leica***	E7

3.2 Combined Treatment Modalities for High-Energy Proton Irradiation: Exploiting Specific DNA Repair Dependencies

Simon Deycmar[1] and Martin Pruschy[1]

[1]Department of Radiation Oncology, Laboratory for Applied Radiobiology, University Hospital Zurich, Zurich, Switzerland

Status of the manuscript: Published in IJPT 2018

Author contribution Simon Deycmar:

- Literature Research
- Drafting and proofreading manuscript
- Minor revisions of the manuscript

Combined Treatment Modalities for High-Energy Proton Irradiation: Exploiting Specific DNA Repair Dependencies

Simon Deycmar, MSc[1]; Martin Pruschy, PhD[1]

[1]Department of Radiation Oncology, Laboratory for Applied Radiobiology, University Hospital Zurich, University of Zurich, Zurich, Switzerland

Abstract

DNA repair deficiencies and genome instability are common features and hallmarks of cancer and are ubiquitously found in the full spectrum of malignant diseases. Heritable DNA repair deficiencies, for example, due to *BRCA1* and *BRCA2* mutations, and subsequent loss of heterozygosity in mammary, ovarian, and prostate carcinoma, are risk factors for the early development of cancer. Despite their detrimental role in tumorigenesis, these deficiencies also provide novel opportunities for treatment options. Current and future pharmacologic approaches in medical oncology rely on the exploitation of such genetically defined, tumor-specific Achilles' heels and integrate the genetic background of a tumor into the treatment strategy. For example, homologous recombination–corrupted, BRCA1/2-mutated tumors are becoming hypersensitive to inhibitors of an additional DNA-damage-repair mechanism and are successfully treated with respective molecular targeting agents such as PARP1 inhibitors.

Patient stratification in radiation oncology today is primarily based on clinical parameters and uses highly sophisticated diagnostic imaging for treatment planning on the individual level. Radiation oncology only minimally takes the genetic makeup of tumors into account, and little attention has been given to the fact that the different modalities of ionizing radiation, such as photon and proton irradiation, may also induce differential damages and biological processes, which might again be influenced by the genetic makeup and mutational status of the tumor. However, radiation oncology is nowadays challenged to understand subtle differences induced by the different qualities of ionizing radiation, and to efficiently exploit and to integrate these differential responses in a personalized treatment approach alone and as part of combined treatment modalities with pharmacologic agents. Here we will review recent insights on the differential DNA damage responses to photon and proton irradiation and discuss their implications for combined treatment modalities with chemotherapeutical agents and small molecular targeting compounds.

Keywords: proton irradiation; combined treatment modality DNA damage response; homologous recombination

Submitted 27 Mar 2018
Accepted 05 Jul 2018
Published 21 Sep 2018

Corresponding Author:
Martin Pruschy
Department of Radiation Oncology
University Hospital Zurich
Raemistr. 100
CH-8091 Zurich, Switzerland
Phone: +41 44 255 8549
Fax: +41 44 255 4435
martin.pruschy@usz.ch

Review Article

DOI
10.14338/IJPT-18-00020.1

http://theijpt.org

Introduction

Approximately 50% of all cancer patients have an indication for radiation therapy at least once during the course of their disease, with an absolute number of patients steadily increasing assuming overall cancer rates remain unchanged ([Borras et al [1] and

references therein). The main pillar of radiotherapy is photon irradiation with linear accelerators as source of ionizing radiation. Nevertheless, charged-particle–based approaches such as proton or carbon beams are stepping out of their niche and are becoming a reasonable alternative [2–4]. The high-dose deposition at the distal end followed by a steep decline as well as minimal lateral scattering allows superior tissue sparing and a dose reduction outside the planned margin [5]. The reduced volume of healthy tissue exposed to intermediate and low doses suggests a reduced risk of secondary malignancies accompanied by a reduced co-irradiation of dose-limiting organs-at-risk such as brain stem, spinal cord, oral cavity, or the optic nerve [6, 7]. Hence, current treatment decisions for particle beam therapy are primarily based on vulnerable tumor locations near organs-at-risk, and treated entities comprise uveal melanoma, skull-based and intracranial tumors, prostate and head and neck tumors [8, 9]. Moreover, the most common solid tumors in pediatric patients arise in the central nervous system [10] and a long life expectance after treatment becomes aggravated by minimal safety margins in a delicate developmental stage. Since pediatric patients are prone to impaired brain development as well as progressive cognitive decline after conventional cranial radiation therapy, particle beam treatment emerges as a beneficial tool to reduce side effects in adult and especially in pediatric patients [11, 12].

Proton radiation therapy is characterized by its advantageous dose deposition and physics attributes, thereby taking primarily clinical aspects for treatment stratification into consideration. Preclinical experiments revealed an enhanced efficacy for proton versus photon irradiation. However, the cause for this increased efficacy is insufficiently known and differential biological stress responses induced by photon-based and particle-based irradiation are minimally investigated so far [13]. Differential "biologies" induced by the different sources of ionizing radiation may become relevant for the determination of optimal therapeutic strategies and be important for the concept of personalized medicine. It may allow adapting the therapy of an individual patient situation, taking both clinical and physical but also biological parameters into account.

Here we will provide an overview on recent preclinical insights on the differential DNA damage responses to photon and proton irradiation and their implications for combined treatment modalities with chemotherapeutical agents and small molecular targeting compounds.

Differential Biological Responses to Photon and Proton Irradiation

Intense preclinical in vitro and in vivo studies comparing photon and proton irradiation have illustrated differing relative biological effectiveness (RBEs) in dependence of endpoint, tissue, and positioning in the spread-out Bragg peak (SOBP) [14–17]. RBE deviations result from and clearly point to differential physicochemical and subsequent differential responses on the molecular and cellular level to photon versus proton irradiation. For example, faster production of reactive oxygen species [18] and enhanced levels of cell apoptosis [19] were identified after irradiation with low linear energy transfer (LET) proton irradiation in comparison to photon irradiation. Furthermore, differential gene expression in response to the 2 modalities of irradiation and increasing RBEs of cell killing along the axis of an SOBP also suggest different mechanisms being induced by photon and proton irradiation, which could be exploited as part of a combined treatment modality [20, 21]. These preclinical insights contrast with the generic constant RBE of 1.1 still applied in clinical practice [13, 22].

Exploitation of Differential DNA Repair Dependences

Genetically defined Chinese hamster ovary (CHO) cell lines with defects in different DNA repair systems were originally used to identify and characterize DNA double-strand break (DSB) machineries relevant for the repair of photon irradiation–induced DNA damage. These cell lines are interesting tools to characterize differential DNA damage responses and dependencies for specific DNA repair machineries in response to different qualities of ionizing radiation [23–25].

Cells have evolved 2 major DSB repair pathways, namely, the more error-prone nonhomologous end joining (NHEJ) process and homologous recombination repair (HRR) [26]. NHEJ is active throughout the cell cycle and is responsible for the repair of most ionizing radiation–induced DSBs in eukaryotic cells. Although very efficient in a quantitative way, the quality of repair by NHEJ can steadily decrease with increasing amounts of DNA damage [27].

Double-strand break repair by NHEJ relies on the initial binding of the Ku70/80 heterodimer, which results in the recruitment of DNA-dependent protein kinase, catalytic subunit, also known as DNA-PKcs. If required, specialized DNA nucleases and polymerases process the "dirty" ends before relegation of the broken strands by XRCC4–DNA ligase IV complex. HRR is initiated through the recognition of DSBs by the MRN complex followed by MRN- and CtIP-dependent 3′-5′ DNA resection [28]. The resulting single-stranded DNA (ssDNA) overhangs are first stabilized by the heterotrimeric ssDNA-binding complex RPA, which is later on replaced by Rad51 with the help of BRCA2. Rad51 nucleoprotein filaments then search for homology

and form Holliday junctions when complementary sequences are found. After ideally error-free rewriting of the damaged DNA site by DNA polymerases, these structures get resolved by several Holliday junction processing factors, including Rad51C-XRCC3 complex [29–31].

Detection and quantification of ionizing radiation–induced and subsequently repaired DNA DSBs represent major challenges in experimental radiobiology. Ideally, several complementary approaches should be combined that include both direct determination of DNA damage at the molecular level, including chromosomal aberrations, and indirect DNA damage–related signaling readouts, which are more easily detectable, such as γH2AX foci. Phosphorylation of the histone variant H2AX has become a powerful tool to monitor DNA DSBs induced by ionizing radiation and was named γH2AX because it was first observed in cells exposed to γ-rays [32]. Large numbers of γH2AX molecules form at the site of DNA breaks and create bright foci that allow detection of individual DSBs. Thereby γH2AX foci can be easily counted by using specific antibodies. γH2AX foci counting has become a major experimental readout in basic and translational radiobiology to probe induction and repair of DNA DSBs at different time points following irradiation. Nevertheless, it only remains an indirect biomarker for DNA DSBs [33].

Using this set of CHO cells with defects in either the NHEJ (XR-C1; DNA-PKcs–deficient CHO cells) or HRR machinery (XRCC3–/–), our own group recently demonstrated differential DNA repair pathway choices in response to photon and proton irradiation. To avoid additional influences due to increasing LETs across the SOBP, cells were always irradiated in the middle of an SOBP with a length of 5 cm and a maximum proton energy of 138 MeV (Center for Proton Therapy at the Paul Scherrer Institute, PSI-Villigen, Switzerland) [34]. The formation of so-called γH2AX foci at the site of DSBs was used to quantify irradiation-induced DSBs. No significant differences in the number of DNA DSBs induced by the 2 types of irradiation could be detected; however, the repair kinetics in XRCC3-lacking cells were clearly delayed after proton irradiation with elevated numbers of residual γH2AX foci after irradiation. Additionally, the HRR-defective cells proved to be markedly hypersensitive to proton irradiation, resulting in an increased RBE in comparison to the RBE determined in wild-type cells. The RBE (survival fraction as endpoint) increased from $RBE_{37\%}$: 1.25 ± 0.05 and $RBE_{10\%}$: 1.29 ± 0.04 in the wild-type cells to $RBE_{37\%}$: 1.54 ± 0.10 and $RBE_{10\%}$: 1.44 ± 0.06 in the HRR-deficient cells. While DNA-PKcs–defective cells were overall more sensitive to both types of ionizing radiation than wild-type cells, defective DNA-PKcs did not result in hypersensitivity towards proton irradiation. Even though these quantitative readouts were only correlated with the γH2AX-foci assay, these results indicate a differential quality of DNA damage by proton versus photon irradiation with a specific requirement for HRR for efficient DNA repair and enhanced cell survival in response to low LET proton irradiation. Interestingly, differential patterns of chromosomal aberrations were also identified in response to the 2 types of ionizing radiation and in dependence of the HRR status. Of note, lack of NHEJ activity in genetically defined knockout mouse embryo fibroblasts was shown to play the more important role for cell survival in response to high LET irradiation than to photon irradiation and thus, targeting of NHEJ might preferentially sensitize to high LET irradiation [35]. A differential response and involvement of the 2 major DNA DSB machineries in dependence of high versus low LET radiation might be further affected by the mutational status of the targeted cells and additional DNA DSB repair backup mechanisms, such as alternative or B-NHEJ [36].

HRR dependence for proton irradiation–induced DNA damage was also tested in established cancer cell lines. Interestingly and in contrast to their wild-type counterpart cell line, ovarian carcinoma cells lacking intact BRCA2 expression were also hypersensitive towards proton in comparison to photon irradiation, which corroborated this hypothesis originally tested in the CHO-based model cell system. Likewise, A549 non-small cell lung cancer cells depleted of the HRR essential protein Rad51 were clearly hypersensitive to proton irradiation in comparison to control cells [37]. Rad51 downregulation also induced a tremendous delay in γH2AX-foci repair kinetics. As such, a preference of proton-induced DNA damage towards HRR might become relevant for clinical stratification of patients carrying mutations in this DNA repair pathway.

Combined Treatment Modalities with HRR-Interfering Agents

Likewise, a state of corrupted HRR activity and thus enhanced sensitivity towards proton irradiation could be achieved by a combined treatment modality with specific inhibitors of HRR. Direct pharmacologic targeting of the HRR machinery has proven to be largely unsuccessful in the past years. However, several chemotherapeutic agents exist, which eventually downregulate Rad51 protein levels—including the broad-range clinically relevant histone deacetylase inhibitor SAHA (Vorinostat) [38]—and thereby also reduce HRR. Low dose exposure to SAHA for 24 hours was sufficient to reduce Rad51 levels down to approximately 10% of the basal level, without affecting critical elements of NHEJ such as Ku80 or DNA-PKcs protein levels. Similar to the results obtained in the tumor cells with a corrupted HRR machinery, DNA repair was also strongly delayed in

SAHA-pretreated cells after proton irradiation, but only minimally after photon irradiation, corroborating this HRR-oriented mechanism of action of SAHA.

Recently, Gerelchuluun et al [39] investigated SAHA-based radiosensitization in lung carcinoma and normal human fibroblasts irradiated with photon, low LET proton, and carbon ion–based irradiation. SAHA sensitized to low LET radiation to a greater extent than to carbon ion–based irradiation and even more so to proton irradiation at low SAHA concentrations. Even though they could not directly link their results to HRR, SAHA also delayed DNA repair kinetics. More important, SAHA-induced radiosensitization was not prominent in normal fibroblasts, which suggests a selective cancer cell–related mechanism, of interest towards an enhanced therapeutic window.

Complementary experiments were performed with pharmacologic agents selectively inhibiting NHEJ. Interestingly, the DNA-PKCs inhibitor NU7026 sensitized lung carcinoma and glioblastoma cells in response to both types of irradiation, yet to a higher extent for photon irradiation, with a dose modifying factor at 10% survival (DMF_{10}) of 1.91 $\pm$ 0.05, than for proton radiation (1.49 $\pm$ 0.06) for lung and with a DMF_{10} of 1.49 $\pm$ 0.02 versus 1.2 $\pm$ 0.11 for the glioblastoma cells. Strikingly, NU7026 treatment only minimally interfered with repair of proton-induced DNA damage, while more than half of γH2AX foci remained unrepaired after 24 hours in the photon-irradiated cells [37]. Thus, while inhibitors of NHEJ more specifically sensitize to photon irradiation, pharmacologic agents that directly downregulate the DNA repair capacity of HRR might more specifically sensitize to proton irradiation.

An RBE-oriented lung cancer cell line screen performed by Liu et al [40] (research group of Henning Willers at Massachusetts General Hospital, Boston) also linked defects in a specific DNA-damage-repair machinery to hypersensitivity to proton irradiation [40]. A selection of NSCLC cell lines was irradiated in the middle of an SOBP, and in 3 of 17 cell lines an increased RBE could be linked to alterations of the Fanconi anemia (FA)/BRCA pathway of DNA repair, which is part of replication-coupled HRR [40]. Control experiments performed in wild-type and FANCD2-depleted but otherwise isogenic lung cancer cells validated the relevance of this pathway and also supported the hypothesis of specific proton hypersensitivity due to HRR defects. Furthermore, the role of FA/BRCA pathway in hypersensitization against proton irradiation was further backed up by the same group focusing on 2 additional downstream elements of this pathway, namely, Slx4(FancP) and Mus81 [41]. Slx4- and Mus81-deficient cells also demonstrated enhanced sensitivity towards proton irradiation as compared to their isogenic wild-type counterpart cells. As such, genomic profiling of DNA damage repair–associated genes might become relevant in the future for clinical stratification of patients and be part of personalized biology-adapted treatment regimens.

DNA damage can be traced in vitro and ex vivo by the generation of so-called foci, which represent specific protein aggregates at the site of DSBs. Interestingly, these studies also revealed that proton irradiation– and photon irradiation–induced foci exhibit a different size, in particular in dependence of the HRR status. As suggested, DNA repair–associated foci could therefore be used as functional biomarker to identify repair-defective and proton irradiation hypersensitive tumors [40, 42]. It will be of interest to determine the phenotype of proton-induced foci in genetically HRR intact cancer cells but cotreated with HRR-directed pharmaceutical inhibitors. A large amount of data and calculations on DNA damage in response to particle irradiation exist, which are derived from different sources of ionizing radiation and which have been incorporated into relevant modeling studies [43, 44]. However, we have only limited experimental data on differential DNA damage, which were obtained in parallel in the same genetically defined cell systems with specific DNA damage repair deficiencies, and which were induced by clinically relevant proton and photon irradiation. The initial amount of DSBs per physical dose of proton irradiation is similar to the number of lesions caused by the same dose of photon irradiation, based on the initial formation of γH2AX foci [34, 37]. However, proton irradiation might cause slightly more complex clustered DNA damage, which is most probably due to the slightly increased LET values even in the middle of the SOBP. While DNA DSB-proficient cells repair these damages equally well, FA/BRCA pathway– and thus replication-coupled HRR-corrupted cells encounter greater difficulties in repairing replication forks that collide with clustered proton damage. Eventually, impaired repair in these mutated tumor cells will translate into a hypersensitivity towards proton irradiation. As such, the genetic status could make tumors more susceptible to proton radiation therapy and could contribute to the definition of a variable instead of a generic RBE [45].

Similar to SAHA, other clinically relevant pharmaceutical agents and compounds in early developmental stage exist, which directly or indirectly reduce HRR activity and have been tested in combination with photon irradiation. For example, Gleevec (Novartis Pharma, Switzerland), which is used to treat chronic myelogenous leukemia, gastrointestinal stromal tumors, and a number of other malignancies, also reduces RAD51 and sensitizes for ionizing radiation [46]. Likewise, inhibitors of the hepatocyte growth factor receptor MET (mesenchymal-epithelial transition), which is overexpressed in numerous types of human tumors and considered a prime target in clinical oncology, sensitize for ionizing radiation via

reduced formation of the RAD51-BRCA2 complex [47]. Even classic chemotherapeutic agents like gemcitabine, which are clinically applied in combination with radiation therapy, sensitize via selective targeting of HRR [48]. As such, treatment combinations with agents cotargeting HRR might require a reduced dose of proton radiation to achieve the same treatment outcome as with photon irradiation. On the other hand, agents targeting NHEJ might be less effective in combination with proton irradiation. Most combined treatment modalities have been investigated with photon irradiation. It will be now important to qualitatively as well as quantitatively determine the differential outcome combining these agents also with clinically relevant proton irradiation.

ADDITIONAL INFORMATION AND DECLARATIONS

Conflicts of Interest: The authors have no conflicts of interest to disclose.
Acknowledgments: Simon Deycmar is an early stage researcher and Martin Pruschy is a beneficiary in the RADIATE-ITN and as such have received funding from the European Union's Horizon 2020 research and innovation programme under the Marie Sklodowska-Curie grant agreement No 642623.

References

1. Borras JM, Lievens Y, Barton M, Corral J, Ferlay J, Bray F, Grau C. How many new cancer patients in Europe will require radiotherapy by 2025: an ESTRO-HERO analysis. *Radiother Oncol.* 2016;119:5–11.
2. Wilson RR. Radiological use of fast protons. *Radiology.* 1946;47:487–91.
3. Durante M, Loeffler JS. Charged particles in radiation oncology. *Nat Rev Clin Oncol.* 2010;7:37–43.
4. Durante M, Orecchia R, Loeffler JS. Charged-particle therapy in cancer: clinical uses and future perspectives. *Nat Rev Clin Oncol.* 2017;14:483–95.
5. Baumann M, Krause M, Overgaard J, Debus J, Bentzen SM, Daartz J, Richter C, Zips D, Bortfeld T. Radiation oncology in the era of precision medicine. *Nat Rev Cancer.* 2016;16:234–49.
6. Romesser PB, Cahlon O, Scher E, Zhou Y, Berry SL, Rybkin A, Sine KM, Tang S, Sherman EJ, Wong R, Lee NY. Proton beam radiation therapy results in significantly reduced toxicity compared with intensity-modulated radiation therapy for head and neck tumors that require ipsilateral radiation. *Radiother Oncol.* 2016;118:286–92.
7. Vogel J, Both S, Kirk M, Chao HH, Bagatell R, Li Y, Womer R, Balamuth N, Reilly A, Kurtz G, Lustig R, Tochner Z, Hill-Kayser C. Proton therapy for pediatric head and neck malignancies. *Pediatr Blood Cancer.* 2018;65.
8. Schulz-Ertner D, Tsujii H. Particle radiation therapy using proton and heavier ion beams. *J Clin Oncol.* 2007;25:953–64.
9. Schiller KC, Habl G, Combs SE. Protons, photons, and the prostate: is there emerging evidence in the ongoing discussion on particle therapy for the treatment of prostate cancer? *Front Oncol.* 2016;6:8.
10. International Agency for Research on Cancer. In: Stewart B, Wild C, eds. *World Cancer Report 2014.* Geneva, Switzerland: WHO Press; 2014.
11. Mizumoto M, Oshiro Y, Yamamoto T, Kohzuki H, Sakurai H. Proton beam therapy for pediatric brain tumor. *Neurol Med Chir (Tokyo).* 2017;57:343–55.
12. Sands SA. Proton beam radiation therapy: the future may prove brighter for pediatric patients with brain tumors. *J Clin Oncol.* 2016;34:1024–6.
13. Paganetti H. Relative biological effectiveness (RBE) values for proton beam therapy: variations as a function of biological endpoint, dose, and linear energy transfer. *Phys Med Biol.* 2014;59:R419–72.
14. Urano M, Verhey LJ, Goitein M, Tepper JE, Suit HD, Mendiondo O, Gragoudas ES, Koehler A. Relative biological effectiveness of modulated proton beams in various murine tissues. *Int J Radiat Oncol Biol Phys.* 1984;10:509–14.
15. Hojo H, Dohmae T, Hotta K, Kohno R, Motegi A, Yagishita A, Makinoshima H, Tsuchihara K, Akimoto T. Difference in the relative biological effectiveness and DNA damage repair processes in response to proton beam therapy according to the positions of the spread out Bragg peak. *Radiat Oncol.* 2017;12:111.
16. Tang JT, Inoue T, Inoue T, Yamazaki H, Fukushima S, Fournier-Bidoz N, Koizumi M, Ozeki S, Hatanaka K. Comparison of radiobiological effective depths in 65-MeV modulated proton beams. *Br J Cancer.* 1997;76:220–5.

17. Britten RA, Nazaryan V, Davis LK, Klein SB, Nichiporov D, Mendonca MS, Wolanski M, Nie X, George J, Keppel C. Variations in the RBE for cell killing along the depth-dose profile of a modulated proton therapy beam. *Radiat Res*. 2013; 179:21–8.
18. Giedzinski E, Rola R, Fike JR, Limoli CL. Efficient production of reactive oxygen species in neural precursor cells after exposure to 250 MeV protons. *Radiat Res*. 2005;164:540–4.
19. Green LM, Murray DK, Bant AM, Kazarians G, Moyers MF, Nelson GA, Tran DT. Response of thyroid follicular cells to gamma irradiation compared to proton irradiation, I: initial characterization of DNA damage, micronucleus formation, apoptosis, cell survival, and cell cycle phase redistribution. *Radiat Res*. 2001;155:32–42.
20. Biaggi M, Ballarini F, Burkard W, Egger E, Ferrari A, Ottolenghi A. Physical and biophysical characteristics of a fully modulated 72 MeV therapeutic proton beam: model predictions and experimental data. *Nucl Instrum Methods Phys Res B*. 1999;159:89–100.
21. Nielsen S, Bassler N, Grzanka L, Swakon J, Olko P, Andreassen CN, Overgaard J, Alsner J, Sorensen BS. Differential gene expression in primary fibroblasts induced by proton and cobalt-60 beam irradiation. *Acta Oncol*. 2017;56:1406–12.
22. Paganetti H, Niemierko A, Ancukiewicz M, Gerweck LE, Goitein M, Loeffler JS, Suit HD. Relative biological effectiveness (RBE) values for proton beam therapy. *Int J Radiat Oncol Biol Phys*. 2002;53:407–21.
23. Rothkamm K, Kruger I, Thompson LH, Lobrich M. Pathways of DNA double-strand break repair during the mammalian cell cycle. *Mol Cell Biol*. 2003;23:5706–15.
24. Hinz JM, Yamada NA, Salazar EP, Tebbs RS, Thompson LH. Influence of double-strand-break repair pathways on radiosensitivity throughout the cell cycle in CHO cells. *DNA Repair (Amst)*. 2005;4:782–92.
25. Kuhfittig-Kulle S, Feldmann E, Odersky A, Kuliczkowska A, Goedecke W, Eggert A, Pfeiffer P. The mutagenic potential of non-homologous end joining in the absence of the NHEJ core factors Ku70/80, DNA-PKcs and XRCC4-LigIV. *Mutagenesis*. 2007;22:217–33.
26. Iliakis G, Murmann T, Soni A. Alternative end-joining repair pathways are the ultimate backup for abrogated classical non-homologous end-joining and homologous recombination repair: implications for the formation of chromosome translocations. *Mutat Res Genet Toxicol Environ Mutagen*. 2015;793:166–75.
27. Povirk LF. Biochemical mechanisms of chromosomal translocations resulting from DNA double-strand breaks. *DNA Repair (Amst)*. 2006;5:1199–212.
28. Sartori AA, Lukas C, Coates J, Mistrik M, Fu S, Bartek J, Baer R, Lukas J, Jackson SP. Human CtIP promotes DNA end resection. *Nature*. 2007;450:509–14.
29. Hiom K. Coping with DNA double strand breaks. *DNA Repair (Amst)*. 2010;9:1256–63.
30. Lieber MR. The mechanism of double-strand DNA break repair by the nonhomologous DNA end-joining pathway. *Annu Rev Biochem*. 2010;79:181–211.
31. Pardo B, Gomez-Gonzalez B, Aguilera A. DNA repair in mammalian cells: DNA double-strand break repair: how to fix a broken relationship. *Cell Mol Life Sci*. 2009;66:1039–56.
32. Rogakou EP, Boon C, Redon C, Bonner WM. Megabase chromatin domains involved in DNA double-strand breaks in vivo. *J Cell Biol*. 1999;146:905–16.
33. Ivashkevich A, Redon CE, Nakamura AJ, Martin RF, Martin OA. Use of the gamma-H2AX assay to monitor DNA damage and repair in translational cancer research. *Cancer Lett*. 2012;327:123–33.
34. Grosse N, Fontana AO, Hug EB, Lomax A, Coray A, Augsburger M, Paganetti H, Sartori AA, Pruschy M. Deficiency in homologous recombination renders Mammalian cells more sensitive to proton versus photon irradiation. *Int J Radiat Oncol Biol Phys*. 2014;88:175–81.
35. Takahashi A, Kubo M, Ma H, Nakagawa A, Yoshida Y, Isono M, Kanai T, Ohno T, Furusawa Y, Funayama T, Kobayashi Y, Nakano T. Nonhomologous end-joining repair plays a more important role than homologous recombination repair in defining radiosensitivity after exposure to high-LET radiation. *Radiat Res*. 2014;182:338–44.
36. Mladenov E, Iliakis G. Induction and repair of DNA double strand breaks: the increasing spectrum of non-homologous end joining pathways. *Mutat Res*. 2011;711:61–72.
37. Fontana AO, Augsburger MA, Grosse N, Guckenberger M, Lomax AJ, Sartori AA, Pruschy MN. Differential DNA repair pathway choice in cancer cells after proton- and photon-irradiation. *Radiother Oncol*. 2015;116:374–80.

38. Chen X, Wong P, Radany EH, Stark JM, Laulier C, Wong JY. Suberoylanilide hydroxamic acid as a radiosensitizer through modulation of RAD51 protein and inhibition of homology-directed repair in multiple myeloma. *Mol Cancer Res*. 2012;10:1052–64.
39. Gerelchuluun A, Maeda J, Manabe E, Brents CA, Sakae T, Fujimori A, Chen DJ, Tsuboi K, Kato TA. Histone deacetylase inhibitor induced radiation sensitization effects on human cancer cells after photon and hadron radiation exposure. *Int J Mol Sci*. 2018;19:pii:E496.
40. Liu Q, Ghosh P, Magpayo N, Testa M, Tang S, Gheorghiu L, Biggs P, Paganetti H, Efstathiou JA, Lu HM, Held KD, Willers H. Lung cancer cell line screen links fanconi anemia/BRCA pathway defects to increased relative biological effectiveness of proton radiation. *Int J Radiat Oncol Biol Phys*. 2015;91:1081–9.
41. Liu Q, Underwood TS, Kung J, Wang M, Lu HM, Paganetti H, Held KD, Hong TS, Efstathiou JA, Willers H. Disruption of SLX4-MUS81 function increases the relative biological effectiveness of proton radiation. *Int J Radiat Oncol Biol Phys*. 2016;95:78–85.
42. Costes SV, Boissiere A, Ravani S, Romano R, Parvin B, Barcellos-Hoff MH. Imaging features that discriminate between foci induced by high- and low-LET radiation in human fibroblasts. *Radiat Res*. 2006;165:505–15.
43. Friedland W, Jacob P, Bernhardt P, Paretzke HG, Dingfelder M. Simulation of DNA damage after proton irradiation. *Radiat Res*. 2003;159:401–10.
44. Li Y, Reynolds P, O'Neill P, Cucinotta FA. Modeling damage complexity-dependent non-homologous end-joining repair pathway. *PLoS One*. 2014;9:e85816.
45. Held KD, Kawamura H, Kaminuma T, Paz AE, Yoshida Y, Liu Q, Willers H, Takahashi A. Effects of charged particles on human tumor cells. *Front Oncol*. 2016;6:23.
46. Choudhury A, Zhao H, Jalali F, Al Rashid S, Ran J, Supiot S, Kiltie AE, Bristow RG. Targeting homologous recombination using imatinib results in enhanced tumor cell chemosensitivity and radiosensitivity. *Mol Cancer Ther*. 2009;8:203–13.
47. Medova M, Aebersold DM, Zimmer Y. MET inhibition in tumor cells by PHA665752 impairs homologous recombination repair of DNA double strand breaks. *Int J Cancer*. 2012;130:728–34.
48. Wachters FM, van Putten JW, Maring JG, Zdzienicka MZ, Groen HJ, Kampinga HH. Selective targeting of homologous DNA recombination repair by gemcitabine. *Int J Radiat Oncol Biol Phys*. 2003;57:553–62.

3.3 The Relative Biological Effectiveness of Proton Irradiation in Dependence of DNA Damage Repair

Simon Deycmar[1], Erica Faccin[1], Tamara Kazimova[1], Philip Knobel[1], Irma Telarovic[1], Fabienne Tschanz[1], Verena Waller[1], Rona Winkler[1], Carmen Yong[1], Dario Zingariello[1], and Martin Pruschy[1]

[1]Laboratory for Applied Radiobiology, Department of Radiation Oncology, University Hospital Zurich, Zurich, Switzerland

Status of the manuscript: Published in BJR 2019

Author contribution Simon Deycmar:

- Literature Research
- Drafting and proofreading manuscript
- Minor revisions of the manuscript

BJR

https://doi.org/10.1259/bjr.20190494

Received: 03 June 2019 | Revised: 30 October 2019 | Accepted: 01 November 2019

Cite this article as:
Deycmar S, Faccin E, Kazimova T, Knobel PA, Telarovic I, Tschanz F, et al. The relative biological effectiveness of proton irradiation in dependence of DNA damage repair. *Br J Radiol* 2019; **92**: 20190494.

PROTON THERAPY SPECIAL FEATURE: REVIEW ARTICLE

The relative biological effectiveness of proton irradiation in dependence of DNA damage repair

SIMON DEYCMAR, MSc, ERICA FACCIN, MSc, TAMARA KAZIMOVA, MSc, PHILIP A. KNOBEL, PhD, IRMA TELAROVIC, MD, FABIENNE TSCHANZ, MSc, VERENA WALLER, MSc, RONA WINKLER, BSc, CARMEN YONG, PhD, DARIO ZINGARIELLO, MSc and MARTIN PRUSCHY, PhD

Laboratory for Applied Radiobiology Department of Radiation Oncology, University Hospital Zurich, University of Zurich, Raemistrasse 100, CH-8091 Zurich, Switzerland

Address correspondence to: Mr Martin Pruschy
E-mail: *martin.pruschy@uzh.ch*

ABSTRACT

Clinical parameters and empirical evidence are the primary determinants for current treatment planning in radiation oncology. Personalized medicine in radiation oncology is only at the very beginning to take the genetic background of a tumor entity into consideration to define an individual treatment regimen, the total dose or the combination with a specific anticancer agent. Likewise, stratification of patients towards proton radiotherapy is linked to its physical advantageous energy deposition at the tumor site with minimal healthy tissue being co-irradiated distal to the target volume. Hence, the fact that photon and proton irradiation also induce different qualities of DNA damages, which require differential DNA damage repair mechanisms has been completely neglected so far. These subtle differences could be efficiently exploited in a personalized treatment approach and could be integrated into personalized treatment planning. A differential requirement of the two major DNA double-strand break repair pathways, homologous recombination and non-homologous end joining, was recently identified in response to proton and photon irradiation, respectively, and subsequently influence the mode of ionizing radiation-induced cell death and susceptibility of tumor cells with defects in DNA repair machineries to either quality of ionizing radiation.

This review focuses on the differential DNA-damage responses and subsequent biological processes induced by photon and proton irradiation in dependence of the genetic background and discusses their impact on the unicellular level and in the tumor microenvironment and their implications for combined treatment modalities.

INTRODUCTION

Radiotherapy alone or in multimodality approaches is applied in 45–60% of all cancer patients, but despite technical innovations approximately only 50% are cured ([1] and references therein). At present, the most commonly used mode of radiotherapy with high energy linear accelerators is using an externally generated photon beam directed towards the exact delineated tumor site. Other forms of radiation include radiotherapy with charged particles such as electron beams, protons and heavier charged ions such as ^{12}C. Of these, proton radiotherapy is becoming a reasonable alternative worldwide.[2–4] Stratification towards a specific quality of ionizing radiation is primarily based on clinical parameters, not taking any biological aspects into consideration.

The major difference between photon- and particular proton-based radiotherapy is the spatial distribution of energy deposition. Photon beams have the highest dose deposition close to the entrance surface and continuously deposit dose at the whole path throughout the tissue. Generally, this involves healthy tissue being co-irradiated proximal and distal to the target volume. In contrast, proton beams commonly deposit a lower dose in the entry field, and maximum dose deposition occurs within the so-called Bragg peak at a depth defined by the velocity of the applied protons. Behind this Bragg peak region—or spread-out Bragg peak (SOBP) in clinical applications—no significant dose is deposited[5] (Figure 1). Thereby, a reduced exposure of dose-limiting organs-at-risk (OARs), *e.g.* the brain stem, the optical nerve and the oral cavity, to low and intermediate doses of ionizing radiation is achieved by proton radiotherapy.[6,7] Eventually, this will result in a reduced risk of normal tissue toxicities and secondary malignancies in these co-irradiated organs close to treated entities such as skull-based and intracranial tumors, uveal melanoma and head and neck tumors, respectively.[8–10]

Figure 1. Differential depth dose distributions of photons versus protons. Photon beams have the highest dose deposition close to the entrance surface and continuously deposit dose at the whole path throughout the tissue. In contrast, proton beams deposit a lower dose in the entry field, and maximum dose deposition occurs within the so-called Bragg peak or SOBP in clinical applications. The reduced volume of healthy tissue exposed to intermediate and low doses of proton radiotherapy results in a reduced co-irradiation of dose-limiting OAR. OARs, organs-at-risk; SOBP, spread-out Bragg peak.

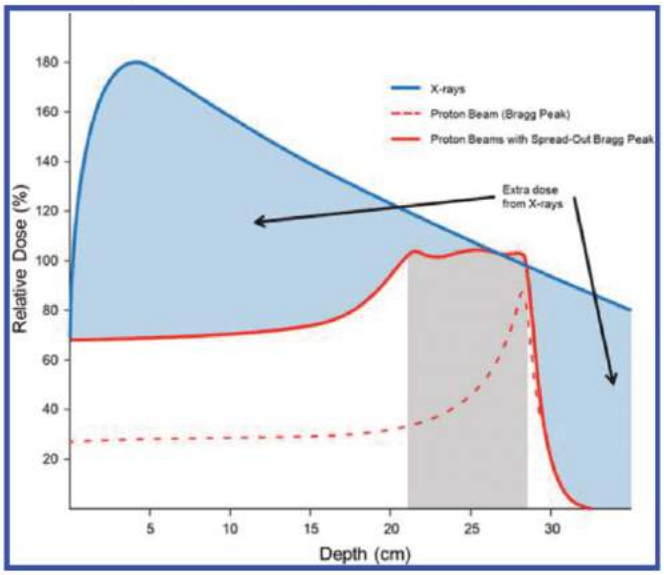

Progressive cognitive decline and impaired brain development represent major risk factors after conventional cranial radiotherapy in pediatric patients. Thus, particle radiotherapy represents an ideal treatment modality to reduce these side-effects in the central nervous system in pediatric tumor patients.[11,12]

Preclinical *in vitro* and *in vivo* experiments suggest an enhanced potency for proton- *vs* photon-irradiation. This enhanced relative biological effectiveness (RBE) is accounted for by the generic RBE value of 1.1 used in the clinics. In general, the RBE depends on the linear energy transfer (LET), the radiation dose, the number of fractions applied, the dose range and the biological system or end point analyzed.

The RBE is the ratio of the dose of high-energy photons, *e.g.* 60Co γ-rays or linear accelerator generated X-rays, relative to that of protons required to produce the same biological response. This effect is generally considered to be relatively small for protons, and a generic RBE of 1.1 has been used throughout its history for dose specification with virtually no exceptions being made for the dose/fraction, position in the SOBP, initial beam energy, or the tissue being irradiated. The global use of an RBE value of 1.1, *i.e.* a 10% higher biologic effectiveness of protons compared to photons, is based primarily on radiobiology experiments conducted in the 70's and 80's.[13] However, the LET varies along a clinically relevant SOBP. For example, in case of a 62 MeV proton beam with a 10 mm SOBP centered at 25 mm depth, the LET ranges from approximately 1 keV/μm at the entrance field, to 4 keV in the SOBP and reaches up to 25 keV/μm at the Bragg Peak.

Eventually, several groups also demonstrated a varying RBE depending on the position cells and tissue were placed within the SOBP, with the highest RBE when cells were positioned in the Bragg peak area.[14,15] This corresponds to enhanced cell killing per gray of irradiation as LET increases. These considerations result in "LET painting" as an approach to shift distal end, high LET and thus high RBE irradiation away from critical organs into the tumor treatment volume.[16–18] However, the clinical decision at the leading proton facility, the Harvard Cyclotron Laboratory, was made to proceed with a RBE factor of 1.1 as the basis of treating patients.[19] Subsequent clinical data of the last 20–30 years have though confirmed the usefulness of the factor of 1.1 in clinical practice.

Based on the improved experimental systems, the increased knowledge gained during the last decades on ionizing radiation-induced biological responses and the increasing amount of proton radiotherapy centers with integrated radiobiological research facilities, molecular and cellular-oriented studies are now routinely performed to investigate differential stress responses and differential damage profiles induced by proton *vs* photon irradiation. Thereby, the RBE will be characterized not only in relation to the differential energies but also from the differential processes induced on the molecular, cellular and (patho-) physiological level. These putative differences could eventually be important for different treatment strategies (*e.g.* as part of combined treatment modalities) and for patient stratification, challenge the use of a generic RBE and asks to integrate biological parameters into treatment planning.[20,21]

Recent insights from our own and other research laboratories indicate that differential qualities of DNA damage and subsequently differential DNA-damage responses (DDR) are induced in response to photon and proton irradiation. These differential "biologies" may be important for the concept of personalized medicine in radiotherapy. Nowadays, treatment planning of an individual patient primarily takes clinical and physical parameters into account. Eventually, stratification towards proton *vs* photon irradiation might also take these differential "biologies" on the personalized level into consideration.

Ionizing radiation induced cytotoxicity on the individually targeted cell

Ionizing radiation induces DNA double-strand breaks (DNA DSB), which represent the major cytotoxic insult. These DSBs are to a large extent correctly repaired by the two major DNA DSB repair pathways, namely the error-free homologous recombination repair (HRR) and the more error-prone non-homologous end joining (NHEJ) process.[22] NHEJ is quantitatively highly efficient to repair most of the DSBs throughout the cell. However, the quality of repair steadily decreases with increasing amounts of DNA DSBs and NHEJ-mediated chromosomal translocations might even lead to toxic chromosomal aberrations.[23] In an initial step, Ku70/80 heterodimers are formed at the broken end, which leads to the recruitment of DNA-PKcs, followed by processing of the "dirty" ends by specific DNA nucleases and polymerases and religation of the broken strands by the XRCC4-DNA Ligase IV complex.

Figure 2. Ionizing radiation induced cytotoxicity on the individually targeted cell level and via the tumor microenvironment. Incorrectly repaired DNA double strand breaks might lead to chromosomes containing reciprocal translocations of chromosomal regions. These monocentric chromosomes can still be segregated into the two surviving daughter cells following mitosis. On the other hand, most cells with dicentric chromosomes (shown) will undergo cell death. These chromosomal aberrations activate a mitotic checkpoint and will eventually undergo mitotic catastrophe in the initial or in one of the following cell cycles, respectively (direct cytotoxicity). Acentric DNA fragments (shown) are at the same time encapsulated into micronuclei, which are often leaky, and subsequently release small DNA fragments into the cytosol. These small DNA fragments stimulate the expression and secretion of imunostimulatory cytokines via the cGAS-STING pathway, and are now regarded as co-factors and starting point for ionizing radiation-induced immunogenic cell death. Immunogenic cell death contributes to tumor control acting also against tumor cells (indirect cytotoxicity), which initially survived direct targeting by ionizing radiation.

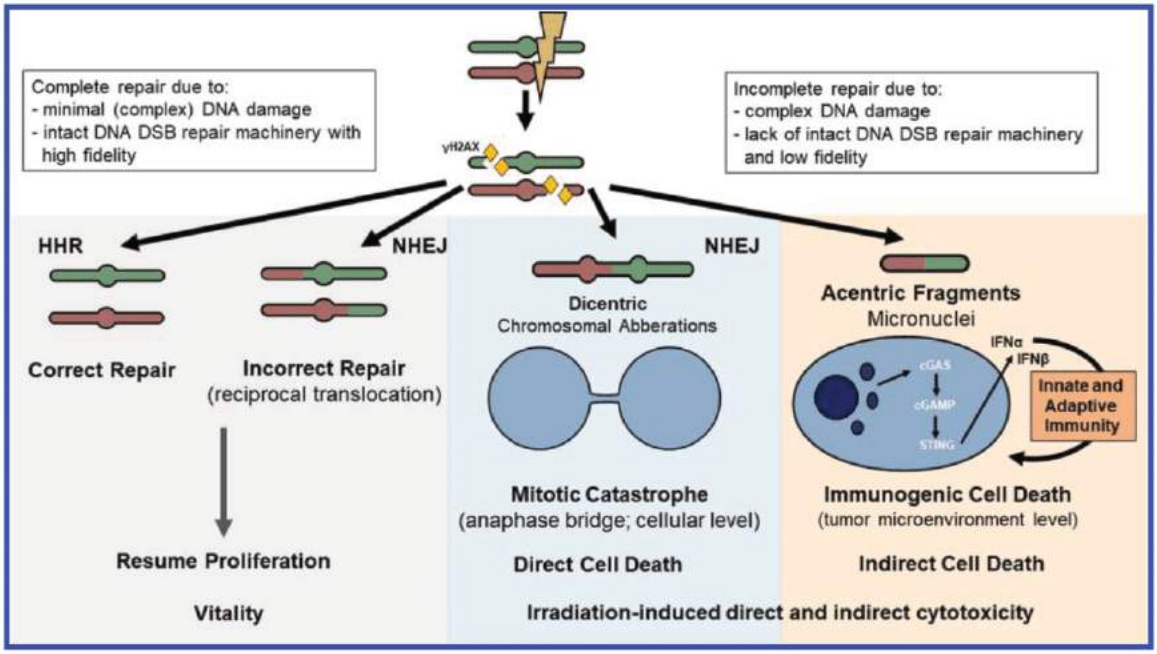

In contrast to NHEJ, HRR is an error-free process. Following MRN- and CtIP-dependent 3`−5`DNA resection, the single-stranded DNA overhangs are stabilized by the heterotrimeric ssDNA-binding complex RPA.[24] With the help of the tumor suppressor BRAC2, RPA is then replaced by RAD51 to form RAD51 nucleoprotein filaments and Holliday junctions (HJ) with complementary sequences on the adjacent sister chromatid. Eventually, these structures are resolved by several HJ processing factors on completion of DNA polymerase-dependent error-free rewriting of the damaged DNA sites.[25–27]

Incorrectly repaired DNA DSB might lead to reciprocal translocations of chromosomal regions. These newly rearranged, duplicated but still monocentric chromosomes can still be segregated into the two surviving daughter cells following mitosis. On the other hand, most cells with dicentric chromosomes undergo cell death. These chromosomal aberrations are formed due to incorrect DNA DSB repair and form unresolvable anaphase bridges during chromosomal segregation in M-phase and activate a mitotic checkpoint. Cells with unresolved, prolonged mitotic checkpoints or cells with extended chromosomal aberrations, which managed to slip into the next cell cycle, will eventually undergo mitotic catastrophe in the initial or in one of the following cell cycles, respectively. Overall, these cells undergo cell death as a direct consequence of ionizing radiation-induced DNA damage, incomplete DNA damage repair and the formation of chromosomal aberrations, which can not be properly segregated into the two daughter cells (Figure 2).

Cellular hypersensitivity towards proton irradiation in dependence of the genetic background

As part of an RBE-oriented non-small cell lung cancer (NSCLC) cell line screen, hypersensitivity to proton irradiation could be linked to defects in a specific DNA damage repair machinery.[28] Subsequently, the research group of H. Willers (Massachusetts General Hospital, Boston) could identify specific alterations of the Fanconi-Anemia (FA)/BRCA- replication-coupled HRR pathway of DNA repair in three out of 17 cell lines with an increased RBE.[28] For these comparative experiments, lung cancer cell lines were positioned at the mid-SOBP of a clinical proton beam (235 MeV). Control experiments with genetically modified lung cancer cells validated the relevance of this pathway, and supported the hypothesis of specific proton hypersensitivity due to HRR-defects (RBE-shift from 1.1 to 1.39 in dependence of FANCD2-expression level). The same group performed additional control experiments on two downstream elements of the FA/BRCA-pathway, namely Slx4(FancP) and Mus81.[29] Slx4- and Mus81-deficient cells were also hypersensitive towards proton irradiation in comparison to their isogenic wildtype counterpart cells (RBE-shift from 1.1 to 1.29 in dependence of Mus81-mutational status).

In parallel to this genomic profiling approach, hypersensitivity towards proton irradiation in HRR-deficient cells has been corroborated in several established cancer cell lines. PEO1-ovarian carcinoma cells that are lacking intact BRCA2-expression but are otherwise genetically identical to PEO4-ovarian carcinoma cells, were hypersensitive towards proton in comparison to photon irradiation. Likewise, clonogenic survival of A549 NSCLC cells that were depleted of Rad51, was strongly reduced in response to proton irradiation in comparison to control cells that were irradiated with either quality of ionizing radiation.[30] Downregulation of Rad51 also resulted in delayed γH2AX-foci repair kinetics (see below). These experiments were also performed with cells positioned in the middle of the SOBP and with a clinical proton beam. Of note, besides HHR and NHEJ as major DNA DSB repair machineries, additional DNA DSB damage repair pathways exist, which also co-determine the cellular response to ionizing radiation. However, at this stage and due to the lack of defined comparative experiments, we cannot estimate, *e.g.* the impact of alternative NHEJ (Alt-NHEJ) to a putative shift of the RBE and thus a differential radiation response to proton *vs* photon radiation.

A set of well-characterized chinese hamster ovary (CHO) cell lines was traditionally used in radiobiology to define the involvement of the different DNA DSB repair machineries for photon irradiation-induced DNA damage. These CHO cell lines have defined defects in different DNA repair machineries and are now also very suitable to characterize subtles differences in the cellular response to different qualities of ionizing radiation.[31–33]

In comparison to the corresponding wildtype cells, an increased RBE was determined in the HRR-defective cells, indicating hypersensitivity of HRR-deficient cells towards proton irradiation ($RBE_{37\%}$: 1.54 ± 0.10 and $RBE_{10\%}$: 1.44 ± 0.06 HRR-deficient cells *vs* $RBE_{37\%}$: 1.25 ± 0.05 and $RBE_{10\%}$: 1.29 ± 0.04 wildtype cells).The RBE (survival fraction as end point) was determined with cell positioned in the middle of the SOBP, with a length of 5 cm and maximum proton energy of 138 MeV. NHEJ-defective cells (XR-C1; DNA-PKcs-deficient CHO cells) were overall more sensitive to both types of ionizing radiation in comparison to wildtype cells. However, no hypersensitivity towards proton irradiation was identified in the NHEJ-defective cells.[34] Of note, differential patterns of chromosomal aberrations, in particular with an increased amount of smaller fragments, were identified in response to proton and photon irradiation (see below).

The HRR status of tumors predicts treatment sensitivity to several anticancer agents such as cisplatinum and taxanes. Furthermore, the concept of synthetic lethality was developed based on the identification of BRCA1/BRCA2-mutations leading to enhanced sensitivity to PARP-inhibitors.[35] Large-scale next generation sequencing studies on molecular profiling of solid tumors beyond BRCA1/2 suggest that more than 15% carry mutations in HRR.[36] Based on the enhanced sensitivity of tumor cells with HRR-mutations to proton irradiation and preference of proton-induced DNA damage to be repaired by HRR, stratification of patients towards proton *vs* photon radiotherapy should also take the mutational status of the tumor into consideration.

Damages at the molecular DNA level and DNA damage-related signaling should be determined to detect and quantify ionizing radiation-induced DSBs and repair of DNA DSBs over time. However, for the sake of convenience, most studies only focus on the formation and processing of γH2AX-foci in response to ionizing radiation, which are easily detectable. As part of the initial DNA damage response to DSB, the histone variant H2AX are posttranslationally phosphorylated in order to mark the site of the DNA DSB and to initiate DNA DSB repair. γH2AX-foci detection has now become a powerful method to quantify DNA DSBs induced by ionizing radiation. Phosphorylated H2AX was originally named γH2AX as it was first observed in γ-ray-exposed cells.[37] Clusters of γH2AX molecules at the site of DNA breaks allow detection and quantification of individual DSBs by using γH2AX-oriented antibodies.[38] Interestingly, the specific shape and the kinetics of γH2AX-foci formation and processing (incl. 53BP1-foci, which also accumulate at the site of DNA damage) might be used to mark repair-defective and proton irradiation hypersensitive tumors. Using these foci as biomarkers was suggested by the research group of H. Willers, who identified an increased size of 53 BP-1 foci in FA/BRCA-pathway-deficient tumor cells, in particular in response to proton irradiation. These large foci might be due to an increased complexity of clustered DNA damage in response to proton irradiation.[28,39] Since the FA/BRCA-pathway is specifically involved in replication fork maintenance and repair, increase of foci sizes might result from impaired repair of replication forks that collide with clustered proton damages.

In the genetically defined CHO cell system no significant quantitative differences in the initial amount of DNA DSBs were observed in cells irradiated by the two types of irradiation. However, elevated numbers of residual γH2AX-foci were detected in the HR-deficient cells after proton irradiation, indicative for delayed repair kinetics after proton irradiation. Cells were always irradiated in the middle of the SOBP in order avoid additional LET-depending influences across the SOBP. These results support the notion of a differential quality of DNA damage induced by proton *vs* photon irradiation. Furthermore, the qualitative difference on the level of the DNA damage response correlate with the quantitative clonogenic cell survival data and indicate a specific requirement for FA/HRR for potent DNA DSB repair in response to proton irradiation.

Recently, DNA DSB repair kinetics were investigated in response to photon and proton irradiation analyzing formation and removal of γH2AX and 53BP1-foci in murine prostate adenocarcinoma and murine embryonic fibroblast.[40] In this study, cells were exposed to the same dose but irradiated at different positions with the proton beam (plateau and Bragg Peak). A 105.5 MeV proton beam, was decelerated by a range shifter to approximately 31 MeV within the Bragg-peak. For the plateau proton set-up, a higher energy of 220 MeV was used to ensure that the proton beam was still in the plateau zone when reaching the cells after crossing the same range shifter. Consequently, the cells were hit by a proton beam with 187 MeV. Again, similar amounts of foci were induced in response to photon and proton irradiation, but foci-induction, processing and removal was delayed in cells

irradiated in the Bragg peak of the proton beam. Furthermore, the shape of Bragg peak-induced foci was more irregular and larger than foci induced by photon and plateau-protons. These differential characteristics might be linked to overlapping DNA lesions in close proximity to another, also resulting in more complex, clustered lesions. Such lesions were as also observed on irradiation with high LET charged particles, which also require more time for repair and eventually differential DNA repair machineries.[41,42] An increased complexity of proton-induced DNA damage with more persistent foci but only at the distal end of a SOBP was also demonstrated in detailed comparative irradiation studies with cells positioned along a modulated SOBP proton beam[43] confirming the overall low-LET-quality of proton exposure but with increased LET towards the distal end. Again, these qualitative DNA-damage-oriented results on the unicellular level correlate with differential RBEs (clonogenic cell survival) when cells are irradiated at different positions within a SOBP *in vitro*[44,45] and *in vivo*.[14]

Overall, these preclinical results link a putative differential quality of DNA damage in response to proton *vs* photon irradiation to a hypersensitivity to proton irradiation and increased cytotoxicity on the unicellular level.

Hypersensitivity towards proton irradiation in the tumor microenvironment

Ionizing radiation may induce different modes of cell death, which are primarily linked to the origin of the targeted cells and their differentiation status. Besides mitotic catastrophe (see above), also enhanced cell apoptosis was identified after low LET proton irradiation in comparison to photon irradiation.[46] Recently, the irradiation-induced response of the immune system and its related induction of immunogenic cell death (ICD) has gained of interest, and—even though still to be proven—proton and photon-irradiation might induce different levels of ICD, which again might be linked to the status of the two major DNA DSB repair machineries.

As indicated above, acentric fragments have long been regarded as waste by-products of chromosomal aberrations and less relevant for the direct cytotoxic potency of ionizing radiation. These small acentric fragments are encapsulated into micronuclei (MN) and these MN are actually used as biomarkers for the induction of mitotic catastrophe. Interestingly though, these MNs and the encapsulated small DNA fragments are now regarded as starting point of co-stimulatory factors for ionizing radiation-induced ICD.

Irradiation activates an anti tumor immune response through the release of danger signals and inflammatory cytokines thereby promoting dendritic cells to cross-present released antigens to T cells.[47] A thereby triggered cytotoxic T cell response might be directed toward the primary irradiated tumor, but might also acts against non-irradiated metastasis via an abscopal effect, directed against non-irradiated lesions. Interestingly though, the acentric DNA fragments, classified as by-products of the incorrectly repaired chromosomes, act as initial co-factors for the activation of this so called cancer-immunity cycle in response to irradiation.

While compartmentalization of the cell separates nuclear-located chromosomes from the cytosol and prevents sensing of DNA in the cytosol, rupture of micronuclei gives access of cytosolic proteins to DNA. Likewise, small DNA fragments may also leak out from MN into the cytosol. DNA fragments trigger the formation of the second messenger cGMP-AMP (cGAMP) by the cytoplasmic protein GMP-AMP synthase (cGAS), and cGAMP activates the Stimulator of Interferon Genes (STING)-dependent signal transduction cascade leading to the expression and secretion of pro-inflammatory cytokines such as interferone α and β[48,49]. These cytokines contribute to tumor recruitment and activation of Batf3-lineage dendritic cells, which are responsible for correct priming of T-cells as part of the cancer immunity cycle[47] (Figure 2).

As such, incorrectly repaired ionizing radiation-induced DNA damage results in DNA-insults (dicentric chromosomes) directly acting in a cytotoxic way on the unicellular level and may indirectly (acentric fragments) stimulate an immune-mediated tumor-oriented toxic microenvironment. Both mechanisms are induced in response to different qualities of ionizing radiation, but to different extents and in dependence of different genetic backgrounds.

A few studies have so far directly compared the regulation of immune-stimulatory factors and surface molecules in response to different qualities of ionizing radiation that are required for successful ionizing radiation-triggered ICD. A common signature of surface molecules involved in immune recognition, tumor-associated antigens and calreticulin surface expression was observed in multiple tumor cell lines in response to photon and proton irradiation, relevant for successful cytotoxic T-lymphocyte mediated cell killing.[50] On the other hand, inflammatory factors such as IL6, IL8 and CXCL12 were generally less extensively upregulated by proton irradiation in comparison to photon irradiation.[51] Of interest, proton irradiation in particular at higher dosages results in increased rates of micronuclei formation in comparison to photon irradiation as characterized in thyroid follicular cells (0–12 Gy) and human peripheral blood lymphocytes (2–4 Gy).[46,52] Since micronuclei encapsulate small DNA fragments, an enhanced rate of micronuclei formation may also correlate with a higher rate of acentric and small DNA fragments generated in response to proton irradiation.[34]

The generation of small DNA fragments in response to irradiation is also determined by an intact DNA damage response. Interestingly, micronuclei formation and cGAS-STING activation was specifically increased in a BRCA2- and thus HR-deficient background in tumor cells as part of replicative stress even in absence of irradiation-induced DNA damage.[53] Given the hypersensitivity of HR-defective tumor cells to proton irradiation on the unicellular level, it will be of interest to determine activation of the cancer immunity cycle and induction of ICD in tumors derived from HR-intact and HR-defective tumor cells in response to proton irradiation but in an otherwise intact tumor microenvironment.

Combined treatment modalities with HRR-interfering agents

A combined treatment modality with specific inhibitors of HRR could also lead to enhanced sensitivity towards proton versus photon irradiation. However, the development of pharmacological agents directly targeting moieties of the HRR machinery has been largely unsuccessful so far. Nevertheless, several chemotherapeutic agents exist, which eventually affect HRR, *e.g.* by the downregulation of respective HRR-elements. For example, low dose exposure of lung adenocarcinoma cells to the histone deacetylase inhibitor SAHA (Vorinostat) downregulates Rad51 protein levels but not critical elements of NHEJ, and thereby specifically reduces HRR activity.[54] Of note, DNA repair in SAHA-pretreated cells was in particular delayed after proton irradiation and much less so in response to photon irradiation, and cellular pretreatment with SAHA also translated into enhanced radiosensitivity towards proton irradiation.[30]

Interestingly, SAHA-based radiosensitization was also investigated in response to different qualities of ionizing radiation (photon, low LET proton and high LET carbon irradiation) in lung carcinoma cells versus normal human fibroblasts.[55] SAHA specifically sensitized tumor cells and less so normal fibroblasts, which is of interest towards an enhanced therapeutic window. Furthermore, these studies also demonstrated delayed DNA repair and most potent SAHA-based sensitization at low doses for proton irradiation.

Besides SAHA, other pharmaceutical agents in early developmental stage exist, which directly or indirectly reduce HRR-activity. The inhibitor of the heat shock chaperone hsp90 ganetespib counteracts irradiation-enhanced RAD51protein levels and thereby sensitizes lung adenocarcinoma cells for ionizing radiation.[56] The Brc-abl tyrosine kinase inhibitor gleevec, which is used to treat chronic myelogenous leukemia (CML), also reduces RAD51protein levels and thereby sensitizes for irradiation.[57] Likewise, reduced formation of the RAD51-BRCA2 complex is also induced on cellular treatment with inhibitors of the hepatocyte growth factor receptor Mesenchymal-Epithelial Transition (MET). MET is overexpressed in multiple types of human tumors and inhibition of MET kinase activity also sensitizes for ionizing radiation.[58]

Selective targeting of HRR even represents the mechanism of action for clinically applied chemotherapeutic agents and radiosensitizers, *e.g.* gemcitabine, when used in combination with photon radiotherapy.[59] Thus, a reduced dose of proton radiation might be sufficient when combined with HRR-co-targeting agents to achieve the same treatment outcome as when combined with classic radiotherapy.

On the other hand, inhibitors of NHEJ might sensitize more for photon than for proton irradiation. Indeed, the DNA-PKcs inhibitor NU7026 strongly delayed repair of photon- but not proton-induced DNA DSB damage and subsequently sensitized lung carcinoma and glioblastoma to a higher extent to photon than to proton irradiation.[30] These results also indicate that HRR and not NHEJ is the primary repair machinery for proton-induced DNA DSBs.

The identification of immunosuppressive mechanisms and respective blocking immune checkpoint inhibitors boosted an immense level of basic, translational and clinical research at the interface of radiotherapy and immunology leading to promising clinical trials of radiotherapy in combination with immune checkpoint inhibitors.[60] Radiotherapy has long been classified as immunosuppressive. However, preclinical studies with hypofractionated regimens have revealed that increased doses of ionizing radiation induce potent anti tumor immune responses, and several strategies have been developed to heat-up the cancer immunity cycle and to increase irradiation-induced immunogenic cell death.[61] Likewise, we also start to identify mechanisms on the molecular level how DNA damage drives the regulation of immune checkpoints.[62,63] In order to follow this line of research there is a great need to explore how the different qualities of ionizing radiation interfere with immunogenic cell death and the cancer immunity cycle. For example, TREX1 is an endonuclease, degrades small DNA fragments and thereby downregulates irradiation-induced immunogenic cell death (see above). TREX1 is upregulated in particular in response to single high doses of ionizing radiation, and thus, TREX1 inhibitors could be of great interest to stimulate immunogenic cell death in particular as part of a hypofractionated treatment regimen.[64] However, due to the different qualities of proton irradiation-induced DNA damage and a differential requirement for HRR as major DNA repair mechanism, the expression of TREX1 might also be regulated in a differential way and thereby influence immunogenic cell death in a differential way.

Recently, a novel inhibitor of the HRR-upstream-situated serine/threonine-specific protein kinase ATR (AZD6738) was demonstrated to sensitize for ionizing radiation *in vitro* and *in vivo*.[65] Interestingly, AZD6738 in combination with irradiation not only reduced clonogenicity, but also increased the amount of irradiation-induced cellular micronuclei. Thus, the ATR and other HR-oriented inhibitors could thereby not only increase hypersensitivity on the unicellular level but even increase immunogenic cell death on the tumor level in response to proton irradiation.

However, most treatment combinations have only been investigated with classic photon irradiation. It will be now important to perform both efficacy- and mechanistic-oriented studies with these clinically relevant agents in combination with proton radiotherapy. Eventually, these investigations could lead to the integration of biological parameters for patient's stratification to either quality of ionizing radiation.

ACKNOWLEDGMENT

Martin Pruschy is a beneficiary of the MSCA ITN RADIATE (Marie Sklodowska-Curie grant agreement No 642623). He received funding from this European Union's Horizon 2020 research and innovation programme. Simon Deycmar and Tamara Kazimova are early stage researchers of this ITN.

REFERENCES

1. Borras JM, Lievens Y, Barton M, Corral J, Ferlay J, Bray F, et al. How many new cancer patients in Europe will require radiotherapy by 2025? an ESTRO-HERO analysis. *Radiother Oncol* 2016; **119**: 5–11. doi: https://doi.org/10.1016/j.radonc.2016.02.016
2. Wilson RR. Radiological use of fast protons. *Radiology* 1946; **47**: 487–91. doi: https://doi.org/10.1148/47.5.487
3. Durante M, Loeffler JS. Charged particles in radiation oncology. *Nat Rev Clin Oncol* 2010; **7**: 37–43. doi: https://doi.org/10.1038/nrclinonc.2009.183
4. Durante M, Orecchia R, Loeffler JS. Charged-Particle therapy in cancer: clinical uses and future perspectives. *Nat Rev Clin Oncol* 2017; **14**: 483–95. doi: https://doi.org/10.1038/nrclinonc.2017.30
5. Baumann M, Krause M, Overgaard J, Debus J, Bentzen SM, Daartz J, et al. Radiation oncology in the era of precision medicine. *Nat Rev Cancer* 2016; **16**: 234–49. doi: https://doi.org/10.1038/nrc.2016.18
6. Romesser PB, Cahlon O, Scher E, Zhou Y, Berry SL, Rybkin A, et al. Proton beam radiation therapy results in significantly reduced toxicity compared with intensity-modulated radiation therapy for head and neck tumors that require ipsilateral radiation. *Radiother Oncol* 2016; **118**: 286–92. doi: https://doi.org/10.1016/j.radonc.2015.12.008
7. Vogel J, Both S, Kirk M, Chao H-H, Bagatell R, Li Y, et al. Proton therapy for pediatric head and neck malignancies. *Pediatr Blood Cancer* 2018; **65**: e2685823 10 2017. doi: https://doi.org/10.1002/pbc.26858
8. Schulz-Ertner D, Tsujii H. Particle radiation therapy using proton and heavier ion beams. *J Clin Oncol* 2007; **25**: 953–64. doi: https://doi.org/10.1200/JCO.2006.09.7816
9. Schiller KC, Habl G, Combs SE, Protons CSE. Protons, Photons, and the Prostate - Is There Emerging Evidence in the Ongoing Discussion on Particle Therapy for the Treatment of Prostate Cancer? *Front Oncol* 2016; **6**: 8. doi: https://doi.org/10.3389/fonc.2016.00008
10. Stewart, B., and Wild, C. World cancer report. 71. 2014.
11. Mizumoto M, Oshiro Y, Yamamoto T, Kohzuki H, Sakurai H. Proton beam therapy for pediatric brain tumor. *Neurol Med Chir* 2017; **57**: 343–55. doi: https://doi.org/10.2176/nmc.ra.2017-0003
12. Sands SA. Proton beam radiation therapy: the future may prove brighter for pediatric patients with brain tumors. *J Clin Oncol* 2016; **34**: 1024–6. doi: https://doi.org/10.1200/JCO.2015.65.4350
13. Urano M, Verhey LJ, Goitein M, Tepper JE, Suit HD, Mendiondo O, et al. Relative biological effectiveness of modulated proton beams in various murine tissues. *Int J Radiat Oncol Biol Phys* 1984; **10**: 509–14. doi: https://doi.org/10.1016/0360-3016(84)90031-2
14. Sørensen BS, Bassler N, Nielsen S, Horsman MR, Grzanka L, Spejlborg H, et al. Relative biological effectiveness (RBE) and distal edge effects of proton radiation on early damage in vivo. *Acta Oncol* 2017; **56**: 1387–91. doi: https://doi.org/10.1080/0284186X.2017.1351621
15. Wouters BG, Skarsgard LD, Gerweck LE, Carabe-Fernandez A, Wong M, Durand RE, et al. Radiobiological intercomparison of the 160 MeV and 230 MeV proton therapy beams at the Harvard cyclotron laboratory and at Massachusetts General Hospital. *Radiat Res* 2015; **183**: 174–87. doi: https://doi.org/10.1667/RR13795.1
16. Cao W, Khabazian A, Yepes PP, Lim G, Poenisch F, Grosshans DR, et al. Linear energy transfer incorporated intensity modulated proton therapy optimization. *Phys Med Biol* 2017; **63**: 015013. doi: https://doi.org/10.1088/1361-6560/aa9a2e
17. McMahon SJ, Paganetti H, Prise KM. LET-weighted doses effectively reduce biological variability in proton radiotherapy planning. *Phys Med Biol* 2018; **63**: 225009. doi: https://doi.org/10.1088/1361-6560/aae8a5
18. Mohan R, Peeler CR, Guan F, Bronk L, Cao W, Grosshans DR. Radiobiological issues in proton therapy. *Acta Oncol* 2017; **56**: 1367–73. doi: https://doi.org/10.1080/0284186X.2017.1348621
19. Suit HD, Goitein M, Munzenrider J, Verhey L, Urie M, Gragoudas E, et al. Increased efficacy of radiation therapy by use of proton beam. *Strahlenther Onkol* 1990; **166**: 40–4.
20. Dosanjh M, Jones B, Pawelke J, Pruschy M, Sørensen BS. Overview of research and therapy facilities for radiobiological experimental work in particle therapy. Report from the European particle therapy network radiobiology group. *Radiother Oncol* 2018; **128**: 14–18. doi: https://doi.org/10.1016/j.radonc.2018.03.008
21. Lühr A, von Neubeck C, Pawelke J, Seidlitz A, Peitzsch C, Bentzen SM, et al. "Radiobiology of Proton Therapy": Results of an international expert workshop. *Radiother Oncol* 2018; **128**: 56–67. doi: https://doi.org/10.1016/j.radonc.2018.05.018
22. Iliakis G, Murmann T, Soni A. Alternative end-joining repair pathways are the ultimate backup for abrogated classical non-homologous end-joining and homologous recombination repair: implications for the formation of chromosome translocations. *Mutat Res Genet Toxicol Environ Mutagen* 2015; **793**: 166–75. doi: https://doi.org/10.1016/j.mrgentox.2015.07.001
23. Povirk LF. Biochemical mechanisms of chromosomal translocations resulting from DNA double-strand breaks. *DNA Repair* 2006; **5**(9-10): 1199–212. doi: https://doi.org/10.1016/j.dnarep.2006.05.016
24. Sartori AA, Lukas C, Coates J, Mistrik M, Fu S, Bartek J, et al. Human CtIP promotes DNA end resection. *Nature* 2007; **450**: 509–14. doi: https://doi.org/10.1038/nature06337
25. Hiom K. Coping with DNA double strand breaks. *DNA Repair* 2010; **9**: 1256–63. doi: https://doi.org/10.1016/j.dnarep.2010.09.018
26. Lieber MR. The mechanism of double-strand DNA break repair by the nonhomologous DNA end-joining pathway. *Annu Rev Biochem* 2010; **79**: 181–211. doi: https://doi.org/10.1146/annurev.biochem.052308.093131
27. Pardo B, Gómez-González B, Aguilera A. Dna repair in mammalian cells: DNA double-strand break repair: how to fix a broken relationship. *Cell Mol Life Sci* 2009; **66**: 1039–56. doi: https://doi.org/10.1007/s00018-009-8740-3
28. Liu Q, Ghosh P, Magpayo N, Testa M, Tang S, Gheorghiu L, et al. Lung cancer cell line screen links Fanconi anemia/BRCA pathway defects to increased relative biological effectiveness of proton radiation. *Int J Radiat Oncol Biol Phys* 2015; **91**: 1081–9. doi: https://doi.org/10.1016/j.ijrobp.2014.12.046
29. Liu Q, Underwood TSA, Kung J, Wang M, Lu H-M, Paganetti H, et al. Disruption of SLX4-MUS81 function increases the relative biological effectiveness of proton radiation. *Int J Radiat Oncol Biol Phys* 2016; **95**: 78–85. doi: https://doi.org/10.1016/j.ijrobp.2016.01.046
30. Fontana AO, Augsburger MA, Grosse N, Guckenberger M, Lomax AJ, Sartori AA, et al. Differential DNA repair pathway choice in cancer cells after proton- and photon-irradiation. *Radiother Oncol* 2015; **116**: 374–80. doi: https://doi.org/10.1016/j.radonc.2015.08.014
31. Rothkamm K, Krüger I, Thompson LH, Löbrich M. Pathways of DNA double-strand break repair during the mammalian cell cycle. *Mol Cell Biol* 2003; **23**: 5706–15. doi: https://doi.org/10.1128/MCB.23.16.5706-5715.2003

32. Hinz JM, Yamada NA, Salazar EP, Tebbs RS, Thompson LH. Influence of double-strand-break repair pathways on radiosensitivity throughout the cell cycle in CHO cells. *DNA Repair* 2005; **4**: 782–92. doi: https://doi.org/10.1016/j.dnarep.2005.03.005
33. Kuhfittig-Kulle S, Feldmann E, Odersky A, Kuliczkowska A, Goedecke W, Eggert A, et al. The mutagenic potential of non-homologous end joining in the absence of the NHEJ core factors Ku70/80, DNA-PKcs and XRCC4-LigIV. *Mutagenesis* 2007; **22**: 217–33. doi: https://doi.org/10.1093/mutage/gem007
34. Grosse N, Fontana AO, Hug EB, Lomax A, Coray A, Augsburger M, et al. Deficiency in homologous recombination renders mammalian cells more sensitive to proton versus photon irradiation. *Int J Radiat Oncol Biol Phys* 2014; **88**: 175–81. doi: https://doi.org/10.1016/j.ijrobp.2013.09.041
35. Lord CJ, Ashworth A. Parp inhibitors: synthetic lethality in the clinic. *Science* 2017; **355**: 1152–8. doi: https://doi.org/10.1126/science.aam7344
36. Heeke AL, Pishvaian MJ, Lynce F, Xiu J, Brody JR, Chen W-J, et al. Prevalence of homologous Recombination–Related gene mutations across multiple cancer types. *JCO Precis Oncol* 2018; **2018**: 1–13. doi: https://doi.org/10.1200/PO.17.00286
37. Rogakou EP, Boon C, Redon C, Bonner WM. Megabase chromatin domains involved in DNA double-strand breaks in vivo. *J Cell Biol* 1999; **146**: 905–16. doi: https://doi.org/10.1083/jcb.146.5.905
38. Ivashkevich A, Redon CE, Nakamura AJ, Martin RF, Martin OA. Use of the γ-H2AX assay to monitor DNA damage and repair in translational cancer research. *Cancer Lett* 2012; **327**(1-2): 123–33. doi: https://doi.org/10.1016/j.canlet.2011.12.025
39. Costes SV, Boissière A, Ravani S, Romano R, Parvin B, Barcellos-Hoff MH. Imaging features that discriminate between foci induced by high- and low-LET radiation in human fibroblasts. *Radiat Res* 2006; **165**: 505–15. doi: https://doi.org/10.1667/RR3538.1
40. Oeck S, Szymonowicz K, Wiel G, Krysztofiak A, Lambert J, Koska B, et al. Relating linear energy transfer to the formation and resolution of DNA repair foci after irradiation with equal doses of X-ray photons, Plateau, or Bragg-peak protons. *Int J Mol Sci* 2018; **19**: 3779. doi: https://doi.org/10.3390/ijms19123779
41. Hagiwara Y, Niimi A, Isono M, Yamauchi M, Yasuhara T, Limsirichaikul S, et al. 3D-structured illumination microscopy reveals clustered DNA double-strand break formation in widespread γH2AX foci after high let heavy-ion particle radiation. *Oncotarget* 2017; **8**: 109370–81. doi: https://doi.org/10.18632/oncotarget.22679
42. Nakajima NI, Brunton H, Watanabe R, Shrikhande A, Hirayama R, Matsufuji N, et al. Visualisation of γH2AX foci caused by heavy ion particle traversal; distinction between core track versus non-track damage. *PLoS One* 2013; **8**: e70107. doi: https://doi.org/10.1371/journal.pone.0070107
43. Chaudhary P, Marshall TI, Currell FJ, Kacperek A, Schettino G, Prise KM. Variations in the processing of DNA double-strand breaks along 60-MeV therapeutic proton beams. *Int J Radiat Oncol Biol Phys* 2016; **95**: 86–94. doi: https://doi.org/10.1016/j.ijrobp.2015.07.2279
44. Cuaron JJ, Chang C, Lovelock M, Higginson DS, Mah D, Cahlon O, et al. Exponential increase in relative biological effectiveness along distal edge of a proton Bragg peak as measured by deoxyribonucleic acid double-strand breaks. *Int J Radiat Oncol Biol Phys* 2016; **95**: 62–9. doi: https://doi.org/10.1016/j.ijrobp.2016.02.018
45. Hojo H, Dohmae T, Hotta K, Kohno R, Motegi A, Yagishita A, et al. Difference in the relative biological effectiveness and DNA damage repair processes in response to proton beam therapy according to the positions of the spread out Bragg peak. *Radiat Oncol* 2017; **12**: 111. doi: https://doi.org/10.1186/s13014-017-0849-1
46. Green LM, Murray DK, Bant AM, Kazarians G, Moyers MF, Nelson GA, et al. Response of thyroid follicular cells to gamma irradiation compared to proton irradiation. I. initial characterization of DNA damage, micronucleus formation, apoptosis, cell survival, and cell cycle phase redistribution. *Radiat Res* 2001; **155**(1 Pt 1): 32–42. doi: https://doi.org/10.1667/0033-7587(2001)155[0032:ROTFCT]2.0.CO;2
47. Chen DS, Mellman I. Oncology meets immunology: the cancer-immunity cycle. *Immunity* 2013; **39**: 1–10. doi: https://doi.org/10.1016/j.immuni.2013.07.012
48. Harding SM, Benci JL, Irianto J, Discher DE, Minn AJ, Greenberg RA. Mitotic progression following DNA damage enables pattern recognition within micronuclei. *Nature* 2017; **548**: 466–70. doi: https://doi.org/10.1038/nature23470
49. Mackenzie KJ, Carroll P, Martin C-A, Murina O, Fluteau A, Simpson DJ, et al. cGAS surveillance of micronuclei links genome instability to innate immunity. *Nature* 2017; **548**: 461–5. doi: https://doi.org/10.1038/nature23449
50. Gameiro SR, Malamas AS, Bernstein MB, Tsang KY, Vassantachart A, Sahoo N, et al. Tumor cells surviving exposure to proton or photon radiation share a common immunogenic modulation signature, rendering them more sensitive to T cell-mediated killing. *Int J Radiat Oncol Biol Phys* 2016; **95**: 120–30. doi: https://doi.org/10.1016/j.ijrobp.2016.02.022
51. Nielsen S, Bassler N, Grzanka L, Swakon J, Olko P, Andreassen CN, et al. Differential gene expression in primary fibroblasts induced by proton and cobalt-60 beam irradiation. *Acta Oncol* 2017; **56**: 1406–12. doi: https://doi.org/10.1080/0284186X.2017.1351623
52. Miszczyk J, Rawojć K, Panek A, Swakoń J, Prasanna PG, Rydygier M. Response of human lymphocytes to proton radiation of 60 MeV compared to 250 kV x-rays by the cytokinesis-block micronucleus assay. *Radiother Oncol* 2015; **115**: 128–34. doi: https://doi.org/10.1016/j.radonc.2015.03.003
53. Heijink AM, Talens F, Jae LT, van Gijn SE, Fehrmann RSN, Brummelkamp TR, et al. Brca2 deficiency instigates cGAS-mediated inflammatory signaling and confers sensitivity to tumor necrosis factor-alpha-mediated cytotoxicity. *Nat Commun* 2019; **10**: 100. doi: https://doi.org/10.1038/s41467-018-07927-y
54. Chen X, Wong P, Radany EH, Stark JM, Laulier C, Wong JYC. Suberoylanilide hydroxamic acid as a radiosensitizer through modulation of Rad51 protein and inhibition of homology-directed repair in multiple myeloma. *Mol Cancer Res* 2012; **10**: 1052–64. doi: https://doi.org/10.1158/1541-7786.MCR-11-0587
55. Gerelchuluun A, Maeda J, Manabe E, Brents C, Sakae T, Fujimori A, et al. Histone deacetylase inhibitor induced radiation sensitization effects on human cancer cells after photon and Hadron radiation exposure. *Int J Mol Sci* 2018; **19**: 496. doi: https://doi.org/10.3390/ijms19020496
56. Gomez-Casal R, Bhattacharya C, Epperly MW, Basse PH, Wang H, Wang X, et al. The Hsp90 inhibitor Ganetespib radiosensitizes human lung adenocarcinoma cells. *Cancers* 2015; **7**: 876–907. doi: https://doi.org/10.3390/cancers7020814
57. Choudhury A, Zhao H, Jalali F, Al Rashid S, Ran J, Supiot S, et al. Targeting homologous recombination using imatinib results in enhanced tumor cell chemosensitivity and radiosensitivity. *Mol Cancer Ther* 2009; **8**: 203–13. doi: https://doi.org/10.1158/1535-7163.MCT-08-0959

58. Medová M, Aebersold DM, Zimmer Y. Met inhibition in tumor cells by PHA665752 impairs homologous recombination repair of DNA double strand breaks. *Int J Cancer* 2012; **130**: 728–34. doi: https://doi.org/10.1002/ijc.26058
59. Wachters FM, van Putten JWG, Maring JG, Zdzienicka MZ, Groen HJM, Kampinga HH. Selective targeting of homologous DNA recombination repair by gemcitabine. *Int J Radiat Oncol Biol Phys* 2003; **57**: 553–62. doi: https://doi.org/10.1016/S0360-3016(03)00503-0
60. Pilones KA, Vanpouille-Box C, Demaria S. Combination of radiotherapy and immune checkpoint inhibitors. *Semin Radiat Oncol* 2015; **25**: 28–33. doi: https://doi.org/10.1016/j.semradonc.2014.07.004
61. Golden EB, Pellicciotta I, Demaria S, Barcellos-Hoff MH, Formenti SC. The convergence of radiation and immunogenic cell death signaling pathways. *Front Oncol* 2012; **2**: 88. doi: https://doi.org/10.3389/fonc.2012.00088
62. Sato H, Niimi A, Yasuhara T, Permata TBM, Hagiwara Y, Isono M, et al. Dna double-strand break repair pathway regulates PD-L1 expression in cancer cells. *Nat Commun* 2017; **8**: 1751. doi: https://doi.org/10.1038/s41467-017-01883-9
63. Permata TBM, Hagiwara Y, Sato H, Yasuhara T, Oike T, Gondhowiardjo S, et al. Base excision repair regulates PD-L1 expression in cancer cells. *Oncogene* 2019; **38**: 4452–66. doi: https://doi.org/10.1038/s41388-019-0733-6
64. Vanpouille-Box C, Alard A, Aryankalayil MJ, Sarfraz Y, Diamond JM, Schneider RJ, et al. DNA exonuclease TREX1 regulates radiotherapy-induced tumour immunogenicity. *Nat Commun* 2017; **8**: 15618. doi: https://doi.org/10.1038/ncomms15618
65. Dillon MT, Barker HE, Pedersen M, Hafsi H, Bhide SA, Newbold KL, et al. Radiosensitization by the ATR inhibitor AZD6738 through generation of acentric micronuclei. *Mol Cancer Ther* 2017; **16**: 25–34. doi: https://doi.org/10.1158/1535-7163.MCT-16-0239

3.4 Investigating the impact of alpha/beta and LET on RBE in scanned proton beams: an in vitro study

Elisabeth Mara[1,2], Monika Clausen[1], Suphalak Khachonkham[1,3], **Simon Deycmar[4]**, Clara Pessy[1], Wolfgang Dörr[1], Peter Kuess [1, 5], Dietmar Georg[1,5] , Sylvia Gruber[1,5]

[1] Department of Radiation Oncology/ Christian Doppler Laboratory for Medical Radiation Research for Radiation Oncology, Medical University of Vienna, Austria
[2] University of Applied Science, Wiener Neustadt, Austria
[3] Division of Radiation Therapy, Department of Diagnostic and Therapeutic Radiology, Faculty of Medicine Ramathibodi Hospital, Mahidol University, Bangkok, Thailand
[4] Laboratory of Applied Radiobiology, Department of Radiation Oncology, University Hospital Zürich, Switzerland
[5] EBG MedAustron GmbH, Wiener Neustadt, Austria

Key words: relative biological effectiveness, proton therapy, pencil beam scanning, α/ß-ratio, linear energy transfer, RBE modelling

Status of the manuscript: Submitted to MedPhys at the end of 2019

Author contribution Simon Deycmar:

- Minor contributions in drafting and conduction of experiments
    - Proton beam irradiation
    - Clonogenic cell survival assay

        see Table 2

        Figure 2
- Drafting and proofreading of the manuscript
- Managing collaboration

Investigating the impact of alpha/beta and LET_d on relative biological effectiveness in scanned proton beams: an in vitro study based on human cell lines

Running title: RBE in scanned proton beams

Elisabeth Mara[1,2], Monika Clausen[1], Suphalak Khachonkham[1,3], Simon Deycmar[4], Clara Pessy[1], Wolfgang Dörr[1], Peter Kuess[1, 5], Dietmar Georg[1,5], Sylvia Gruber[1,5]

[1] Department of Radiation Oncology/ Christian Doppler Laboratory for Medical Radiation Research for Radiation Oncology, Medical University of Vienna, Austria

[2] University of Applied Science, Wiener Neustadt, Austria

[3] Division of Radiation Therapy, Department of Diagnostic and Therapeutic Radiology, Faculty of Medicine Ramathibodi Hospital, Mahidol University, Bangkok, Thailand

[4] Laboratory of Applied Radiobiology, Department of Radiation Oncology, University Hospital Zürich, Switzerland

[5] EBG MedAustron GmbH, Wiener Neustadt, Austria

Key words: relative biological effectiveness, proton therapy, pencil beam scanning, α/ß-ratio, linear energy transfer, RBE modeling

Corresponding author:

Univ. Prof. DI Dr. Dietmar Georg

Medical University of Vienna

Dept. Radiotherapy

Währinger Gürtel 18-20

A-1090 Wien

Austria

E-mail: dietmar.georg@meduniwien.ac.at

Abstract

Purpose: A relative biological effectiveness (RBE) of 1.1 is commonly used in clinical proton therapy, irrespective of tissue type and depth. This *in-vitro* study was conducted to quantify the RBE of scanned protons as a function of the dose-averaged linear energy transfer (LET_d) and the sensitivity factor $(\alpha/ß)_X$. Additionally, three phenomenological models (McNamara, Rørvik and Jones) and one mechanistic model (double strand break, DSB) were applied to the experimentally derived data.

Methods: Four human cell lines (FaDu, HaCat, Du145, SKMel) with differential $(\alpha/ß)_X$ ratios were irradiated in a custom-designed irradiation setups with doses between 0 and 6 Gy at proximal, central and distal positions of an 80 mm spread-out Bragg peak (SOBP) centered at 80 mm (set-up A: proton energies 66.5-135.6 MeV) and 155 mm (set-up B: proton energies 127.2-185.9 MeV) depth, respectively. LET_d values at the respective cell positions were derived from Monte Carlo simulations performed with the treatment planning system (TPS, RayStation). Dosimetric measurements were conducted to verify dose homogeneity and dose delivery accuracy. RBE values were derived for doses that resulted in 90 % (RBE_{90})and 10 % (RBE_{10}) of cell survival, and survival after a 0.5 Gy dose ($RBE_{0.5Gy}$), 2 Gy dose (RBE_{2Gy}) and 6 Gy dose (RBE_{6Gy}).

Results: LET_d values at sample positioning were 1.9, 2.1, 2.5, 2.8, 4.1 and 4.5 keV/µm. For the cell lines with high $(\alpha/ß)_X$ ratios (FaDu, HaCat), the LET_d did not impact on the RBE. For low $(\alpha/ß)_X$ cell lines (Du145, SKMel), LQ-derived survival curves indicated a clear correlation of LET_d and RBE. RBE_{90} values up to 2.9 and RBE_{10} values between 1.4 and 1.8 were obtained. Model-derived RBE predictions slightly overestimated the RBE for the high $(\alpha/ß)_X$ cell lines, although all models except the Jones model provided RBE values within the experimental uncertainty. For low $(\alpha/ß)_X$ cell lines, no agreement was found between experiments and model predictions, i.e all models underestimated the RBE.

Conclusions: The sensitivity parameter $(\alpha/ß)_X$ was observed to be a major influencing factor for the RBE of protons and its sensitivity towards LET_d changes. RBE prediction models are applicable for high $(\alpha/ß)_X$ cell lines but do not estimate RBEs with sufficient accuracy in low $(\alpha/ß)_X$ cell lines.

Introduction

Proton therapy (PT) is an emerging treatment modality within radiation oncology with 77 facilities currently in operation (www.ptcog.ch). Compared to most advanced treatment techniques with high energy photon beams, the advantageous physical ballistics of protons enable highly conformal treatments with reduced organs-at-risk doses, especially in the low and medium dose range, and a substantially reduced integral dose[1]. Due to the effective sparing of normal tissues without compromised target coverage, PT is primarily applied in paediatric oncology and for malignancies close to critical anatomical structures, i.e. for head-and-neck and skull base region as well as re-irradiations [2–4].

Besides the favorable inverted depth dose profile, protons are biologically more effective than high-energy photon beams. Hence, the relative biological effectiveness (RBE) was introduced as a conversion factor, defined as the ratio of physical doses required to yield the same biological effect [5,6]. Today's clinical practice in PT is still based on a generic RBE of 1.1, a value which was chosen conservatively in the 1960s and 1970s [7,8]. However, the knowledge gained from several studies suggests a variable, rather than a constant RBE. Fractional doses, physical beam characteristics, biological parameters and the investigated endpoint were identified as influencing factors. Especially the increased linear energy transfer at the distal end of the spread-out Bragg Peak (SOBP) is associated with increased biological efficacy [9,10]. However, none of these parameters have so far been implemented in clinical routine, largely due to uncertainties within these complex interactions and the broad range of reported RBE of 0.8 to 2 [11,12]. These variations in RBE can be partly attributed to the use of different reference irradiation qualities, beam delivery techniques and energies, endpoint assessment at different positions within the beam line, and chosen radiobiological model systems [11,13–15].

To account for a potential variable RBE, several mathematical models have been developed to predict the RBE. All phenomenological models are empirical data-based, generally taking into account the dose, dose-averaged linear energy transfer (LET_d) and the tissue-specific parameters generated from

78 a collection of *in vitro* data with clonogenic death as biological endpoint. In contrast to that,
79 mechanistic models are derived from predicting the interaction probability of particles within the
80 biological system, including, to a varying extent, DNA double-strand break repair dynamics. Again,
81 clinical implementation so far was hindered due to uncertainties in the fitting data [16]. Concerning the
82 beam delivery, pencil beam scanning with active or passive depth modulation has eclipsed the
83 traditional passive scattering techniques. The latter was the basic mode of beam delivery in which
84 almost all experimentally available RBE data have been determined. As very recently pointed out, the
85 physical characterization of particle beams and the standardization of dosimetric reporting are
86 essential steps to reduce uncertainties in RBE determination [13,17]. In summary, during the last decades
87 the scientific knowledge, methodological approaches and the mode of proton beam delivery have
88 changed and progressed considerably.

89 The aim of the present study was to investigate the correlation of RBE, LET_d and the tissue specific
90 fractionation sensitivity factor of photons $(\alpha/\beta)_x$ by employing scanned proton beams with an active
91 energy variation in experimental conditions that mimic typical clinical scenarios (e.g. dose, energy
92 range). More specifically, the LET_d dependency of the proton RBE was assessed for four human cell
93 lines with high and low $(\alpha/\beta)_x$ using typical clinical proton energy ranges, provided by the synchrotron
94 at the MedAustron facility. Our experimentally derived RBE values were compared to 3
95 phenomenological models (McNamara[18], Rørvik [19] and Jones[20]) as well as one mechanistic model
96 (double strand break (DSB) model[21]). The phenomenological models were chosen based on their
97 different database characteristics. From the applied models, the McNamara's model (MCN) contains
98 the largest amount of datapoints, 285 in total as compared to 85 datapoints for the Rørvik model (RØR)
99 and 28 datapoints for the Jones model (JON), respectively. MCN and RØR included a variety of cell lines
100 with different $(\alpha/\beta)_x$ in their databases, while the model from JON is exclusively based on low $(\alpha/\beta)_x$
101 data. All three phenomenoglical models depend on the LET_d. The RØR database has the most uniform
102 range of LET_d, MCN is dominated by LET_d values below 5 keV/µm and JON exclusively contains
103 datapoints with LET_d larger than 5 keV/µm. In contrast to MCN and RØR, JON´s tissue dependency is

based on the absolute values of α_x and β_x independently of each other and the input data are solely from tissues with low $(\alpha/\beta)_x$ values [22]. The applied mechanistic model (DSB) for normoxic cells is based on Monte Carlo damage simulation and estimates double strength strand breaks and other simple and more complex clusters of DNA lesions[21]. The DSB model predictions were based on the treatment plans, which were generated for cell irradiations, and directly calculated in the treatment planning system (TPS, Raystation 5.99), where the model is integrated. The predicted values were therefore determined directly at the positions of the cells.

Material and Methods

Cell cultures and procedures

Four human cell lines were chosen, which represent two *in-vitro* models with a high $(\alpha/\beta)_x$ ratio, head-and-neck squamous cell carcinoma (FaDu) and normal skin keratinocytes (HaCat), as well as two models with a low $(\alpha/\beta)_x$, melanoma (SKMel) and prostate carcinoma (Du145).

HaCat were cultured in DMEM (Dulbecco's Modified Eagle Medium), supplemented with 10 % fetal calf serum, 25 mM HEPES, 1 % sodium pyruvate and 100 U/ml penicillin and streptomycin. FaDu were maintained in RPMI 1640 (Roswell Park Memorial Institute), supplemented with 10 % fetal calf serum , 25 mM HEPES, and 100 U/ml penicillin and streptomycin. Du145 and SKMel were cultivated in MEM (Minimum Essential Medium Eagle), supplemented with 10 % fetal calf serum, 25 mM HEPES, 2 mM L-Glutamin and 100 U/ml penicillin and streptomycin.

All cells were cultured at 37°C in a humidified atmosphere with 95 % air and 5 % CO_2. Cells were seeded in chamber slide flasks (Nunc™ Lab-Tek™ II Chamber Slide™ System) with plastic slides at 2.5 to 5 x 10^5 cells per flask 24 to 48 hours before irradiation to achieve 70-80 % confluency at the time of irradiation. Immediately prior to the irradiation, the chamber slide flasks were filled air-bubble free with the respective unsupplemented medium.

Photon and proton irradiation and dosimetry

For both, reference X-ray as well as proton irradiation, dedicated PMMA irradiation setups were developed to accommodate for the horizontal beam geometry and to ensure standardized sample positioning. Detailed dosimetric verification of the PMMA irradiation set-ups preceded the experiments [23]. Cells were irradiated with 0.5 Gy, 1 Gy, 2 Gy, 4 Gy and 6 Gy physical dose. For each experiment an equally processed, non-irradiated negative control was carried out. The negative control was filled with unsupplemented medium and left inside of the irradiation rooms (X-rays as well as proton treatment room) for the duration of a 6 Gy irradiation. The flask holder itself was designed so that the transition zones between PMMA and cell medium were limited (see Figure S1 in supplementary material). This is of essential importance as dose levels can change significantly in such transition zones. The dosimetric impact caused by different cell media and water was investigated in a preceding experiment, where no significant differences were found. For each dose level and beam quality, at least three independent irradiation sessions were conducted.

Reference X-ray irradiation: Reference irradiation was performed in a 200 kV beam, generated by a YXLON unit (Type TU 32-D03, YXLON GmbH, Hamburg, Germany). For details of the dosimetric commissioning of this reference X-ray irradiator please see Kuess et al, 2014 [24]. For the experiments described in this study, the following filtration was used: 3 mm Be + 3 mm Al + 0.5 mm Cu. The cell layer was positioned at 40 cm distance from the beam exit window (see Figure S1 in supplementary material). Absolute dosimetry was conducted for this irradiation geometry with a Farmer type ionization chamber (T31013, PTW Freiburg, Germany) within a cell flask to account for attenuation of the plastic walls. Furthermore, dosimetric measurements were conducted using EBT3-type Gafchromic films to verify dose homogeneity and with PinPoint Ionisation chambers (T31015, PTW Freiburg, Germany) for absolute dosimetry, applying dose determination methodologies similar to patient-specific quality assurance procedures [24–26].

Films were cut in a size to completely cover the cell flask slide where the cells are growing. Using films in combination with the ionization chamber was beneficial to account for realistic X-ray backscatter

produced by the cell medium and the flasks itself. The dose homogeneity of the irradiated area of the chamber slide flask was within +/-3 %.

Proton irradiation: A dedicated PMMA setup was developed for the horizontal beam line at MedAustron (see Figure S2 in supplementary material). A depth of 40 cm allows chamber slide flasks or detectors to be positioned along the entire range of clinically relevant energies up to 250 MeV. Multiple chamber slide flasks can be inserted and irradiated simultaneously. The remaining space of either unused slots or around inserted chamber slide flasks was filled with water to prevent range uncertainties caused by air gaps in the set-up. A computed tomography (CT) scan of the set-up in experimental condition (filled with flasks and water) was used for treatment planning. Using the TPS RayStation (V5.99, Raysearch Laboratories, Sweden), two different irradiation scenarios were planned, each with a SOBP of 80 mm longitudinal dimension. The employed Monte Carlo code in the TPS Raystation 5.99 considers primary protons and secondary ions (protons, deuterons and alpha particles). Primary and secondary protons are accounted for by class II transport method while the energy loss of heaverier secondaries is approximated via a continous slowing down approximation. In set-up A, the more proximal target, the centre of the SOBP was located at 80 mm, with beam energies ranging from 66.5 to 135.6 MeV to cover the entire SOBP. In the more distal located set-up B, the centre of the SOPB was positioned at a depth of about 155 mm with beam energies ranging from 127.2 to 185.9 MeV. The TPS has been specifically commissioned for the proton beam line in the research room at MedAustron following the procedures in the clinical beam lines [27]. In contrast to the experimental validation of the dose calculation, LET_d calculations of the TPS have been validated against independent Monte Carlo particle transport simulations using GATE/Geant4, which itself also applies a dedicated proton beam model tracking all particles through the entire Nozzle. The LET_d of the TPS agreed very well with the independent Monte Carlo simulations for all tested voxel sizes, where only a minor deviation (max. 5 % at the distal edge) could be observed towards the end of the beam range due to the steep LET_d gradient and the moderate beam range differences of the TPS and the Monte Carlo simulations.[28]

Chamber slide flasks were positioned at a proximal, a central and a distal SOBP position for each set-up. More specifically, cell layers were located at 55 mm, 80 mm and 105 mm in set-up A, and at 130 mm, 155 mm and 180 mm in set-up B, respectively. Corresponding LET_d values were derived from Monte Carlo calculations performed with the TPS, based on the energy and beam spot information of the underlying treatment plan [29].

Clonogenic survival assay

Standard clonogenic survival assays were performed after reference X-ray or proton irradiation. Cells were harvested immediately after irradiation, diluted with supplemented medium appropriate for the cell line and seeded in 6-well plates in concentrations according to the dose level: 250 cells (0 Gy and 0.5 Gy), 500 cells (1 Gy, 2 Gy), 1000 cells (4 Gy) and 2000 cells (6 Gy) per well, respectively. Following a cell line specific incubation period (7-14 days), cells were fixed with 96 % methanol, stained with 0.5 % crystal violet solution and colonies of more than 50 cells were considered as surviving clones.

RBE modeling and statistical analysis

Data points in all following tables and figures represent the mean including the standard deviation of ≥ 3 independent experiments. Correlation of the parameters was tested using an F-test on data fitted with linear regression. GraphPad Prism (GraphPad Software, Inc.) and Python 3.6 programming language (Python Software Foundation, https://www.python.org/) were used for statistical procedures and the graphical illustration [30,31].

Linear-quadratic model: Based on the linear-quadratic (LQ) formalism, surviving fractions in relation to the plating efficiency of non-irradiated control samples were calculated for each value of the delivered physical dose in Gy. The mean and standard deviation results from a minimum of 18 individual values, corresponding to a minimum of 3 independent 6-well plates per dose group. Standard errors result from error propagation. A $1/\sigma$-weighted minimum chi-square estimation was applied to the linear-quadratic model for survival curve fitting [32]. Both parameters, α and β, were calculated for both

radiation types using the same fitting method. For cells irradiated in proton beams, RBEs were calculated for the physical doses that reduced the cell survival to 90 %, and 10 %, respectively. To compare the experimental data to the model-based predictions, RBEs were determined as a function of the LQ model parameters and the physical proton dose [33]:

$$RBE\left(D_p, \alpha_x \beta_x, \alpha_p, \beta_p\right) = \frac{\sqrt{\alpha_x^2 + 4\beta_x D_p\left(\alpha_p + \beta_p D_p\right)} - \alpha_x}{2\beta_x D_p}$$

Equation 1: Calculation of the RBE [33,34]

The equation 1 can be rewritten as a function of RBE_{max} and the RBE_{min} [35]

$$RBE\left(D_p, \left(\frac{\alpha}{\beta}\right)_x, RBE_{max}, RBE_{min}\right)$$

$$= \frac{1}{2D_p}\left(\sqrt{\left(\frac{\alpha}{\beta}\right)_x^2 + 4D_p\left(\frac{\alpha}{\beta}\right)_x RBE_{max} + 4{D_p}^2 RBE_{min}^2} - \left(\frac{\alpha}{\beta}\right)_x\right)$$

Equation 2: RBE as a function of the RBE_{max} and the RBE_{min}

All applied phenomenological models have equation 2 in common but differ in their definition of the RBE_{max} and RBE_{min} functions. More details on the RBE models are summarized in the supplementary information (S4-S6). RBE values derived from the experiments and models were determined at dose levels of 0.5 Gy, 2 Gy and 6 Gy.

Results

Reference dosimetry and LET_d

Within the area of interest of 550 × 800 mm^2 (area covering chamber slide flask) the dose homogeneity in both the 200 kV reference irradiation set-up and the two proton set-ups was within 3 %. For the reference irradiation the dose rate at the object surface was 1.28 ± 0.02 Gy/min. This value was measured with EBT3 radiochromic films, which were calibrated against Farmer type ionization

chamber in PMMA. Table 1 summarizes the LET_d values for proton irradiations, determined directly in TPS with Monte Carlo methods.

Table 1: Sample positions within the irradiation setup with corresponding LET_d values

	set-up A proton energies: 66.5-135.6 MeV		set-up B proton energies: 127.2-185.9 MeV	
relative position	depth (mm)	LET_d (keV/µm)	depth (mm)	LET_d (keV/µm)
proximal	55	2.1	130	1.9
central	80	2.8	155	2.5
distal	105	4.5	180	4.1

Figure 1 depicts the central axis depth dose distribution of set-up A and set-up B, including sample positioning and LET_d, respectively.

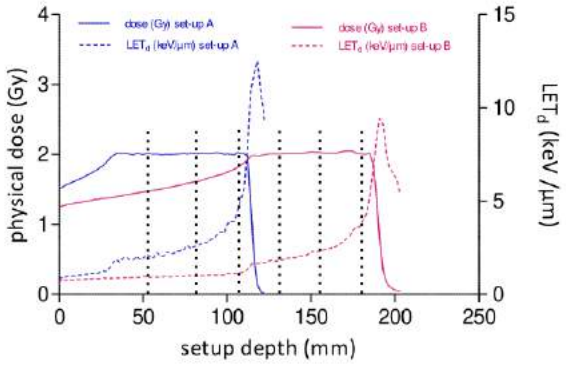

Fig. 1: Central axis depth dose distribution of the proximal set-up A and the distal set-up B, based on Monte Carlo calculation. The solid lines represent TPS data for both targets. The dashed lines illustrate the LET_d. The proximal target is indicated in blue, the distal target in pink. The SOBPs of both targets encompassed 3 positions each (proximal, middle and distal), indicated by black dotted stripes.

X-ray sensitivity

α_x values of 0.30 ± 0.02, 0.30 ± 0.02, 0.14 ± 0.02, and 0.12 ± 0.01 for HaCat, FaDu, Du145, and SKMel, respectively, were obtained from the X-ray survival curves. Corresponding β_x values were 0.02 ± 0.00

(HaCat), 0.03 ± 0.00 (FaDu), 0.03 ± 0.00 (Du145), and 0.04 ± 0.00 (SKMel). The four cell lines were categorized according to their $(\alpha/\beta)_X$ ratios in high $(\alpha/\beta)_X$ cell lines (FaDu and HaCat, $\alpha/\beta \geq 10$) and low $(\alpha/\beta)_X$ cell lines (Du145 and SKMel, $\alpha/\beta < 5$) for subsequent analysis in proton beams. The respective survival parameters are summarized in the left part of table 2.

Proton sensitivity

After proton irradiation, survival curves and (α/β) parameters were calculated for all four cell lines, the respective survival parameters are summarized in table 2. Cell survival curves as a function of dose are depicted in figure 2, sorted from lowest LET_d to highest LET_d (also see figure S3 in supplementary material).

Table 2: LQ-derived cell survival parameters and RBE values

	200 kV X-ray			protons				
Cell line	α_x (Gy^{-1})	β_x (Gy^{-2})	α/β_x (Gy)	LET_d (keV/µm)	α (Gy^{-1})	β (Gy^{-2})	α/β (Gy)	$expRBE_{90}$	$expRBE_{10}$
HaCat	0.30 ± 0.02	0.02 ± 0.00	15.0	1.9	0.20 ± 0.03	0.04 ± 0.01	5.53 ± 1.73	0.72 ± 0.09	1.00 ± 0.02
				2.1	0.25 ± 0.09	0.03 ± 0.02	9.37 ± 9.30	0.84 ± 0.26	0.97 ± 0.05
				2.5	0.25 ± 0.06	0.03 ± 0.01	7.52 ± 4.66	0.87 ± 0.19	1.05 ± 0.04
				2.8	0.25 ± 0.11	0.04 ± 0.02	6.82 ± 6.73	0.87 ± 0.32	1.07 ± 0.05
				4.1	0.22 ± 0.03	0.04 ± 0.01	5.77 ± 1.78	0.79 ± 0.10	1.05 ± 0.02
				4.5	0.33 ± 0.06	0.02 ± 0.01	15.88 ± 10.37	1.13 ± 0.18	1.09 ± 0.03
FaDu	0.30 ± 0.02	0.03 ± 0.00	10.0	1.9	0.31 ± 0.02	0.03 ± 0.00	10.65 ± 2.51	1.04 ± 0.09	1.02 ± 0.02
				2.1	0.25 ± 0.02	0.03 ± 0.00	7.11 ± 1.19	0.85 ± 0.06	0.97 ± 0.02
				2.5	0.23 ± 0.01	0.04 ± 0.00	5.10 ± 0.41	0.80 ± 0.04	1.02 ± 0.01
				2.8	0.20 ± 0.03	0.05 ± 0.01	4.36 ± 1.33	0.72 ± 0.10	0.99 ± 0.02
				4.1	0.29 ± 0.04	0.04 ± 0.01	8.05 ± 3.01	0.99 ± 0.14	1.06 ± 0.03
				4.5	0.26 ± 0.01	0.04 ± 0.00	6.41 ± 0.56	0.90 ± 0.05	1.04 ± 0.01
Du145	0.14 ± 0.02	0.03 ± 0.00	4.7	1.9	0.34 ± 0.02	0.02 ± 0.00	18.51 ± 6.08	2.19 ± 0.22	1.28 ± 0.03
				2.1	0.30 ± 0.01	0.04 ± 0.00	8.34 ± 0.84	1.95 ± 0.17	1.37 ± 0.03
				2.5	0.31 ± 0.01	0.03 ± 0.00	10.25 ± 1.25	2.12 ± 0.19	1.39 ± 0.03
				2.8	0.33 ± 0.03	0.03 ± 0.00	10.22 ± 2.90	2.11 ± 0.24	1.39 ± 0.04
				4.1	0.37 ± 0.03	0.03 ± 0.01	10.97 ± 2.72	2.40 ± 0.26	1.51 ± 0.03
				4.5	0.39 ± 0.04	0.03 ± 0.01	12.54 ± 4.67	2.52 ± 0.29	1.53 ± 0.05
SKMel	0.12 ± 0.01	0.04 ± 0.00	3.0	1.9	0.32 ± 0.02	0.04 ± 0.01	8.67 ± 1.78	2.22 ± 0.21	1.36 ± 0.03
				2.1	0.35 ± 0.02	0.04 ± 0.00	9.15 ± 1.50	2.41 ± 0.22	1.43 ± 0.03
				2.5	0.29 ± 0.03	0.06 ± 0.01	4.71 ± 1.00	2.05 ± 0.23	1.49 ± 0.03
				2.8	0.43 ± 0.02	0.03 ± 0.00	12.84 ± 2.30	2.92 ± 0.25	1.56 ± 0.03
				4.1	0.34 ± 0.01	0.07 ± 0.00	5.20 ± 0.41	2.42 ± 0.19	1.64 ± 0.03
				4.5	0.42 ± 0.04	0.06 ± 0.01	6.60 ± 1.54	2.88 ± 0.23	1.76 ± 0.05

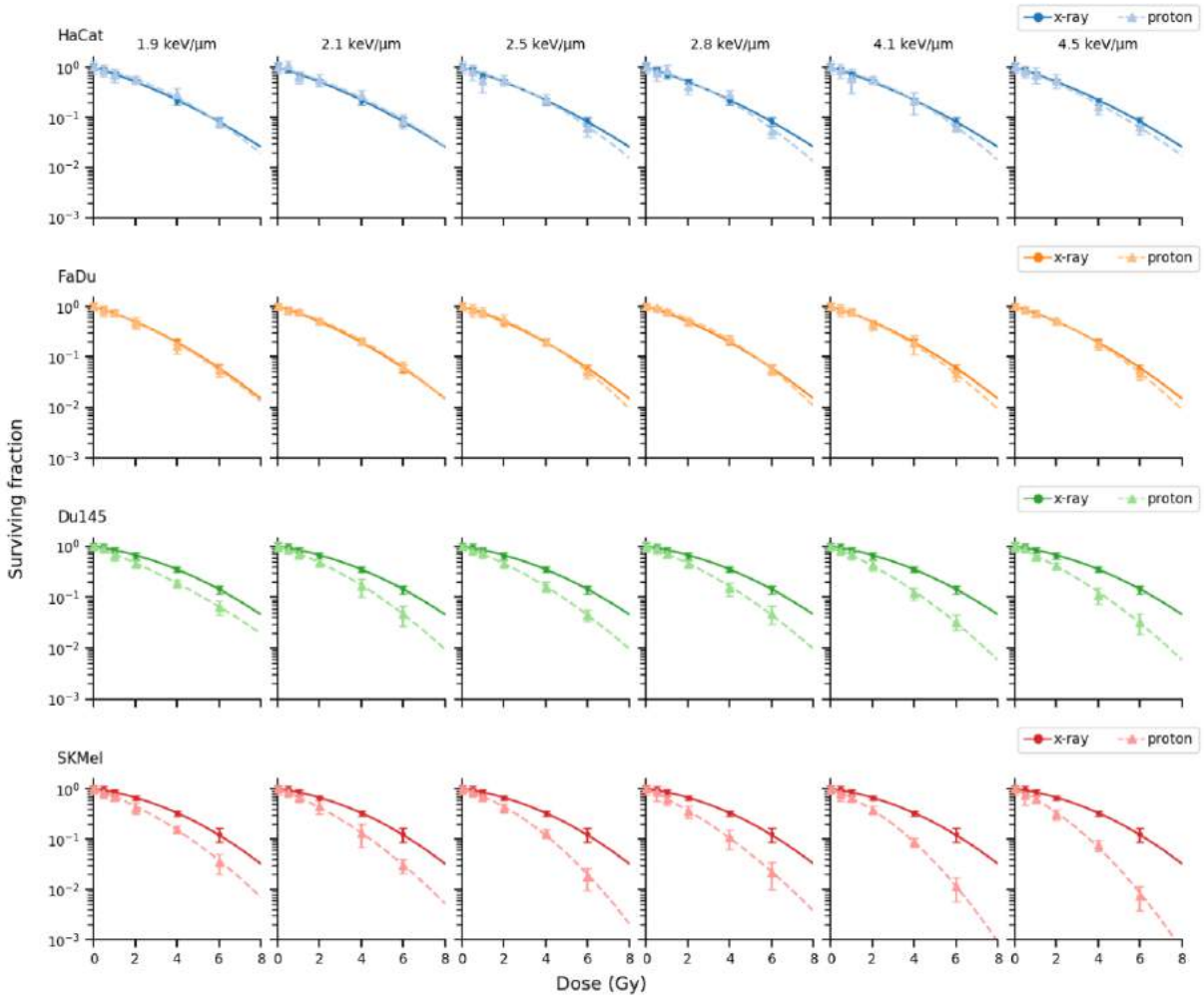

Fig.2: Cell survival curves of HaCat, FaDu, Du145, and SKMel after X-ray (solid lines) and proton irradiation (dashed lines) sorted from the lowest to the highest LET_d. Data points represent a mean of a minimum of 3 independent experiments ± standard errors.

For HaCat and FaDu, the RBE values ranged from 0.72 ± 0.09 to 1.13 ± 0.18 for all levels of cell survival and for every LET_d value. In contrast, the low $(\alpha/\beta)_x$ cell lines, Du145 and SKMel exhibited RBE values substantially higher than the currently clinically used 1.1 for all levels of cell survival. For Du145 and SKMel cells, RBE values between 1.95 ± 0.17 and 2.92 ± 0.25 were obtained for the low dose range at 90 % of cell survival and between 1.28 ± 0.03 and 1.76 ± 0.05 for 10 % of cell survival (table 2).

To test a potential correlation of LET_d and RBE, the experimental RBE values were fitted with linear regression (Fig.3). No correlation was found for HaCat and FaDu. RBE values remained around unity across the whole investigated LET_d range. For HaCat, p-values of 0.0834 (RBE_{10}) and 0.1545 (RBE_{90}) were calculated. F-tests on FaDu linear regression fits resulted in p-values of 0.1134 (RBE_{10}) and 0.8265

(RBE$_{90}$). A significant correlation between LET$_d$ and RBE was found for Du145 at both levels of cell survival (RBE$_{10}$ = p ≤ 0.0021, RBE$_{90}$ = p ≤ 0.0183). SKMel displayed a significant correlation at RBE$_{10}$ with p ≤ 0.0013 but not at RBE$_{90}$ with p ≤ 0.2723.

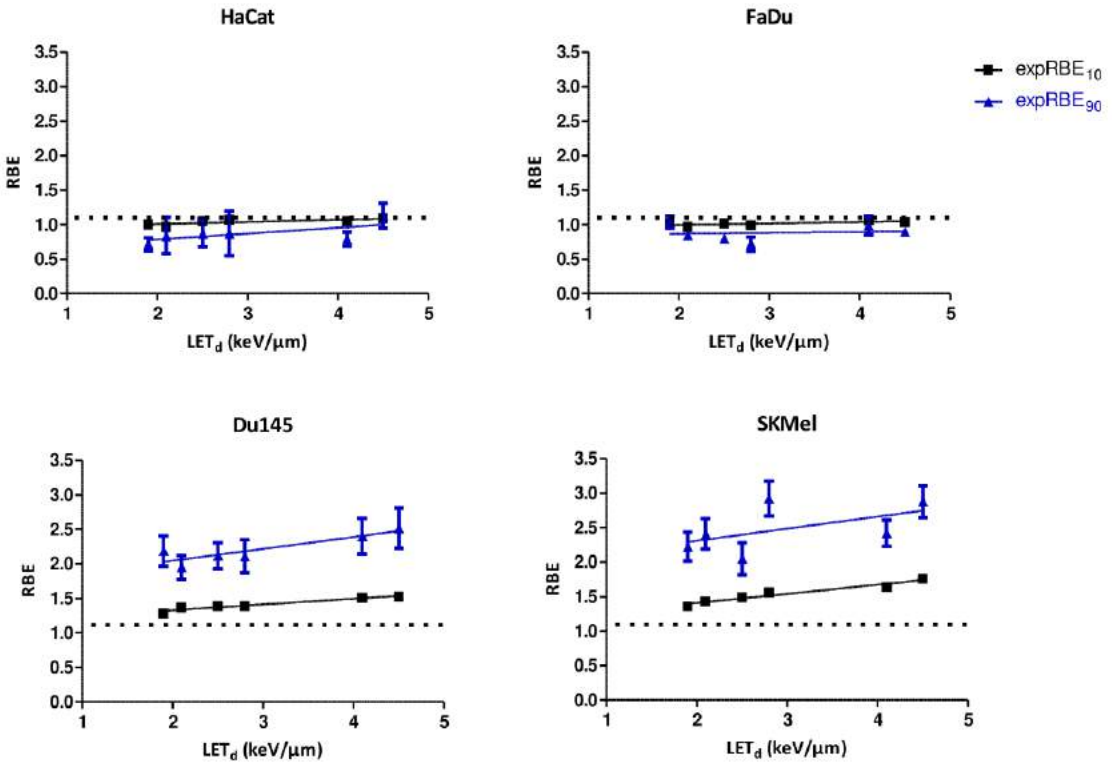

Fig. 3: RBE as a function of LET$_d$: RBE values as a funtion of LET$_d$ at cell survival levels of 10 % (black squares) and 90 % (blue triangles). The constant RBE level of 1.1. is illustrated with dotted lines. Linear fits were obtained from linear regression. Slopes were tested with F-test. Data points represent a mean of a minimum of 3 independent experiments including the corresponding standard errors.

RBE model prediction at the dose level of 2 Gy are summarized in table 3 and plotted against LET$_d$ in comparision to the experimentally derived RBE$_{2Gy}$ in Fig. 4.

280 **Table 3: Model-derived RBE predictions**

Cell line	LET_d (keV/µm)	$expRBE_{2Gy}$	MCN_{2Gy}	$RØR_{2Gy}$	JON_{2Gy}	DSB_{2Gy}
HaCat	1.9	0.84 ± 0.11	1.04 ± 0.00	1.06 ± 0.00	1.23 ± 0.01	1.16
	2.1	0.92 ± 0.27	1.05 ± 0.00	1.07 ± 0.00	1.25 ± 0.01	1.16
	2.5	0.92 ± 0.18	1.05 ± 0.00	1.09 ± 0.01	1.31 ± 0.01	1.20
	2.8	0.97 ± 0.31	1.06 ± 0.00	1.10 ± 0.01	1.35 ± 0.01	1.17
	4.1	0.89 ± 0.89	1.08 ± 0.01	1.14 ± 0.01	1.51 ± 0.02	1.23
	4.5	1.08 ± 0.17	1.08 ± 0.10	1.15 ± 0.01	1.56 ± 0.02	1.22
FaDu	1.9	1.02 ± 0.07	1.07 ± 0.00	1.09 ± 0.01	1.21 ± 0.01	1.16
	2.1	0.88 ± 0.07	1.07 ± 0.00	1.10 ± 0.01	1.23 ± 0.01	1.16
	2.5	0.88 ± 0.05	1.08 ± 0.00	1.11 ± 0.01	1.28 ± 0.01	1.20
	2.8	0.85 ± 0.10	1.08 ± 0.00	1.13 ± 0.01	1.31 ± 0.01	1.17
	4.1	1.02 ± 0.12	1.11 ± 0.01	1.18 ± 0.01	1.46 ± 0.02	1.23
	4.5	0.95 ± 0.05	1.12 ± 0.01	1.20 ± 0.01	1.50 ± 0.02	1.22
Du145	1.9	1.61 ± 0.11	1.11 ± 0.01	1.14 ± 0.02	1.21 ± 0.02	1.16
	2.1	1.61 ± 0.10	1.12 ± 0.01	1.15 ± 0.02	1.23 ± 0.02	1.16
	2.5	1.64 ± 0.13	1.13 ± 0.01	1.18 ± 0.02	1.28 ± 0.02	1.20
	2.8	1.64 ± 0.13	1.14 ± 0.01	1.20 ± 0.03	1.32 ± 0.02	1.17
	4.1	1.75 ± 0.14	1.19 ± 0.02	1.29 ± 0.04	1.46 ± 0.03	1.23
	4.5	1.81 ± 0.16	1.20 ± 0.02	1.31 ± 0.05	1.50 ± 0.03	1.22
SKMel	1.9	1.61 ± 0.09	1.14 ± 0.02	1.17 ± 0.04	1.17 ± 0.01	1.16
	2.1	1.69 ± 0.07	1.15 ± 0.02	1.18 ± 0.04	1.19 ± 0.01	1.16
	2.5	1.63 ± 0.10	1.17 ± 0.03	1.22 ± 0.05	1.23 ± 0.01	1.20
	2.8	1.84 ± 0.07	1.18 ± 0.03	1.24 ± 0.05	1.26 ± 0.01	1.17
	4.1	1.81 ± 0.05	1.23 ± 0.04	1.34 ± 0.08	1.38 ± 0.02	1.23
	4.5	1.95 ± 0.11	1.25 ± 0.05	1.37 ± 0.09	1.42 ± 0.02	1.22

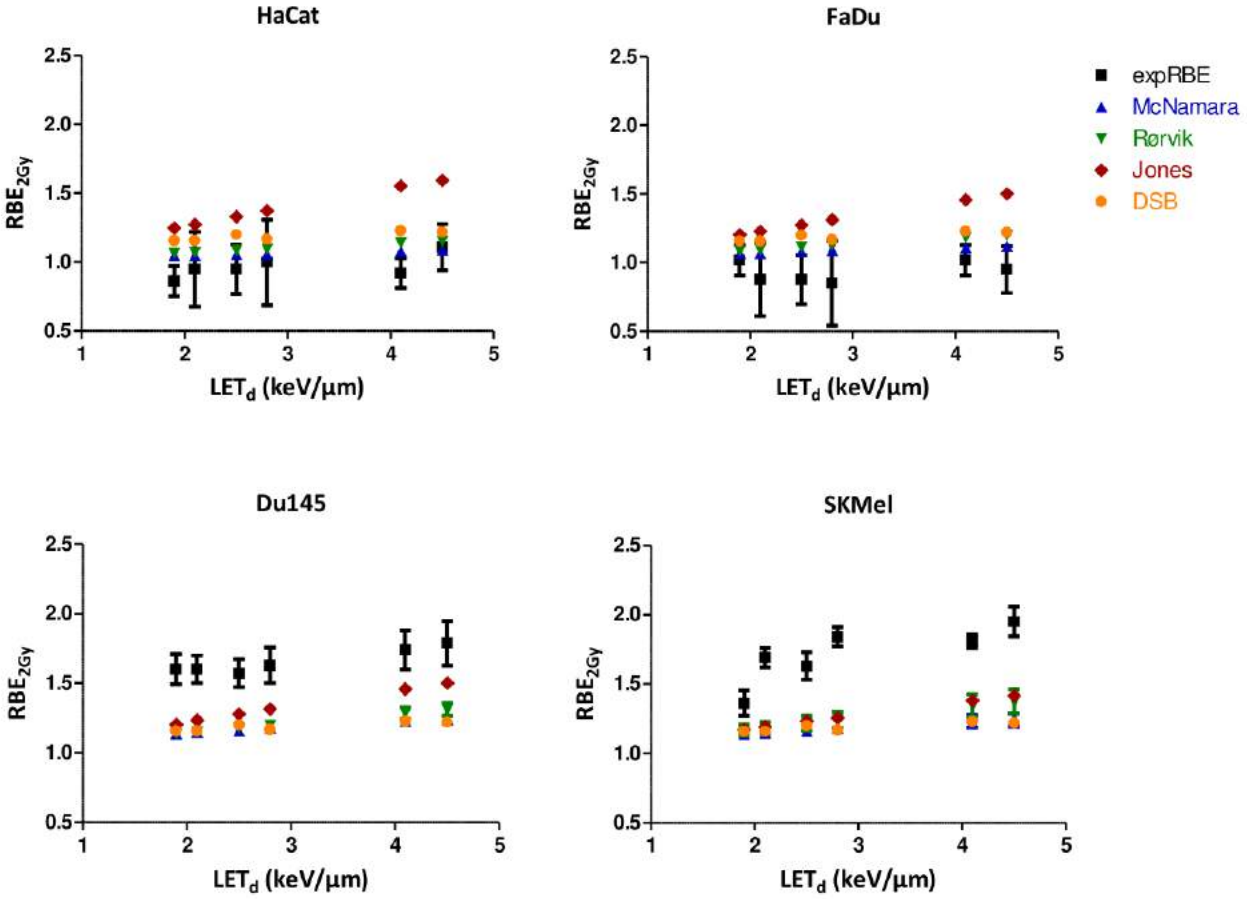

281

282 Fig. 4: Experimental and model-derived RBE_{2Gy} estimates as a function of the LET_d. Data points represent a mean
283 of a minimum of 3 independent experiments. The error bars indicate the estimated standard deviation obtained
284 by error propagation of the measurement uncertainties on the alpha/beta values, for both, experimentally and
285 model-derived RBE values.

286

287 All three phenomenological models predicted an increase of the RBE with increasing LET_d. RBE
288 calculations according to the McNamara model resulted in values ranging from 1.04 to 1.12 for both
289 high $(\alpha/\beta)_x$ cell lines (HaCat and FaDu) and from 1.11 to 1.25 for Du145 and SKMel. The RØR model
290 predicted RBE_{2Gy} between 1.06 and 1.20 for HaCat and FaDu and 1.14 and 1.37 for Du145 and SKMel.
291 The JON modeling resulted in RBE_{2Gy} of 1.21 to 1.56 for HaCat and FaDu and 1.17 to 1.50 for Du145
292 and SKMel. The MCN and RØR models assumed higher RBE values for the low $(\alpha/\beta)_x$ cell lines Du145

293 and SKMel as compared to the high $(\alpha/\beta)_x$ cell lines HaCat and FaDu. The JON model predicted RBE
294 values of the same range for all cell lines. The mechanistic DSB model does not utilize tissue-dependent
295 parameters and hence gives the same RBE_{2Gy} values for all 4 cell lines. While the JON model predicted
296 the steepest increase of the RBE for all 4 cell lines, the DSB model assumed the least sensitivity towards
297 LET_d changes.
298 For both high $(\alpha/\beta)_x$ cell lines, HaCat and FaDu, MCN predictions agreed well with the experimentally
299 derived RBE_{2Gy} values for most of the data points. Similar agreement, even though slightly worse than
300 for the MCN model, was observed for the RØR and DSB models.
301 All models clearly underestimated the RBEs for the investigated low $(\alpha/\beta)_x$ cell lines. While the model
302 estimates were found to agree for all RBE values over the LET_d range, no overlap with the experimental
303 RBE_{2Gy} range was observed, even though the model databases contain low $(\alpha/\beta)_x$ and low LET_d (<
304 5keV/um) data points.
305
306 **Discussion**
307 With the increasing number of patients treated with proton therapy, the concept of using a constant
308 RBE of 1.1 is increasingly discussed but will probably remain an accepted approximation until the
309 uncertainties concerning physical and biological parameters can be substantially reduced [36,37]. Recent
310 reports raised concerns that a constant RBE is not beneficial for certain tissues and can cause adverse
311 effects after PT [12,38,39].

312 Most of the published studies on RBE dependencies focused only on one factor of influence and often
313 assessed only one position within a SOBP. In addition, they were conducted using passive scattering,
314 which historically was the most widely used beam delivering technique [9,40,41]. This study aimed to
315 overcome some of the limitations of previous studies. The above mentioned considerable
316 uncertainties in reported RBE from *in vitro* and *in vivo* studies can partly be attributed to non-
317 standardized experimental techniques and limited reporting on the experiment´s physical aspects,
318 such as beam characteristics and dosimetry.

In order to minimize experimental uncertainties in radiobiological experiments for subsequent correlation between biological response and physical parameters, standardized irradiation setups for both X-ray reference and proton irradiation were subjected to extensive dosimetric assessment prior to this study [23]. The focus was set on clinically relevant proton energies and corresponding LET_d values. Finally, four human cell lines were selected to address differences in RBE dependencies for high and low $(\alpha/\beta)_x$.

As far as LET_d dependencies of RBE are concerned, multiple studies demonstrated that the RBE increases with LET_d and thus towards the distal end of an SOBP even in proton beams [42–44]. Our study confirms such an LET_d - RBE relationship, however, only for low $(\alpha/\beta)_x$ cell lines. In this context our results complement previous studies, which suggest higher RBE values for tissues with low $(\alpha/\beta)_x$ [45,46]. In our study we tried to mimic clinical scenarios conserning the irradiation conditions, e.g. the SOPB size and the target depth. Despite the low LET_d values resulting from clinically relevant proton energy ranges for an irradiation volume of (8 x 10 x 10 cm^3) located at a depth of 80 mm and 155 mm, still substantial RBE variations could be observed.

An inverse relationship between RBE and dose per fraction was proposed [5,11,47] and confirmed by our study, however, only for low $(\alpha/\beta)_x$ cell lines. We observed the highest RBE values in the low dose range for melanoma and prostate carcinoma cells, both having an $(\alpha/\beta)_x < 5$. No marked increase of the RBE with the LET_d was found for the high $(\alpha/\beta)_x$ lines: squamous cell carcinoma cell line FaDu and the normal keratinocyte cell line HaCat. RBE_{2Gy} determined in our study are in agreement with published data. Wang et al, who assessed the impact of the HPV status on the RBE of protons in different head-and-neck squamous cell carcinoma cell lines, report RBE_{2Gy} values between 1.15 and 1.19 [48]. Zlobinskaya et al. found a RBE_{10} of 1.1 in a FaDu xenofgraft model [49]. Skin reactions following proton irradiation with moist desquamation as endpoint were quantified by Sørensen et al, who calculated RBE values between 0.9 and 1.06 [50].

Compared to cell lines with high $(\alpha/\beta)_x$ values, less literature data are available for human low $(\alpha/\beta)_x$ lines and thus for benchmarking our melanoma or prostate carcinoma data. Petrovic et al. determined

an RBE_{2Gy} in a range of 1.69 to 2.14 for their melanoma cell line, which agrees well with our data [51]. Petringa et al. investigated the RBE of protons in Du145 but, in contrast to our study, concluded a good agreement between model RBE predictions (Local Effect Model, MCN) and experimental values [52].

The higher LET_d associated with scanned protons and range uncertainties might result in excess dose and LET_d outside of the planning target volume. Assuming that the cell/tissue sensitivity towards increased LET_d is determined by its $(\alpha/\beta)_x$ value, RBE values that differ considerably from the constant 1.1 can be expected towards the distal end of the SOBP, predominantly for low doses per fraction and low $(\alpha/\beta)_x$ ratio systems. The current policy of treatment planning with a static RBE of 1.1 for protons, regardless of tumor type and depth, is based on averaged historical data obtained with scattered proton beams [11,34]. Typical low $(\alpha/\beta)_x$ normal tissues adjacent to the PTV, such as the central nervous system, may need special attention in treatment planning given the current practice of treatment planning.

For tissues with high $(\alpha/\beta)_x$, the higher LET_d of scanned protons appears to be negligible. RBE values around unity, as found in this study and previously reported for tumors displaying high α/β values (e.g. medulloblastoma and head-and-neck malignancies), indicate a slight RBE overestimation in current practice [45 53].

Based on the concerns regarding a constant RBE value of 1.1, several RBE models have been developed to predict RBE values taking into account the physical and biological factors. The phenomenological models are based on the widely accepted- and used LQ formalism and incorporate tissues specific survival parameters, dose and LET_d. Differences in input parameters and model assumptions, however, were recently shown to result in variations of the RBE predictions [19]. In this study 3 phenomenological models and 1 mechanistic model were selected to predict the RBE values. The experimental *in vitro* data were systematically compared to model predictions. In contrast to the mechanistic DSB model, the applied phenomenological models assume an inverse relationship of RBE and photon-derived $(\alpha/\beta)_x$. For the high $(\alpha/\beta)_x$ cell lines, all models slightly overestimated the RBE values. MCN predictions were the closest and mainly agreeing with experimental values within the statistical uncertainties. JON

calculated the highest RBE, deviating the most from the experimentally derived RBE_{2Gy} values for FaDu and HaCat. The JON database consists of not only proton data but also experiments with heavier ions. The combination of particles in the modeling may result in higher RBE predictions for protons, as observed in our study. JON´s model is exclusively derived from experiments based on a small range of low $(\alpha/\beta)_x$ values and while deviating the most for the high $(\alpha/\beta)_x$ cell lines, the predictions deviate the least from all applied models for the low $(\alpha/\beta)_x$ cell lines. When the phenomenological models were compared at different dose levels, it was noted that in-between model agreement as well as prediction accuracy increased for higher doses (see results presented in supplementary material). Smaller errors as well as decreased deviation from the RBE_{exp} were obtained for survival at 6 Gy (RBE_{6Gy}) as compared to 2Gy (RBE_{2Gy}) or 0.5Gy ($RBE_{0.5Gy}$), respectively (S7-8).

The observed deviations of model-derived RBE estimates and experimentally derived RBE values may be based on differences in model input parameters and/or reference irradiation. MCN and RØR accounted for the higher efficiency of low kV X-rays [19] and normalized their model input data to a 6 MeV radiation quality. In this study, we report RBE values derived from experiments with a 200 kV X-ray reference beam. Rørvik et al. provides a systematic comparison of $(\alpha/\beta)_x$ values, LET_d inputs and different RBE models [22]. Two chosen phenomenological models MCN and RØR applied in this study were chosen based on their LET_d range which covers the low LET_d values (< 5 keV/µm) relevant for our study. Furthermore, all chosen models include low $(\alpha/\beta)_x$ cell lines in their databases. In contrast to our study, however, the databases of all 3 phenomenological models are dominated by non-human low $(\alpha/\beta)_x$ cell lines, such as the V-79 chinese hamster fibroblasts, which may contribute to the differences between model predictions and experimentally derived RBE_{2Gy} values.

A major challenge remains if and how to account for the growing body of evidence that the RBE of protons is not constant. Accounting for the increase of LET_d with depth, similar to the clinical practice of carbon ion therapy, and the adaptation of an α/β-weighing factor could improve PT treatment planning and consequently safety and effectiveness. Given the reliance of treatment planning and modeling in both proton and carbon ion therapy on *in vitro* data, research to complement the

increasing clinical utilization of particle therapy needs to build on high dosimetric accuracy and detailed reporting on relevant physical data. Only then model refinement can improve patient outcomes, but will directly depend on well-characterized experiments to generate data with minimized physical and biological uncertainties.

This study focused on the irradiation response of 2D monocultures. This is in line with the fact that several biological optimisation algorithms used in TPS for particle therapy, especially for heavier ions, are based on 2D *in vitro* data. Most of the studies concerning RBE determination are in essence done with 2D cultures because of their simple and fast handling and well established endpoint methods [43–45,54]. What differentiates this study from others is the application of clinically relevant doses and energy ranges and the use of a scanning pencil beam delivery system. However, multicellular 3D models of malignancies gain increasing importance in cancer research. Stromal disease components and 3D-associated factors such as signaling gradients and diffusion as well as perfusion limitations contribute significantly to the therapy response *in vivo* [55–59]. These factors have not been considered in our study, as the main intention was to benchmark our data with already existing *in vitro* data and to specifically assess the RBE as a function of $(\alpha/\beta)_x$, derived from the basic LQ formula that is only applicable to 2D *in vitro* data [60].

Conclusions

The tissue specific fractionation sensitivity factor of photons, i.e. the $(\alpha/ß)_x$ ratio, is a clear determinant of the RBE of protons and a predictor for its sensitivity towards LET_d changes. Higher RBE values than 1.1 can be expected for low $(\alpha/ß)_x$ tissues at proton beam end-of-range positions within the clinical practice of applied fractional doses. Current practice might slightly overestimate the RBE of protons for tissues with high $(\alpha/ß)_x$ ratios.

Acknowledgements

The authors wish to thank Mr. Anton Kerschbaum, BSc, MedAustron Control Systems Group, for providing the python script used for data analyses in this study. The introduction into python programming and the valuable continuous support in python programming is greatly acknowledged.

Funding details

Simon Deycmar is beneficiary of the ITN RADIATE funded by the European Union`s Horizon 2020 research and innovation programme under the Marie Sklodowska-Curie grant agreement (No. 642623) and supported by the Swiss State Secretariat for Education, Research and Innovation (SBFI, No. 15.0066)

Conflict of interest statement

The authors state that there are no conflicts of interest.

References

1. Schulz-Ertner D, Tsujii H. Particle Radiation Therapy Using Proton and Heavier Ion Beams. *J Clin Oncol*. 2007;25(8):953-964. doi:10.1200/JCO.2006.09.7816.
2. Hess CB, Indelicato DJ, Paulino AC, et al. An Update From the Pediatric Proton Consortium Registry. *Front Oncol*. 2018;8:165. doi:10.3389/fonc.2018.00165.
3. El Shafie RA, Czech M, Kessel KA, et al. Clinical outcome after particle therapy for meningiomas of the skull base: toxicity and local control in patients treated with active rasterscanning. *Radiat Oncol*. 2018;13(1):54. doi:10.1186/s13014-018-1002-5.
4. El Shafie RA, Czech M, Kessel KA, et al. Evaluation of particle radiotherapy for the re-irradiation of recurrent intracranial meningioma. *Radiat Oncol*. 2018;13(1):86. doi:10.1186/s13014-018-1026-x.
5. Wambersie A, Hendry JH, Andreo P, et al. The RBE issues in ion-beam therapy: conclusions of a joint IAEA/ICRU working group regarding quantities and units. *Radiat Prot Dosimetry*. 2006;122(1-4):463-470. http://dx.doi.org/10.1093/rpd/ncl447.
6. Wambersie A, Menzel HG, Andreo P, et al. Isoeffective dose: a concept for biological weighting of absorbed dose in proton and heavier-ion therapies. *Radiat Prot Dosimetry*. 2011;143(2-4):481-486. http://dx.doi.org/10.1093/rpd/ncq410.
7. Tepper J, Verhey L, Goitein M, Suit HD, Phil D, Koehler AM. In vivo determinations of RBE in a high energy modulated proton beam using normal tissue reactions and fractionated dose schedules. *Int J Radiat Oncol • Biol • Phys*. 1977;2(11):1115-1122. doi:10.1016/0360-3016(77)90118-3.
8. ICRU. Prescribing, Recording, and Reporting Proton-Beam Therapy (ICRU Report 78). *ICRU Rep 78*. 2007.
9. Maeda K, Yasui H, Matsuura T, et al. Evaluation of the relative biological effectiveness of spot-scanning proton irradiation in vitro. *J Radiat Res*. 2016;57(3):307-311. doi:10.1093/jrr/rrv101.
10. Gridley DS, Pecaut MJ, Mao XW, Wroe AJ, Luo-Owen X. Biological Effects of Passive Versus Active Scanning Proton Beams on Human Lung Epithelial Cells. *Technol Cancer Res Treat*. 2015;14(1):81-98. doi:10.7785/tcrt.2012.500392.
11. Paganetti HAP, Iemierko ANN, Ncukiewicz MAA, et al. Relative Biological Effectiveness (RBE) values for proton beam therapy. 2002;53(2):407-421.
12. Sethi R V, Giantsoudi D, Raiford M, et al. Patterns of Failure After Proton Therapy in Medulloblastoma; Linear Energy Transfer Distributions and Relative Biological Effectiveness Associations for Relapses. *Int J Radiat Oncol • Biol • Phys*. 2014;88(3):655-663. doi:10.1016/j.ijrobp.2013.11.239.
13. Paganetti H, Blakely E, Carabe-Fernandez A, et al. Report of the AAPM TG-256 on the relative biological effectiveness of proton beams in radiation therapy. *Med Phys*. 2019;0(0). doi:10.1002/mp.13390.
14. Wambersie A, Hendry JH, Andreo P, et al. THE RBE ISSUES IN ION-BEAM THERAPY : CONCLUSIONS OF A JOINT IAEA / ICRU WORKING GROUP REGARDING QUANTITIES AND UNITS. *Radiat Prot Dosimetry*. 2006;122(1):463-470. doi:10.1093/rpd/ncl447.
15. Liu Q, Ghosh P, Magpayo N, et al. Lung Cancer Cell Line Screen Links Fanconi Anemia / BRCA Pathway Defects to Increased Relative Biological Effectiveness of Proton Radiation. *Radiat Oncol Biol*. 2015;91(5):1081-1089. doi:10.1016/j.ijrobp.2014.12.046.
16. Smith EAK, Henthorn NT, Warmenhoven JW, et al. In Silico Models of DNA Damage and Repair in Proton Treatment Planning: A Proof of Concept. *Sci Rep*. 2019;9(1):19870. doi:10.1038/s41598-019-56258-5.
17. Durante M, Paganetti H, Pompos A, Kry SF, Wu X, Grosshans DR. Report of a National Cancer Institute special panel: Characterization of the physical parameters of particle beams for biological research. *Med Phys*. 2019;46(2):e37-e52. doi:10.1002/mp.13324.
18. McNamara AL, Schuemann J, Paganetti H. A phenomenological relative biological effectiveness (RBE) model for proton therapy based on all published in vitro cell survival data. *Phys Med Biol*. 2015;60(21):8399-8416. doi:10.1088/0031-9155/60/21/8399.

19. Rørvik E, Thörnqvist S, Stokkevåg CH, Dahle TJ, Fjæra LF, Ytre-Hauge KS. A phenomenological biological dose model for proton therapy based on linear energy transfer spectra. *Med Phys*. 2017;44(6):2586-2594. doi:10.1002/mp.12216.
20. Jones B. A Simpler Energy Transfer Efficiency Model to Predict Relative Biological Effect for Protons and Heavier Ions. *Front Oncol*. 2015;5:184. doi:10.3389/fonc.2015.00184.
21. Stewart RD, Streitmatter SW, Argento DC, et al. Rapid MCNP simulation of DNA double strand break (DSB) relative biological effectiveness (RBE) for photons, neutrons, and light ions. *Phys Med Biol*. 2015;60(21):8249-8274. doi:10.1088/0031-9155/60/21/8249.
22. Rørvik E, Fjæra LF, Dahle TJ, et al. Exploration and application of phenomenological RBE models for proton therapy. *Phys Med Biol*. 2018;63(18):185013. doi:10.1088/1361-6560/aad9db.
23. Clausen M, Khachonkham S, Gruber S, et al. Phantom design and dosimetric characterization for multiple simultaneous cell irradiations with active pencil beam scanning. *Radiat Environ Biophys*. 2019;58(4):563-573. doi:10.1007/s00411-019-00813-1.
24. Kuess P, Bozsaky E, Hopfgartner J, Seifritz G, Dörr W, Georg D. Dosimetric challenges of small animal irradiation with a commercial X-ray unit. *Z med Phys*. 2014. doi:10.1016/j.zemedi.2014.08.005.
25. Placidi L, Tongo W, Weber D, Lomax A, Hrbacek J. Range resolution and reproducibility of a dedicated phantom for proton PBS daily quality assurance. *Z Med Phys*. 2018;4:310-317. doi:doi: 10.1016/j.zemedi.2018.02.001.
26. Palmans H, Vatnitsky SM. Beam monitor calibration in scanned light-ion beams. *Med Phys*. 2016;43(11):5835-5847. doi:10.1118/1.4963808.
27. Carlino A, Kragl G, Böhlen TT, et al. 10. Dosimetric commissioning of PB and MC algorithms for a synchrotron based proton PBS delivery. *Phys Medica Eur J Med Phys*. 2018;56:66-67. doi:10.1016/j.ejmp.2018.04.020.
28. Martino G, Van Lobenstein N, Carlino A, Resch A, Stock M, Kragl G. OC-0673 LET variation as a function of different optimization approaches in proton beam therapy. *Radiother Oncol*. 2019;133:S354. doi:10.1016/S0167-8140(19)31093-X.
29. Saini J, Maes D, Egan A, et al. Dosimetric evaluation of a commercial proton spot scanning Monte-Carlo dose algorithm: comparisons against measurements and simulations. *Phys Med Biol*. 2017;62(19):7659-7681. doi:10.1088/1361-6560/aa82a5.
30. Hunter JD. Matplotlib: A 2D Graphics Environment. *Comput Sci Eng*. 2007;9(3):90-95. doi:10.1109/MCSE.2007.55.
31. Seabold, Skipper, Perktold. Statsmodels: Econometric and statistical modeling with python. *Proc 9th Python Sci Conf*. 2010.
32. M N, T S, D A, A I. LMFIT: Non-Linear Least-Square Minimization and Curve-Fitting for Python. 2014. doi:10.5281/ZENODO.11813.
33. Wilkens JJ, Oelfke U. A phenomenological model for the relative biological effectiveness in therapeutic proton beams. *Phys Med Biol*. 2004;49(13):2811-2825. doi:10.1088/0031-9155/49/13/004.
34. Paganetti H. Relative biological effectiveness (RBE) values for proton beam therapy. Variations as a function of biological endpoint, dose, and linear energy transfer. *Phys Med Biol*. 2014;59(22):R419-72. doi:10.1088/0031-9155/59/22/R419.
35. Manuscript A. Ac ce pt. 2018.
36. Jones B. Towards Achieving the Full Clinical Potential of Proton Therapy by Inclusion of LET and RBE Models. *Cancers (Basel)*. 2015;7(1):460-480. doi:10.3390/cancers7010460.
37. Jones B. Why RBE must be a variable and not a constant in proton therapy. *Br J Radiol*. 2016;89(1063):20160116. doi:10.1259/bjr.20160116.
38. Giantsoudi D, Sethi R V, Yeap BY, et al. Incidence of CNS Injury for a Cohort of 111 Patients Treated With Proton Therapy for Medulloblastoma: LET and RBE Associations for Areas of Injury. *Int J Radiat Oncol • Biol • Phys*. 2016;95(1):287-296. doi:10.1016/j.ijrobp.2015.09.015.
39. Indelicato DJ, Flampouri S, Rotondo RL, et al. Incidence and dosimetric parameters of

pediatric brainstem toxicity following proton therapy. *Acta Oncol (Madr)*. 2014;53(10):1298-1304. doi:10.3109/0284186X.2014.957414.

40. Iwata H, Ogino H, Hashimoto S, et al. Spot Scanning and Passive Scattering Proton Therapy: Relative Biological Effectiveness and Oxygen Enhancement Ratio in Cultured Cells. *Int J Radiat Oncol • Biol • Phys*. 2018;95(1):95-102. doi:10.1016/j.ijrobp.2016.01.017.
41. Moteabbed M, Yock TI, Depauw N, Madden TM, Kooy HM, Paganetti H. Impact of Spot Size and Beam-Shaping Devices on the Treatment Plan Quality for Pencil Beam Scanning Proton Therapy. *Int J Radiat Oncol Biol Phys*. 2016;95(1):190-198. doi:10.1016/j.ijrobp.2015.12.368.
42. Britten RA, Nazaryan V, Davis LK, et al. Variations in the RBE for Cell Killing Along the Depth-Dose Profile of a Modulated Proton Therapy Beam. *Radiat Res*. 2012;179(1):21-28. doi:10.1667/RR2737.1.
43. Carante M Pietro, Ballarini F. Calculating Variations in Biological Effectiveness for a 62 MeV Proton Beam. *Front Oncol*. 2016;6:76. doi:10.3389/fonc.2016.00076.
44. Marshall TI, Chaudhary P, Michaelidesová A, et al. Investigating the Implications of a Variable RBE on Proton Dose Fractionation Across a Clinical Pencil Beam Scanned Spread-Out Bragg Peak. *Int J Radiat Oncol Biol Phys*. 2016;95(1):70-77. doi:10.1016/j.ijrobp.2016.02.029.
45. Jones B, McMahon SJ, Prise KM. The Radiobiology of Proton Therapy: Challenges and Opportunities Around Relative Biological Effectiveness. *Clin Oncol*. 2018;30(5):285-292. doi:10.1016/j.clon.2018.01.010.
46. Wedenberg M, Lind BK, Hårdemark B. A model for the relative biological effectiveness of protons : The tissue specific parameter a / b of photons is a predictor for the sensitivity to LET changes. 2013;(April 2012):580-588. doi:10.3109/0284186X.2012.705892.
47. Paganetti H. Relating the proton relative biological effectiveness to tumor control and normal tissue complication probabilities assuming interpatient variability in α/β. *Acta Oncol (Madr)*. 2017;56(11):1379-1386. doi:10.1080/0284186X.2017.1371325.
48. Wang L, Wang X, Li Y, et al. Human papillomavirus status and the relative biological effectiveness of proton radiotherapy in head and neck cancer cells. *Head Neck*. 2017;39(4):708-715. doi:10.1002/hed.24673.
49. Zlobinskaya O, Siebenwirth C, Greubel C, et al. The Effects of Ultra-High Dose Rate Proton Irradiation on Growth Delay in the Treatment of Human Tumor Xenografts in Nude Mice. *Radiat Res*. 2014;181(2):177-183. https://doi.org/10.1667/RR13464.1.
50. Sørensen BS, Bassler N, Nielsen S, et al. Relative biological effectiveness (RBE) and distal edge effects of proton radiation on early damage in vivo. *Acta Oncol (Madr)*. 2017;56(11):1387-1391. doi:10.1080/0284186X.2017.1351621.
51. Petrović I, Ristić-Fira A, Todorović D, Valastro L, Cirrone P, Cuttone G. Radiobiological analysis of human melanoma cells on the 62 MeV CATANA proton beam. *Int J Radiat Biol*. 2006;82(4):251-265. doi:10.1080/09553000600669859.
52. Petringa G, Romano F, Manti L, et al. Radiobiological quantities in proton-therapy: Estimation and validation using Geant4-based Monte Carlo simulations. *Phys Medica Eur J Med Phys*. 2019;58:72-80. doi:10.1016/j.ejmp.2019.01.018.
53. Leeuwen CM Van, Oei AL, Crezee J, et al. The alfa and beta of tumours : a review of parameters of the linear-quadratic model , derived from clinical radiotherapy studies. *Radiat Oncol*. 2018:1-11.
54. Maeda K, Yasui H, Matsuura T, et al. Evaluation of the relative biological effectiveness of spot-scanning proton irradiation in vitro. 2016;57(3):307-311. doi:10.1093/jrr/rrv101.
55. Mueller-klieser W, Kunz-schughart LA. Multicellular tumor spheroids: An underestimated tool is catching up again. *J Biotechnol*. 2010. doi:10.1016/j.jbiotec.2010.01.012.
56. Longati P, Jia X, Eimer J, et al. 3D pancreatic carcinoma spheroids induce a matrix-rich, chemoresistant phenotype offering a better model for drug testing. *BMC Cancer*. 2013;13:95. doi:10.1186/1471-2407-13-95.
57. Gupta SK, Torrico Guzmán EA, Meenach SA. Coadministration of a tumor-penetrating peptide improves the therapeutic efficacy of paclitaxel in a novel air-grown lung cancer 3D spheroid

model. *Int J Cancer*. 2017;141(10):2143-2153. doi:10.1002/ijc.30913.
58. Nc D. Three-Dimensional Culture Systems in Cancer Research: Focus on Tumor Spheroid Model. 2017:94-108. doi:10.1016/j.pharmthera.2016.03.013.Three-Dimensional.
59. Ho WY, Yeap SK, Ho CL, Rahim RA, Alitheen NB. Development of Multicellular Tumor Spheroid (MCTS) Culture from Breast Cancer Cell and a High Throughput Screening Method Using the MTT Assay. 2012;7(9). doi:10.1371/journal.pone.0044640.
60. Horas JA, Olguin OR, Rizzotto MG. On the surviving fraction in irradiated multicellular tumour spheroids: calculation of overall radiosensitivity parameters, influence of hypoxia and volume effects. *Phys Med Biol*. 2005;50(8):1689-1701. doi:10.1088/0031-9155/50/8/005.

3.5 Proton irradiation increases the necessity for homologous recombination repair along with the indispensability of non-homologous end joining

Klaudia Szymonowicz [1,*], Adam Krysztofiak [1,*], Jansje van der Linden [1], Ajvar Kern [2], Simon Deycmar [3], Sebastian Oeck [1,4], Anthony Squire [5], Benjamin Koska [2], Julian Hlouschek [1], Melanie Vüllings [2], Christian Neander [6,7], Jens T. Siveke [6,7], Johann Matschke [1], Martin Pruschy [3], Beate Timmermann [2,7,8], and Verena Jendrossek [1,#]

[1] Institute of Cell Biology (Cancer Research), University Hospital Essen, University of Duisburg-Essen, 45122 Essen, Germany; klaudia.szymonowicz@uk-essen.de (K.S.), adam.krysztofiak@uk-essen.de (A.K.), janettevanderlinden@hotmail.com (J.v.d.L.), sebastian.oeck@uk-essen.de (S.O.), julian.hlouschek@uk-essen.de (J.H.), johann.matschke@uk-essen.de (J.M.), verena.jendrossek@uni-due.de (V.J.)

[2] West German Proton Therapy Centre Essen (WPE), West German Cancer Center (WTZ), University Hospital Essen, 45147 Essen, Germany; ajvar.kern@uk-essen.de (A.K.2), benjamin.koska@uk-essen.de (B.K.), melanie.vuellings@uk-essen.de (M.V.), beate.timmermann@uk-essen.de (B.T.)

[3] Department of Radiation Oncology, Laboratory for Applied Radiobiology, University Hospital Zurich, Zurich, Switzerland; simon.deycmar@uzh.ch (S.D.), martin.pruschy@uzh.ch (M.P.)

[4] Department of Therapeutic Radiology, Yale University School of Medicine, New Haven, CT 06520, USA; sebastian.oeck@uk-essen.de (S.O.)

[5] Institute of Experimental Immunology and Imaging, Imaging Center Essen, University Hospital Essen, 45122 Essen, Germany; anthony.squire@uk-essen.de (A.S.)

[6] Institute of Developmental Cancer Therapeutics, West German Cancer Center, University Hospital Essen, Essen, Germany; christian.neander@uk-essen.de (C.N), jens.siveke@uk-essen.de (J.T. S.)

[7] Division of Solid Tumor Translational Oncology, German Cancer Consortium (DKTK, partner site Essen) and German Cancer Research Center, DKFZ, Heidelberg, Germany

[8] Department of Particle Therapy, West German Proton Therapy Center Essen (WPE), West German Cancer Center (WTZ), University Hospital Essen, 45147 Essen, Germany

Correspondence: verena.jendrossek@uni-due.de; +49-201-723-3380 (V.J.)

* These authors contributed equally to this work

Status of the manuscript: Submitted to Cells (ISSN 2073-4409) in February 2020

Author contribution Simon Deycmar:

- Minor contributions in drafting and conduction of experiments
    - Proton beam irradiation
    - COMET assay

        see Figure 3
- Drafting and proofreading of the manuscript
- Managing collaboration

cells

MDPI

Article

Proton irradiation increases the necessity for homologous recombination repair along with the indispensability of non-homologous end joining

Klaudia Szymonowicz [1,*], Adam Krysztofiak [1,*], Jansje van der Linden [1], Ajvar Kern [2], Simon Deycmar [3], Sebastian Oeck [1,4], Anthony Squire [5], Benjamin Koska [2], Julian Hlouschek [1], Melanie Vüllings [2], Christian Neander [6,7], Jens T. Siveke [6,7], Johann Matschke [1], Martin Pruschy [3], Beate Timmermann [2,7,8], and Verena Jendrossek [1,#]

[1] Institute of Cell Biology (Cancer Research), University Hospital Essen, University of Duisburg-Essen, 45122 Essen, Germany; klaudia.szymonowicz@uk-essen.de (K.S.), adam.krysztofiak@uk-essen.de (A.K.), janettevanderlinden@hotmail.com (J.v.d.L.), sebastian.oeck@uk-essen.de (S.O.), julian.hlouschek@uk-essen.de (J.H.), johann.matschke@uk-essen.de (J.M.), verena.jendrossek@uni-due.de (V.J.)

[2] West German Proton Therapy Centre Essen (WPE), West German Cancer Center (WTZ), University Hospital Essen, 45147 Essen, Germany; ajvar.kern@uk-essen.de (A.K.2), benjamin.koska@uk-essen.de (B.K.), melanie.vuellings@uk-essen.de (M.V.), beate.timmermann@uk-essen.de (B.T.)

[3] Department of Radiation Oncology, Laboratory for Applied Radiobiology, University Hospital Zurich, Zurich, Switzerland; simon.deycmar@uzh.ch (S.D.), martin.pruschy@uzh.ch (M.P.)

[4] Department of Therapeutic Radiology, Yale University School of Medicine, New Haven, CT 06520, USA; sebastian.oeck@uk-essen.de (S.O.)

[5] Institute of Experimental Immunology and Imaging, Imaging Center Essen, University Hospital Essen, 45122 Essen, Germany; anthony.squire@uk-essen.de (A.S.)

[6] Institute of Developmental Cancer Therapeutics, West German Cancer Center, University Hospital Essen, Essen, Germany; christian.neander@uk-essen.de (C.N), jens.siveke@uk-essen.de (J.T. S.)

[7] Division of Solid Tumor Translational Oncology, German Cancer Consortium (DKTK, partner site Essen) and German Cancer Research Center, DKFZ, Heidelberg, Germany

[8] Department of Particle Therapy, West German Proton Therapy Center Essen (WPE), West German Cancer Center (WTZ), University Hospital Essen, 45147 Essen, Germany

Correspondence: verena.jendrossek@uni-due.de; +49-201-723-3380 (V.J.)

* These authors contributed equally to this work

Received: date; Accepted: date; Published: date

Abstract: *Background*: Technical improvements in clinical radiotherapy for maximizing cytotoxicity to the tumor while limiting negative impact on co-irradiated healthy tissues include the increasing use of particle therapy (e.g. proton therapy) worldwide. Yet potential differences in the biology of DNA damage induction and repair between irradiation with X-ray photons and protons remained elusive. *Methods*: We compared the differences in DNA double strand break (DSB) repair and survival of cells compromised in non-homologous end joining (NHEJ), homologous recombination repair (HRR) or both, after irradiation with an equal dose of X-ray photons, entrance plateau (EP), and mid Spread-Out Bragg Peak (SOBP) protons. We used super-resolution microscopy to investigate potential differences in spatial distribution of DNA damage foci upon irradiation. *Results:* While DNA damage foci were equally distributed throughout the nucleus after X-ray photon irradiation, we observed more clustered DNA damage foci upon proton irradiation. Furthermore, deficiency in essential NHEJ proteins delayed DNA repair kinetics and sensitized cells to both, X-ray photon and proton irradiation, whereas deficiency in HRR proteins sensitized cells only to proton irradiation. *Conclusions*: We assume that NHEJ is indispensable for processing DNA DSB independent of the irradiation source, whereas importance of HRR rises with increasing energy of applied irradiation.

Keywords: ionizing radiation; DNA damage foci; DNA repair; Spread-Out Bragg Peak (SOBP); Relative Biological Effectiveness (RBE); Entrance Plateau (EP) protons; Linear Energy Transfer (LET), DNA double-strand break (DSB), non-homologous end joining (NHEJ), homologous recombination repair (HRR)

1. Introduction

Radiotherapy is a part of standard treatment for more than 50% of cancer patients and has a documented contribution to local tumor control and improved overall survival. Clinical radiotherapy aims to achieve maximal tumor control rates while reducing the risk for dose-limiting adverse late effects in normal tissues [1,2]. Depending on the disease stage, radiotherapy is therefore either given alone or as a part of multimodal combinations with surgery, chemotherapy as well as molecularly targeted drug therapy or immunotherapy [1,3]. Overcoming dose-limiting toxicity to normal tissues is still a major challenge in clinical radiotherapy, particularly when tumors grow adjacent to critical structures or within tissues or organs with pronounced radiation sensitivity. Enhancing the accuracy of dose delivery to the tumor volume, e.g. by stereotactic radiotherapy or intensity-modulated radiation therapy, has allowed to improve the safety profile of radiotherapy for many solid tumors [4]. Moreover, recent technical developments have led to broader application of particle therapy in clinical practice. It is expected that the favorable depth-dose curves and linear energy transfer (LET) characteristics of charged particles will allow a precise targeting of deep-seated tumors while reducing ionizing dose and irradiated volume of normal tissue. It is expected that these attempts to achieve a precise and more target-specific irradiation have helped to lower the toxicity rates and the risk of developing secondary tumors [5–11]. In fact, particles pass through normal tissues on their track without losing much energy but instead releasing the main carried energy at a specific tissue depth shortly before their complete stop. This maximized dose deposition at the end of particles range is represented as a Bragg peak of depth-dose curve. In contrast, photons lose their energy exponentially, with higher values at the entry point and lower at the deep-seated tissues [12–14]. Additionally, the rising number of particle therapy centers worldwide facilitates the use of protons or heavy ions in the clinical care of cancer patients and allows the validation of the suspected superiority of particle beams compared to photon beams in terms of normal tissue protection [15,16].

To allow for irradiation of a three-dimensional tumor volume, therapeutic proton beam therapy is performed using a so called Spread-Out Bragg peak (SOBP), which is composed of several single Bragg peaks with slightly varying energies [17]. Despite divergent physical properties of proton and photon beams, it is assumed that the relative biological effectiveness (RBE) of proton beams resemble those of photon beams, mostly when put in relation to high LET particle beams such as carbon ions [18]. As a consequence, treatment planning for proton beam radiotherapy has been developed based on data originating from therapy with gamma-ray photons generated by a ^{60}Co source, using a correction factor for RBE of 1.1 [18–22]. Herein, RBE is defined as the ratio of biological effectiveness of two radiation modalities, measured by absorbed dose for a given effect (reference irradiation type/irradiation type under investigation), which is inversely related to a given dose (Equation (3) in Material and Methods section) [13,23]. Generally, the higher the deposited energy, the higher the density of ionizing events, and the higher the resulting RBE per unit of dose, as defined by a more severe DNA damage [17,24].

However, it is increasingly appreciated that not only the physical characteristics of the beam but also the microscopic pattern of energy deposition differs between photons and protons, particularly at the distal edge of the Bragg-peak, with potential impact on the resulting biological effects [14,20]. In fact, depending on the tissue, the measured endpoint, dose and LET of the beam, the RBE values reported for protons vary between ~ 1.1 – 1.7, with increasing RBE values for protons along the distal edge of the Bragg peak [18,21,25–27]. Moreover, first *in vitro* studies implicate that cancer-associated genetic defects in DNA repair - homologous recombination repair (HRR) or the Fanconi Anemia (FA) pathway are associated with an increase in the RBE values for irradiation with proton beams compared to irradiation with gamma-ray photons or X-ray photons [28–31]. These observations point

to potential differences in the biology of DNA damage induced by irradiation with proton beams compared to irradiation with gamma-ray photons or X-ray photons. Moreover, these findings suggest that genetic alterations affecting DNA damage response (DDR) and DNA repair pathways may not only contribute to heterogeneity in cancer cell radiosensitivity *per se*, but might also cause variations in proton RBE [32].

Independent of the radiation quality, the cytotoxic effects of ionizing radiation are based on its ability to cause damage to cellular macromolecules, particularly the DNA. Herein, DNA double strand breaks (DSB) are considered as the most toxic lesions induced by ionizing radiation so that the capacity of cells to repair radiation-induced DNA DSB constitutes a major determinant of cellular radiosensitivity [33,34]. Radiation-induced DNA DSB are mainly repaired by non-homologous end joining (NHEJ) and HRR [35]. However, if both pathways are disrupted, alternative end joining (alt-EJ) can be activated [36,37]. NHEJ is a cell cycle independent and rapid, but error-prone DNA repair pathway that is mediated by a DNA-PK (DNA-dependent protein kinase) complex consisting of KU70/80 heterodimer and a catalytic subunit (DNA-PKcs) [35]. DNA-PKcs is essential for the recruitment of repair proteins of the NHEJ complex, including XRCC4 (X-ray repair cross-complementing protein 4), Lig IV (DNA ligase IV), the nuclease Artemis as well as the stabilizing factors XLF (XRCC4-like factor) and PAXX (Paralog of XRCC4 and XLF) [38–41]). In contrast, HRR is a precise, but slow and cell cycle-dependent DNA repair mechanism requiring homology of a sister chromatid [35,42,43]. HRR efficiency relies on numerous proteins and protein complexes, e.g. BRCA2 (breast cancer 2) and Rad54. BRCA2 is a tumor suppressor and one of the most essential proteins regulating HRR; it promotes binding of Rad51 to a single-stranded DNA during DNA damage processing [44]. Rad54 induces DNA synthesis and promotes dissociation of Rad51 from DNA strand, ensuring annealing of the synthesized DNA to the ends of damaged DNA strand [45]. In this context, 53BP1 (p53 binding protein 1) functions as a sensor of DNA damage and has been proposed to mediate DNA repair pathway choice by promoting NHEJ [45,46].

Though an increasing number of reports points to different patterns of DNA damage induced by photon and proton irradiation with potential relevance for DNA repair [14,28–30,47]. There is a gap of knowledge about potential microscopic differences in the DNA damage pattern induced by protons from the entrance plateau (EP) versus protons from SOBP. Moreover, only limited data are available on variations in RBE caused by genetic deficiencies in components of the two major DNA DSB repair pathways, NHEJ and HRR, which are also observed in human cancer. Such investigations are particularly important in view of the increasing interest in combining DNA repair pathway inhibitors with radiotherapy for inducing synthetic lethality in tumors with intrinsic or acquired DNA repair-deficiencies [48–51].

In the present study, we used STED (stimulated emission depletion) microscopy to compare the microscopic pattern of DNA damage induced by irradiation with equal physical doses of SOBP protons, EP protons and X-ray photons. Moreover, we used fibroblasts and cancer cells without and with deficiencies in specific proteins of NHEJ, HRR or both, to explore potential differences in RBE upon irradiation with a similar physical dose of protons (SOBP, EP) and X-ray photons for the endpoints clonogenic cell survival and DNA DSB repair kinetics. We observed the induction of more clustered γH2A.X foci in cells exposed to irradiation with SOBP protons. This may contribute to the more pronounced dependency of cells exposed to proton irradiation from integrity of the HRR pathway for efficient DNA repair and survival. The definition of signaling molecules specifically enhancing RBE values upon irradiation with proton beams will help to identify patients that might particularly benefit from proton beam radiotherapy according to the molecular characteristics of their tumors. This will also help to define combinatorial treatments suited to harness the full potential of radiotherapy with SOBP protons whilst avoiding increased toxicity.

2. Materials and Methods

2.1. Chemicals and antibodies

Alexa Fluor 647-coupled antibody against γH2A.X protein was obtained from Becton Dickinson (Heidelberg, Germany). Anti-53BP1 rabbit polyclonal antibody was purchased from Santa Cruz (Heidelberg, Germany). Secondary antibody Alexa Fluor 555 (anti-rabbit) and Hoechst33342 were purchased from Invitrogen (Eugene, OR, USA). DAKO Fluorescent mounting medium from Dako North America Inc. (Carpinteria, CA, USA) was used. All media, fetal bovine serum (FBS) and penicillin-streptomycin (pen/strep) were acquired from Thermo Fisher Scientific (Waltham, MA, USA). All other chemicals were purchased from Sigma-Aldrich (Deisenhofen, Germany) unless otherwise specified.

2.2. Cell culture

M059K (DNA-PKcs-proficient) and M059J (DNA-PKcs-deficient) glioblastoma cell lines [52], wild type MEFs (murine embryonic fibroblasts) and MEFs with genetic deficiency in DNA repair proteins (Rad54$^{-/-}$, Lig IV$^{-/-}$, Rad54$^{-/-}$/Lig IV$^{-/-}$) [53], Capan-1 (human pancreatic adenocarcinoma BRCA2$^{-/+}$) and BxPC3 (human pancreatic adenocarcinoma) [54], 2BN hTERT human fibroblasts XLF$^{-/-}$ and control fibroblasts [55], RPE-1 human retinal PAXX-deficient (PAXX$^{-/-}$) and control cells [56] were kindly provided by Prof. Dr. George Iliakis (Institute of Medical Radiation Biology, University of Duisburg-Essen, Germany). 2BN hTERT control and XLF-deficient (XLF$^{-/-}$ cells) were cultured in MEM supplemented with 10% FBS (fetal bovine serum), non-essential amino acids and 1% pen/strep. RPE-1 control and PAXX$^{-/-}$ cells were cultured in DMEM/F12 supplemented with 10% FBS and 1% pen/strep. All other cell lines were cultured in DMEM supplemented with 10% FBS and 1% pen/strep. All cell lines were routinely checked for mycoplasma contamination

2.3. Irradiation

Cells were exposed to an equal physical dose of 3 Gy for γH2A.X assay or 1, 2, 4, 6 and 8 Gy for long-term clonogenic survival assays, independent of different beams and irradiators used. We present the model of irradiation in Figure 1A and show the distribution of relative dose in percent.

2.3.1. X-ray photon irradiation

X-ray photon irradiation by X-RAD 320 X-Ray Biological Irradiator with a MIR-324 X-ray tube (Precision X-Ray Inc., North Branford, CT, USA) 3.75 Gy/min at a distance of 50cm from the X-ray tube window was controlled by a parallel dosimetry with the PTW 7862 parallel plate transmission chamber and PTW UNIDOS dosimeter (Precision X-Ray Inc., North Branford, CT, USA).

2.3.2. Proton irradiation

Proton irradiation was performed on a Proteus Plus with a 230 MeV cyclotron (IBA International, Louvain-La-Neuve, Belgium). The plates with cells monolayer covered with 2 ml of culture medium for 12-well and 6-well plates were placed on a treatment table and irradiated in pencil beam mode in a defined source axis distance in the isocenter. Cells were exposed to either mid SOBP or EP proton irradiation. A narrow SOBP was necessary to account for uncertainties in range and scattering as well as exact cell positions while maintaining the SOBP region. The maximum energy of 110 MeV (range approx. 9 cm in water) and the lowest energy of 100 MeV (range approx. 7.6 cm in water) of the SOBP (in total six layers) must therefore be transmitted through a range shifter (thickness 7.4 cm). The range shifter offers the possibility to reach the desired measuring depth. A 2 mm solid plate phantom was used as build up to position the cells in the EP region of the depth dose curve. SOBP was composed of 6 single Bragg peaks with following energies in MeV: 1: 109.9; 2: 107.6; 3: 105.1; 4: 103.1; 5: 100.9; 6: 100. To achieve the same dose for EP proton region as for SOBP, the range shifter was not applied and the time of irradiation was increased.

196 Irradiation fields were created and optimized by the clinical planning system and calibrated by
197 measuring the dose with a 2D array detector MatriXX PT (IBA International, Louvain-La-Neuve,
198 Belgium) at the same depth as the cells were placed during the irradiation.

199 *2.4. Colony formation assay*

200 Clonogenic cell survival was tested in response to ionizing radiation with doses between 1 and
201 8 Gy as previously described [57]. Exponentially grown cells were seeded in 6-well plates and 24 h
202 later irradiated. For determination of colony formation cells were fixed after 7-10 days in 3.7%
203 formaldehyde and 70% ethanol, stained with 0.05% Coomassie blue. Colonies of at least 50 cells were
204 counted. Survival data were calculated using linear-quadratic model and following equation:

$$S_{(D)} = \exp\left[-(\alpha D + \beta D^2)\right] \quad (1)$$

205 where $S_{(D)}$ – survival fraction probability at a given radiation dose (D), α – linear and β – quadratic
206 parameter of cells' radiosensitivity [58].
207 The linear (α) and quadratic (β) parameters were calculated for each survival curve form
208 stratified and fitted to the liner-quadratic model colony formation survival data. The dose $D_{(S)}$ to
209 achieve a given survival level (S) was calculated using transformed equation (1):

$$D_{(S)} = -(\alpha/2\beta) \pm [0.25(\alpha/\beta)^2 - (\ln(S)/\beta)]^{0.5} \quad (2)$$

210 The RBE values were calculated as previously described using equation (3):

$$RBE_{(S)} = D_{(S)\ \text{X-rays}} / D_{(S)\ \text{particle}} \quad (3)$$

211 where $RBE_{(S)}$ – RBE at given cell survival level (10%), $D_{(S)\ \text{X-rays}}$ – dose of X-ray photons and $D_{(S)\ \text{particle}}$ –
212 dose of EP/SOBP protons required to achieved given cell survival (S) [23,59].

213 *2.5. Immunofluorescence staining*

214 Cells were fixed and permeabilized with 3% paraformaldehyde (PFA) and 0.2% Triton X-100 in
215 PBS for 15 min at indicated time points after irradiation. After washing with PBS, cells were blocked
216 overnight with 2% goat serum in PBS. Antibodies were diluted in blocking buffer. Incubation with
217 antibody against 53BP1 was performed for 1 h in a 1:100 dilution. Alexa Fluor 647-conjugated anti-
218 γH2A.X antibody was incubated for 1 h at a 1:100 dilution. Staining with secondary antibody - Alexa
219 Fluor 555 (anti-rabbit) was performed in the dark for 1 h at a dilution 1:400. Samples were washed
220 after each incubation step three times with PBS followed by staining for 15 min in the dark with 0.2%
221 (w/v) Hoechst33342 diluted in PBS. Samples were again washed with PBS, mounted with the DAKO
222 mounting medium and stored at 4°C in the dark. Single layer fluorescence images were taken with a
223 Zeiss AxioCam MRm (1388 x 1040 pixels) at a Zeiss Axio Observer Z1 fluorescence microscope with
224 Plan-Apochromat 63x/1.40 Oil M27 lens, 49 DAPI, 38 HE, 43HE and 78 HE ms filter and a
225 transmission grid VH "ApoTome" (Carl Zeiss, Goettingen, Germany). Images were taken with three
226 fourth of the maximum intensity without overexposure. The pictures were saved as 16-bit multi-
227 channel Carl Zeiss Image files (CZI) with no further editing. Foci were analyzed with the Focinator
228 software [60,61]. Software, instructions and supporting information are provided at
229 https://www.focinator.com.
230 For super resolution STED microscopy 100.000 cells were seeded in full growth medium on #1.5
231 thickness high precision (18mm x 18mm) coverslips (Scientific Thermo Fisher; Waltham, MA, USA),
232 placed in standard 6-well plates, and irradiated 24 h after seeding with 3 Gy of either photon or SOBP
233 proton. Cells were fixed and permeabilized (3% paraformaldehyde (PFA) and 0.2% Triton X-100 in
234 PBS; 15 min; RT). After washing with PBS, cells were blocked overnight with 2% goat serum in PBS.
235 γH2A.X antibody was diluted in blocking buffer. Incubation with antibody against γH2A.X was
236 performed for 1 h in a 1:100 dilution. Alexa-Fluor 488 (anti-rabbit) diluted 1:100 in 2% goat serum
237 was incubated for 1 h in dark. Mounting was performed using the TDE mounting medium [62].
238

2.6. Superresolution STED microscopy

Gated Stimulated emission depletion (STED) microscopy was performed using a Leica TCS SP8 epifluorecence-confocal-microscope equipped with a picosecond pulsed white light laser for excitation at 488 nm and a 592 nm STED depletion laser (Leica, Wetzlar, Germany). STED confocal images were acquired with a pixel resolution of 21nm using the Leica HCX PL APO 100x/1.4 Oil STED objective. These images were later deconvolved using the STED deconvolution option of Huygens Professional (v. 16.05, SVI, Hilversum, Netherlands), which resulted in a final transverse resolution of 76.22 nm +/- 3.47 nm (n=6). The coordinates and number of foci in was measured by intensity of foci using ImageJ. From the foci coordinates a nearest neighbor analysis was performed with a script written in R using the spatial statistics package 'spatstat' [63].

2.7. Alkaline single cell gel electrophoresis (comet) assay

Exponentially growing cells cultured in 6-well plates were irradiated with 8 Gy photon or proton irradiation. Alkaline buffers were prepared according to literature [64]. Cells were collected at defined time points after irradiation (30 min, 4 h, 8 h, 24 h) by trypsinization. 100 µl cell suspension were mixed with 200 µl agarose (40°C, 1% in ddH_2O, low melting, Sigma-Aldrich, Deisenhofen, Germany) and pipetted onto an agarose-precoated slide. The agarose clot was covered with a cover slip which was removed after solidification of the agarose and subsequently placed in alkaline lysis buffer (pH > 13.0) for 1 h. The slides were then placed in alkaline electrophoresis buffer (pH > 12.3) for 10 min to allow buffer exchange prior to electrophoresis for 1 h (0,75 V/cm electrode distance). Subsequently, the slides were transferred in ddH2O for 10 min and allowed to air-dry overnight at room temperature. For fluorescence microscopy, propidium iodide solution (50 µg/ml in ddH2O) was added onto the dried slide and sealed with a cover slip. The comets were imaged by the Axio Scanner Z.1 with 10x objective magnification and using the ZEN 2 Blue edition software (Carl Zeiss AG, Germany) and the tail length determined with ImageJ (1.51j8 available at https://imagej.nih.gov/ij/; U.S. National Institutes of Health, Bethesda, MD, USA) and the plugin OpenComet (OpenComet v1.3.1) [65].

2.8. Statistical analysis and reproducibility

Data represent mean values of at least 3 independent experiments. Data were first tested for normal distribution using the D'Agostino-Pearson omnibus normality test. Further, data analysis was performed by standard one-way ANOVA test with Tukey two-pair comparison post-test for normally distributed values or non-parametric Kruskal-Wallis test for values lacking normal distribution. Two-way ANOVA test with Tukey's or Sidak's multiple comparisons comparison post-tests were applied for statistical calculation of influence of two different parameters. Calculations were done using Prism6™ software (GraphPad Inc., La Jolla, CA, USA). p-values ≤ 0.05 were considered as statistically significant and indicated as a star symbol where * p≤ 0.05, ** p< 0.01, *** p< 0.001 and ****p< 0.0001.

3. Results

3.1. Proton irradiation induces larger DNA repair γH2A.X foci when compared to irradiation with X-ray photons

To explore suggested differences in the biology of DNA damage induced by proton and photon irradiation, we exposed *in vitro* cultured cells to irradiation with a physical dose of 3 Gy generated by X-ray photons, mid SOBP protons (SOBP composed of 6 single Bragg peaks) and EP protons (Figure 1A). First, we irradiated MEFs and analyzed the distribution of γH2A.X foci in the nucleus 1 h and 8 h after irradiation using a STED super resolution microscopy (Figure 1B). While X-ray photon irradiation mainly resulted in a formation of small γH2A.X foci equally distributed within the nucleus, SOBP protons created a more heterogeneous foci distribution with a high number of larger γH2A.X foci (Figure 1B).

STED microscopy analysis revealed that the pattern of DNA damage foci consisted of several small sub clusters of γH2A.X foci in close proximity to each other and with larger distance to neighboring γH2A.X foci accumulations within a pattern of a larger cluster formations within the nucleus; we therefore termed the γH2A.X foci with the larger appearance "foci clusters" throughout the manuscript (Figure 1B). Instead, spatial distribution of foci upon irradiation of the MEFs with EP protons, was characterized by a mixture of both types of DNA damage foci described above, namely homogenously distributed small foci, as well as heterogeneously distributed foci clusters (Figure 1B). ImageJ-based quantitative analysis of STED pictures confirmed a significantly higher number of γH2A.X foci clusters after irradiation with SOBP or EP protons at 1 h post-irradiation than after X-ray photon irradiation, where we barely observed γH2A.X foci clusters (Figure 1C). Over time, the number of clustered γH2A.X foci declined significantly, or clusters were no longer detectable.

For STED analysis, we picked spots of accumulated γH2A.X foci and used those for more detailed analysis. To better define the features of clusters, we determined the distance between single γH2A.X foci within each cluster. As shown in Figure 1D, the distance between foci was significantly lower in SOBP- and EP-induced clusters. However, this distance increased over time pointing to a time-dependent removal of single γH2A.X foci indicative of ongoing DNA repair (Figure 1D).

Besides the number of γH2A.X foci clusters, we determined the number of non-clustered γH2A.X foci (Figure 1E). Expectedly, X-ray photon irradiation caused the highest level of equally distributed DNA damage foci (Figure 1E). Interestingly, irradiation with EP protons evoked a significantly higher number of non-clustered γH2A.X foci compared to SOBP proton irradiation (Figure 1E). However, the equally distributed DNA damage was mostly resolved within 8 h after EP proton irradiation but was still highly present in nuclei irradiated by X-ray photons (Figure 1E). Taken together, these findings about the spatial distribution of γH2A.X foci suggest that irradiation with SOBP protons evokes more clustered DNA damage when compared to X-ray photons, whereas EP proton induce both, SOBP protons-like and X-ray photons like DNA damage distribution.

3.2. Deficiency in Lig IV strongly sensitizes MEFs to irradiation with proton beams and X-ray photons

The distinct spatial distribution of γH2A.X foci upon irradiation with protons and X-ray photons observed in our STED analysis pointed to differences in biology of the DNA damage induced by different irradiation sources. This prompted us to explore whether the observed variations in the biology of the damage might result in distinct radiosensitivity of cells depending on the applied radiation quality and cellular proficiency in DNA repair. To this end, we first compared clonogenic survival of wild type MEFs after exposure to irradiation with X-ray photons, EP protons or SOBP protons, respectively. However, we did not observe significant differences in clonogenic survival of wild type MEFs exposed to the different radiation qualities (Figure 2A, E), revealing a comparable sensitivity of MEFs to irradiation with X-ray photons and protons. Next, we explored potential differences in the sensitivity of cells with defects in DNA repair pathways to proton vs. X-ray photon irradiation, since others suggested differences in DNA damage response in cells with deficiencies in HRR or FA [28–30]. Therefore, we compared clonogenic survival of MEFs with defects in specific DNA repair proteins, including Lig IV$^{-/-}$ (NHEJ), Rad54$^{-/-}$ (HRR) or both, Lig IV$^{-/-}$ and Rad54$^{-/-}$ upon irradiation with a similar physical dose of X-ray photons, EP protons or SOBP protons (Figure 2B-D and 2F-H). In contrast to wild type MEFs, MEF cell lines with a deficiency in Lig IV (MEF Lig IV$^{-/-}$) or Rad54 (MEF Rad54$^{-/-}$) turned out to be significantly more sensitive to irradiation with protons compared to X-ray photons, as depicted exemplarily for 8 Gy (Figures 2E-H). Of note, values for double-deficient MEF Rad54$^{-/-}$ / Lig IV$^{-/-}$ did not reach statistical significance (Figure 2H). Interestingly, none of the tested cell lines showed a significant difference in clonogenic survival after irradiation with EP or SOBP protons (Figure 2E-H).

Further, comparing the responses of wild type MEFs and the DNA repair-deficient MEFs to irradiation with X-ray photons, EP protons or SOBP protons, we found that deficiency in Lig IV exerted the most pronounced effect on clonogenic survival, irrespective of the radiation quality used (Figure 2J-L).

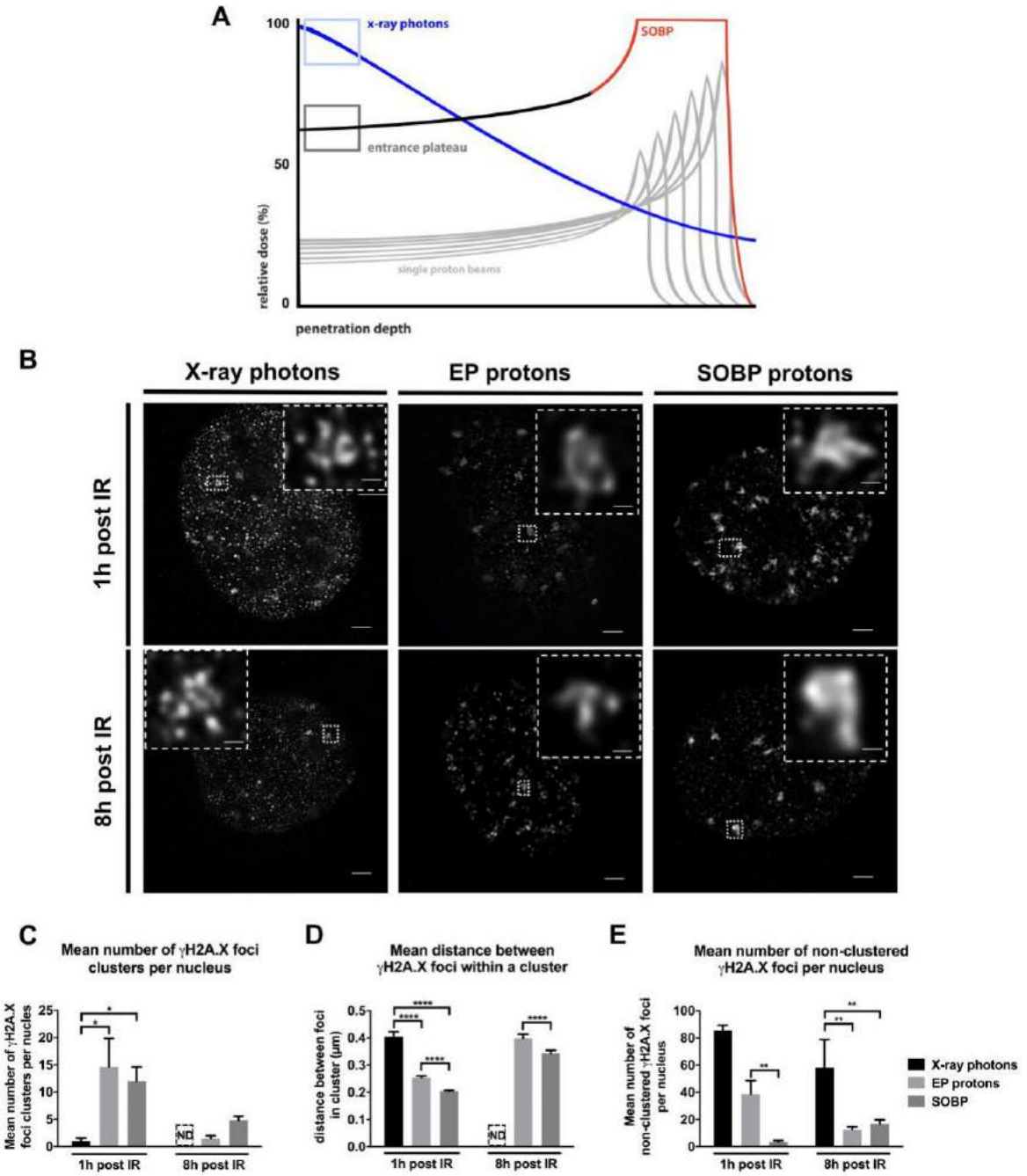

Figure 1. Time-dependent induction and removal of γH2A.X foci in MEFs irradiated with a physical dose of 3 Gy of X-ray photons, EP and SOBP protons visualized by γH2A.X staining. (**A**) Model of irradiation setup. Depth-dose curves of an X-ray photons beam and a proton beam highlighting the depth area where the cells were irradiated with X-ray photons, Bragg-peak protons and plateau protons. (**B**) STED microscopy pictures of a single nucleus of MEFs after 1 h and 8 h of 3 Gy irradiation with X-ray photons, EP protons or SOBP protons (objective 100x); scale bar: 0.1 µm. Clustered γH2A.X foci were additionally zoomed in 40x (small squares in the edge). Scale bar: 0.1 µm. (**C**-**E**) Quantification of γH2A.X foci in MEFs irradiated with 3 Gy of X-ray photons, EP and SOBP protons. (**C**) Average number of clusters per nucleus. (**D**) Average distance between γH2A.X foci in clusters. (**E**) Average number of foci per nucleus beyond clusters. Data represent mean ± SEM; One-way ANOVA with Tukey's multiple comparisons post-test and Kruskal-Wallis test; *p<0.05; **p<0.01; ****p<0.0001; ND – not detectable.

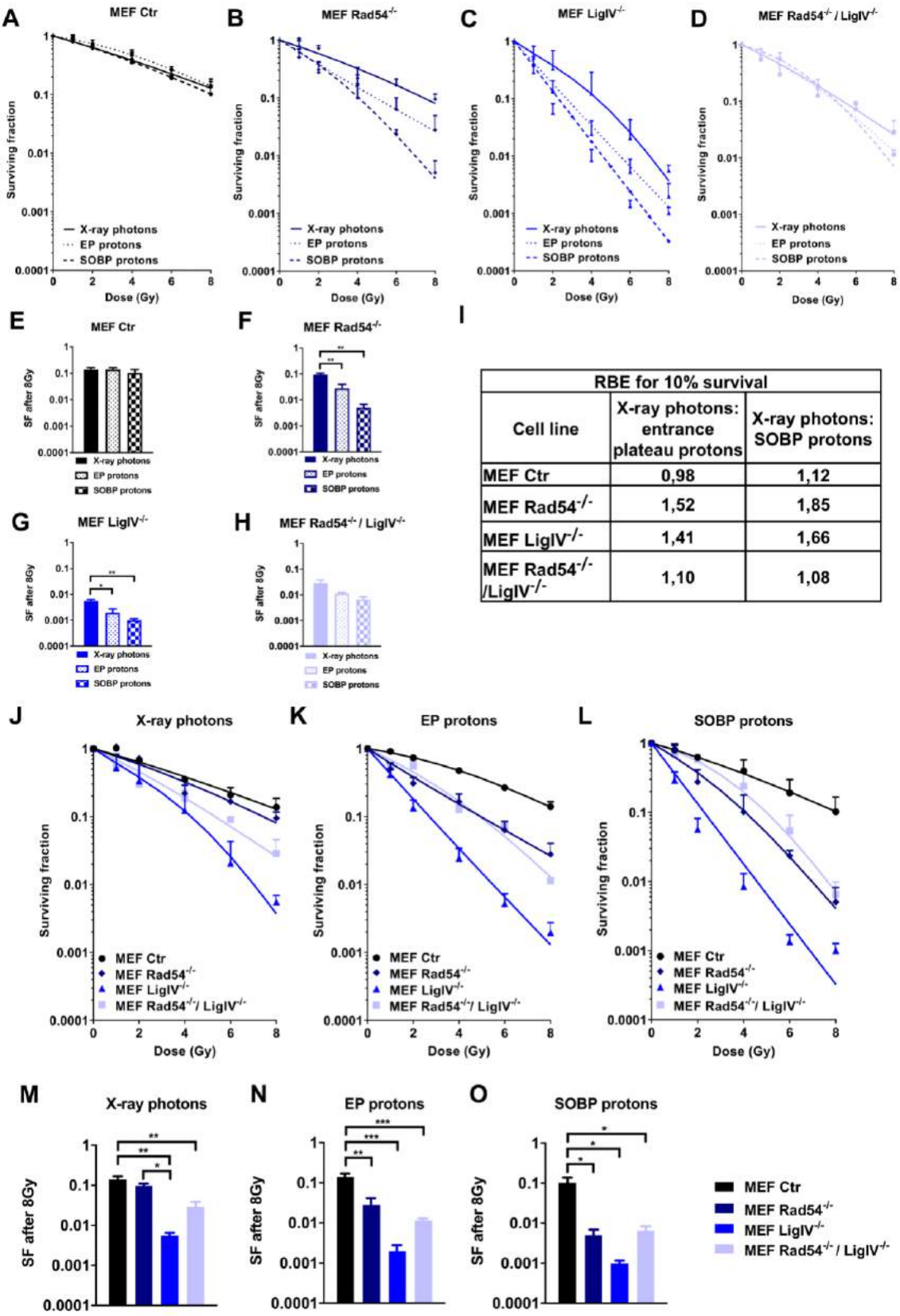

RBE for 10% survival		
Cell line	X-ray photons: entrance plateau protons	X-ray photons: SOBP protons
MEF Ctr	0,98	1,12
MEF Rad54$^{-/-}$	1,52	1,85
MEF LigIV$^{-/-}$	1,41	1,66
MEF Rad54$^{-/-}$ /LigIV$^{-/-}$	1,10	1,08

Figure. 2 Effects of X-ray photons, EP and SOBP protons on clonogenic cell survival. (**A-H**) Results of colony formation assay in wild type MEFs (Ctr) and MEFs harboring genetic deficiency ($^{-/-}$) in Rad54 (Rad54$^{-/-}$), Lig IV (Lig IV$^{-/-}$) or Rad54 and Lig IV (Rad54$^{-/-}$ / Lig IV$^{-/-}$), upon irradiation with X-ray photons, EP protons or SOBP protons (1-8 Gy) as indicated. (**I**) RBE values of clonogenic survival calculated for 10% survival of the indicated MEF cell lines. (**J-L**) Clonogenic survival curves of MEFs

upon irradiation with 1-8 Gy of X-ray photons (**J**), EP protons (**K**) or SOBP protons (**L**). (**M-O**) Comparison of cell survival between MEFs harboring distinct DNA repair protein-deficiencies as described above upon irradiation with 8 Gy of X-ray photons (**M**), EP protons (**N**) or SOBP protons (**O**). Data represent mean values ± SD (**A-D**, **J-L**) or ± SEM (**E-H**, **M-O**) of 3 independent experiments. One-way ANOVA with Tukey's multiple comparisons post-test; *p<0.05; ** p<0.01; ***p<0.001;

Moreover, while single loss of Rad54 failed to significantly affect survival of MEFs upon X-ray photon irradiation, loss of Lig IV alone or both, Lig IV and Rad54, increased the sensitivity of MEFs to irradiation with X-ray photons significantly (Figure 2M). Additionally, loss of Lig IV significantly increased the radiosensitivity to X-ray photons than Rad54-deficiency (Figure 2M). However, loss of Rad54, Lig IV or both, rendered MEFs significantly more sensitive to irradiation with 8 Gy of either EP protons or SOBP protons (Figures 2N, O). Here, additional loss of Lig IV did not render Rad54-deficient MEFs more sensitive to proton irradiation (EP or SOBP) compared to Rad54-deficiency alone (Figure 2N, O).

To correlate variations in the efficiency of EP and SOBP proton irradiation to the different DNA repair-deficiencies, we subsequently calculated variations in RBE for 10% of clonogenic survival. The highest RBE values (1.84 and 1.66) were achieved after SOBP proton irradiation in Rad54$^{-/-}$ and Lig IV$^{-/-}$ MEFs, respectively (Figure 2I). In general, RBE values for SOBP protons were higher than those determined after EP proton irradiation.

To explore if deficiency in other proteins with relevance to NHEJ might reproduce the strong effects of Lig IV-deficiency on the survival of irradiated fibroblasts, we included two immortalized fibroblast cell lines deficient in XLF and PAXX in our investigations. However, neither deletion of XLF (Figure S1A, B) nor PAXX (Figure S1F, G) significantly affected long-term survival of MEFs after irradiation with X-ray photons and SOBP protons. However, XLF-deficiency slightly radiosensitized MEFs to EP proton irradiation at 8 Gy of dose leading to a higher RBE for EP proton irradiation (Figure S1B, C). Unexpectedly, SOBP proton irradiation was less efficient than X-ray photon irradiation in RPE-1 control cells resulting in lower RBE of 0.7 (Figure S1H).

3.3 Lig IV is essential for the repair of DNA damage induced in MEFs by irradiation with X-ray photons and SOBP protons

To gain insight into the relative importance of the above-mentioned NHEJ and HRR proteins for the repair of DNA damage induced by irradiation with X-ray photons vs. SOBP protons, we next determined potential differences in DNA damage induction and time-dependent removal of γH2A.X and 53BP1 foci in wild type MEFs as well as in MEFs harboring deficiencies in Lig IV, Rad54 or both, Lig IV and Rad54. Since we have not observed substantial differences in clonogenic survival of MEFs between irradiation with SOBP and EP protons (Figure 2), we focused on SOBP protons in our further experiments.

Quantification of DNA damage by using the alkaline comet assay demonstrated that exposure to X-ray photons and SOBP protons significantly increased DNA damage in wild type MEFs as well as in MEFs deficient in NHEJ or HRR proteins at 30 min after irradiation compared to non-irradiated control cells (Figure 3A, C left panel). Interestingly, the initial overall amount of DNA damage induced by SOBP protons was slightly increased when compared to X ray photons, independent of the cell line (Figure 3A, C left panel). However, deficiency in Lig IV, Rad54 or both, did not significantly alter the overall amount of initial amount of DNA damage induced by SOBP protons vs. X-ray photons at 30 min after irradiation (Figure 3A, C left panel). To corroborate these findings, we additionally used the γH2A.X and 53BP1 foci staining as a marker for DNA damage induction. However, we did not detect significant differences in the number of initial foci between tested cell lines when using X-ray photons vs. SOBP protons (Figure 3D, E).

However, despite similarities in the amount of initial DNA damage, cells with genetic deficiencies in DNA repair proteins may differ in the capacity for and kinetics of repair of radiation-induced DNA damage. Therefore, we additionally quantified the amount of residual DNA damage 24 h after irradiation. As depicted in Figures 3B and 3C (right panel), the highest amount of residual

DNA damage 24 h after irradiation with SOBP protons was observed in Rad54$^{-/-}$ MEFs, followed by Lig IV$^{-/-}$ MEFs and Rad54$^{-/-}$/ Lig IV$^{-/-}$ MEFs (Figure 3B, C right panel); though the double-deficient MEFs were characterized by an accumulation of residual DNA damage after irradiation with both, X-ray photons and SOBP protons (Figure 3B, C right panel). Next, we compared the capacity of wild type MEFs as well as of MEFs with genetic deficiencies in DNA repair proteins for the time-dependent removal of γH2A.X foci after irradiation with X-ray photons (Figure 3F) and SOBP protons (Figure 3G). Of note, when irradiation was performed with X-ray photons, only loss of Lig IV caused a significant delay in the removal of γH2A.X foci at 4 and 8 h after irradiation and an accumulation of residual γH2A.X foci at 24 h after irradiation. In contrast, MEFs deficient in Rad54 or both, Rad54 and Lig IV, displayed almost similar DNA repair kinetics as wildtype MEFs (Figure 3F). However, upon irradiation with SOBP protons, a significant delay in the removal of γH2A.X foci was observed in all cell lines with deficiency in NHEJ or HRR proteins when compared to wild type MEFs, at least at 4 h after irradiation (Figure 3G).

Taken together, while deficiency in Lig IV delayed DNA repair kinetics after irradiation with both, X-ray photons and SOBP protons compared to wild type MEFs, the removal of γH2A.X foci was only delayed by deficiency in Rad54 or both, Rad54 and Lig IV$^{-/-}$ compared to wild type MEFs when irradiation was performed with SOBP protons (Figure 3F, G). Moreover, a direct comparison between the response of the different MEFs to X-ray photons and SOBP protons further revealed that the most pronounced difference in the removal of γH2A.X foci between X-ray photon and proton irradiation was observed in Rad54$^{-/-}$ MEFs pointing to a more pronounced dependency of MEFs from integrity of HRR proteins when irradiated with SOBP protons than with X-ray photons (Figure 3H). An opposite trend was observed in Lig IV$^{-/-}$ MEFs where the removal of γH2A.X foci was slightly more efficient upon X-ray photon irradiation (Figure 3H).

In line with the findings obtained with Lig IV-deficient MEFs, XLF-deficiency significantly delayed DNA repair kinetics after irradiation with both, X-ray photons (Figure S1D) and SOBP protons (Figure S1E) in the 2BN fibroblast cell line. As expected, PAXX-deficiency had no effect on the removal of radiation-induced γH2A.X foci (Figure S1I, J). Moreover, a direct comparison of time-dependent γH2A.X foci removal in XLF$^{-/-}$ cells and the respective control cells revealed a difference after both, X-ray photon and SOBP proton irradiation (Figure S1K). Again, PAXX-deficiency had no effect on γH2A.X foci removal after X-ray photon irradiation, however we noticed a not significantly higher amount of γH2A.X foci after SOBP proton irradiation (Figure S1L).

3.4. Impairment of NHEJ or HRR shows a different impact on sensitivity of cancer cells to irradiation with X-ray photons or protons

So far, our data indicated that deficiency in NHEJ and HRR proteins has a different impact on effects on the repair of radiation-induced DNA damage and survival of normal MEFs. However, ionizing radiation is mostly used to treat cancer. We thus next investigated if we observe similar differences in cancer cells with deficiency in proteins relevant to NHEJ or HRR. To this end, we used glioblastoma cells proficient (M059K) and deficient (M059J) in DNA-PKcs, as well as pancreatic cancer cells without (BxPC3) and with loss of function of BRCA2 (Capan-1). Similar to the investigations in the MEFs, we irradiated cancer cells with a similar physical dose of X-ray photons, SOBP protons, or EP protons (Figure 4A, B and F, G). Deficiency in DNA-PKcs caused a dramatic radiosensitization independent of the radiation quality used (Figure 4A). Of note, comparison of different irradiation sources in DNA-PKcs-deficient vs. DNA-PKcs-proficient cells at a dose of 8 Gy revealed no difference in clonogenic survival (Figure 4B). As a consequence of the very high sensitivity of the DNA-PKcs-deficient cells to irradiation with X-ray photons, the RBE values for clonogenic cell survival turned out to be rather similar for all 3 radiation qualities in both cell lines, since irradiation with X-ray photons served as reference radiation quality (Figure 4C). Interestingly both, BRCA2-proficient BxPC3 and Capan-1 pancreatic cancer cells with BRCA2-deficiency turned out to be more sensitive to SOBP proton irradiation when compared to X-ray photon irradiation (Figure 4F, G). Though this effect was much more pronounced in Capan-1 cells with BRCA2-deficiency (Figure 4G).

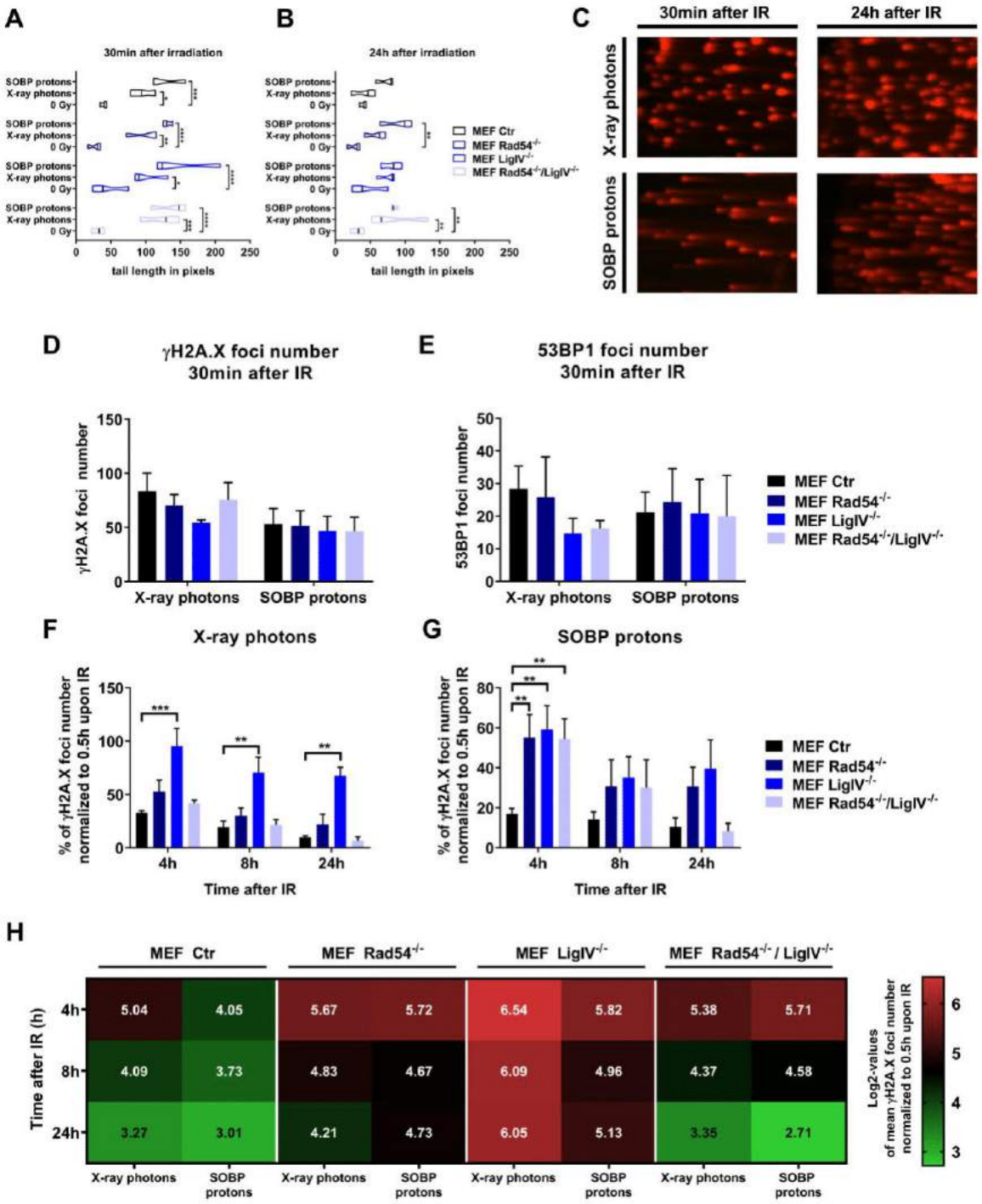

Figure 3. DNA damage repair induced by X-ray photons or SOBP protons in MEFs. (**A, B**) Quantification of alkaline Comet assay in wild type, Lig IV-deficient (Lig IV$^{-/-}$), Rad54-deficient (Rad54$^{-/-}$) or Lig IV/Rad54 double-deficient MEFs (Rad54$^{-/-}$/Lig IV$^{-/-}$) at 30 min (**A**) and 24 h (**B**) after irradiation with 3 Gy of X-ray photons or SOBP protons. (**C**) Exemplary pictures of alkaline Comet assay of wild type MEFs (MEF ctr) 30 min or 24 h after X-ray photon or SOBP proton irradiation. (**D**) γH2A.X and (**E**) 53BP1 foci number 30 min after irradiation with 3 Gy of X-ray photons and SOBP protons. (**F, G**) Quantification of DNA repair kinetics of MEFs harboring deficiencies in Rad54, Lig IV or Rad54 and Lig IV determined by quantification of γH2A.X foci. Data represent values normalized to 30 min after irradiation with 3 Gy. (**H**) Comparison of radiation source effects in tested cell lines as log2 values of γH2A.X foci quantification. Data represent mean SEM from 3 independent experiments. Two-way ANOVA with Tukey's multiple comparisons post-test; *p<0.05; **p<0.01; ***p<0.001; ****p<0.0001.

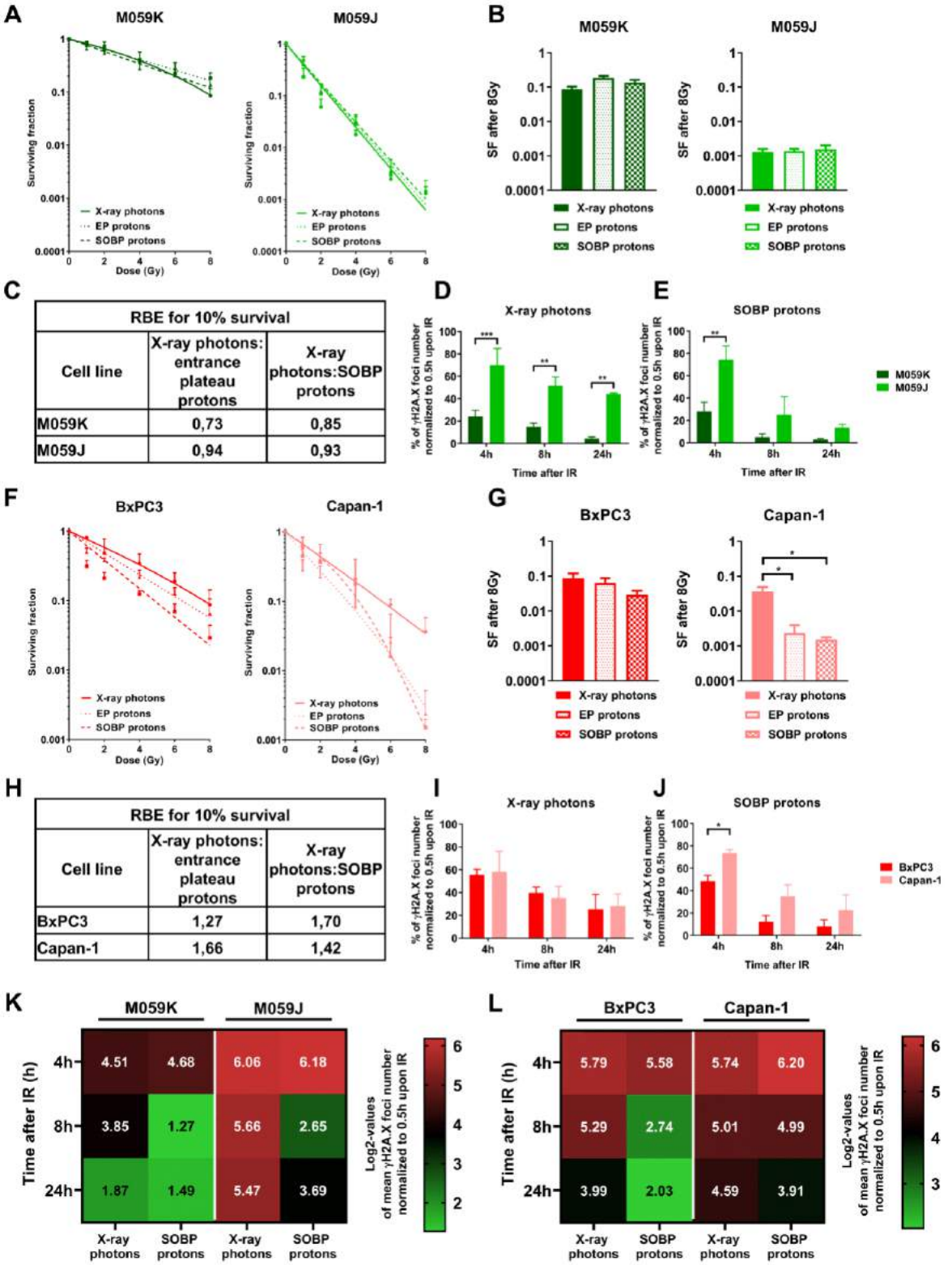

Figure 4. Effects of X-ray photons, EP and SOBP protons on clonogenic cell survival and kinetics in formation and removal of γH2A.X foci in cancer cells. (**A**, **B**) Clonogenic survival assay of DNA-PKcs-deficient M059J and DNA-PKcs-proficient M059K glioblastoma cells irradiated with X-ray photons, EP and SOBP protons (1-8 Gy). (**C**) RBE values calculated for 10% of clonogenic cell survival of the indicated cell lines. (**D**, **E**) γH2A.X foci removal over time (4-24 h) normalized to initial foci number at 30 min in M059J and M059K cells upon irradiation with 3 Gy of X-ray photons (**D**) and SOBP protons (**E**). (**F**, **G**) Clonogenic survival assay of pancreatic cancer cells with BRCA2-deficiency (Capan-1) and BRCA2-proficiency (BxPC3). (**H**) RBE values calculated for 10% of clonogenic cell

survival of the indicated cell lines. (**I, J**) γH2A.X foci removal over time (4-24 h) normalized to initial foci number at 30 min in Capan-1 and BxPC3 cells upon irradiation with 3 Gy of X-ray photons (**I**) and SOBP protons (**J**). (**K, L**) Comparison of radiation quality effects in tested cell lines as log2 values of γH2A.X foci quantification. Data represent mean values ± SD (**A, F**) or ± SEM (**B, D, E, G, I, J**) from 3 independent experiments. One-way ANOVA with Tukey's multiple comparisons post-test (**B, G**) or two-way ANOVA with Tukey's multiple comparisons post-test (**D, E, I, J**); *p<0.05; **p<0.01; ***p<0.001.

Instead, loss of BRCA2 only slightly sensitized Capan-1 cells to X-ray photon irradiation, when compared to BRCA2-proficient BxPC3 cells (Figure 4G). Of note, BRCA2-deficiency had a significantly higher sensitizing effect, when cells were exposed to irradiation with SOBP protons than to X-ray photon irradiation (Figure 4F, G). Furthermore, RBE values calculated for clonogenic cell survival of BxPC3 and Capan-1 cell lines after EP and SOBP proton irradiation were much higher than those determined for M059J and M059K cells, suggesting a particular benefit in using proton irradiation for pancreatic cancer cells when compared to X-ray photons (Figure 4H).

Next, we explored the effects of deficiency in DNA-PKcs and BRCA2 on the kinetics of DNA repair by measuring the time-dependent removal of γH2A.X foci in the respective cell lines (Figure 4 E-H). Consistent with the results gained from the long-term survival experiments, the time-dependent removal of γH2A.X foci was significantly delayed in DNA-PKcs-deficient M059J cells when compared to M059K DNA-PKcs-proficient cells (Figure 4D, E). Interestingly, X-ray photons evoked a stronger delay in DNA repair kinetics on M059J cells than SOBP proton irradiation resulting in a higher amount of residual DNA damage at 24 h after irradiation (Figure 4D, E). In contrast, in deficiency in BRCA2 in pancreatic cancer cells caused a pronounced delay in time-dependent removal of γH2A.X foci compared to BRCA2-proficient BxPC3 cells upon irradiation with SOBP, but not after irradiation with X-ray photons, reaching significant values at the 4 h time point (Figure 4I, J).

To better visualize the effects of both irradiation modalities, X-ray photons and SOBP protons, on DNA repair kinetics of M059J and M059K as well as Capan-1 and BxPC3, we performed a direct comparison of normalized γH2A.X foci numbers at 4 h, 8 h and 24 h dependent on irradiation source (Figure 4K, L). First, a more pronounced delay in the time-dependent removal of γH2A.X foci compared to M059K cells, including the residual DNA damage after 24 h, was observed in M059J cells when using X-ray photon irradiation, whereas the effect was weaker upon SOBP proton irradiation (Figure 4K). Second, we only observed minor differences in DNA repair kinetics between the two radiation qualities in control cell line M059K (Figure 4K). On the other hand, removal of γH2A.X foci occurred with similar efficiency in BRCA2 proficient BxPC3 and Capan-1 pancreatic cancer cells with BRCA2 deficiency, resulting in similar DNA repair kinetics upon irradiation with X-ray photons (Figure 4L). However, removal of γH2A.X foci was slower in Capan-1 cells than in BxPC3 cells upon irradiation with SOBP protons (Figure 4L). This resulted in almost similar DNA repair kinetics and comparable levels of residual DNA damage foci in Capan-1 cells upon irradiation with X-ray photons and SOBP protons (Figure 4L).

4. Discussion

While the physical characteristics of photon irradiation have been investigated in much detail during recent decades, potential specificities in biological effects of proton irradiation are less well understood. Dose-deposition profiles of therapeutic proton beams are characterized by a low-dose plateau at small depths EP) and the SOBP. In the SOBP the major part of energy is deposited shortly before the sharp distal energy fall-off. First, by using STED we reveal here that irradiation with X-ray photons resulted in homogenously distributed small DNA damage foci, whereas SOBP proton irradiation induced clusters of several smaller γH2A.X foci in closer proximity that we termed "foci clusters". Interestingly, EP proton irradiation caused both, clustered and homogenously distributed small γH2A.X foci within the nucleus of MEFs. Second, we demonstrate that loss of important components of HRR has a more severe impact on DNA repair kinetics and survival of cancer cells

and MEFs exposed to a similar physical radiation dose of mid SOBP or EP protons than upon irradiation with X-ray photons. We assume that the increasing importance of repair by HRR in cancer cells irradiated with SOBP protons compared to X-ray photon irradiation will also be caused by the induction of more clustered DNA lesions composed of multiple DNA damage sites in close proximity, as demonstrated in MEFs by visualizing γH2A.X foci using STED microscopy. We speculate that an increased dependence of cancer cells exposed to proton irradiation from the integrity of the HRR pathway may be relevant for patient stratification to proton vs. photon irradiation and a biological optimization of combinatorial treatments using proton irradiation with inhibitors of HRR.

In more detail, we first hypothesized that irradiation with protons (SOBP, EP) and X-ray photons may induce distinct microscopic patterns of DNA damage since the physical characteristics of proton beams include a higher LET and a deposition of more dose per path length than gamma-ray or X-ray photons [66]. Indeed, we observed that irradiation with SOBP protons induced γH2A.X DNA foci-clusters, whereas DNA damage foci induced by X-ray photons were smaller and more randomly distributed over the whole nucleus. These observations are consistent with the described action of particles, including protons, that induce a direct DNA damage within their defined track and therefore tend to induce accumulated DNA damage in closer proximity [13,14,67,68]. It has been previously suggested that the high energy of particles, e.g. protons, strongly correlates with clustered DNA damage in form of coalesced DNA DSB due to denser ionizing events [6,13,14,67,69]. Moreover, a prediction analysis done by a new computational track structure model which simulates complexity of DNA damage after proton irradiation, endorses our assumption of a more complex DNA damage induced by proton irradiation [70]. Interestingly, we observed that EP proton irradiation caused both – clustered and randomly distributed DNA damage. Therefore, we speculate that high energy protons of the EP region deposit their energy more randomly causing less ionizing events than the 'precise' SOBP protons and result therefore in lower probability to hit the cell nucleus and to induce only clustered DNA lesions [71]. Our findings support assumptions proposed by others that differences in dose deposition between photons and protons induce different DNA lesions. Thereby, more complex DNA damage induced by protons may result in less efficient repair and more effective eradication of clonogenic cells [14,28,29,72,73]. Furthermore, the time-dependent increase in distance between γH2A.X foci observed in our study suggests that the initial clusters are removed over time leaving smaller but longer-lasting foci [68,74].

Since X-ray photons, SOBP and EP protons induced different patterns of DNA damage, we further determined radiosensitivity of wildtype MEFs to all three radiation modalities and observed higher RBE values for 10% of clonogenic survival upon SOBP proton than upon EP proton irradiation. We therefore conclude that the effects of EP on survival are more similar to X-ray photons, at least as long as the MEFs have an intact DNA repair machinery (NHEJ, HRR). These observations corroborate findings obtained by others describing higher RBE values in a zebrafish model at mid SOBP compared to EP proton irradiation [75].

However, when analyzing MEFs harboring deficiencies in specific DNA repair proteins associated with NHEJ (Lig IV$^{-/-}$), HRR (Rad54$^{-/-}$) or both (Rad54$^{-/-}$/Lig IV$^{-/-}$), we observed divergent results. In fact, MEFs deficient in Lig IV turned out to be highly radiosensitive, independent of the radiation quality used. In contrast, only proton irradiation showed a radiosensitizing effect in MEFs deficient in Rad54. However, for both cell lines, the RBE values determined for SOBP proton irradiation were higher than for EP, as observed in wildtype MEFs. Interestingly, co-depletion of proteins involved in NHEJ and HRR (Rad54$^{-/-}$/Lig IV$^{-/-}$) showed a similar survival as wildtype fibroblasts which might be explained by activation of alt-EJ as an adaptation to the lack of both major DNA repair pathways [36]. Instead, neither loss of XLF nor loss of PAXX had a significant impact on survival of fibroblasts after any type of irradiation, pointing to a redundant function of those NHEJ factors. We speculate that only the loss of key factors of the NHEJ complex, as Lig IV, XRCC4 or DNA-PKcs, has a significant impact on clonogenic survival. However, XLF-deficiency affected the proper DNA repair kinetics after SOBP proton irradiation, pointing to its role in DNA repair and

presumably in stabilizing the NHEJ-complex, but not in long-term survival. We speculate that loss of XLF can be compensated and is therefore not essential for cells to survive.

To corroborate our findings about the impact of DNA repair-deficiencies on radiation response in cancer cell models, we used the DNA-PKcs-deficient M059J and DNA-PKcs-proficient M059K glioblastoma cell lines as well as the pancreatic cell lines BxPC3 with intact BRCA2 and Capan-1 with reported deficiency in BRCA2 expression. Similar to fibroblasts with impaired NHEJ due to loss of Lig IV, DNA-PKcs-deficient glioblastoma cells were more sensitive than DNA-PKcs proficient M059K cells to irradiation with both, X-ray photons as well as protons (EP and SOBP). However, calculated RBE values for 10% of clonogenic survival for EP and SOBP were approx. 1, which has already been observed by others [28,76]. These findings reveal that deficiency in NHEJ caused by the loss of DNA-PKcs causes a dramatic radiosensitization already to X-ray photon irradiation that overrides potential small differences in survival caused by the distinct biology of the DNA damage induced by X-ray photon and proton irradiation, respectively.

Though both, BRCA2-proficient BxPC3 pancreatic cancer cells as well as Capan-1 pancreatic cancer cells with BRCA2-deficiency, were more sensitive to irradiation with SOBP protons compared to irradiation with X-ray photons, the increase in the cytotoxic effects of proton irradiation compared to X-ray photon irradiation was more pronounced in Capan-1 pancreatic cancer cells. We assume that the 6174delT mutation on the remaining copy of BRCA2, which results in C-terminal truncation and removal of the DNA repair domain, strongly contributed to the radiosensitizing effect [77]. However, it is important to bear in mind that BxPC3 and Capan-1 cells are not isogenic but constitute distinct cell lines and thus have a different genetic background [54,78]. Therefore, it cannot be excluded that the radiation effects observed in BxPC3 and Capan-1 cells may be altered due to further, yet unknown, variations in other proteins or pathways involved in the regulation or execution of DNA DSB repair by NHEJ, HRR or both [54,78]. So far, pancreatic cancer has been reported to be strongly radioresistant with lowest RBE values compared to other tumor entities [71,79–84]. Importantly, our findings suggest that proton radiotherapy may offer a better treatment option for pancreatic cancer patients than photon irradiation and also limit normal tissue toxicity. Moreover, since BRCA2-deficiency in Capan-1 cells was associated with an increased the sensitivity of pancreatic cancer cells to proton irradiation, inhibitors of BRCA2 or another HRR-factors may be suited to enhance the efficacy of proton radiotherapy and thereby improve the outcome of patients suffering from pancreatic cancer. Despite first promising results, so far the number of reports describing combined treatment of pancreatic cancer with radiotherapy and targeted therapy with DNA repair inhibitors, (e.g. ATM, ATR, DNA-PK) is very limited [48].

Despite severe impact of DNA-PKcs-deficiency on DNA repair kinetics in M059J cells upon proton and photon irradiation, X-ray photons had the highest impact on the number of the induction and removal of γH2A.X foci, as revealed by increased number of initial γH2A.X foci at 4 h and 8 h after irradiation. Moreover, deficiency in DNA-PKcs resulted in more pronounced damage persistence, as revealed by enhanced residual DNA damage foci in M059J cells 24 h upon irradiation with X-ray photons compared to SOBP protons. Our observations corroborate the major role of NHEJ for survival of irradiated cancer cells irrespective of the radiation quality, thereby confirming previous observations by others [73,76]. The importance of NHEJ in ensuring cell survival upon both, proton and photon irradiation, also corresponds to the reported involvement of NHEJ in the repair of approx. 80% of all DNA DSB occurring upon X-ray photon irradiation [47].

Taken together, while fibroblasts and cancer cells deficient in NHEJ (Lig IV$^{-/-}$ or DNA-PKcs$^{-/-}$) responded to proton and X-ray photon irradiation with a comparable reduction of clonogenic cell survival, the increase in residual DNA damage was higher after X-ray photon irradiation. We speculate that the repair of smaller DNA lesions induced by X-ray photons will mainly rely on NHEJ, so that cells with a deficiency in proper NHEJ will accumulate residual DNA damage [28,29]. In contrast, a delay in DNA repair kinetics of HRR-deficient cell lines was only observed after SOBP proton irradiation underlining the increased importance of HRR for the repair of clustered DNA damage induced by irradiation with SOBP protons [14,28,29,47,68,71,76]. However, the delay was less pronounced than the delay observed in NHEJ-deficient cells after X-ray photon irradiation. This

633 suggests that NHEJ is also involved in repair of clustered DNA lesions induced by SOBP proton
634 irradiation and that HRR plays an additional and supportive role in processing the induced DNA
635 DSB, as suggested by others [47,76].
636 Summarizing, the genetic makeup impacts patient-specific radiosensitivity and represents a
637 valuable factor for patient stratification in the clinic. However, uncertainties in RBE, which are
638 estimated to be 10-20%, remain a current obstacle in the use particle or heavy ion therapy, since the
639 delivered dose depends on estimated RBE [19]. Another limiting factor is the uncertainty in RBE in
640 specific tissue types as it is not possible to estimate a tissue-related RBE. Therefore, RBE-related
641 uncertainties strongly complicate an optimization of treatment planning based on RBE models [85].
642 So far, patient stratification for proton versus photon radiotherapy is mainly based on the
643 localization of the tumor and critical organs at risk. However, our findings emphasize that it may be
644 useful to additionally use molecular markers for patient stratification according to the biological
645 characteristics of the respective tumor, e.g. integrity of the major DNA repair pathways. A better
646 understanding of the characteristics and consequences of DNA damage induced by proton
647 irradiation in normal tissues and tumors, and potential different molecular requirements for repair
648 of DNA damage induced by proton irradiation will allow us to harness the full potential of proton
649 irradiation for clinical radiotherapy by combining proton radiotherapy with chemotherapy, targeted
650 drug therapy, metabolic inhibitors and/or immunotherapy in the future.

651 **5. Conclusions**

652 Super-resolution STED microscopy of wildtype fibroblasts MEFs exposed to a similar physical dose
653 of X-ray photons or SOBP protons revealed that SOBP protons induced increased numbers of
654 clustered γH2A.X foci composed of several smaller foci. In contrast, irradiation with X-ray photons
655 caused homogenously distributed small DNA damage foci. Furthermore, we demonstrate that
656 deficiency in key proteins involved in NHEJ, Lig IV and DNA-PKcs, delayed DNA repair after X-
657 ray photon and proton irradiation compared to DNA repair-proficient control cells. Of note,
658 deficiency in components of HRR compromised DNA repair and removal of γ-H2A.X foci
659 particularly in response to SOBP proton irradiation. In line with these findings, NHEJ-deficiency
660 resulted in significant sensitization of normal fibroblasts and cancer cells to both, X-ray photons and
661 protons, whereas deficiency in HRR proteins resulted in a specific sensitization to proton
662 irradiation. We conclude that NHEJ plays an essential role in processing DNA DSB induced by
663 proton and photon irradiation, whereas HRR gains increasing importance when proton irradiation
664 is used, presumably for proper repair of the more clustered DNA lesions. This has also implications
665 for combinatorial treatments with inhibitors of DNA repair pathways.
666

667 **Supplementary Materials:** The following are available online at www.mdpi.com/xxx/s1, Figure S1: Clonogenic
668 survival and DNA damage response of RPE-1 PAXX$^{-/-}$ and 2BN hTERT XLF$^{-/-}$ cells as well as respective control
669 cells.

670 **Author Contributions:** K.S., A.K., and V.J. designed and conceptualized the research and wrote the original
671 manuscript draft; K.S. and A.K. designed methodology, performed experiments as well analyzed, curated and
672 validated the data and visualized the results; J.v.d.L. performed and analyzed experiments; A.K.2 and M.V.
673 performed proton irradiation, validation and formal analysis of irradiation fields; B.K. designed proton
674 irradiation fields and performed their calculations, validation and formal analysis; A.S. and S.O. analyzed and
675 visualized experiments; S.D., J.H., C.N. and J.M. performed experiments; J.T.S. provided resources; M.P., B.T.
676 and V.J. supervised the work; V.J. acquired the funding. All authors critically revised, edited and approved the
677 final version of the manuscript.

678 **Funding:** This work was supported by a grant of the German Research Foundation DFG GRK1739/2 to V.J. and
679 by a grant for ITN RADIATE from European Union's Framework Programme for Research and Innovation
680 Horizon 2020 (2014-2020) under Marie Skłodowska-Curie Grant Agreement No. 642623 to V.J. and M.P.; J.T.S. is
681 supported by the German Cancer Consortium (DKTK) and the German Research Foundation (DFG) through
682 grant SI1549/3-1 (Clinical Research Unit KFO337) and Collaborative Research Center SFB824 (project C4).

Acknowledgments: We would like to thank Prof. Dr. George Iliakis (Institute of Medical Radiation Biology, University Hospital Essen, Germany) for providing cells used in this work and for the opportunity to use the X-RAD 320 X-Ray Biological Irradiator. We would like to thank Michael Piel (Institute of Medical Radiation Biology, University Hospital Essen, Germany) for providing information regarding photon irradiation.

Conflicts of Interest: The authors declare no conflict of interest.

References

1. Begg, A.C.; Stewart, F.A.; Vens, C. Strategies to improve radiotherapy with targeted drugs. *Nat. Rev. Cancer* **2011**, *11*, 239–253.
2. De Ruysscher, D.; Niedermann, G.; Burnet, N.G.; Siva, S.; Lee, A.W.M.; Hegi-Johnson, F. Radiotherapy toxicity. *Nat. Rev. Dis. Prim.* **2019**, *5*, 13.
3. Bristow, R.G.; Alexander, B.; Baumann, M.; Bratman, S. V; Brown, J.M.; Camphausen, K.; Choyke, P.; Citrin, D.; Contessa, J.N.; Dicker, A.; et al. Combining precision radiotherapy with molecular targeting and immunomodulatory agents: a guideline by the American Society for Radiation Oncology. *Lancet Oncol.* **2018**, *19*, e240–e251.
4. Orth, M.; Lauber, K.; Niyazi, M.; Friedl, A.A.; Li, M.; Maihöfer, C.; Schüttrumpf, L.; Ernst, A.; Niemöller, O.M.; Belka, C. Current concepts in clinical radiation oncology. *Radiat. Environ. Biophys.* **2014**, *53*, 1–29.
5. Baumann, B.C.; Mitra, N.; Harton, J.; Xiao, Y.; Wojcieszynski, A.; Gabriel, P.E.; Zhong, H.; Geng, H.; Doucette, A.; Wei, J.J.; et al. Comparative effectiveness of proton therapy versus photon therapy as part of concurrent chemoradiotherapy for locally advanced cancer. *J. Clin. Oncol.* **2019**, *37*, 6521.
6. Durante, M.; Loeffler, J.S. Charged particles in radiation oncology. *Nat. Rev. Clin. Oncol.* **2010**, *7*, 37–43.
7. McDonald, M.W.; Zolali-Meybodi, O.; Lehnert, S.J.; Estabrook, N.C.; Liu, Y.; Cohen-Gadol, A.A.; Moore, M.G. Reirradiation of Recurrent and Second Primary Head and Neck Cancer With Proton Therapy. *Int. J. Radiat. Oncol.* **2016**, *96*, 808–819.
8. Rombi, B.; Vennarini, S.; Vinante, L.; Ravanelli, D.; Amichetti, M. Proton radiotherapy for pediatric tumors: review of first clinical results. *Ital. J. Pediatr.* **2014**, *40*, 74.
9. Amichetti, M.; Cianchetti, M.; Amelio, D.; Enrici, R.M.; Minniti, G. Proton therapy in chordoma of the base of the skull: a systematic review. *Neurosurg. Rev.* **2009**, *32*, 403–416.
10. Tallen, G.; Resch, A.; Calaminus, G.; Wiener, A.; Leiss, U.; Pletschko, T.; Friedrich, C.; Langer, T.; Grabow, D.; Driever, P.H.; et al. Strategies to improve the quality of survival for childhood brain tumour survivors. *Eur. J. Paediatr. Neurol.* **2015**, *19*, 619–639.
11. Timmermann, B. Proton Beam Therapy for Childhood Malignancies: Status Report. *Klin. Pädiatrie* **2010**, 222, 127–133.
12. Tommasino, F.; Durante, M. Proton radiobiology. *Cancers (Basel).* **2015**, *7*, 353–81.
13. Jones, B. Proton radiobiology and its clinical implications. *Ecancermedicalscience* **2017**, *11*, 777.
14. Oeck, S.; Szymonowicz, K.; Wiel, G.; Krysztofiak, A.; Lambert, J.; Koska, B.; Iliakis, G.; Timmermann, B.; Jendrossek, V. Relating Linear Energy Transfer to the Formation and Resolution of DNA Repair Foci After Irradiation with Equal Doses of X-ray Photons, Plateau, or Bragg-Peak Protons. *Int. J. Mol. Sci.* **2018**, *19*, 3779.
15. Jermann, M. Particle Therapy Statistics in 2014. *Int. J. Part. Ther.* **2015**, *2*, 50–54.
16. Montay-Gruel, P.; Meziani, L.; Yakkala, C.; Vozenin, M.C. Expanding the therapeutic index of radiation therapy by normal tissue protection. *Br. J. Radiol.* **2019**, *92*.
17. Nickoloff, J.A. Photon, light ion, and heavy ion cancer radiotherapy: paths from physics and biology to clinical practice. *Ann. Transl. Med.* **2015**, *3*, 336.

18. Paganetti, H. Relative biological effectiveness (RBE) values for proton beam therapy. Variations as a function of biological endpoint, dose, and linear energy transfer. *Phys. Med. Biol.* **2014**, *59*, R419–R472.
19. Paganetti, H.; Niemierko, A.; Ancukiewicz, M.; Gerweck, L.E.; Goitein, M.; Loeffler, J.S.; Suit, H.D. Relative biological effectiveness (RBE) values for proton beam therapy. *Int. J. Radiat. Oncol.* **2002**, *53*, 407–421.
20. Paganetti, H.; van Luijk, P. Biological Considerations When Comparing Proton Therapy With Photon Therapy. *Semin. Radiat. Oncol.* **2013**, *23*, 77–87.
21. Karger, C.P.; Peschke, P. RBE and related modeling in carbon-ion therapy. *Phys. Med. Biol.* **2018**, *63*.
22. Willers, H.; Allen, A.; Grosshans, D.; McMahon, S.J.; von Neubeck, C.; Wiese, C.; Vikram, B. Toward A variable RBE for proton beam therapy. *Radiother. Oncol.* **2018**, *128*, 68–75.
23. Paganetti, H.; Olko, P.; Kobus, H.; Becker, R.; Schmitz, T.; Waligorski, M.P.R.; Filges, D.; Müller-Gärtner, H.-W. Calculation of relative biological effectiveness for proton beams using biological weighting functions. *Int. J. Radiat. Oncol.* **1997**, *37*, 719–729.
24. Scalliet, P.; Gueulette, J. Radiobiological Characterization of Clinical Proton and Carbon-Ion Beams. **2018**.
25. Held, K.D.; Kawamura, H.; Kaminuma, T.; Paz, A.E.S.; Yoshida, Y.; Liu, Q.; Willers, H.; Takahashi, A. Effects of Charged Particles on Human Tumor Cells. *Front. Oncol.* **2016**, *6*, 23.
26. Lühr, A.; von Neubeck, C.; Krause, M.; Troost, E.G.C. Relative biological effectiveness in proton beam therapy – Current knowledge and future challenges. *Clin. Transl. Radiat. Oncol.* **2018**, *9*, 35–41.
27. Suzuki, M.; Kase, Y.; Yamaguchi, H.; Kanai, T.; Ando, K. Relative biological effectiveness for cell-killing effect on various human cell lines irradiated with heavy-ion medical accelerator in Chiba (HIMAC) carbon-ion beams. *Int. J. Radiat. Oncol.* **2000**, *48*, 241–250.
28. Grosse, N.; Fontana, A.O.; Hug, E.B.; Lomax, A.; Coray, A.; Augsburger, M.; Paganetti, H.; Sartori, A.A.; Pruschy, M. Deficiency in Homologous Recombination Renders Mammalian Cells More Sensitive to Proton Versus Photon Irradiation. *Int. J. Radiat. Oncol.* **2014**, *88*, 175–181.
29. Fontana, A.O.; Augsburger, M.A.; Grosse, N.; Guckenberger, M.; Lomax, A.J.; Sartori, A.A.; Pruschy, M.N. Differential DNA repair pathway choice in cancer cells after proton- and photon-irradiation. *Radiother. Oncol.* **2015**, *116*, 374–380.
30. Liu, Q.; Ghosh, P.; Magpayo, N.; Testa, M.; Tang, S.; Gheorghiu, L.; Biggs, P.; Paganetti, H.; Efstathiou, J.A.; Lu, H.-M.; et al. Lung Cancer Cell Line Screen Links Fanconi Anemia/BRCA Pathway Defects to Increased Relative Biological Effectiveness of Proton Radiation. *Int. J. Radiat. Oncol.* **2015**, *91*, 1081–1089.
31. Peeler, C.R.; Mirkovic, D.; Titt, U.; Blanchard, P.; Gunther, J.R.; Mahajan, A.; Mohan, R.; Grosshans, D.R. Clinical evidence of variable proton biological effectiveness in pediatric patients treated for ependymoma. *Radiother. Oncol.* **2016**, *121*, 395–401.
32. Willers, H.; Allen, A.; Grosshans, D.; McMahon, S.J.; von Neubeck, C.; Wiese, C.; Vikram, B. Toward A variable RBE for proton beam therapy. *Radiother. Oncol.* **2018**, *128*, 68–75.
33. Mladenov, E.; Magin, S.; Soni, A.; Iliakis, G. DNA Double-Strand Break Repair as Determinant of Cellular Radiosensitivity to Killing and Target in Radiation Therapy. *Front. Oncol.* **2013**, *3*, 113.
34. Roos, W.P.; Thomas, A.D.; Kaina, B. DNA damage and the balance between survival and death in cancer biology. *Nat. Rev. Cancer* **2015**, *16*, 20–33.
35. Schipler, A.; Iliakis, G. DNA double-strand-break complexity levels and their possible contributions to the probability for error-prone processing and repair pathway choice. *Nucleic Acids Res.* **2013**, *41*, 7589–605.

769 36. Iliakis, G.; Murmann, T.; Soni, A. Alternative end-joining repair pathways are the ultimate backup for
770 abrogated classical non-homologous end-joining and homologous recombination repair: Implications
771 for the formation of chromosome translocations. *Mutat. Res. Toxicol. Environ. Mutagen.* **2015**, *793*, 166–
772 175.
773 37. Soni, A.; Siemann, M.; Pantelias, G.E.; Iliakis, G. Marked contribution of alternative end-joining to
774 chromosome-translocation-formation by stochastically induced DNA double-strand-breaks in G2-phase
775 human cells. *Mutat. Res. Toxicol. Environ. Mutagen.* **2015**, *793*, 2–8.
776 38. Critchlow, S.E.; Bowater, R.P.; Jackson, S.P. Mammalian DNA double-strand break repair protein
777 XRCC4 interacts with DNA ligase IV. *Curr. Biol.* **1997**, *7*, 588–598.
778 39. Andres, S.N.; Modesti, M.; Tsai, C.J.; Chu, G.; Junop, M.S. Crystal structure of human XLF: a twist in
779 nonhomologous DNA end-joining. *Mol. Cell* **2007**, *28*, 1093–101.
780 40. Davis, A.J.; Chen, B.P.C.; Chen, D.J. DNA-PK: A dynamic enzyme in a versatile DSB repair pathway.
781 *DNA Repair (Amst).* **2014**, *17*, 21–29.
782 41. Ochi, T.; Blackford, A.N.; Coates, J.; Jhujh, S.; Mehmood, S.; Tamura, N.; Travers, J.; Wu, Q.; Draviam,
783 V.M.; Robinson, C. V; et al. DNA repair. PAXX, a paralog of XRCC4 and XLF, interacts with Ku to
784 promote DNA double-strand break repair. *Science* **2015**, *347*, 185–188.
785 42. Heyer, W.-D.; Ehmsen, K.T.; Liu, J. Regulation of Homologous Recombination in Eukaryotes. *Annu. Rev.*
786 *Genet.* **2010**, *44*, 113–139.
787 43. Lamarche, B.J.; Orazio, N.I.; Weitzman, M.D. The MRN complex in double-strand break repair and
788 telomere maintenance. *FEBS Lett.* **2010**, *584*, 3682–95.
789 44. Narod, S.A.; Salmena, L. BRCA1 and BRCA2 mutations and breast cancer. *Discov. Med.* **2011**, *12*, 445–53.
790 45. Chapman, J.R.; Taylor, M.R.G.; Boulton, S.J. Playing the End Game: DNA Double-Strand Break Repair
791 Pathway Choice. *Mol. Cell* **2012**, *47*, 497–510.
792 46. Bothmer, A.; Robbiani, D.F.; Di Virgilio, M.; Bunting, S.F.; Klein, I.A.; Feldhahn, N.; Barlow, J.; Chen, H.-
793 T.; Bosque, D.; Callen, E.; et al. Regulation of DNA end joining, resection, and immunoglobulin class
794 switch recombination by 53BP1. *Mol. Cell* **2011**, *42*, 319–29.
795 47. Gerelchuluun, A.; Manabe, E.; Ishikawa, T.; Sun, L.; Itoh, K.; Sakae, T.; Suzuki, K.; Hirayama, R.;
796 Asaithamby, A.; Chen, D.J.; et al. The Major DNA Repair Pathway after Both Proton and Carbon-Ion
797 Radiation is NHEJ, but the HR Pathway is More Relevant in Carbon Ions HHS Public Access. *Radiat Res*
798 **2015**, *183*, 345–356.
799 48. Yang, S.-H.; Kuo, T.-C.; Wu, H.; Guo, J.-C.; Hsu, C.; Hsu, C.-H.; Tien, Y.-W.; Yeh, K.-H.; Cheng, A.-L.;
800 Kuo, S.-H. Perspectives on the combination of radiotherapy and targeted therapy with DNA repair
801 inhibitors in the treatment of pancreatic cancer. *World J. Gastroenterol.* **2016**, *22*, 7275.
802 49. Biau, J.; Chautard, E.; Verrelle, P.; Dutreix, M. Altering DNA Repair to Improve Radiation Therapy:
803 Specific and Multiple Pathway Targeting. *Front. Oncol.* **2019**, *9*, 1009.
804 50. Bhattacharya, S.; Asaithamby, A. Repurposing DNA repair factors to eradicate tumor cells upon
805 radiotherapy. *Transl. Cancer Res.* **2017**, *6*, S822–S839.
806 51. Gavande, N.S.; VanderVere-Carozza, P.S.; Hinshaw, H.D.; Jalal, S.I.; Sears, C.R.; Pawelczak, K.S.; Turchi,
807 J.J. DNA repair targeted therapy: The past or future of cancer treatment? *Pharmacol. Ther.* **2016**, *160*, 65–
808 83.
809 52. DiBiase, S.J.; Zeng, Z.C.; Chen, R.; Hyslop, T.; Curran, W.J.; Iliakis, G. DNA-dependent protein kinase
810 stimulates an independently active, nonhomologous, end-joining apparatus. *Cancer Res.* **2000**, *60*, 1245–
811 1253.

53. Wu, W.; Wang, M.; Wu, W.; Singh, S.K.; Mussfeldt, T.; Iliakis, G. Repair of radiation induced DNA double strand breaks by backup NHEJ is enhanced in G2. *DNA Repair (Amst).* **2008**, *7*, 329–338.
54. Abbott, D.W.; Holt, J.T.; Freeman, M.L. Double-Strand Break Repair Deficiency and Radiation Sensitivity in BRCA2 Mutant Cancer Cells. *JNCI J. Natl. Cancer Inst.* **1998**, *90*, 978–985.
55. Riballo, E.; Woodbine, L.; Stiff, T.; Walker, S.A.; Goodarzi, A.A.; Jeggo, P.A. XLF-Cernunnos promotes DNA ligase IV–XRCC4 re-adenylation following ligation. *Nucleic Acids Res.* **2009**, *37*, 482–492.
56. Ochi, T.; Blackford, A.N.; Coates, J.; Jhujh, S.; Mehmood, S.; Tamura, N.; Travers, J.; Wu, Q.; Draviam, V.M.; Robinson, C. V; et al. DNA repair. PAXX, a paralog of XRCC4 and XLF, interacts with Ku to promote DNA double-strand break repair. *Science* **2015**, *347*, 185–188.
57. Franken, N.A.P.; Rodermond, H.M.; Stap, J.; Haveman, J.; van Bree, C. Clonogenic assay of cells in vitro. *Nat. Protoc.* **2006**, *1*, 2315–2319.
58. McMahon, S.J. The linear quadratic model: usage, interpretation and challenges. *Phys. Med. Biol.* **2018**, *64*, 01TR01.
59. Staab, A.; Zukowski, D.; Walenta, S.; Scholz, M.; Mueller-Klieser, W. Response of Chinese Hamster V79 Multicellular Spheroids Exposed to High-Energy Carbon Ions. *Radiat. Res.* **2004**, *161*, 219–227.
60. Oeck, S.; Malewicz, N.M.; Hurst, S.; Rudner, J.; Jendrossek, V. The Focinator - a new open-source tool for high-throughput foci evaluation of DNA damage. *Radiat. Oncol.* **2015**, *10*, 163.
61. Oeck, S.; Malewicz, N.M.; Hurst, S.; Al-Refae, K.; Krysztofiak, A.; Jendrossek, V. The Focinator v2-0 - Graphical Interface, Four Channels, Colocalization Analysis and Cell Phase Identification. *Radiat. Res.* **2017**, *000*, RR14746.1.
62. Staudt, T.; Lang, M.C.; Medda, R.; Engelhardt, J.; Hell, S.W. 2,2′-Thiodiethanol: A new water soluble mounting medium for high resolution optical microscopy. *Microsc. Res. Tech.* **2007**, *70*, 1–9.
63. Baddeley, A.; Rubak, E.; Turner, R. *Spatial Point Patterns: Methodology and Applications with R*; Chapman & Hall/CRC: London, 2015; ISBN 978-1-4822-1020-0.
64. Olive, P.L.; Banáth, J.P. The comet assay: a method to measure DNA damage in individual cells. *Nat. Protoc.* **2006**, *1*, 23–29.
65. Gyori, B.M.; Venkatachalam, G.; Thiagarajan, P.S.; Hsu, D.; Clement, M.-V. OpenComet: An automated tool for comet assay image analysis. *Redox Biol.* **2014**, *2*, 457–465.
66. Krämer, M.; Weyrather, W.K.; Scholz, M. The Increased Biological Effectiveness of Heavy Charged Particles: From Radiobiology to Treatment Planning. *Technol. Cancer Res. Treat.* **2003**, *2*, 427–436.
67. Hojo, H.; Dohmae, T.; Hotta, K.; Kohno, R.; Motegi, A.; Yagishita, A.; Makinoshima, H.; Tsuchihara, K.; Akimoto, T. Difference in the relative biological effectiveness and DNA damage repair processes in response to proton beam therapy according to the positions of the spread out Bragg peak. *Radiat. Oncol.* **2017**, *12*, 111.
68. Reindl, J.; Girst, S.; Walsh, D.W.M.; Greubel, C.; Schwarz, B.; Siebenwirth, C.; Drexler, G.A.; Friedl, A.A.; Dollinger, G. Chromatin organization revealed by nanostructure of irradiation induced γH2AX, 53BP1 and Rad51 foci. *Sci. Rep.* **2017**, *7*, 40616.
69. Chaudhary, P.; Marshall, T.I.; Currell, F.J.; Kacperek, A.; Schettino, G.; Prise, K.M. Variations in the Processing of DNA Double-Strand Breaks Along 60-MeV Therapeutic Proton Beams. *Int. J. Radiat. Oncol.* **2016**, *95*, 86–94.
70. Henthorn, N.T.; Warmenhoven, J.W.; Sotiropoulos, M.; Aitkenhead, A.H.; Smith, E.A.K.; Ingram, S.P.; Kirkby, N.F.; Chadwick, A.L.; Burnet, N.G.; Mackay, R.I.; et al. Clinically relevant nanodosimetric simulation of DNA damage complexity from photons and protons. *RSC Adv.* **2019**, *9*, 6845–6858.

855 71. Ray, S.; Cekanaviciute, E.; Lima, I.P.; Sørensen, B.S.; Costes, S. V. Comparing Photon and Charged
856 Particle Therapy Using DNA Damage Biomarkers. *Int. J. Part. Ther.* **2018**, *5*, 15–24.
857 72. Maeda, K.; Yasui, H.; Yamamori, T.; Matsuura, T.; Takao, S.; Suzuki, M.; Matsuda, A.; Inanami, O.;
858 Shirato, H. A Nucleoside Anticancer Drug, 1-(3-C-Ethynyl-β-D-Ribo-Pentofuranosyl)Cytosine, Induces
859 Depth-Dependent Enhancement of Tumor Cell Death in Spread-Out Bragg Peak (SOBP) of Proton Beam.
860 *PLoS One* **2016**, *11*, e0166848.
861 73. Gerelchuluun, A.; Manabe, E.; Ishikawa, T.; Sun, L.; Itoh, K.; Sakae, T.; Suzuki, K.; Hirayama, R.;
862 Asaithamby, A.; Chen, D.J.; et al. The Major DNA Repair Pathway after Both Proton and Carbon-Ion
863 Radiation is NHEJ, but the HR Pathway is More Relevant in Carbon Ions. *Radiat. Res.* **2015**, *183*, 345–356.
864 74. Timm, S.; Lorat, Y.; Jakob, B.; Taucher-Scholz, G.; Rübe, C.E. Clustered DNA damage concentrated in
865 particle trajectories causes persistent large-scale rearrangements in chromatin architecture. *Radiother.*
866 *Oncol.* **2018**.
867 75. Szabó, E.R.; Brand, M.; Hans, S.; Hideghéty, K.; Karsch, L.; Lessmann, E.; Pawelke, J.; Schürer, M.;
868 Beyreuther, E. Radiobiological effects and proton RBE determined by wildtype zebrafish embryos. *PLoS*
869 *One* **2018**, *13*, e0206879.
870 76. Bright, S.J.; Flint, D.B.; Chakraborty, S.; McFadden, C.H.; Yoon, D.S.; Bronk, L.; Titt, U.; Mohan, R.;
871 Grosshans, D.R.; Sumazin, P.; et al. Nonhomologous End Joining Is More Important Than Proton Linear
872 Energy Transfer in Dictating Cell Death. *Int. J. Radiat. Oncol. Biol. Phys.* **2019**, *105*, 1119–1125.
873 77. Holt, J.T.; Toole, W.P.; Patel, V.R.; Hwang, H.Y.; Brown, E.T. Restoration of CAPAN-1 cells with
874 functional BRCA2 provides insight into the DNA repair activity of individuals who are heterozygous
875 for BRCA2 mutations. *Cancer Genet. Cytogenet.* **2008**, *186*, 85–94.
876 78. Deer, E.L.; González-Hernández, J.; Coursen, J.D.; Shea, J.E.; Ngatia, J.; Scaife, C.L.; Firpo, M.A.;
877 Mulvihill, S.J. Phenotype and genotype of pancreatic cancer cell lines. *Pancreas* **2010**, *39*, 425–35.
878 79. Held, K.D.; Kawamura, H.; Kaminuma, T.; Paz, A.E.S.; Yoshida, Y.; Liu, Q.; Willers, H.; Takahashi, A.
879 Effects of Charged Particles on Human Tumor Cells. *Front. Oncol.* **2016**, *6*, 23.
880 80. Loeffler, J.S.; Durante, M. Charged particle therapy—optimization, challenges and future directions. *Nat.*
881 *Rev. Clin. Oncol.* **2013**, *10*, 411–424.
882 81. Kamada, T.; Tsujii, H.; Blakely, E.A.; Debus, J.; De Neve, W.; Durante, M.; Jäkel, O.; Mayer, R.; Orecchia,
883 R.; Pötter, R.; et al. Lawrence Berkeley National Laboratory Recent Work Title Carbon ion radiotherapy
884 in Japan: an assessment of 20 years of clinical experience Publication Date Policy Review Carbon ion
885 radiotherapy in Japan: an assessment of 20 years of clinical experience. *Lancet Oncol.* **2015**, *16*, e93–e100.
886 82. Shafie, R.A. El; Habermehl, D.; Rieken, S.; Mairani, A.; Orschiedt, L.; Brons, S.; Haberer, T.; Weber, K.-J.;
887 Debus, J.; Combs, S.E. In vitro evaluation of photon and raster-scanned carbon ion radiotherapy in
888 combination with gemcitabine in pancreatic cancer cell lines. **2013**.
889 83. Bouchard, M.; Amos, R.A.; Briere, T.M.; Beddar, S.; Crane, C.H. Dose escalation with proton or photon
890 radiation treatment for pancreatic cancer. *Radiother. Oncol.* **2009**, *92*, 238–243.
891 84. Nichols, R.C.; Huh, S.; Li, Z.; Rutenberg, M. Proton therapy for pancreatic cancer. *World J. Gastrointest.*
892 *Oncol.* **2015**, *7*, 141–7.
893 85. Paganetti, H.; Giantsoudi, D. Relative Biological Effectiveness Uncertainties and Implications for Beam
894 Arrangements and Dose Constraints in Proton Therapy. *Semin. Radiat. Oncol.* **2018**, *28*, 256–263.

895

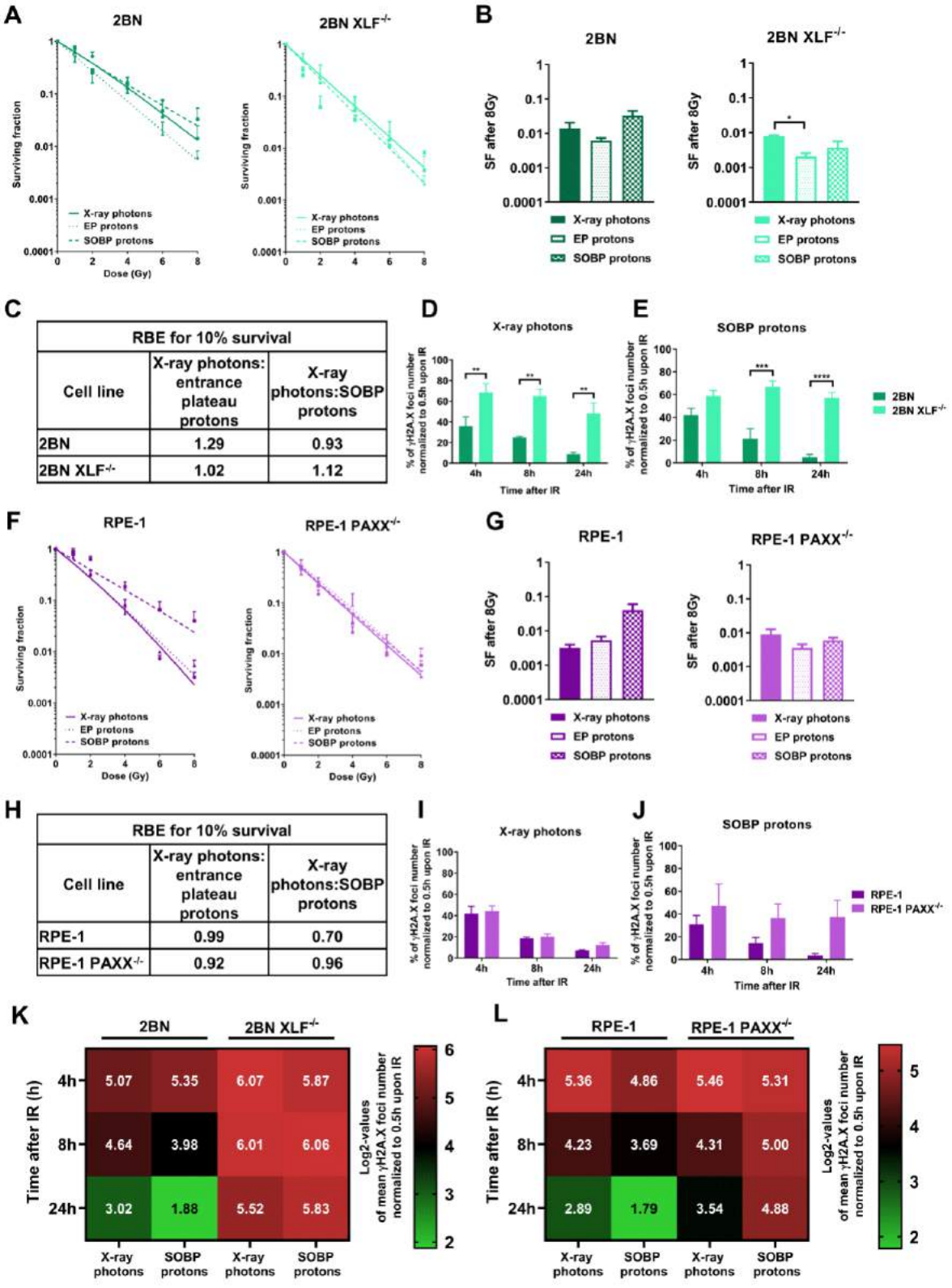

Figure S1. Clonogenic survival and DNA damage response of 2BN hTERT XLF$^{-/-}$ and RPE-1 PAXX$^{-/-}$ cells as well as respective control cells. (**A, B**) Clonogenic survival assay of 2BN hTERT XLF$^{-/-}$ cells irradiated with X-ray photons, EP and SOBP protons (1-8 Gy). (**C**) RBE values calculated for 10% survival of the indicated cell lines. (**D, E**) γH2A.X foci removal over time (4-24 h) normalized to initial foci number at 30 min in 2BN hTERT XLF$^{-/-}$ cells as well as respective control cells upon irradiation with 3 Gy of X-ray photons (**D**) and SOBP protons (**E**). (**F, G**) Clonogenic survival assay of RPE-1

PAXX$^{-/-}$ cells irradiated with X-ray photons, EP and SOBP protons (1-8 Gy). Data represent mean values ± SD from 3 independent experiments. One-way ANOVA. (**H**) RBE values calculated for 10% clonogenic survival of the indicated cell lines. (**I, J**) γH2A.X foci removal over time (4-24 h) normalized to initial foci number at 30 min in RPE-1 PAXX$^{-/-}$ cells as well as respective control cells upon irradiation with 3 Gy of X-ray photons (**I**) and SOBP protons (**J**). (**K, L**) Comparison of radiation source effects in tested cell lines as log2 values of γH2A.X foci quantification. Data represent mean values ± SD (**A**, **F**) or ± SEM (**B**, **D**, **E**, **G**, **I**, **J**) from 3 independent experiments. One-way ANOVA with Tukey's multiple comparisons post-test (**B**,**G**) or two-way ANOVA with Tukey's multiple comparisons post-test (**D**,**E**,**I**,**J**); *p<0.05; **p<0.01; ***p<0.001.

4. Discussion

4.1 Current Proton Radiotherapy

Proton therapy is an outstanding method and bears the potential to supplement or even substitute photon irradiation in certain clinical situations. The demand for a more confined treatment which limits damage to healthy tissue and maximizes tumor control is imminent and supports a wide spread application of proton radiotherapy despite the financial burden.

Nowadays, proton treatment plans are frequently superior as illustrated by a reduced dose to healthy tissue and the specific sparring of critical structures. Unfortunately, tumors are seldomly confined capsules but present themselves with diffuse rims and evading tumor cells. Thus, a safety margin surrounding the gross tumor volume is established to avoid underdosing in these regions of uncertainty. Optimizing the treatment plan between a more confined treatment volume and adding an extensive safety margin reaching into healthy tissue demands an experienced radiation oncologist, careful planning and robust imaging.

A drawback which specifically emerges in the distal safety margin, is the increase in LET towards the end of the proton beam path. The dose deposited by protons of an increased LET corresponds to a higher RBE but is widely unexplored in affected healthy cells. Thus, a broader understanding and possibly adaptations in treatment planning such as LET painting could help to minimize high-LET respectively high-RBE dose deposition into healthy tissue [176, 177] and circumvent this drawback of proton radiotherapy.[178]

Importantly, the generally increased LET of proton irradiation in comparison to photon irradiation and these prementioned LET variations not just impose a threat to healthy tissue but also illustrate a promising cue for a different cellular response. Understanding biological differences provides clinicians with a point of leverage to target the weak points of the respective tumor cells. In detail, a growing body of evidence supports a different utilization of NHEJ and HRR, respectively, in response to photon or proton radiotherapy.

The following section intends to outline this promising area of research and to provide a more detailed statement

4.2 The role of DNA repair in response to proton radiotherapy and how to modulate it

DNA repair is an important process to maintain genome integrity in unstressed but even more so in cells stressed by ionizing irradiation. Numerous papers investigated the differential recruitment of DSB repair machineries (see also 1.3.5 Repair) in response to photon or proton irradiation and astonishing results were obtained.

In 2013, Grosse et al. [179] investigated the response to photon and proton irradiation in Chinese hamster ovary (CHO) cells with a DSB repair deficiency respectively their isogenic repair-proficient counterparts. Similar numbers of DSB were induced as determined by

immunofluorescence staining of γH2AX foci. However, cells with an HRR-deficient background as well as upon treatment with siRad51 were markedly hypersensitive for proton irradiation. These findings were confirmed in human cancer cells by Fontana et al. [180] who treated A549 NSCLC cells with siRad51 and additionally investigated a BRCA2-deficient ovarian cancer cell line. Rad51 downregulation as well as BRCA2-deficiency resulted in hypersensitivity towards proton irradiation.

This hypothesis of an increased relevance of HRR in response to proton irradiation was supported by the research group headed by Prof. Dr. Henning Willers. A screening of lung cancer cells for their RBE demonstrated an increased proton sensitivity in HRR-deficient cells while a cell line overexpressing Rad51 mRNA and protein displayed a more proton-resistant phenotype.[181] In addition, an increased size of 53BP1 foci was detected in HRR-deficient but not in HRR-proficient cell lines which was moreover limited to proton-irradiated cells. Further corroborating findings were provided by immortalized human fibroblasts with different deficiencies in HRR-relevant proteins.[182] Likewise, HRR-deficiency was linked to a proton-sensitive phenotype which was accompanied by an impaired removal of DSBs during S/G2 phase in response to proton irradiation.

This sound evidence implies that deficiencies in HRR could act as a predictive marker for an increased sensitivity towards proton irradiation. Unfortunately, these deficiencies are not limited to tumor tissue but also present in healthy tissue as seen in BRCA1 mutation carriers. A mutation and/or loss of heterozygosity in the BRCA1 gene can abrogate HRR but on the other hand, a secondary mutation deactivating 53BP1 can restore HRR capacity. Conclusively, a detailed consideration of the patient and the tumor situation by the radiation oncologist is necessary to balance between a promising chance for clinical exploitation and a potentially dose-limiting factor due to side effects in healthy tissue.

These apparent differences also illustrate that combinatorial regimens established with conventional photon radiotherapy cannot simply be transferred to proton radiotherapy without any reconsideration. On the other hand, induction of specific repair deficiencies and thus increasing the sensitivity for proton radiotherapy represents a promising rational similar to synthetic lethality. This combinatorial approach could supply radiation oncologists with an off-the-shelf pharmaceutical agent to increase the efficacy of proton radiotherapy.

A number of drugs have been investigated for their role as RBE-modulating agents but research on proton radiobiology and especially research on drug combinations is very limited. Nonetheless, a promising candidate for a combinatorial approach is the histone deacetylase inhibitor (HDACi) SAHA.[183] SAHA sensitized A549 cells for proton and carbon irradiation at low concentrations and no cell cycle alterations but reduced Rad51 foci formation were observed. This sensitization by HDACi was limited to cancer cells and not an altered DNA repair but the different chromatin structure and accessibility in cancer cells suggested as pharmaceutical mode of action.

Conclusively, a broader literature search was conducted to determine additional small-molecule inhibitors with a promising pharmaceutical profile as well as an established HRR-downregulating effect. As a result, Triapine, Gemcitabine, and Ganetespib were selected for further experimental research.

Ribonucleotide reductase (RNR) is a protein complex active during S phase and facilitates the synthesis of dNTP precursors.[184] Triapine inactivates RNR by quenching the catalytic pocket and thus stalls DNA replication and depletes the dNTP pool in proliferative cells. Triapine administration is conclusively linked to a decreased HRR activity and sensitizes tumor cells to a variety of DNA-damaging agents including cisplatin and doxorubicin. In addition, Triapine is of high clinical relevance and currently being investigated in a phase III clinical trial in combination with cisplatin and photon radiotherapy.[185]

Gemcitabine is an already established chemotherapeutic and metabolized intracellularly to a dCDP analogue which also inhibits RNR.[186, 187] Gemcitabine thus depletes the dNTP pool and upon further phosphorylation competes with native dCTP for incorporation into DNA. As a result of incorporation, DNA polymerization is being terminated and replication forks stalled. The radiosensitizing effect of Gemcitabine is limited to HRR-proficient cell lines [188] and delays Rad51 foci formation but prolongs the Rad51 foci persistence in response to photon irradiation.[189] A suggested mechanism is the stabilization of Gemcitabine-induced stalled forks by BRCA2 and Rad51, the conversion into complex HRR intermediates despite abrogated DNA resynthetization, and the subsequent detrimental Mus81- and XPF-dependent cleavage resulting in unrepaired DSBs.[190] A more extended recruitment of HRR subsequent to proton radiotherapy is therefore expected to be decelerated due to a lack of nucleotides and potentially provides more stalled forks than obtained by photon irradiation.

The third drug investigated is the HSP90 inhibitor Ganetespib. Ganetespib in combination with DNA-damaging carboplatin but not alone induced a phenotype of global chromosome fragmentation.[163] HSP90 inhibition by Ganetespib downregulates key proteins of HRR such as FancD2 and the described phenotype could as a result be rescued by overexpression of FancA. Additionally, also the depletion of nuclease DNA2 prevented chromosomal fragmentation. This indicates a defective DNA repair in combination with uncontrolled nuclease activity upon combination of Ganetespib with a DNA damaging agent. Moreover, cell cycle checkpoint proteins such as CHK1 and Wee1 were also depleted by Ganetespib administration. In addition, other HSP90 inhibitors such as 17AAG are also found to downregulate HRR-relevant proteins such as BRCA2, Rad51, and BRCA1 and furthermore shifted the repair pathway choice away from HRR and towards NHEJ. [191, 192]

To investigate the radiosensitization be the respective drug, the sublethal concentration of each drug was established in advance. This implies that cells continue exponential growth and only the combination with irradiation is severe enough to significantly reduce cellular proliferation. This low dosing therefore increases the relative change observed and is also more translatable than clinically unfeasible overdosing.

Unfortunately, proton beam time was strictly limited and we therefore selected A549 (wtTP53) and FaDu (mutTP53) as cell lines of interest and Ganetespib as drug of interest.

The following section is intended to provide the context to our study and discuss supporting and contradicting research.

4.3 Context and clinical relevance of this study

Firstly, research on proton radiobiology is complicated due to the highly restricted access and limited beam times, facilities usually being located at remote sides, and the understandable design for optimal patient treatment implying a lack of adjoining cell culture and laboratory facilities. MedAustron on the other hand provided me with the unique opportunity of an up-to-date pencil beam scanning proton beam, extensive lab space and equipment as well as support by physicists and operators. I occupied nearly all shifts allocated for biological research between the end of 2018 and the beginning of 2020. During this time, I was approached by multiple PhD-students- and PostDocs and asked on how I got access to a proton beam line. This illustrates that not lack of research interest but access and sufficient beam time are the largest limitation in current proton radiobiology as well as my gratitude for this privileged access.

What also limits proton radiobiology is the far more complex physics involved in comparison to photon irradiation. Photons can be easily and reproducible administered by commercial irradiation cabinets or small-animal irradiation platforms while each proton facility is customized with different beam lines, different accelerators, different dose rates, and different set-ups for radiobiological irradiations. Proton radiobiology thus requires a more sophisticated experimental approach to provide robustness of results and thus comparability in between facilities.

This study therefore intends to exclude as many uncertainties as feasible which is achieved by a water/PMMA phantom to position cell culture flasks at clinically relevant depths and administer proton irradiation by most advanced spot scanning. The phantom allows to place the slides at two positions of a SOBP and positioning can be assured by the laser alignment system of the treatment room. Thus, the LET and dose delivered are reproducible and mimic the situation in the gross tumor volume upon treatment with clinical radiotherapy.

Our data indicated a significant increase in RBE of approximately 20% to 30% for proximal as well as distal SOBP protons in Ganetespib-treated A549 cells. This was confirmed in a second cell line and a comparable increase of RBE by 15% to 30% for proximal and distal SOBP protons was observed in Ganetespib-treated FaDu cells. These increases in RBE move in the same range as determined in HRR-deficient lung cancer cells compared to proficient cell lines [181] as well as by siRNA-mediated knockdown of Rad51 in A549 and CHO cells.[179, 180]

We are the first ones to demonstrate such a proton-specific radiosensitization by HSP90 inhibition which is supported by data demonstrating sensitization being observed in high-LET carbon [193-196] but not in photon-irradiated cells.

As described above, Rad51 requires HSP90 chaperon activity and is downregulated upon HSP90 inhibition.[191, 193] Despite the low doses of Ganetespib administered, a significant and persistent decrease in Rad51 protein levels could be observed in A549 cells. We

moreover demonstrated higher levels of Rad51 8h, 24, and 48h in sham-treated cells after proton irradiation than observed after photon irradiation.

In accordance with previous research [179], we also determined similar numbers of γH2AX foci, a surrogate marker for DSBs, being induced irrespective of the administration of photon or proximal or distal SOBP proton irradiation. Moreover, sham-treated A549 cells exhibited a similar removal of γH2AX foci which was also independent of the irradiation administered and thus corresponds to previous findings [180, 181]. Fontana et al. described a delayed removal of γH2AX foci upon siRNA-mediated suppression of Rad51. In addition, also HSP90 inhibition is indicated to reduce Rad51 foci recruitment [193] and γH2AX removal.[194, 195] In contrast, a reduction in Rad51 protein levels due to Ganetespib treatment as observed by western blotting did not alter the number of persisting γH2AX foci per nucleus and low foci numbers close to baseline were achieved within 24h. This implies that Rad51 levels remained either sufficient to facilitate HRR or missing HRR capacity was potentially replaced by Rad51-independent but more error-prone alternatives such as NHEJ or microhomology-mediated end joining.[197]. This shift towards more erroneous pathways entails the risk of mutations or chromosomal alterations but was not further investigated in this study.

Another not investigated mode of action of Ganetespib may be provided by cell cycle checkpoint proteins and their inhibition upon Ganetespib treatment. CHK1, a protein arresting cells in G2/M phase upon activation by ATR, is described to be downregulate by HSP90 inhibition.[163, 192] This abrogated G1 check point limits the time cells can utilize HRR and is further aggravated by premature progression into M phase and the risk of mitotic catastrophe and ultimately cell death. We could observe a marginally more extensive G2 phase arrest upon proton irradiation in sham-treated A549 cells. In addition, 10nM Ganetespib was found to distort this post-irradiation G2 phase accumulation and conclusively decreased the fraction of S/G2/M phase cells. Unfortunately, due to limited beam time we could only obtained a duplicate of samples for A549 cells and could not repeat cell cycle analysis with FaDu cells. Thus, additional research and repetitions to investigate cell cycle accumulation, cell cycle checkpoint proteins and a potential abrogation of both by Ganetespib are strongly suggested.

In conclusion, we are the first to demonstrate a reproducible and significant radiosensitizing effect of low dose Ganetespib in A549 and FaDu cells for clinically relevant SOBP proton irradiation but not for conventional photon irradiation. A potential mode of action of Ganetespib was determined in A549 cells by the persistent downregulation of Rad51 protein and a potential shift towards more error-prone DNA repair pathway. Nevertheless, beam time limitations prevent the repetition of western blotting, repair foci analysis and flow cytometry with FaDu cells as well as the conduction of more elaborate experiments to investigate additional end points.

5. Outlook

Proton radiobiology only represents a small niche in cancer therapy but increases in importance with each newly opened treatment facility. The different nature of irradiation implies a different pattern of damage induced as well as a different subsequent cellular response. Such differences bear the opportunity for clinical opportunity. In this PhD thesis, we demonstrated for the first time the proton-specific radiosensitization by low doses of HSP90 inhibitor Ganetespib. We moreover investigated the cellular response upon Ganetespib treatment in combination with SOBP proton and reference photon irradiation and suggested potential MOAs explaining the demonstrated proton-specific radio-sensitization.

Ganetespib and other HSP90 inhibitors are shown to specifically sensitize for carbon irradiation. We are the first ones to transfer this to clinically relevant SOBP proton beam irradiation and confirmed these findings in two cell lines. Unfortunately, a phase III clinical trial combining Ganetespib with Paclitaxel in NSCLC was discontinued and followed by an obvious decrease in research interest. A new rational for a combination of Ganetespib with particle therapy could renew the interest and initiate further preclinical and clinical investigations but the main driver of these efforts is expected to be academia.

The determined downregulation of Rad51 protein by Ganetespib and marginally increased fractions of cells in S/G2 phase suggests an increased importance of HRR in response to proton radiotherapy and also agrees with previous findings by numerous research groups. We nevertheless could not define a LET dependence throughout the SOBP but also cannot exclude relevance at the more distal fall off region. Moreover, we cannot explain the indifferent repair of DNA DSBs despite Rad51 protein downregulation.

The most important but often forgotten issue is the broad variation in experimental set-up in between proton treatment facilities. Conclusively, large efforts will be required to standardize testing and proton irradiation itself to foster the transferability of obtained results. We addressed this issue by mimicking the clinical situation as close as feasible and by detailing all physical, experimental and biological parameters.

Research investigating combinations of chemotherapeutics and immune checkpoint inhibitors is faster, easier to employ, and not limited by the number of treatment facilities and beam time. It will therefore take huge efforts by proton radiobiologists to keep pace and not miss the chance of participation.

Current immune checkpoint blockade prevents the exhaustion of immune cells but radiotherapy could provide the switch to activate and guide them towards the tumor. This perfectly illustrates the superiority of particle therapeutic approaches where immune cells will receive less unintended irradiation due to the more confined treatment fields and thus retain their potential to attack and clear tumor cells. Furthermore, the investigated HSP90 inhibitor Ganetespib not just downregulates repair proteins but could also increase proteotoxic stress in a cancer-specific manner which bears the potential to provide immune cells with neo-antigens and improve their efficacy.

Summarizing, both, HSP90 inhibitors as well as proton radiotherapy, themselves represent promising therapeutic approaches of high clinical relevance but are neither fully understood nor fully exploited.

The presented PhD work indicates that a combination of HSP90-inhibiting Ganetespib results in the sensitization of cancer cells specifically for proximal and distal SOBP proton radiotherapy. Increasing the RBE by 20% to 30% implies a huge leap in radiation oncology and could improve tumor control as well as patient outcome. Taken together, we generated reliable data that promotes the combination of proton radiotherapy with HSP90 inhibition as a novel rational-driven clinical approach against cancer.

Table of References - Thesis

1. Bray, F., et al., *Global cancer statistics 2018: GLOBOCAN estimates of incidence and mortality worldwide for 36 cancers in 185 countries.* CA Cancer J Clin, 2018. **68**(6): p. 394-424.
2. *World Cancer Report 2014*, ed. B.W. Stewart and C.P. Wild. 2014, Lyon: International Agency for Research on Cancer (IARC) - WHO. p.20.
3. Brown, J.C., et al., *Cancer, physical activity, and exercise.* Compr Physiol, 2012. **2**(4): p. 2775-809.
4. Haslam, D.W. and W.P. James, *Obesity.* Lancet, 2005. **366**(9492): p. 1197-209.
5. Lynch, B.M., H.K. Neilson, and C.M. Friedenreich, *Physical activity and breast cancer prevention.* Recent Results Cancer Res, 2011. **186**: p. 13-42.
6. *World Cancer Report 2014*, ed. B.W. Stewart and C.P. Wild. 2014, Lyon: International Agency for Research on Cancer (IARC) - WHO. p.82.
7. Thomas, T.L., *Cancer Prevention: HPV Vaccination.* Semin Oncol Nurs, 2016. **32**(3): p. 273-80.
8. Toh, Z.Q., et al., *Cervical Cancer Prevention Through HPV Vaccination in Low- and Middle-Income Countries in Asia.* Asian Pac J Cancer Prev, 2017. **18**(9): p. 2339-2343.
9. Schmitz, K.H., *Exercise for secondary prevention of breast cancer: moving from evidence to changing clinical practice.* Cancer Prev Res (Phila), 2011. **4**(4): p. 476-80.
10. Hanahan, D. and R.A. Weinberg, *The hallmarks of cancer.* Cell, 2000. **100**(1): p. 57-70.
11. Hanahan, D. and R.A. Weinberg, *Hallmarks of cancer: the next generation.* Cell, 2011. **144**(5): p. 646-74.
12. Jancik, S., et al., *Clinical relevance of KRAS in human cancers.* J Biomed Biotechnol, 2010. **2010**: p. 150960.
13. Davies, M.A. and Y. Samuels, *Analysis of the genome to personalize therapy for melanoma.* Oncogene, 2010. **29**(41): p. 5545-55.
14. Yuan, T.L. and L.C. Cantley, *PI3K pathway alterations in cancer: variations on a theme.* Oncogene, 2008. **27**(41): p. 5497-510.
15. Jiang, B.H. and L.Z. Liu, *PI3K/PTEN signaling in angiogenesis and tumorigenesis.* Adv Cancer Res, 2009. **102**: p. 19-65.
16. Collado, M. and M. Serrano, *Senescence in tumours: evidence from mice and humans.* Nat Rev Cancer, 2010. **10**(1): p. 51-7.
17. Evan, G.I. and F. d'Adda di Fagagna, *Cellular senescence: hot or what?* Curr Opin Genet Dev, 2009. **19**(1): p. 25-31.
18. Flaherty, K.T., et al., *Inhibition of mutated, activated BRAF in metastatic melanoma.* N Engl J Med, 2010. **363**(9): p. 809-19.
19. Chapman, P.B., et al., *Improved survival with vemurafenib in melanoma with BRAF V600E mutation.* N Engl J Med, 2011. **364**(26): p. 2507-16.
20. Kim, G., et al., *FDA approval summary: vemurafenib for treatment of unresectable or metastatic melanoma with the BRAFV600E mutation.* Clin Cancer Res, 2014. **20**(19): p. 4994-5000.
21. European_Medicines_Agency. *Zelboraf (vemurafenib)*. 2018 21.11.2019]; Available from: https://www.ema.europa.eu/en/medicines/human/EPAR/zelboraf.
22. Zhu, Y. and S.X. Qian, *Clinical efficacy and safety of imatinib in the management of Ph(+) chronic myeloid or acute lymphoblastic leukemia in Chinese patients.* Onco Targets Ther, 2014. **7**: p. 395-404.
23. Kurzrock, R., et al., *Philadelphia chromosome-positive leukemias: from basic mechanisms to molecular therapeutics.* Ann Intern Med, 2003. **138**(10): p. 819-30.
24. Hochhaus, A., et al., *Long-Term Outcomes of Imatinib Treatment for Chronic Myeloid Leukemia.* N Engl J Med, 2017. **376**(10): p. 917-927.
25. drugs.com. *Gleevec Approval History*. 21.11.2019]; Available from: https://www.drugs.com/history/gleevec.html.
26. Wong, S.F., *Cetuximab: an epidermal growth factor receptor monoclonal antibody for the treatment of colorectal cancer.* Clin Ther, 2005. **27**(6): p. 684-94.
27. European_Medicines_Agency. *Erbitux (cetuximab)*. 26.11.2019]; Available from: https://www.ema.europa.eu/en/medicines/human/EPAR/erbitux.
28. European_Medicines_Agency. *Xalkori (crizotinib)*. 26.11.2019]; Available from: https://www.ema.europa.eu/en/documents/overview/xalkori-epar-summary-public_de.pdf.

29. Ou, S.H., *Crizotinib: a novel and first-in-class multitargeted tyrosine kinase inhibitor for the treatment of anaplastic lymphoma kinase rearranged non-small cell lung cancer and beyond.* Drug Des Devel Ther, 2011. **5**: p. 471-85.
30. Sahu, A., et al., *Crizotinib: A comprehensive review.* South Asian J Cancer, 2013. **2**(2): p. 91-7.
31. European_Medicines_Agency. *Tarceva (erlotinib)*. 26.11.2019]; Available from: https://www.ema.europa.eu/en/documents/overview/tarceva-epar-medicine-overview_de.pdf.
32. Rocha-Lima, C.M. and L.E. Raez, *Erlotinib (tarceva) for the treatment of non-small-cell lung cancer and pancreatic cancer.* P T, 2009. **34**(10): p. 554-64.
33. Deshpande, A., P. Sicinski, and P.W. Hinds, *Cyclins and cdks in development and cancer: a perspective.* Oncogene, 2005. **24**(17): p. 2909-15.
34. Burkhart, D.L. and J. Sage, *Cellular mechanisms of tumour suppression by the retinoblastoma gene.* Nat Rev Cancer, 2008. **8**(9): p. 671-82.
35. Sherr, C.J. and F. McCormick, *The RB and p53 pathways in cancer.* Cancer Cell, 2002. **2**(2): p. 103-12.
36. Zilfou, J.T. and S.W. Lowe, *Tumor suppressive functions of p53.* Cold Spring Harb Perspect Biol, 2009. **1**(5): p. a001883.
37. Suh, Y., et al., *Clinical update on cancer: molecular oncology of head and neck cancer.* Cell Death Dis, 2014. **5**: p. e1018.
38. Watson, M., et al., *Using population-based cancer registry data to assess the burden of human papillomavirus-associated cancers in the United States: overview of methods.* Cancer, 2008. **113**(10 Suppl): p. 2841-54.
39. Chrysostomou, A.C., et al., *Cervical Cancer Screening Programs in Europe: The Transition Towards HPV Vaccination and Population-Based HPV Testing.* Viruses, 2018. **10**(12).
40. Mboumba Bouassa, R.S., et al., *High prevalence of cervical high-risk human papillomavirus infection mostly covered by Gardasil-9 prophylactic vaccine in adult women living in N'Djamena, Chad.* PLoS One, 2019. **14**(6): p. e0217486.
41. Motz, G.T., et al., *Tumor endothelium FasL establishes a selective immune barrier promoting tolerance in tumors.* Nat Med, 2014. **20**(6): p. 607-15.
42. Shay, J.W. and W.E. Wright, *Hayflick, his limit, and cellular ageing.* Nat Rev Mol Cell Biol, 2000. **1**(1): p. 72-6.
43. Armstrong, C.A. and K. Tomita, *Fundamental mechanisms of telomerase action in yeasts and mammals: understanding telomeres and telomerase in cancer cells.* Open Biol, 2017. **7**(3).
44. Pech, M.F., et al., *High telomerase is a hallmark of undifferentiated spermatogonia and is required for maintenance of male germline stem cells.* Genes Dev, 2015. **29**(23): p. 2420-34.
45. Teichroeb, J.H., J. Kim, and D.H. Betts, *The role of telomeres and telomerase reverse transcriptase isoforms in pluripotency induction and maintenance.* RNA Biol, 2016. **13**(8): p. 707-19.
46. Oladipupo, S., et al., *VEGF is essential for hypoxia-inducible factor-mediated neovascularization but dispensable for endothelial sprouting.* Proc Natl Acad Sci U S A, 2011. **108**(32): p. 13264-9.
47. Kurihara, T., P.D. Westenskow, and M. Friedlander, *Hypoxia-inducible factor (HIF)/vascular endothelial growth factor (VEGF) signaling in the retina.* Adv Exp Med Biol, 2014. **801**: p. 275-81.
48. Shweiki, D., et al., *Vascular endothelial growth factor induced by hypoxia may mediate hypoxia-initiated angiogenesis.* Nature, 1992. **359**(6398): p. 843-5.
49. Mac Gabhann, F. and A.S. Popel, *Systems biology of vascular endothelial growth factors.* Microcirculation, 2008. **15**(8): p. 715-38.
50. Stefanini, M.O., et al., *A compartment model of VEGF distribution in blood, healthy and diseased tissues.* BMC Syst Biol, 2008. **2**: p. 77.
51. European_Medicines_Agency. *Avastin (bevacizumab)*. 25.11.2019]; Available from: https://www.ema.europa.eu/en/medicines/human/EPAR/avastin.
52. Ferrara, N., *Vascular endothelial growth factor.* Arterioscler Thromb Vasc Biol, 2009. **29**(6): p. 789-91.
53. Golombek, S.K., et al., *Tumor targeting via EPR: Strategies to enhance patient responses.* Adv Drug Deliv Rev, 2018. **130**: p. 17-38.
54. Maeda, H., G.Y. Bharate, and J. Daruwalla, *Polymeric drugs for efficient tumor-targeted drug delivery based on EPR-effect.* Eur J Pharm Biopharm, 2009. **71**(3): p. 409-19.
55. Green, A.E. and P.G. Rose, *Pegylated liposomal doxorubicin in ovarian cancer.* Int J Nanomedicine, 2006. **1**(3): p. 229-39.
56. Tsubakihara, Y. and A. Moustakas, *Epithelial-Mesenchymal Transition and Metastasis under the Control of Transforming Growth Factor beta.* Int J Mol Sci, 2018. **19**(11).

57. Jolly, M.K., et al., *EMT and MET: necessary or permissive for metastasis?* Mol Oncol, 2017. **11**(7): p. 755-769.
58. Bachmayr-Heyda, A., et al., *Small RNAs and the competing endogenous RNA network in high grade serous ovarian cancer tumor spread.* Oncotarget, 2016. **7**(26): p. 39640-39653.
59. Westermarck, J. and V.M. Kahari, *Regulation of matrix metalloproteinase expression in tumor invasion.* FASEB J, 1999. **13**(8): p. 781-92.
60. Das, A., et al., *MMP proteolytic activity regulates cancer invasiveness by modulating integrins.* Sci Rep, 2017. **7**(1): p. 14219.
61. Roomi, M.W., et al., *Inhibition of invasion and MMPs by a nutrient mixture in human cancer cell lines: a correlation study.* Exp Oncol, 2010. **32**(4): p. 243-8.
62. Hosaka, K., et al., *Pericyte-fibroblast transition promotes tumor growth and metastasis.* Proc Natl Acad Sci U S A, 2016. **113**(38): p. E5618-27.
63. Hao, D., L. Wang, and L.J. Di, *Distinct mutation accumulation rates among tissues determine the variation in cancer risk.* Sci Rep, 2016. **6**: p. 19458.
64. Barroso-Sousa, R., et al., *Prevalence and mutational determinants of high tumor mutation burden in breast cancer.* Ann Oncol, 2020. **31**(3): p. 387-394.
65. Jakobsen, L.S., et al., *Probabilistic approach for assessing cancer risk due to benzo[a]pyrene in barbecued meat: Informing advice for population groups.* PLoS One, 2018. **13**(11): p. e0207032.
66. Kazerouni, N., et al., *Analysis of 200 food items for benzo[a]pyrene and estimation of its intake in an epidemiologic study.* Food Chem Toxicol, 2001. **39**(5): p. 423-36.
67. Alexandrov, L.B., et al., *Signatures of mutational processes in human cancer.* Nature, 2013. **500**(7463): p. 415-21.
68. Govindan, R., et al., *Genomic landscape of non-small cell lung cancer in smokers and never-smokers.* Cell, 2012. **150**(6): p. 1121-34.
69. Lawrence, M.S., et al., *Mutational heterogeneity in cancer and the search for new cancer-associated genes.* Nature, 2013. **499**(7457): p. 214-218.
70. Vogelstein, B., et al., *Cancer genome landscapes.* Science, 2013. **339**(6127): p. 1546-58.
71. Lee, W.H. and T.G. Boyer, *BRCA1 and BRCA2 in breast cancer.* Lancet, 2001. **358 Suppl**: p. S5.
72. Kuchenbaecker, K.B., et al., *Risks of Breast, Ovarian, and Contralateral Breast Cancer for BRCA1 and BRCA2 Mutation Carriers.* JAMA, 2017. **317**(23): p. 2402-2416.
73. Kotsopoulos, J., *BRCA Mutations and Breast Cancer Prevention.* Cancers (Basel), 2018. **10**(12).
74. Gorodetska, I., I. Kozeretska, and A. Dubrovska, *BRCA Genes: The Role in Genome Stability, Cancer Stemness and Therapy Resistance.* J Cancer, 2019. **10**(9): p. 2109-2127.
75. Naik, S.M., et al., *Cutaneous malignancies in xeroderma pigmentosum: earlier management improves survival.* Indian J Otolaryngol Head Neck Surg, 2013. **65**(2): p. 162-7.
76. McGranahan, N. and C. Swanton, *Biological and therapeutic impact of intratumor heterogeneity in cancer evolution.* Cancer Cell, 2015. **27**(1): p. 15-26.
77. Greten, F.R. and S.I. Grivennikov, *Inflammation and Cancer: Triggers, Mechanisms, and Consequences.* Immunity, 2019. **51**(1): p. 27-41.
78. Kadariya, Y., et al., *Inflammation-Related IL1beta/IL1R Signaling Promotes the Development of Asbestos-Induced Malignant Mesothelioma.* Cancer Prev Res (Phila), 2016. **9**(5): p. 406-414.
79. Quail, D.F. and A.J. Dannenberg, *The obese adipose tissue microenvironment in cancer development and progression.* Nat Rev Endocrinol, 2019. **15**(3): p. 139-154.
80. Quail, D.F., et al., *Obesity alters the lung myeloid cell landscape to enhance breast cancer metastasis through IL5 and GM-CSF.* Nat Cell Biol, 2017. **19**(8): p. 974-987.
81. DeBerardinis, R.J. and N.S. Chandel, *Fundamentals of cancer metabolism.* Sci Adv, 2016. **2**(5): p. e1600200.
82. Vajdic, C.M. and M.T. van Leeuwen, *Cancer incidence and risk factors after solid organ transplantation.* Int J Cancer, 2009. **125**(8): p. 1747-54.
83. Pages, F., et al., *Immune infiltration in human tumors: a prognostic factor that should not be ignored.* Oncogene, 2010. **29**(8): p. 1093-102.
84. Nelson, B.H., *The impact of T-cell immunity on ovarian cancer outcomes.* Immunol Rev, 2008. **222**: p. 101-16.
85. Haanen, J.B., et al., *Melanoma-specific tumor-infiltrating lymphocytes but not circulating melanoma-specific T cells may predict survival in resected advanced-stage melanoma patients.* Cancer Immunol Immunother, 2006. **55**(4): p. 451-8.
86. Naito, Y., et al., *CD8+ T cells infiltrated within cancer cell nests as a prognostic factor in human colorectal cancer.* Cancer Res, 1998. **58**(16): p. 3491-4.

87. Yasunaga, M., et al., *Accelerated growth signals and low tumor-infiltrating lymphocyte levels predict poor outcome in T4 esophageal squamous cell carcinoma.* Ann Thorac Surg, 2000. **70**(5): p. 1634-40.
88. Kim, H.R., et al., *PD-L1 expression on immune cells, but not on tumor cells, is a favorable prognostic factor for head and neck cancer patients.* Sci Rep, 2016. **6**: p. 36956.
89. Loeser, S., et al., *Spontaneous tumor rejection by cbl-b-deficient CD8+ T cells.* J Exp Med, 2007. **204**(4): p. 879-91.
90. Smyth, M.J., et al., *Differential tumor surveillance by natural killer (NK) and NKT cells.* J Exp Med, 2000. **191**(4): p. 661-8.
91. Smyth, M.J., N.Y. Crowe, and D.I. Godfrey, *NK cells and NKT cells collaborate in host protection from methylcholanthrene-induced fibrosarcoma.* Int Immunol, 2001. **13**(4): p. 459-63.
92. Liu, M. and F. Guo, *Recent updates on cancer immunotherapy.* Precis Clin Med, 2018. **1**(2): p. 65-74.
93. Blandin Knight, S., et al., *Progress and prospects of early detection in lung cancer.* Open Biol, 2017. **7**(9).
94. Miller, J.W., et al., *Breast and cervical cancers diagnosed and stage at diagnosis among women served through the National Breast and Cervical Cancer Early Detection Program.* Cancer Causes Control, 2015. **26**(5): p. 741-7.
95. National_Cancer_Institute. *Cancer Screening Overview (PDQ)-Patient Version*. 23.10.2019 28.12.2019]; Available from: https://www.cancer.gov/about-cancer/screening/patient-screening-overview-pdq#_1.
96. Tripp, M.K., et al., *State of the science on prevention and screening to reduce melanoma incidence and mortality: The time is now.* CA Cancer J Clin, 2016. **66**(6): p. 460-480.
97. Dik, V.K., L.M. Moons, and P.D. Siersema, *Endoscopic innovations to increase the adenoma detection rate during colonoscopy.* World J Gastroenterol, 2014. **20**(9): p. 2200-11.
98. Mayo-Clinic. *Pap smear*. 2019 28.12.2019]; Available from: https://www.mayoclinic.org/tests-procedures/pap-smear/about/pac-20394841.
99. Mayo-Clinic. *Skin biopsy*. 28.12.2019]; Available from: https://www.mayoclinic.org/tests-procedures/skin-biopsy/about/pac-20384634.
100. Mayo-Clinic. *PSA Test*. 28.12.2019]; Available from: https://www.mayoclinic.org/tests-procedures/psa-test/about/pac-20384731.
101. Fortner, R.T., et al., *Ovarian cancer early detection by circulating CA125 in the context of anti-CA125 autoantibody levels: Results from the EPIC cohort.* Int J Cancer, 2018. **142**(7): p. 1355-1360.
102. American_Cancer_Society. *Imaging (Radiology) Tests for Cancer*. 30.11.2015 28.12.2019]; Available from: https://www.cancer.org/treatment/understanding-your-diagnosis/tests/imaging-radiology-tests-for-cancer.html.
103. National_Cancer_Institute. *Nuclear Medicine Scans for Cancer*. 29.08.2019 28.12.2019]; Available from: https://www.cancer.org/treatment/understanding-your-diagnosis/tests/nuclear-medicine-scans-for-cancer.html.
104. Mayo-Clinic. *BRCA gene test for breast and ovarian cancer risk*. 12.09.2019 28.12.2019]; Available from: https://www.mayoclinic.org/tests-procedures/brca-gene-test/about/pac-20384815.
105. Mayo-Clinic. *Stool DNA test*. 16.11.2017 28.12.2019]; Available from: https://www.mayoclinic.org/tests-procedures/stool-dna-test/about/pac-20385153.
106. Maritschnegg, E., et al., *Uterine and Tubal Lavage for Earlier Cancer Detection Using an Innovative Catheter: A Feasibility and Safety Study.* Int J Gynecol Cancer, 2018. **28**(9): p. 1692-1698.
107. Maritschnegg, E., et al., *Lavage of the Uterine Cavity for Molecular Detection of Mullerian Duct Carcinomas: A Proof-of-Concept Study.* J Clin Oncol, 2015. **33**(36): p. 4293-300.
108. Salk, J.J., et al., *Ultra-Sensitive TP53 Sequencing for Cancer Detection Reveals Progressive Clonal Selection in Normal Tissue over a Century of Human Lifespan.* Cell Rep, 2019. **28**(1): p. 132-144 e3.
109. Fortner, R.T., et al., *Correlates of circulating ovarian cancer early detection markers and their contribution to discrimination of early detection models: results from the EPIC cohort.* J Ovarian Res, 2017. **10**(1): p. 20.
110. Loeb, S., et al., *Overdiagnosis and overtreatment of prostate cancer.* Eur Urol, 2014. **65**(6): p. 1046-55.
111. Gasnier, A. and N. Parvizi, *Updates on the diagnosis and treatment of prostate cancer.* Br J Radiol, 2017. **90**(1075): p. 20170180.

112. Davis, K.M., et al., *The association of long-term treatment-related side effects with cancer-specific and general quality of life among prostate cancer survivors.* Urology, 2014. **84**(2): p. 300-6.
113. Feng, S.H. and S.T. Yang, *The new 8th TNM staging system of lung cancer and its potential imaging interpretation pitfalls and limitations with CT image demonstrations.* Diagn Interv Radiol, 2019. **25**(4): p. 270-279.
114. American_Society_of_Clinical_Oncology. *What is Cancer Surgery?* 05.2019 28.12.2019]; Available from: https://www.cancer.net/navigating-cancer-care/how-cancer-treated/surgery/what-cancer-surgery.
115. National_Cancer_Institute. *Surgery to Treat Cancer*. 29.04.2015 28.12.2019]; Available from: https://www.cancer.gov/about-cancer/treatment/types/surgery.
116. Saraee, A., et al., *Whipple procedure: a review of a 7-year clinical experience in a referral center for hepatobiliary and pancreas diseases.* World J Surg Oncol, 2015. **13**: p. 98.
117. American_Society_of_Clinical_Oncology. *Understanding Chemotherapy*. 05.2019 [cited 28.12.2019; Available from: https://www.cancer.net/navigating-cancer-care/how-cancer-treated/chemotherapy/understanding-chemotherapy.
118. National_Cancer_Institute. *Chemotherapy to Treat Cancer*. 29.04.2015 28.12.2019]; Available from: https://www.cancer.gov/about-cancer/treatment/types/chemotherapy#chemotherapy-can-cause-side-effects.
119. American_Society_of_Clinical_Oncology. *What to Expect when having Chemotherapy*. 06.2019 28.12.2019]; Available from: https://www.cancer.net/navigating-cancer-care/how-cancer-treated/chemotherapy/what-expect-when-having-chemotherapy.
120. Huang, C.Y., et al., *A review on the effects of current chemotherapy drugs and natural agents in treating non-small cell lung cancer.* Biomedicine (Taipei), 2017. **7**(4): p. 23.
121. Chemocare. *Types of Chemotherapy*. 28.12.2019]; Available from: http://chemocare.com/chemotherapy/what-is-chemotherapy/types-of-chemotherapy.aspx.
122. Wang-Gillam, A., et al., *Nanoliposomal irinotecan with fluorouracil and folinic acid in metastatic pancreatic cancer after previous gemcitabine-based therapy (NAPOLI-1): a global, randomised, open-label, phase 3 trial.* Lancet, 2016. **387**(10018): p. 545-557.
123. Claus, C., et al., *Tumor-targeted 4-1BB agonists for combination with T cell bispecific antibodies as off-the-shelf therapy.* Sci Transl Med, 2019. **11**(496).
124. Mozaffarian, N., A.E. Wiedeman, and A.M. Stevens, *Active systemic lupus erythematosus is associated with failure of antigen-presenting cells to express programmed death ligand-1.* Rheumatology (Oxford), 2008. **47**(9): p. 1335-41.
125. Zheng, Y., Y.C. Fang, and J. Li, *PD-L1 expression levels on tumor cells affect their immunosuppressive activity.* Oncol Lett, 2019. **18**(5): p. 5399-5407.
126. Wu, Y., et al., *PD-L1 Distribution and Perspective for Cancer Immunotherapy-Blockade, Knockdown, or Inhibition.* Front Immunol, 2019. **10**: p. 2022.
127. Callahan, M.K., J.D. Wolchok, and J.P. Allison, *Anti-CTLA-4 antibody therapy: immune monitoring during clinical development of a novel immunotherapy.* Semin Oncol, 2010. **37**(5): p. 473-84.
128. Schmid, P., et al., *Atezolizumab plus nab-paclitaxel as first-line treatment for unresectable, locally advanced or metastatic triple-negative breast cancer (IMpassion130): updated efficacy results from a randomised, double-blind, placebo-controlled, phase 3 trial.* Lancet Oncol, 2019.
129. Gao, X. and D.F. McDermott, *Ipilimumab in combination with nivolumab for the treatment of renal cell carcinoma.* Expert Opin Biol Ther, 2018. **18**(9): p. 947-957.
130. Tamiya, M., et al., *Efficacy and safety of pembrolizumab as first-line therapy in advanced non-small cell lung cancer with at least 50% PD-L1 positivity: a multicenter retrospective cohort study (HOPE-001).* Invest New Drugs, 2019. **37**(6): p. 1266-1273.
131. Ninomiya, K. and K. Hotta, *Pembrolizumab for the first-line treatment of non-small cell lung cancer.* Expert Opinion on Biological Therapy, 2018. **18**(10): p. 1015-1021.
132. Gianfaldoni, S., et al., *An Overview on Radiotherapy: From Its History to Its Current Applications in Dermatology.* Open Access Maced J Med Sci, 2017. **5**(4): p. 521-525.
133. Borras, J.M., et al., *How many new cancer patients in Europe will require radiotherapy by 2025? An ESTRO-HERO analysis.* Radiother Oncol, 2016. **119**(1): p. 5-11.
134. *Basic Clinical Radiobiology*. 4th Edition ed. 2009, Great Britain: Hodder Arnold.
135. Podgorsak, E.B., *Radiation Oncology Physics: A Handbook for Teachers and Students*. 2005, Vienna: IAEA_International_Atomic_Energy_Agency.
136. Schexnayder Jr., C.J., *Tabulated Values of Bond Dissociation Energies, Ionization Potentials, and Electron Affinities for some Molecules found in High-Temperature Chemical Reactions _TN D-1791*. 05.1963, Washington: NASA-National_Aeronautics_and_Space_Administration.

137. Dartnell, L.R., *Ionizing radiation and life.* Astrobiology, 2011. **11**(6): p. 551-82.
138. Braccini, S., *Particle Accelerators and Detectors for Medical Diagnostics and Therapy*. 2013: Bern.
139. Mohan, R. and D. Grosshans, *Proton therapy - Present and future.* Adv Drug Deliv Rev, 2017. **109**: p. 26-44.
140. Tian, X., et al., *The evolution of proton beam therapy: Current and future status.* Mol Clin Oncol, 2018. **8**(1): p. 15-21.
141. Levin, W.P., et al., *Proton beam therapy.* Br J Cancer, 2005. **93**(8): p. 849-54.
142. Deycmar, S. and M. Pruschy, *Combined Treatment Modalities for High-Energy Proton Irradiation: Exploiting Specific DNA Repair Dependencies.* Int J Part Ther, 2018. **5**(1): p. 133-139.
143. Deycmar, S., et al., *The relative biological effectiveness of proton irradiation in dependence of DNA damage repair.* Br J Radiol, 2019: p. 20190494.
144. Baumann, M., et al., *Radiation oncology in the era of precision medicine.* Nat Rev Cancer, 2016. **16**(4): p. 234-49.
145. Son, J., et al., *Development of Optical Fiber Based Measurement System for the Verification of Entrance Dose Map in Pencil Beam Scanning Proton Beam.* Sensors (Basel), 2018. **18**(1).
146. Britten, R.A., et al., *Variations in the RBE for cell killing along the depth-dose profile of a modulated proton therapy beam.* Radiat Res, 2013. **179**(1): p. 21-8.
147. Tang, J.T., et al., *Comparison of radiobiological effective depths in 65-MeV modulated proton beams.* Br J Cancer, 1997. **76**(2): p. 220-5.
148. Hojo, H., et al., *Difference in the relative biological effectiveness and DNA damage repair processes in response to proton beam therapy according to the positions of the spread out Bragg peak.* Radiat Oncol, 2017. **12**(1): p. 111.
149. Urano, M., et al., *Relative biological effectiveness of modulated proton beams in various murine tissues.* Int J Radiat Oncol Biol Phys, 1984. **10**(4): p. 509-14.
150. Weyrather, W.K. and G. Kraft, *RBE of carbon ions: experimental data and the strategy of RBE calculation for treatment planning.* Radiother Oncol, 2004. **73 Suppl 2**: p. S161-9.
151. Karger, C.P., *Medizinische Physik: Grundlagen-Bildgebung-Therapie-Technik*. 2018, Heidelberg, Germany: Springer Nature.
152. Malinen, E. and A. Sovik, *Dose or 'LET' painting--What is optimal in particle therapy of hypoxic tumors?* Acta Oncol, 2015. **54**(9): p. 1614-22.
153. Gerard, M., et al., *Hypoxia Imaging and Adaptive Radiotherapy: A State-of-the-Art Approach in the Management of Glioma.* Front Med (Lausanne), 2019. **6**: p. 117.
154. Tinganelli, W., et al., *Kill-painting of hypoxic tumours in charged particle therapy.* Sci Rep, 2015. **5**: p. 17016.
155. Falchi, F., et al., *Synthetic Lethality Triggered by Combining Olaparib with BRCA2-Rad51 Disruptors.* ACS Chem Biol, 2017. **12**(10): p. 2491-2497.
156. *Clinical Radiation Oncology - Indications, Techniques and Results*. Third Edition ed. 2017: Wiley Blackwell.
157. Fortini, P., et al., *The type of DNA glycosylase determines the base excision repair pathway in mammalian cells.* J Biol Chem, 1999. **274**(21): p. 15230-6.
158. Caldecott, K.W., *Single-strand break repair and genetic disease.* Nat Rev Genet, 2008. **9**(8): p. 619-31.
159. Brandsma, I. and D.C. Gent, *Pathway choice in DNA double strand break repair: observations of a balancing act.* Genome Integr, 2012. **3**(1): p. 9.
160. Lieber, M.R., *The mechanism of double-strand DNA break repair by the nonhomologous DNA end-joining pathway.* Annu Rev Biochem, 2010. **79**: p. 181-211.
161. Wyatt, H.D. and S.C. West, *Holliday junction resolvases.* Cold Spring Harb Perspect Biol, 2014. **6**(9): p. a023192.
162. Rass, U., et al., *Mechanism of Holliday junction resolution by the human GEN1 protein.* Genes Dev, 2010. **24**(14): p. 1559-69.
163. Kramer, D., et al., *Strong antitumor synergy between DNA crosslinking and HSP90 inhibition causes massive premitotic DNA fragmentation in ovarian cancer cells.* Cell Death Differ, 2017. **24**(2): p. 300-316.
164. Bouwman, P., et al., *53BP1 loss rescues BRCA1 deficiency and is associated with triple-negative and BRCA-mutated breast cancers.* Nat Struct Mol Biol, 2010. **17**(6): p. 688-95.
165. Jaspers, J.E., et al., *Loss of 53BP1 causes PARP inhibitor resistance in Brca1-mutated mouse mammary tumors.* Cancer Discov, 2013. **3**(1): p. 68-81.
166. Schwartz, R. and A.A. Schaffer, *The evolution of tumour phylogenetics: principles and practice.* Nat Rev Genet, 2017. **18**(4): p. 213-229.

167. Alves, J.M., T. Prieto, and D. Posada, *Multiregional Tumor Trees Are Not Phylogenies.* Trends Cancer, 2017. **3**(8): p. 546-550.
168. Kamran, S.C., J.O. Light, and J.A. Efstathiou, *Proton versus photon-based radiation therapy for prostate cancer: emerging evidence and considerations in the era of value-based cancer care.* Prostate Cancer Prostatic Dis, 2019. **22**(4): p. 509-521.
169. Carrier, F., et al., *Three Discipline Collaborative Radiation Therapy (3DCRT) Special Debate: I would treat prostate cancer with proton therapy.* J Appl Clin Med Phys, 2019. **20**(7): p. 7-14.
170. *Proton Therapy Lowers Risk of Side-Effects Compared to Conventional Radiation*, in *PennMedicine News*. 22.05.2019: Philadelphia/USA.
171. Bekelman, J.E., et al., *Pragmatic randomised clinical trial of proton versus photon therapy for patients with non-metastatic breast cancer: the Radiotherapy Comparative Effectiveness (RadComp) Consortium trial protocol.* BMJ Open, 2019. **9**(10): p. e025556.
172. Baumann, B.C., et al., *Comparative Effectiveness of Proton vs Photon Therapy as Part of Concurrent Chemoradiotherapy for Locally Advanced Cancer.* JAMA Oncol, 2019.
173. *Proton therapy lowers risk of side effects in cancer compared to traditional radiation*, in *ScienceDaily*. 26.12.2019.
174. Vogel, J., et al., *Proton therapy for pediatric head and neck malignancies.* Pediatr Blood Cancer, 2018. **65**(2).
175. Rombi, B., et al., *Proton radiotherapy for pediatric tumors: review of first clinical results.* Ital J Pediatr, 2014. **40**: p. 74.
176. Cao, W., et al., *Linear energy transfer incorporated intensity modulated proton therapy optimization.* Phys Med Biol, 2017. **63**(1): p. 015013.
177. Bassler, N., et al., *Dose- and LET-painting with particle therapy.* Acta Oncol, 2010. **49**(7): p. 1170-6.
178. Sorensen, B.S., *Commentary: RBE in proton therapy - where is the experimental in vivo data?* Acta Oncol, 2019. **58**(10): p. 1337-1339.
179. Grosse, N., et al., *Deficiency in homologous recombination renders Mammalian cells more sensitive to proton versus photon irradiation.* Int J Radiat Oncol Biol Phys, 2014. **88**(1): p. 175-81.
180. Fontana, A.O., et al., *Differential DNA repair pathway choice in cancer cells after proton- and photon-irradiation.* Radiother Oncol, 2015. **116**(3): p. 374-80.
181. Liu, Q., et al., *Lung cancer cell line screen links fanconi anemia/BRCA pathway defects to increased relative biological effectiveness of proton radiation.* Int J Radiat Oncol Biol Phys, 2015. **91**(5): p. 1081-9.
182. Liu, Q., et al., *Disruption of SLX4-MUS81 Function Increases the Relative Biological Effectiveness of Proton Radiation.* Int J Radiat Oncol Biol Phys, 2016. **95**(1): p. 78-85.
183. Gerelchuluun, A., et al., *Histone Deacetylase Inhibitor Induced Radiation Sensitization Effects on Human Cancer Cells after Photon and Hadron Radiation Exposure.* Int J Mol Sci, 2018. **19**(2).
184. Ratner, E.S., et al., *Triapine potentiates platinum-based combination therapy by disruption of homologous recombination repair.* Br J Cancer, 2016. **114**(7): p. 777-86.
185. Kunos, C.A. and S.P. Ivy, *Triapine Radiochemotherapy in Advanced Stage Cervical Cancer.* Front Oncol, 2018. **8**: p. 149.
186. Pereira, S., P.A. Fernandes, and M.J. Ramos, *Mechanism for ribonucleotide reductase inactivation by the anticancer drug gemcitabine.* J Comput Chem, 2004. **25**(10): p. 1286-94.
187. Toschi, L., et al., *Role of gemcitabine in cancer therapy.* Future Oncol, 2005. **1**(1): p. 7-17.
188. Wachters, F.M., et al., *Selective targeting of homologous DNA recombination repair by gemcitabine.* Int J Radiat Oncol Biol Phys, 2003. **57**(2): p. 553-62.
189. Kobashigawa, S., et al., *Gemcitabine Induces Radiosensitization Through Inhibition of RAD51-dependent Repair for DNA Double-strand Breaks.* Anticancer Res, 2015. **35**(5): p. 2731-7.
190. Jones, R.M., et al., *BRCA2 and RAD51 promote double-strand break formation and cell death in response to gemcitabine.* Mol Cancer Ther, 2014. **13**(10): p. 2412-21.
191. Noguchi, M., et al., *Inhibition of homologous recombination repair in irradiated tumor cells pretreated with Hsp90 inhibitor 17-allylamino-17-demethoxygeldanamycin.* Biochem Biophys Res Commun, 2006. **351**(3): p. 658-63.
192. Stecklein, S.R., et al., *BRCA1 and HSP90 cooperate in homologous and non-homologous DNA double-strand-break repair and G2/M checkpoint activation.* Proc Natl Acad Sci U S A, 2012. **109**(34): p. 13650-5.
193. Hirakawa, H., et al., *The combination of Hsp90 inhibitor 17AAG and heavy-ion irradiation provides effective tumor control in human lung cancer cells.* Cancer Med, 2015. **4**(3): p. 426-36.

194. Segawa, T., et al., *Radiosensitization of human lung cancer cells by the novel purine-scaffold Hsp90 inhibitor, PU-H71.* Int J Mol Med, 2014. **33**(3): p. 559-64.
195. Lee, Y., et al., *The purine scaffold Hsp90 inhibitor PU-H71 sensitizes cancer cells to heavy ion radiation by inhibiting DNA repair by homologous recombination and non-homologous end joining.* Radiother Oncol, 2016. **121**(1): p. 162-168.
196. Li, H.K., et al., *PU-H71, a novel Hsp90 inhibitor, as a potential cancer-specific sensitizer to carbon-ion beam therapy.* J Radiat Res, 2016. **57**(5): p. 572-575.
197. Seol, J.H., E.Y. Shim, and S.E. Lee, *Microhomology-mediated end joining: Good, bad and ugly.* Mutat Res, 2018. **809**: p. 81-87.

Table of Figures -Thesis

Table of Tables - Thesis